Characterization of Recombinant Alternative Oxidase 1A from *Arabidopsis thaliana* and Interaction with Inhibitors, TCA Cycle and Redox Metabolites

A Thesis submitted to the University of Hyderabad for the award of **DOCTOR OF PHILOSOPHY**

BY

TADIBOINA VEERA SANKAR

Enrollment No: 14LTPH02

Supervisor: Prof. K.P.M.S.V. Padmasree





(A Central University established in 1974 by an Act of Parliament)

Department of Biotechnology & Bioinformatics

School of Life Sciences

University of Hyderabad - 500 046,

India

August 2023



University of Hyderabad

(A Central University established by an Act of Parliament)

School of Life Sciences
Department of Biotechnology & Bioinformatics
University of Hyderabad - 500 046, Telangana, India

DECLARATION

I, Tadiboina Veera sankar, hereby declare that the work presented in this thesis entitled "Characterization of Recombinant Alternative Oxidase 1A from Arabidopsis thaliana and Interaction with Inhibitors, TCA Cycle and Redox Metabolites" has been carried out by me under the supervision of Prof. K.P.M.S.V. Padmasree in the Department of Biotechnology & Bioinformatics, School of Life Sciences, University of Hyderabad. This work has not been submitted for any degree or diploma of any other University or Institute.

Tadiboina Veera sankar

To Veerajankar.

Tadibolia veera sankar

(Candidate)

(Reg. No.14LTPH02)

(Co-Supervisor)

Prof. P. Prakash Babu
Prof. P. Prakash Babu
Prof. P. Prakash Babu
Department of Biotechnology & Bioinformatics
School of Life Sciences
University of Hyderabad
Hyderabad-500 046. (T.S.)

(Supervisor)

Prof. K.P.M.S.V. Padmasree

Dr. K.P.M.S.V. Padmasree, Ph.D.
Professor & AvH Research Fellow
Dept. of Biotechnology & Bioinformatics
School of Life Sciences
University of Hyderabad
Hyderabad-500 046
Telangana, INDIA



University of Hyderabad

(A Central University established by an Act of Parliament)

School of Life Sciences
Department of Biotechnology & Bioinformatics
University of Hyderabad - 500 046, Telangana, India

CERTIFICATE

This is to certify that the thesis entitled "Characterization of Recombinant Alternative Oxidase 1A from Arabidopsis thaliana and Interaction with Inhibitors, TCA Cycle and Redox Metabolites" submitted by Mr. Tadiboina Veera sankar, bearing registration number 14LTPH02 in partial fulfillment of the requirements for award of Doctor of Philosophy in the Department of Biotechnology and Bioinformatics, School of Life Sciences is a bonafied work carried out by him under my guidance and supervision.

This thesis is free from plagiarism and has not been submitted in part or in full to this or any other University or Institution for the award of any degree or diploma.

Parts of the work performed in relation to this thesis have been:

A. Published in the following journals:

1. Frontiers in Plant Science, DOI: 10.3389/fpls.2022.871208.

B. Presented in the following conferences:

- Biomedical engineering, Bioscience, Bioinformatics, Biochemistry, Cancer Biology, Molecular Biology and Applied Biotechnology (BCM-2019), held on 1st January at JNU, Delhi, India-110067 (Poster presentation; International).
- Virtual Conference on Proteomics in Agriculture and Healthcare, held on March 13-14th, 2021, at School of Life Sciences, University of Hyderabad, India-500046 (Oral presentation; National).

3. 2nd international conference on INTEGRATIVE BIOLOGY & APPLIED GENETICS (ICIBAG-2022)", held on 20th – 22nd July -2022 at Osmania University, Hyderabad – 500 007 (Poster presentation; International).

Further, the student has passed the following courses towards the fulfillment of the coursework requirement for Ph.D.

Course Code	Name	Credits	Pass/Fail
AS 801	Analytical Techniques	4	Pass
AS 802	Research Ethics, Data Analysis and Biostatistics	3	Pass
AS 803	Lab Work and Seminar	5	Pass

Co-Supervisor

Prof. P. Prakash Babu

Prof. P. Prakash Babu

Department of Biotechnology & Bioinformatics

School of Life Sciences University of Hyderabad Hyderabad-500 046. (T.S.) Supervisor

Prof. K.P.M.S.V. Padmasree

Dr. K.P.M.S.V. Padmasree, Ph.D.,
Professor & AvH Research Fellow
Dept. of Biotechnology & Bioinformatics
School of Life Sciences
University of Hyderabad
Hyderabad-500 046
Telangana, INDIA

Head NW

Dept. of Biotechnology & Bioinformatics

HEAD

Dept. of Biotechnology & Bioinformatics

University of Hyderabad

Hyderabad.

Dean

School of Life Sciences

Muna Kunal

सकाम अध्यक्ष / Dean

जीव विज्ञान सकाय / School of Life Sciences हैदराबाद विश्वानेशालय/University of Hyderabad हैदराबाद / Hyderabad-500 046.

Acknowledgements

I would like to express my profound gratitude with immense pleasure to my supervisor **Prof. K.P.M.S.V. Padmasree** for her unique guidance, suggestions and constant encouragement throughout my Ph.D.

I would like to express my deepest gratitude and appreciation to my co-supervisor **Prof. P. Prakash babu** and doctoral committee members, **Prof. Sarada Devi Tetali** and **Prof. Anand Kumar Kondapi** for their critical comments and valuable suggestions.

I am grateful to **Prof. Renate Scheibe** from University of Osnabrück, Germany for providing *Arabidopsis thaliana* seeds.

My heartfelt thanks to **Prof. Saradadevi Tetali** for critical suggestions and help in cloning & expression of AtAOX1A.

My sincere thanks to **Dr. Moumita Saharay**, Dept. of Systems and Computational Biology, who helped in molecular docking studies. Completion of my thesis would not have been possible without her help and support.

My special thanks to **Prof. A.S. Raghavendra** and **Prof. Saradadevi Tetali**, dept. of Plant Sciences, for extending critical suggestions on experimental protocols/results and their lab facilities during the execution of the project.

I would also like to extend my thanks to **Prof. J.S.S. Prakash**, Head, Dept. of Biotechnology and former Heads **Prof. K.P.M.S.V. Padmasree**, **Prof. Anand Kondapi**, **Prof. Niyaz Ahmad** and **Prof. P. Prakash babu** for providing the necessary facilities in the department to carry out my research work.

I am grateful to **Prof. N. Siva Kumar**, Dean, School of Life Sciences, and former Deans **Prof. S. Dayananda**, **Prof. K. Ramaiah**, **Prof. P. Reddanna**, **Prof. A.S Raghavendra**, **Prof. R.P. Sharma**, late **Prof. Aparna Dutta Gupta**, and **Prof. M. Ramanadham** for providing all the facilities in the school.

My sincere thanks to **Prof. Sharmistha Banerjee** for timely help in the need for metal affinity resin for protein purification.

I would like to thank **Dr. Arunasree** for her critical suggestions during experimental protocols discussion

I am thankful to late **Prof. Aparna Dutta Gupta** for allowing me to utilize her lab facilities.

I am thankful to **Prof. Krishnaveni Mishra**, **Prof. Naresh Babu V. Sepuri**, **Head**, Dept. of Biochemistry, **Dr. Santosh Kumar Padhi** and **Dr. Mohd. Akif** for allowing me to use the incubator and sonicator for *E. coli* work.

I am also thankful to **Prof. Ch. Venkataramana**, **Prof. Padmaja Gudipalli**, and **Prof. Rajagopal Subramanyam**, **Head**, Dept. of Plant Sciences, for allowing me to use lyophilizer and thanks to Mr. Dasaradh for technical assistance in this regard.

Thanks are due to the Office staff (Mr. Rahul, Mrs. Arundati, Mr. Shekar and Mr. Rajashekar) of the Dept. of Biotechnology & Bioinformatics for their technical assistance.

I thank Mr. Arun, and Mr. Prashanth Kumar for their assistance in the lab.

Thanks to Mrs. Monika Kannan (Proteomics Facility, School of Life Sciences, UoH) for helping in MALDI-TOF studies and Dr. Praveen (GE Healthcare Life Sciences) for helping in the analysis of SPR data.

I'm very thankful for the sources that have supported me financially! Funding from the UGC-SAP, DST-FIST UPE, DBT-CREBB, DBT-BUILDER/SAHAJ, UGC DRS, DST-PURSE, UPE-I & II, UoH-IoE for the Department & School of Life Sciences.

I gratefully acknowledge the **DBT-JRF** and **DBT-SRF** for the research fellowship.

I am thankful to the **University of Hyderabad** and the **Dept. of Biotechnology & Bioinformatics** for giving me this opportunity to pursue my Ph.D. degree.

I would like to thank all the Faculty members of the Department and School of Life Sciences.

I am grateful to all my teachers, who taught me and are instrumental in shaping my life.

I also thank my senior lab mates, **Dr. Prasad** and **Dr. Dinakar**, for their contribution to this laboratory.

I am thankful to my senior lab mates **Dr. Srinivasa Rao**, **Dr. Swathi**, **Dr. Abhay Prathap**, **Dr. Mohanraj**, **Dr. Swaroop Kumar and Dr. Lokya** for their encouragement and support during this time.

I am thankful to my lab mates Mariyamma, Mahati, Bharati, Santhosh, Deepali, Spandana and M.Sc. project students for creating a friendly and cheerful environment to work in.

I am thankful to **all my HCU** and **non-HCU** friends......for making my life beautiful with their company.

My deepest gratitude to my loving and supportive wife (Anantha Lakshmi), brother & sister-in-law (Veera Brahmam & Jhansi Rani) and Parents (Srinivasa Rao & Koteswaramma) for their love and care.

I am extremely grateful to **Pastor Prasad reddy Garu** for his motivation and guidance in building up my carrier.

I thank **Smyrna church**, Gopanpally, for the joyful fellowship.

Above all, I praise and thank my **Almighty Lord Jesus Christ** for his faithfulness, love, grace and wisdom from the beginning of my academic life up to this doctoral level.

Veera Sankar

This thesis is dedicated to my Lord and Savior JESUS CHRIST

List of Abbreviations

AA = antimycin A

ABA = abscisic acid

AOX = alternative oxidase

AsA = ascorbic acid

AtAOX1A = A. thaliana alternative oxidase 1A

COX = cytochrome c oxidase

CD = circular dichroism

DDM = n-dodecyl-β-D-maltopyranoside

DEPC = diethylpyrocarbonate

DHA = dehydroascorbate

DQ = duroquinone

 DQH_2 = duroquinol or Reduced duroquinone

ETC = electron transport chain

E. coli/pET28a = E. coli BL21(DE3) cells transformed with pET28a

E. coli/pAtAOX1A = E. coli BL21(DE3) cells transformed with pAtAOX1A

GSH = reduced glutathione

GSSG = oxidized glutathione

IMS = inner membrane space

IPTG = isopropyl-β-D-thiogalactopyranoside

KCN = potassium cyanide

 k_a = association constant

 $k_{\rm d}$ = dissociation constant

 $K_{\rm D}$ = equilibrium dissociation constant

MALDI-TOF = matrix-assisted laser desorption ionization

time-of-flight

miETC = mitochondrial electron transport chain

NAD = nicotinamide adenine dinucleotide

NADH = reduced nicotinamide adenine dinucleotide

NADP = nicotinamide adenine dinucleotide phosphate

NADPH = reduced nicotinamide adenine dinucleotide phosphate

n-PG = n-propyl gallate

OAA = oxaloacetic acid

OD = optical density

OG = n-octyl-β-D-glucopyranoside

pAtAOX1A = plasmid construct (pET28a + AtAOX1A)

PCR = polymerase chain reaction

PMF = proton motive force

PVDF = polyvinylidene difluoride

 Q_1H_2 = ubiquinol-1 or Reduced ubiquinone

RNS = reactive nitrogen species

ROS = reactive oxygen species

RU = resonance unit

rSgAOX = recombinant Sauromatum guttatum

alternative oxidase

rTAO = recombinant trypanosomal alternative oxidase

rAtAOX1A = recombinant *Arabidopsis thaliana* alternative oxidase

SDS-PAGE = sodiumdodecyl sulfate polyacrylamide

gel electrophoresis

SPR = surface plasmon resonance

SHAM = salicylhydroxamic acid

TCA = tricarboxylic acid

Trx = Thioredoxins

UQ = ubiquinone

 UQ_1 = ubiquinone-1

WT = wild-type

 α -KG = alpha-ketoglutarate

Abstract of Thesis

The plant mitochondrial electron transport chain possesses two terminal oxidases, cytochrome oxidase (COX) and alternative oxidase (AOX) pathways for the reduction of molecular oxygen into water. The COX and AOX pathways are known to bifurcate at ubiquinone. The AOX pathway is identified in all plants, fungi, some protists, and a few animal and bacterial species but is absent in mammals, and this pathway is not linked to ATP generation. Though the AOX pathway was initially thought to be an energy-wasteful process, several studies from the past three decades revealed its importance in regulating cellular redox, ROS and metabolic homeostasis under various biotic and abiotic stresses.

The *alternative oxidase1A* (*AOX1A*) from *Arabidopsis thaliana* is the most important among hundreds of known stress-responsive genes of plant mitochondria. *Arabidopsis thaliana* AOX1A is present in the mitochondrial inner membrane towards the matrix side. Despite its important role in cellular redox and metabolic homeostasis, the mechanism of its interaction with different metabolites is poorly understood due to the difficulty in acquiring it in a pure and highly active form of protein from plant sources.

Therefore, in the present study, the *AtAOXIA* from *Arabidopsis thaliana* is cloned into a pET28a vector and induced its expression in *E. coli* using IPTG. The expressed protein is functionally active in *E. coli*, which is evident by KCN (inhibitor of COX pathway) resistance and salicylhydroxamic acid (SHAM) and n-propyl gallate (n-PG) [inhibitors of AOX pathway] sensitive respiration and growth. Later, the rAtAOX1A is purified in its active form from *E. coli* membranes by solubilizing in DDM and passing through a cobalt affinity column. The purified rAtAOX1A has shown stability in its structure to a wide range of temperature and pH conditions.

In the literature, it has been reported that AOX isoforms are posttranslationally activated by different TCA cycle metabolites in an isoform-specific manner. Therefore, we made an attempt to examine the molecular interaction of purified rAtAOX1A with its activator (pyruvate), TCA cycle, and redox metabolites by employing techniques such as surface plasmon resonance (SPR), CD, and fluorescence spectroscopy. In addition, molecular docking was performed to identify the binding pocket, while point mutational docking studies revealed potent residues involved in the binding with its inhibitors/metabolites. Overall, the strategy gave us an understanding of different inhibitor and metabolite interactions with rAtAOX1A and associated conformational changes.

Chapter 1Introduction and review of literature

Introduction and Review of Literature

Mitochondrial respiration is the fundamental physiological process that occurs in every living cell. All eukaryotes contain mitochondria, an important cellular organelle to generate readily utilizable energy in the form of adenosine triphosphate (ATP) through the process of aerobic respiration, which occurs in three steps: (i) glycolysis; (ii) citric acid cycle and (iii) oxidative phosphorylation. Glycolysis takes place in the cytoplasm, where glucose is broken down into two molecules of pyruvate and during this process, ATP and NADH are generated. The pyruvate produced during glycolysis is converted to acetyl-CoA by the action of pyruvate dehydrogenase in the mitochondria, and it enters into the tricarboxylic acid (TCA)/Krebs cycle, which operates in the mitochondrial matrix. The operation of the TCA cycle generates reduced cofactors such as NADH and FADH₂. The reduced cofactors generated during glycolysis and the TCA cycle are, in turn, oxidized by the mitochondrial electron transport chain (miETC) (Millar et al., 2011; Meyer et al., 2019).

The miETC, which is present in the inner mitochondrial membrane (IMM), is the hub for different protein complexes. The electrons generated by the oxidation of NADH and FADH₂ are passed through different protein complexes (I to IV complexes) in miETC and finally transferred to molecular oxygen, during which a proton gradient is generated across the IMM. The energy stored in the proton gradient is utilized for the phosphorylation of ADP to ATP by ATP synthase (complex V). Thus, the ATP generated through aerobic respiration is utilized by the cell for various cellular functions (Braun, 2020; Meyer et al., 2022). Although the electron transport through complex I to IV operated in eukaryotes is energy-conserving, there are several other energy/non-energy conserving alternative electron

transport pathways identified in some bacteria, protists, fungi, plants and a few animals (Siedow and Umbach, 2000; Vanlerberghe and Ordog, 2002; Millenaar and Lambers, 2003; Rasmusson et al., 2004).

Structure of miETC in higher plants

The plant miETC possesses a classical miETC, which consists of four protein complexes (Complexes I, II, III and IV). The protein complex I (NADH dehydrogenase) and complex II (succinate dehydrogenase) accept electrons from NADH and succinate, respectively, and transfer them to ubiquinone (UQ). The UQ is a lipid-soluble electron carrier and delivers electrons to complex III (cytochrome c reductase). Complex III then passes the electrons to a small protein, 'cytochrome c', a water-soluble electron carrier. The cytochrome c carries electrons to complex IV (cytochrome c oxidase), which reduces oxygen to water. The pathway for the transport of electrons from UQ to complex III and complex IV, which is sensitive to antimycin A (AA) and cyanide, respectively, is broadly called as cytochrome oxidase (COX) pathway (Fig. 1.1) (Millar et al., 2004, 2011).

Along with the COX pathway, there are three different types of alternative electron transport pathways in plant mitochondria and they are operated by (a) Type II NAD(P)H dehydrogenases, (b) Alternative oxidase (AOX), and (c) Uncoupling proteins (UCPs) (Fig.1.1). Type-II NAD(P)H dehydrogenases, which are located on both sides of IMM, bypasses electron transport from complex I and they are insensitive to rotenone and regulated by cytosolic Ca²⁺ levels. Many bacteria, protists and fungi also contain these type–II dehydrogenases (Friedrich et al., 1995; Kerscher, 2000; Joseph-Horne et al., 2001; Møller,

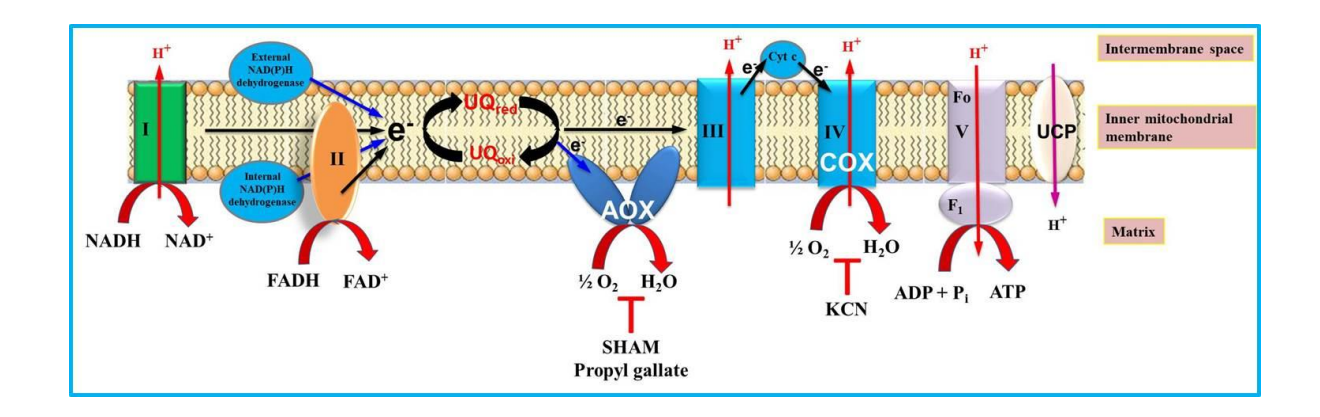


Fig. 1.1. Diagrammatic representation of miETC of higher plants. The mitochondrial inner membrane of higher plants is the site for the ETC, which consists of different protein complexes (complex I, II, III and IV), ubiquinone (UQ) and cytochrome *c* (Cyt c). Complex V produces ATP by utilizing the proton motive force generated by Complexes I, III, and IV. The alternative electron transport pathways include internal and external NAD(P)H dehydrogenases, alternative oxidase (AOX), and uncoupling proteins (UCPs). The inhibitors of the AOX and cytochrome oxidase (COX) pathways were shown below each pathway. The alternative route of electron transport is indicated with blue color arrows. Abbreviations: SHAM- salicylhydroxamic acid, KCN- Potassium cyanide.

2001; Melo et al., 2004; Rasmusson et al., 2004). The activity of external NADH dehydrogenases is up regulated in response to any increase in cytosolic NADH concentration to balance the cellular redox state (Escobar et al., 2006; Fedotova et al., 2023).

The UCPs, which are located on the IMM of plants, are encoded by multiple genes and they show differential expression patterns in different tissues and organs. The UCPs are involved in proton conductance across the IMM and dissipate the proton motive force (PMF) in response to increased reactive oxygen species (ROS) and free fatty acids. Overall, though the activity of UCPs seems to reduce the generation of ATP, nevertheless, it helps in minimizing the ROS production in mitochondria under stress conditions (Vercesi et al., 2006; Barreto et al., 2020). In plants, protists, fungi, a few bacteria and some animal species, an additional electron transport pathway is operated between UQ and molecular O₂ and this pathway is catalyzed by an enzyme AOX. Also, this pathway is insensitive to cyanide, hence called as cyanide-resistant AOX pathway (Rich and Moore, 1976; Vanlerberghe and McIntosh, 1997; McDonald et al., 2009; Dunn, 2023). The AOX pathway is specifically inhibited by n-propyl gallate (n-PG), ascofuranone, and hydroxamic acids such as salicylhydroxamic acid (SHAM) (Hoefnagel et al., 1995; Kido et al., 2010).

Alternative oxidase pathway (AOX Pathway)

The AOX pathway was first identified in the floral tissues of the thermogenic plant Araceae. The electron transport through the AOX pathway of mitochondrial respiration causes a high rate of electron flux in thermogenic plants, which generates heat that is equivalent to as much as a rise in temperature by approximately 25°C. As a result, some organic compounds that are present in the spadix of thermogenic plants are known to get volatilized to attract insect

pollinators (Meeuse and Buggeln, 1969; Meeuse, 1975). The operation of the AOX pathway reduces electron flow through complexes III and IV, which in turn dramatically decreases the synthesis of ATP. Thus, once upon a time, operation of the AOX pathway was thought to be an energy-wasteful process, but now it is well understood that the AOX pathway plays an important role in energy homeostasis and cellular metabolism besides participating in thermogenesis (Strodtkötter et al., 2009; Moore et al., 2013; Vanlerberghe, 2013; Vishwakarma et al., 2015; Dahal and Vanlerberghe, 2017; Florez-Sarasa et al., 2020).

Under normal physiological conditions, little or sometimes no AOX pathway activity was observed in plants. However, on exposure of plants to any stress that is associated with disturbance in cellular redox/carbon status, NAD(P)H supply greatly increased the AOX pathway activity, indicating that the expression of AOX occurs in response to various signals (Vanlerberghe, 2013; Chadee et al., 2022). The AOX pathway is known to play a vital role in regulating the cellular redox balance whenever the cytochrome pathway is over-reduced or chemically inhibited and during the exposure of plants to abiotic stresses, such as high light, drought, temperature, UV-B stress, and high levels of greenhouse gasses (Berthold et al., 2000; Moore et al., 2002, 2013; Giraud et al., 2008; Vanlerberghe, 2013; Vishwakarma et al., 2014, 2015; Dahal and Vanlerberghe, 2017; Florez-Sarasa et al., 2020; Garmash et al., 2020). Besides, the AOX pathway is known to benefit plants by lowering ROS production, either by keeping miETC components upstream of the ubiquinone pool in a more oxidized state or preventing over-reduction of the COX pathway during stress conditions (Maxwell et al., 1999; Vishwakarma et al., 2015). In addition, the role of the AOX pathway in optimizing photosynthesis is well accepted not only under normal environmental conditions but also under various stress conditions. Also, the AOX pathway is known to operate at much higher levels than the conventional COX pathway under stress conditions (Padmasree and Raghavendra, 1999a; Yoshida et al., 2006; Strodtkötter et al., 2009; Dinakar et al., 2010a,b; Zhang et al., 2012, 2016; Vishwakarma et al., 2014, 2015).

Structure of AOX

The AOX basically exists in two states (i) monomeric and (ii) dimeric forms. In fungi like *Neurospora crassa* and *Pichia stipitis*, it exists as a monomer (Siedow and Umbach, 2000), but in plants and parasite like *Trypanosoma brucei*, it exist as a homodimer (Umbach and Siedow 1993; Vanlerberghe et al., 1995; Umbach et al., 2002; McDonald, 2008; Moore et al., 2013; Shiba et al., 2013). The AOX from fungal and protists is generally activated by adenosine diphosphate (ADP), adenosine monophosphate (AMP) and guanosine monophosphate (GMP) (Jarmuszkiewicz et al., 2005; Barsottini et al., 2020). In contrast, AOX from the plant is activated by different organic acids (Millar et al., 1993; Umbach et al., 2002; Moore et al., 2013; Selinski et al., 2018a; Xu et al., 2021). Though AOX from different organisms has conserved active enzymatic sites, the mechanism of activation is found to be different (Moore et al., 2013; May et al., 2017; Xu et al., 2021).

The structural studies on the plant and trypanosomal AOX (TAO) revealed that it possessed a non-heme diiron carboxylate active site (Berthold et al., 2001, 2002; Affourtit et al., 2002; Moore and Albury, 2008; Moore et al., 2008, 2013; Albury et al., 2009; Maréchal et al., 2009). Besides, the studies on the crystal structure of TAO revealed that it exists as a homodimer and each monomer consists of a four-helix bundle (α 2, α 3, α 5, and α 6) ligated to a diiron core by highly conserved four glutamate residues (E123, E162, E213, and E266) and two histidine residues (H165 and H269). Overall, in each monomer, there are six long and

four short α -helices, along with two hydrophobic cavities in TAO. The $\alpha 1$ and $\alpha 4$ helices of TAO contained large hydrophobic regions that are involved in membrane binding. Furthermore, the binding of ubiquinol (UQH₂) to Tyr220 of TAO leads to the catalysis of O₂ reduction (Moore et al., 2013; Shiba et al., 2013; May et al., 2017).

Further, the studies of Elliott et al. (2014) revealed the secondary structure of a recombinant AOX in the thermogenic plant *Sauromatum guttatum* (rSgAOX). However, such a secondary structure is not yet unveiled for AOX from non-thermogenic plants. Also, despite the identification of several inhibitors and activators, the information on how these molecules interact with AOX is not yet known (Xu et al., 2021).

Mechanism of reduction of O₂ to H₂O by AOX

The AOX from different organisms varied in their catalytic activity. For example, the purified rAOX from *Trypanosoma brucei* has shown more UQH₂ oxidase activity compared to the purified rAOX from *S. guttatum* and *A. thaliana* (Kido et al., 2010; Elliott et al., 2014; Xu et al., 2021; Sankar et al., 2022). This variation in the activity of AOX from different sources could be due to their origin and variability in the polar residues surrounding the hydrophobic cavity of the quinol binding site, which in turn might change the size of the cavity. This, in turn, may lead to differences in the strength of attraction of quinol into the active site and, thereby, affect the activity of AOX enzyme (May et al., 2017; Xu et al., 2021).

During the AOX activity, oxygen binds to the active diiron center of the enzyme (**Fig. 1.2**). This binding will lead to the formation of two short-lived intermediates (superoxo and

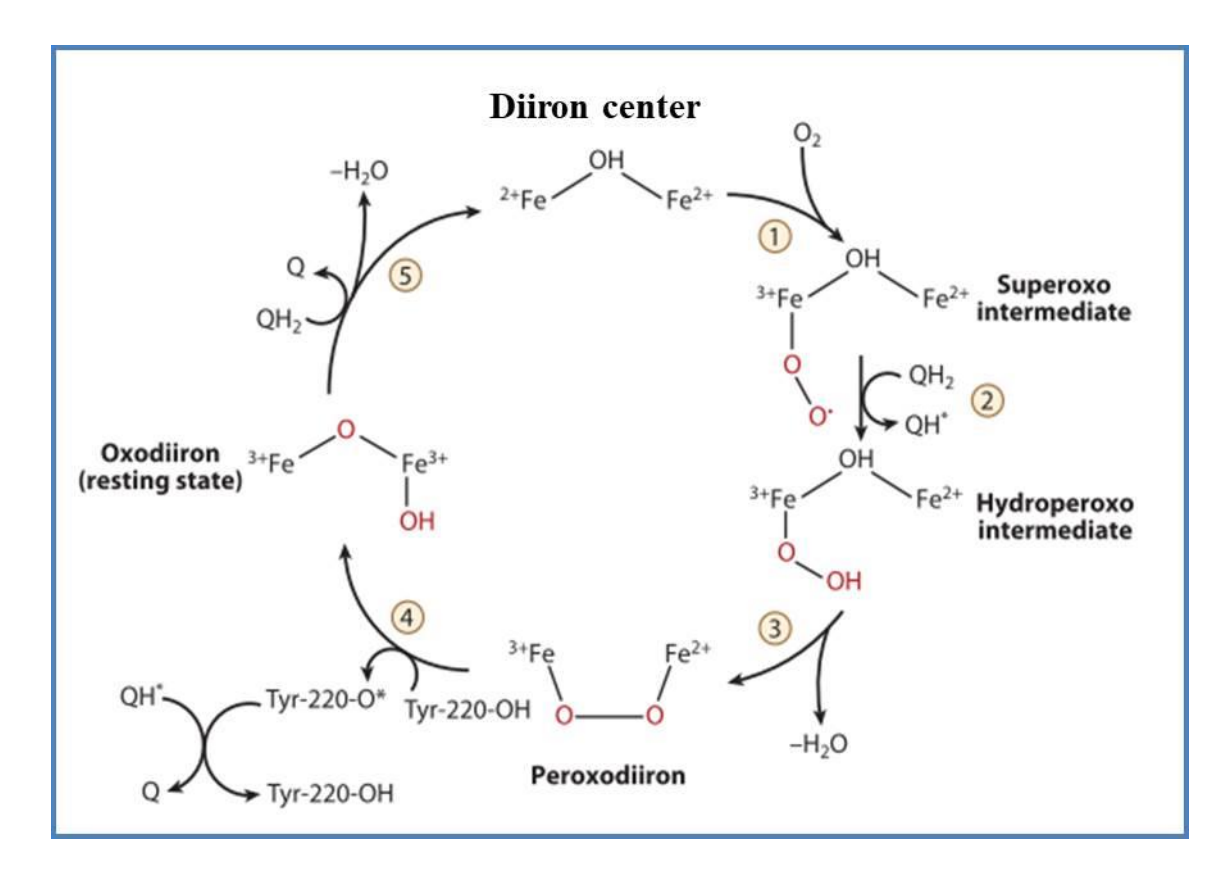


Fig. 1.2. Diagrammatic representation of AOX redox cycle, which involves the conversion of O₂ to 2H₂O. Different reactions are involved in this process; reaction 1: oxygen binds to the active diiron center of the enzyme, which leads to the formation of superoxo intermediate; Reaction 2: reduction of superoxo intermediate by UQH₂ forms Hydroperoxo intermediate; Reaction 3: formation of peroxodiiron species by losing water; Reaction 4: formation of an oxodiiron species by oxidation of Tyrosyl residue which in turn is reduced by semiubiquinone formed in reaction 2; Reaction 5: reduction of oxodiiron species with the second UQH₂ and this reaction generates an active diiron state by losing one water molecule. Overall, AOX catalyzes the reduction of one O₂ molecule to two water molecules (adapted from Moore et al., 2013).

hydroperoxo intermediates). The superoxo species, which is initially formed by the binding of O₂ to the diiron center, receives a proton and an electron from ubiquinol and gets reduced immediately to form a hydroperoxo intermediate, while semiubiquinone is formed in this process (reactions 1 and 2) (Shan and Que, 2005; Friedle et al., 2010; Moore et al., 2013). Further, peroxodiiron species is formed from the hydroperoxo intermediate by losing a water molecule (reaction 3). In the next step, peroxodiiron species take an electron and a proton from Tyr-220 and cause homolytic cleavage of the O-O bond and forms an oxodiiron species (reaction 4). During this process, tyrosyl radical is generated and ubisemiquinone which is formed in reaction 2, helps in the re-reduction of tyrosyl radicle. The second UQH₂ then reduces the oxodiiron species and generates an active diiron state by losing one water molecule (reaction 5) (Moore et al., 2013).

Structure of AOX Gene

Mitochondrial AOX is encoded by nuclear genes. In many plants, it is known to exist as a multi-gene family. In the case of *A. thaliana*, mitochondrial AOX is encoded by two different nuclear gene subfamilies, namely *AOX1* and *AOX2* (Whelan et al., 1996; Saisho et al., 1997; Clifton et al., 2006; Millar et al., 2011). The *AOX1* gene subfamilies (*AOX1A-D*) are expressed in both monocot and dicot plants, and these gene groups show stress-responsive expression. Contrarily, *AOX2* is expressed constitutively and it has no other isoforms (Considine et al., 2002; Clifton et al., 2005; Borecký et al., 2006; Clifton et al., 2006). However, each isoform of AOX genes is expressed differently under various stress conditions and their expression patterns also vary both spatially and temporally. For example, in *A. thaliana*, *AOX1A* is well-known as the most stress-responsive gene among the AOX isoforms. The isoforms *AOX1A* and *AOX1C* expression is identified in rosettes, stems, buds,

flowers, and roots, whereas *AOX1B* is detected in buds and flowers. *AOX2* is found in roots, stems and rosettes. Further, gene expression analysis of *A. thaliana* by using microarray gene chip data indicated that different AOX genes are expressed in almost all developmental stages (Saisho et al., 1997; Clifton et al., 2006).

Retrograde and transcriptional regulation of AOX gene expression

The regulation of nuclear gene expression by the signals received from cellular organelles such as chloroplast and mitochondria is known as retrograde regulation. AOX, which is encoded by a nuclear gene, is a well-known model for retrograde regulation. In plants, mitochondria are the major targets and source of ROS generation in response to different stresses and metabolic disturbances. The ROS generated by miETC under stress conditions acts as a signaling molecule for the AOX gene expression (Gray et al., 2004; Vanlerberghe, 2013; Ng et al., 2014). Further, the mitochondria-localized RRL (Retarded Root Growth-Like) protein of *A. thaliana* is also known to play a crucial role in Abscisic acid (ABA) signaling of AOX gene expression (Bartoli et al., 2004; Fujita et al., 2006; Gechev et al., 2006; Giraud et al., 2008; Yao et al., 2015; Qiao et al., 2023).

The expression of AtAOX1A is regulated by different retrograde signaling described above as well as transcription factors such as (i) Abscisic acid insensitive4 (ABI4): The ABI4 represses the constitutive expression of AOX by binding to the B element of its promoter under normal conditions. Under stress conditions, ABA binds to ABI4 and allows the expression of AOX (Giraud et al., 2009); (ii) Cyclin-dependent kinase E1 (CDKE1): The CDKE1 is involved in cell division or elongation by integrating environmental signals with cellular responses. Moreover, it senses certain transcription factors that are induced during

different stresses and actively binds to the promoter and RNA polymerase II. This will help plants to switch between stress responses and their growth under different environmental conditions. Further, CDKE1 is crucial for H₂O₂ and cold stress responses via anterograde pathways. The CDKE1 also integrates the retrograde signals for AOX expression under various stress conditions (Ng et al., 2013; Wang et al., 2018); (iii) WRKY transcription factors: The WRKY transcription factors are involved in regulating stress responses. They belong to the plant-specific class of proteins that consists of at least one highly conserved sequence WRKY along with an additional zinc finger motif. The WRKY transcription factors are majorly involved in biotic stresses and also play an important role in plant immunity under microbe or pathogen-triggered responses. In A. thaliana, around 72 types of WRKY genes were identified (Rushton et al., 1996; Eulgem and Somssich, 2007; Rushton et al., 2010; Van Aken et al., 2013). The binding sites (W-Boxes) for WRKY transcription factors are present in the promoter of the stress-responsive genes. In the case of AtAOX1A, these transcription factors can directly bind to the promoter and act as both activators and repressors (Rushton et al., 1995; Van Aken et al., 2009; Wang et al., 2018); (iV) Arabidopsis NAC domain-containing protein17 (ANAC017): The ROS generated under stress conditions activates the transcription factor 'ANAC017' of AOX1A. The ANAC017 directly interacts with AOXIA and initiates its expression. This is an example of retrograde signaling of ROS to activate AOX expression (Ng et al., 2013; Vanlerberghe et al., 2020).

Posttranslational regulation of AOX

AOX activity remains low in the cell under normal physiological conditions. An increase in activity is often related to high electron flux in mitochondria and the accumulation of TCA-cycle intermediates (Noguchi et al., 2005; Ribas-Carbo et al., 2005). AOX in plant

mitochondria exists as a homodimer, where the monomers of each homodimer are linked with a disulfide bridge. At the N-terminal region of plant AOX isoforms, two highly conserved cysteine residues (CysI and CysII) were localized. These residues were known to play an important role in the posttranslational regulation of AOX (Umbach et al., 2006).

CysI is mainly involved in disulfide bond formation to interact with the adjacent monomeric subunit of the AOX homodimer. Thus, redox-active CysI plays an important role in the formation of AOX homodimer. The disulfide bridged AOX homodimer is in an oxidized inactive state. Several reports on the activation of AOX have suggested that the thioredoxin (Trx) system and Glutaredoxins of mitochondria are involved in the posttranslational regulation of AOX by providing reducing equivalents for the reduction of the disulfide bond, which leads to the formation of reduced active AOX with sulfhydryl group (Rietsch and Beckwith, 1998; Wheeler and Grant, 2004; Herrero et al., 2008). Apart from disulfide bridge formation, CysI also plays a key role in AOX activation by α -keto acids such as pyruvate (Millar et al., 1993; Umbach and Siedow, 1993, 1996; Day et al., 1995; Rhoads et al., 1998). Besides, the second conserved cysteine residue (CysII) is known to act as a target for small α -keto acids, such as glyoxylate (Fig. 1.3) (Rhoads et al., 1998; Siedow and Umbach, 2000; Umbach and Siedow, 2006).

The physiological role of AOX1A in alleviating cellular ROS

The AOX pathway facilitates to bypass electrons from conventional miETC and restricts the generation of ROS from complex I and III (major sources for the generation of ROS in mitochondria) under over-reduced/stress conditions, thereby protecting the cells from

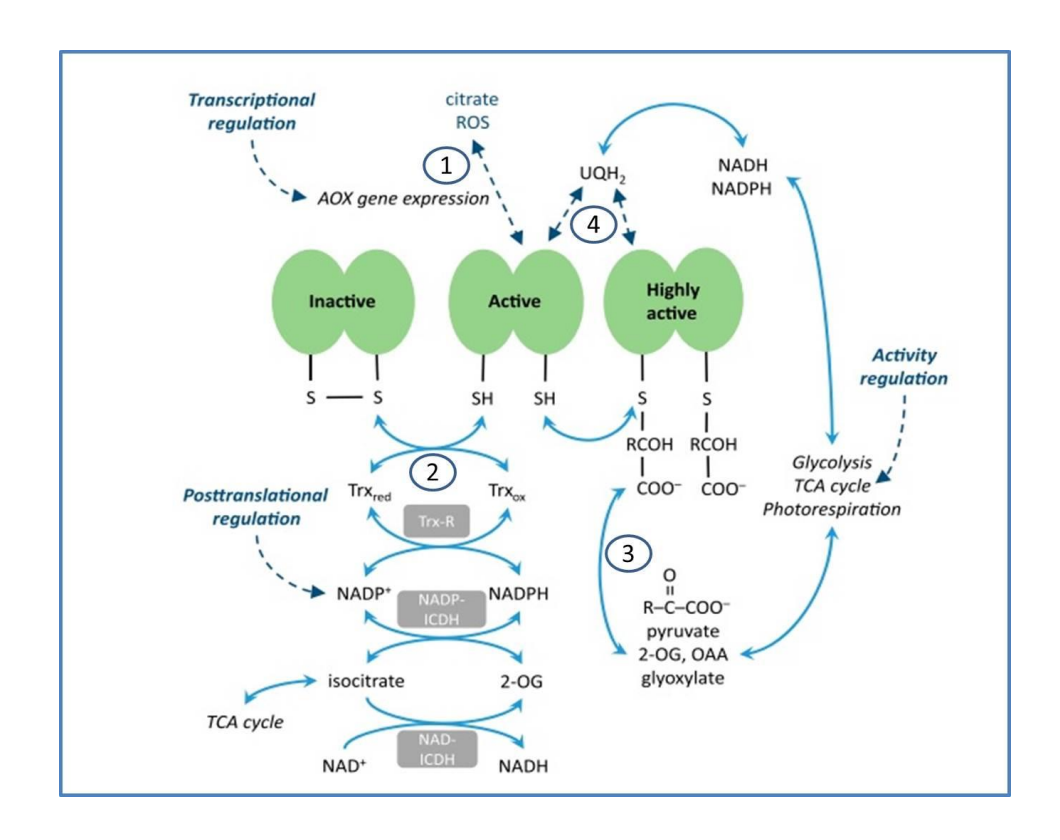


Fig. 1.3. Pictorial representation of the regulation of AOX: (1) biosynthesis of AOX by citrate and ROS levels; (2) posttranslational modification by mitochondrial thioredoxin system; (3) activation of AOX by different metabolites and (4) stimulation of AOX by UQH₂ (adapted from Møller et al., 2020).

damage by ROS and allowing the normal functioning of miETC and maintenance of cellular metabolism (Purvis, 1997; Møller, 2001; Finnegan et al., 2003; Millenaar and Lambers, 2003; Murphy, 2009; Vanlerberghe et al., 2009; Del-Saz et al., 2018). Along with ROS, reactive nitrogen species (RNS) are also generated in mitochondria. The single electrons that are leaked from ETC react with NO₂⁻ and form nitric oxide (NO). The AOX is also known to play a crucial role in reducing RNS levels in mitochondria (Planchet et al., 2005; Gupta et al., 2011, 2012; Cvetkovska and Vanlerberghe, 2012, 2013).

In Arabidopsis, AOXIA is highly induced under different developmental stages as well as under various stress conditions as compared to the other AOX genes, indicating its primary role in stress response. The studies on AOX1A-deficient mutants have shown an increase in ROS generation under different stress conditions in the leaf tissue of A. thaliana (Saisho et al., 1997; Clifton et al., 2006; Giraud et al., 2008; Ho et al., 2008; Strodtkötter et al., 2009; Vishwakarma et al., 2015). In AOX1A deficient A. thaliana, restriction of the COX pathway with antimycin A caused an increase in ROS generation, which in turn caused adverse effects such as apoptosis in the plants (Strodtkötter et al., 2009; Voss et al., 2013; Vishwakarma et al., 2015). Under aluminum phytotoxic conditions, AtAOX1A protected plants from programmed cell death (PCD) by reducing the production of ROS (Liu et al., 2014). Besides, AOX1A over-expressing lines of A. thaliana have shown shoot acclimatization and reduced ROS production under low-temperature treatment. Also, the plants deficient in AOX1A showed acute sensitivity to light, drought, salinity and AA treatment than WT plants (Giraud et al., 2008; Xu et al., 2023). In contrast, overexpression of AtAOX1A induced tolerance to salt (Smith et al., 2009) and hypoxia (Vishwakarma et al., 2018).

The plants lacking AOX were found to be more vulnerable to bacterial pathogens, sucking insects and chewing herbivores as compared to WT plants (Zhang et al., 2012). Furthermore, infection with pathogens caused an increase in AOX transcript as well as protein levels, thereby, AOX respiration in plants, substantiating the importance of AOX in biotic stress tolerance (Liao et al., 2012, 2021; Zhu et al., 2015). Further, as compared to WT Arabidopsis plants, AOX1A over-expressing lines have shown increased rates of Asc levels (Bartoli et al., 2006). The expression of AOX1A is regulated by different mitochondrial retrograde signals under different stress conditions (Rhoads and Subbaiah, 2007; Suzuki et al., 2012).

The important role of AOX in metabolite homeostasis under stress

Under stress conditions, the matrix NADH is found to be high due to the over-reduction of the miETC and it could have a negative feedback effect on the operation of the TCA cycle leading to the accumulation of various organic acid(s), which in turn inhibit different TCA cycle dehydrogenases (Pascal et al., 1990; Tovar-Méndez et al., 2003). When plants experience this situation, the AOX pathway plays a very important role in preventing the over-reduction of the COX pathway by accepting the electrons from the ubiquinol (UQ) pool and thereby reducing the formation of ROS. Plants are frequently exposed to different abiotic and biotic stresses due to their immovable nature. Particularly during environmental stress conditions, optimizing energy metabolism is essential and is managed by coordination between the chloroplast and mitochondria (Raghavendra and Padmasree, 2003; Vanlerberghe et al., 2016; He et al., 2023). The increase in the malate/OAA redox ratio in the matrix leads to the activation of the AOX pathway. Thus, the AOX pathway plays a vital role in the maintenance of the COX pathway by which oxidation of malate and regeneration of OAA

occurs, and this will help in maintaining the oxidized state of ETC carriers of chloroplast and allows optimal photosynthesis (Raghavendra et al., 1994; Padmasree and Raghavendra, 1999b; Raghavendra and Padmasree, 2003; Alber and Vanlerberghe, 2021).

The induction of AOX expression in response to a particular metabolite level was reported earlier, and the level of the metabolite gives key information about the mitochondrial condition. These metabolite levels are very dynamic and their levels may increase or decrease with different stress conditions. For example, the levels of the first TCA cycle metabolite citrate, which acts as a signaling metabolite for the activation of the AOX pathway (Vanlerberghe and McIntosh, 1996), is increased under oxidative stress induced by chlorinated organophosphate esters in *Triticum aestivum* and upon treatment with methyl viologen in *A. thaliana* (Liu et al., 2020; Sipari et al., 2020) and its level is decreased with menadione treatment in suspension cells of *Oryza sativa* and H₂O₂ treatment in heterotrophic cells of Arabidopsis (Ishikawa et al., 2010; Chen et al., 2015).

Besides, the second TCA cycle metabolite 2-oxo-glutarate/ α -keto glutarate (α -KG) is another activator of AtAOX1A (Selinski et al., 2018a, Xu et al., 2021) and its level is known to vary under different stress conditions (**Fig. 1.4**). The α -KG level decreased with menadione treatment (*Oryza sativa* suspension cells and *A. thaliana* roots) methyl viologen treatment (*A. thaliana*) (Ishikawa et al., 2010; Lehmann et al., 2012; Sipari et al., 2020). Further, the levels of succinate increased under menadione treatment (suspension cells of *Oryza sativa*) and H₂O₂ treatment (heterotrophic cells of Arabidopsis) (Ishikawa et al., 2010; Chen et al., 2015) and decreased with menadione treatment (heterotrophic Arabidopsis cell, and *A. thaliana* roots) and methyl viologen (*A. thaliana*) (Baxter et al., 2007; Lehmann et al.,

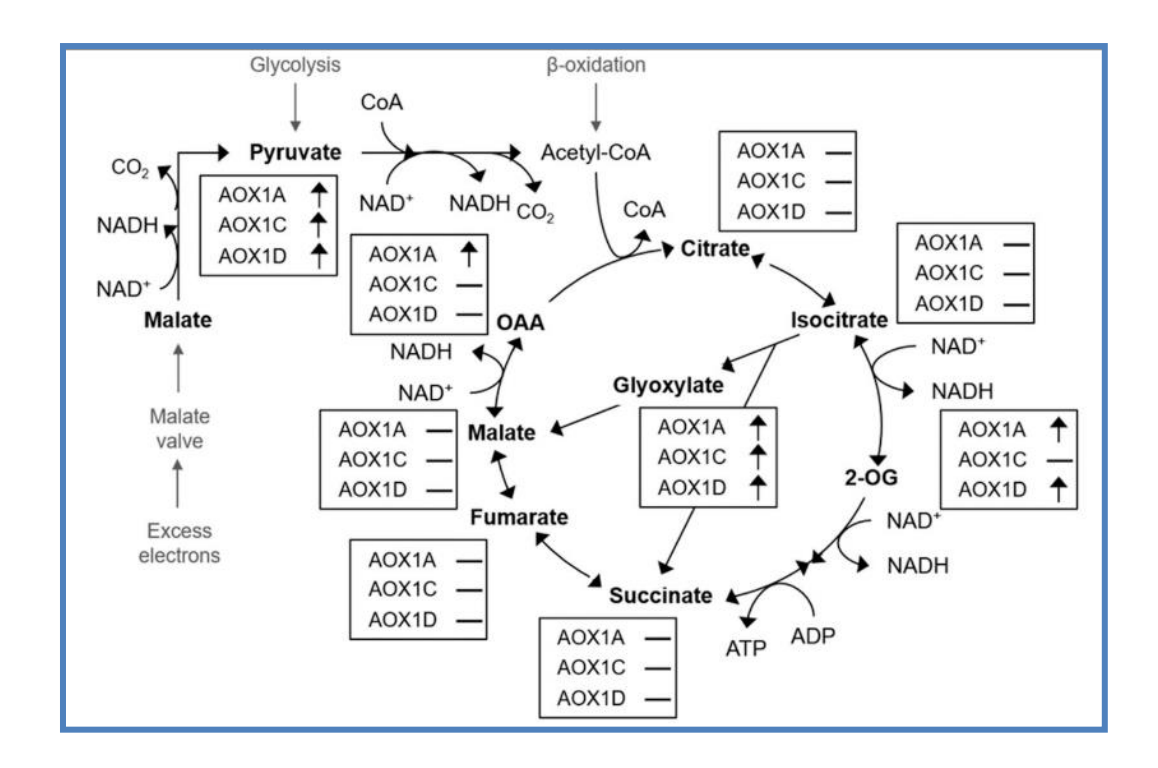


Fig. 1.4. Schematic representation of AtAOX isoforms activation by pyruvate, glyoxylate and TCA cycle metabolites. The activation of AOX isoforms is indicated with up arrows (adapted from Selinski et al., 2018a).

2009; Lehmann et al., 2012; Sipari et al., 2020). Also, the fumarate and malate levels decreased upon treatment with menadione and methyl viologen (Baxter et al., 2007; Ishikawa et al., 2010; Lehmann et al., 2009; Chen et al., 2015; Lehmann et al., 2012; Sipari et al., 2020). However, the malate levels increased oxidative stress induced by chlorinated organophosphate esters and C60 aggregates-induced stress (Du et al., 2017; Liu et al., 2020). In normal plant cells, the levels of malate are higher (60–200 fold) when compared with the levels of OAA. Under light treatment for 10 min, there was a significant increase in malate level (68-77% than the control), and there was a 60% decrease in the OAA levels compared to the control (Padmasree and Raghavendra, 1999b). OAA is also a known activator of AOX1A. Moreover, the metabolites pyruvate and glyoxylate are the well-known key activators of AtAOX1A isoform (Fig. 1.4) (Selinski et al., 2018a; Xu et al., 2021).

Importance of AOX in cellular redox homeostasis

In plants, AOX plays a significant role in cellular redox homeostasis by removing the excess, reducing equivalents and optimizing photosynthesis under oxidative stress. For e.g., a significant increase in the ratio of NADH to NAD⁺ and NADH pool (total amount of NADH) in aox1a mutant was observed upon treatment with AA when compared with the wild-type plants indicating that AOX is important in maintaining the NADH/NAD⁺ ratio, thereby cellular redox levels in the cell (Vishwakarma et al., 2015; Dinakar et al., 2016).

In the plant mitochondria, the well-known mechanism that suppresses excessive ROS is as follows: The superoxide radicals formed in the mitochondria are converted into H_2O_2 and molecular oxygen by the action of the enzyme called Mn superoxide dismutase (MnSOD). This hydrogen peroxide is neutralized by GPX and ascorbate peroxidase (APX)

(Chew et al., 2003; Navrot et al., 2007). Along with this system, alternative NAD(P)H dehydrogenases (NDs) and AOX play an important role in decreasing ROS production (Van Aken et al., 2009). The *A. thaliana* AOX mutant and tobacco suspension cells, which lack AOX, are highly sensitive to high light along with drought and programmed cell death (Robson and Vanlerberghe, 2002; Giraud et al., 2008). Though there are several antioxidant enzymes present in plants, the major benefit of AOX in plants is that it senses a variety of stress signals from different stress conditions and lowers the ROS formation by its activity, which brings metabolic homeostasis and allows normal functioning of ETC, and act as a gauge for programmed cell death (Van Aken et al., 2009).

A reducing environment is essential for the survival of different types of cells and tissues and it is maintained by the coordinated action of various redox metabolite couples such as reduced and oxidized forms of glutathione (GSH-GSSG), ascorbate and dehydroascorbate (AsA-DHA), NAD-NADH and NADP-NADPH (Schafer and Buettner, 2001; 2003). However, the major soluble redox metabolites present in the cells are NAD, NADP, GSH and Asc. These metabolites can act either as independent antioxidant molecules or as a part of redox couple (Noctor, 2006). In plant cells, the various redox couples function not only to equilibrate the redox potential but also to transfer reducing equivalents between cell compartments supporting various metabolic processes such as photosynthesis and respiration (Raghavendra and Padmasree, 2003; Taniguchi and Miyake, 2012; Shiba, 2019).

Among the redox couples, GSH-GSSG is most abundant in a cell and serves to maintain the thiol redox balance in the cytosol as well as in mitochondria (Noctor and Foyer, 1998). In mitochondria, GSH serves as an electron donor for GSH-dependent peroxidases to remove hydroperoxide generated as a by-product in the process of electron transfer to oxygen

(Netto et al., 2002). Besides, Asc is an important antioxidant molecule present abundantly in subcellular compartments of all plants and it plays a crucial role in H₂O₂ detoxification under stress conditions (Smirnoff, 1996; Smirnoff and Wheeler, 2000).

It is well known that the metabolites Asc, GSH and NADPH act as important cofactors for the various enzymes involved in the ascorbate-glutathione cycle. Asc is an important cofactor for ascorbate peroxidase, which is involved in the removal of H₂O₂. In this cycle, monodehydroascorbate (MDHA) and dehydroascorbic acid (DHA) are formed, and a series of reactions occur to recycle the AsA from the MDHA and DHA. Further, the enzyme glutathione reductase reduces GSSG to GSH using NAD(P)H as a co-factor in this cycle (Vanlerberghe et al., 1995; Xiao et al., 2018).

In higher plants, the oxidation of organic acids in the TCA cycle is associated with the reduction of redox metabolite NAD (Noctor, 2006; Igamberdiev and Bykova, 2018; Møller et al., 2020). Besides, the levels of NAD(P) and NAD(P)H are found to be important for the maintenance of cellular redox balance (Møller et al., 2020) since any disproportion in their levels are known to cause different pathological conditions in animals (Ying, 2008; Xiao et al., 2018). Further, in plants, NAD(P)H play a role in the reduction of disulfide bonds present in the homodimer of mitochondrial alternative oxidase (AOX) through the thioredoxin system (Martí et al., 2020; Møller et al., 2020). Also, close coordination between AOX and various redox couples like Asc-DHA, GSH-GSSG, NAD-NADH and NADP-NADPH to maintain cellular redox balance in light and under various abiotic stress conditions was revealed in mesophyll cell protoplast of pea and leaf discs of A. thaliana deficit in AOX (Dinakar et al., 2010a, 2016; Vishwakarma et al., 2014, 2015). Further, higher rates of Asc production were observed in *AOXIA* overexpressed Arabidopsis plants

when compared with the wild-type (WT) plants under high light conditions (Bartoli et al., 2006; Vishwakarma et al., 2014, 2015).

The present study aimed to acquire an adequate amount of AtAOX1A pure protein by expressing it in a routinely used laboratory strain [BL21(DE3)] of *E. coli* and understand its secondary structure and stability toward temperature and pH. Also, the present study intends to examine the interaction of AtAOX1A with well-known inhibitors [salicylhydroxamic acid (SHAM) and n-propyl gallate (n-PG)], activator (pyruvate), TCA cycle metabolites (citrate, α-KG, succinate, fumaric acid, malic acid and OAA) and redox metabolites (GSH, GSSG, AsA, DHA, NAD, NADH, NADP and NADPH) under in vitro conditions by employing surface plasmon resonance (SPR), circular dichroism (CD), fluorescence spectroscopy and molecular docking studies.

Chapter 2

Scope, Rationale, Objectives and Design of the Study

Scope of the present Study

The conventional cyanide-sensitive cytochrome oxidase (COX) pathway is found in the mitochondria of all eukaryotes. In addition to this, an alternative oxidase (AOX) pathway that is insensitive to cyanide is found in plants, fungi, some protists, a few bacteria and some animal species. The AOX pathway bifurcates from the COX pathway at ubiquinone (Vanlerberghe and McIntosh, 1997; McDonald et al., 2009; Dunn, 2023). The AOX pathway was identified during the thermogenic respiration studies on Arum lilies (Meeuse, 1975). AOX is a membrane-bound ubiquinol oxidase present in the inner membrane of mitochondria between ubiquinone and complex III of the electron transport chain toward the mitochondrial matrix (Rasmusson and Møller, 1990; Moore et al., 2013). AOX is involved in a non-phosphorylating mechanism of electron transport from ubiquinone to molecular oxygen, while excess energy is dissipated as heat (Wagner and Moore, 1997; Siedow and Umbach, 2000; Millar et al., 2011; Moore et al., 2013). In higher plants, salicylhydroxamic acid (SHAM) and n-propyl gallate (n-PG) are frequently used to inhibit the activity of AOX, and, thereby, AOX pathway under both in vitro and in vivo conditions to reveal its physiological function(s) during normal growth, as well as biotic/abiotic stress conditions (Diethelm et al., 1990; Padmasree and Raghavendra, 1999a,b; Yoshida et al., 2006; Giraud et al., 2008; Dinakar et al., 2010; Florez-Sarasa et al., 2011; Zhang et al., 2011).

Plants are often exposed to various biotic and abiotic stresses due to their sessile nature. Under stress conditions like high light intensity, drought, salinity, low/high temperatures, and high levels of greenhouse gasses, AOX plays a significant role in sustaining photosynthesis by maintaining redox, ROS and metabolic homeostasis (Strodtkötter et al., 2009; Vanlerberghe, 2013; Vishwakarma et al., 2015; Dahal and

Vanlerberghe, 2017; Florez-Sarasa et al., 2020). Also, AOX plays a vital role in regulating the cellular redox balance when the cytochrome pathway is over-reduced (or) chemically inhibited (Berthold et al., 2000; Moore et al., 2002; Moore et al., 2013). In many plants, AOX is known to exist as a multi-gene family (Whelan et al., 1996; Saisho et al., 1997). As a result, plants possess different isoforms of the AOX. For example, *A. thaliana* has five AOX genes: *AOXIA-D* and *AOX2* (Considine et al., 2002; Clifton et al., 2006; Costa et al., 2017). These AOX isoforms are non-redundant and posttranslationally activated by α-keto acids in an isoform-specific manner (Carré et al., 2011; Selinski et al., 2016; Selinski et al., 2017; Selinski et al., 2018a; Xu et al., 2021). In the case of *A. thaliana*, AOX1A (AtAOX1A) isoform is fully activated by pyruvate and glyoxylate. The TCA cycle metabolites such as 2-oxoglutarate and oxaloacetate are also known to activate AtAOX1A. Contrarily, the isoform AOX1D is activated by 2-oxoglutarate but not by oxaloacetate. However, neither oxaloacetate nor 2-oxoglutarate has shown any effect on AOX1C (Selinski et al., 2018a; Xu et al., 2021).

Upon chemical restriction of the COX pathway, the aox1a mutants of *A. thaliana* have shown increased ROS, lipid peroxidation and disturbance in cellular redox couples such as NAD(P)H and ascorbate, compared to the WT, which shows the importance of AtAOX1A in cellular redox homeostasis under stress (Vishwakarma et al., 2014, 2015). Most of the mitochondrial enzymes that are involved in metabolism are regulated by posttranslational modification (Bykova et al., 2003, Balmer et al., 2004, König et al., 2014, Salvato et al., 2014, Nietzel et al., 2020) and the redox metabolites are known to play an important role in the posttranslational modifications of matrix proteins (Millar et al., 2019; Møller et al., 2020). The information on structural stability and interaction of AtAOX1A with cellular

metabolites is limited and this information is essential to understand the role of AOX in maintaining cellular metabolite and redox homeostasis under biotic/abiotic stress in plants.

Rationale of the study

The model plant *A. thaliana* has different types of AOX genes (*AOX1A-D* and *AOX2*). Among these, *AOX1A* is highly expressed in leaves under most of the given stresses (Clifton et al., 2006; Vishwakarma et al., 2014, 2015). Therefore, in the present study, it is envisaged to examine the structural and biophysical characteristics of AOX1A from *A. thaliana*. To achieve this goal, a large amount of purified AtAOX1A is required and it is difficult to get a sufficient amount of purified native protein from the plant source.

Moreover, metabolite-specific activation of AOX isoforms is reported, which indicates that the demand for AOX-dependent respiration in a particular cell is reflected by the accumulation of specific metabolites (TCA cycle/redox) under different growth and/or stress conditions. Although the secondary structure of AOX from *Sauromatum guttatum* (a thermogenic plant) and *Trypanosoma brucei* (a human pathogen) is reported (Kido et al., 2010; Elliot et al., 2014), no structural data are available for the AOX from non-thermogenic plants. So far, neither binding pocket(s) for these metabolites on AtAOX1A nor structural/conformational changes that occur concurrently in AtAOX1A upon binding with inhibitors and activators/metabolites is revealed in the literature.

Also, the following questions are intriguing to fill the knowledge gap existing in the literature on AOX related to plant species:

1. Do the general laboratory strain like *E. coli* BL21(DE3) suitable to over-express functionally active recombinant AOX1A protein

- 2. Does AOX1A from the non-thermogenic plants show enzyme activity similar to that of *Trypanosoma brucei* AOX (TAO) and *Sauromatum guttatum* AOX (SgAOX)
- 3. What are the secondary structural components of AOX1A
- 4. What are the binding sites of inhibitors and activators on AOX1A, and whether they cause any changes in the protein structure upon binding
- 5. Whether AOX1A interact with the TCA cycle and redox metabolites? If so, do they cause any change in the protein structure upon interaction

Based on the rationale and research gap described above, the following objectives were framed in the present study.

Objectives of the present study

- 1. Cloning, expression and purification of functionally active recombinant *Arabidopsis* thaliana AOX1A (rAtAOX1A) from *E. coli* BL21(DE3)
- 2. Structural and biophysical characterization of rAtAOX1A with its inhibitors
- Interaction of rAtAOX1A with pyruvate, TCA cycle and Redox metabolites using docking and biophysical studies

The rationale for using model plant 'A. thaliana' and E. coli BL21(DE3) cells in the present study

A. thaliana is a familiar model plant because of its unique features: Small flowering plant with a short life cycle, self-fertilization, small in size (20 cm tall), small genome size (157 Mb), completely sequenced, diploid genome and can grow without any seasonal hindrance throughout the year under laboratory conditions. AOXIA is the most stress-responsive gene

among all the AOX gene members and amongst the hundreds of known mitochondrial protein-coding genes of *A. thaliana* (Saisho et al., 1997; Clifton et al., 2006). The isoform AOX1A from *A. thaliana* is selected for this study.

A. thaliana (WT-Columbia) leaves (10 weeks old) are used for total RNA extraction and this total RNA is used for complementary DNA (cDNA) synthesis. The cDNA of AtAOX1A coding for mature protein was amplified and cloned into the pET28a(+) vector. The pAtAOX1A construct was transformed into BL21(DE3) cells for functional expression and purification of functionally active rAtAOX1A for further characterization. The pET system has a lacUV5 promoter that directs transcription of the T7 RNA polymerase gene upon induction with isopropyl-β-D-thiogalactopyranoside (IPTG). The addition of IPTG to a growing E. coli culture induces T7 RNA polymerase, which in turn transcribes the target DNA in the plasmid. BL21(DE3) cells are the expression strains, hence used to express rAtAOX1A in the present study.

The ETC components located in the inner membrane of *E. coli* possess two terminal oxidases, viz., 'cytochrome oxidase *bo*' and 'cytochrome oxidase *bd*,' to reduce molecular oxygen to water molecules and oxidize UQH₂ (Kita et al., 1984a; Anraku and Gennis, 1987; Mogi et al., 1994; Yap et al., 2010; Borisov et al., 2011). Cytochrome oxidase *bo*, which possesses heme-copper oxidase, shares functional similarities with mitochondrial COX of higher plants and is expressed during high oxygen concentrations. In contrast, cytochrome *bd* oxidase, which lacks both copper ion and the Fe–S cluster, is known to predominate in anoxic conditions and is not homologous to any other terminal oxidases, such as heme-copper oxidoreductases or AOX (Reid and Ingledew, 1979; Kita et al., 1984b; Poole and Cook, 2000; Borisov et al., 2011). The properties of both these oxidases (*bo* and *bd*) are quite

distinct from the AOX, which contains a non-heme diiron carboxylate center (Berthold et al., 2002; Berthold and Stenmark, 2003; Moore et al., 2008, 2013).

Design of the present study

Therefore, in this study, BL21(DE3) *E. coli* strain was chosen to examine in vivo functional expression of pAtAOX1A and robust expression of rAtAOX1A protein for purification and in vitro characterization. Further, the purified rAtAOX1A is used to study its structure and molecular interaction with different AOX inhibitors and cellular (pyruvate, TCA cycle and redox) metabolites using SPR, CD, fluorescence spectroscopy and in silico molecular docking techniques.

Chapter 3Materials and methods

Materials and methods

3.1. E. coli strains

The *E. coli* strain DH5α was used to maintain the clone, while the strain BL21(DE3) (InvitrogenTM, Waltham, MA, USA) was used for the expression of recombinant protein (rAtAOX1A), which has a His₆-tag on it. The strain *E. coli* DH5α is a genetically engineered bacteria with inactive recombinase, which is generally used for the transformation of plasmid vectors. The BL21(DE3) *E. coli* strains are used for the expression of recombinant proteins. These strains lack the *E. coli* protease inhibitors so that the expressed protein may not get degraded. The BL21(DE3) strain is generated from the BL21 strain by inserting the lambda phage genome called DE3. The lacUV5 promoter, which controls the T7 RNA polymerase gene, is arranged on this phase genome DE3 in BL21(DE3) cells.

3.2. pET system and protein induction mechanism

The pET system is a plasmid DNA vector and it is a very useful tool for recombinant protein expression in *E. coli*. The vector plasmid with *AtAOX1A* (pAtAOX1A) was constructed as described in Vishwakarma et al. (2016) and the confirmed clone was used for the expression of rAtAOX1A.

a) pET28a(+) vector

The pET28a(+) system offers the advantages of the controlled expression of recombinant protein and its purification with ease. The pET28a(+) vector contains genes encoding for T7 lac promoter, N-terminal 6-His tag, kanamycin resistance and thrombin cleavage site (**Fig.** 3.1). The recombinant protein expression is regulated by the induction with IPTG.

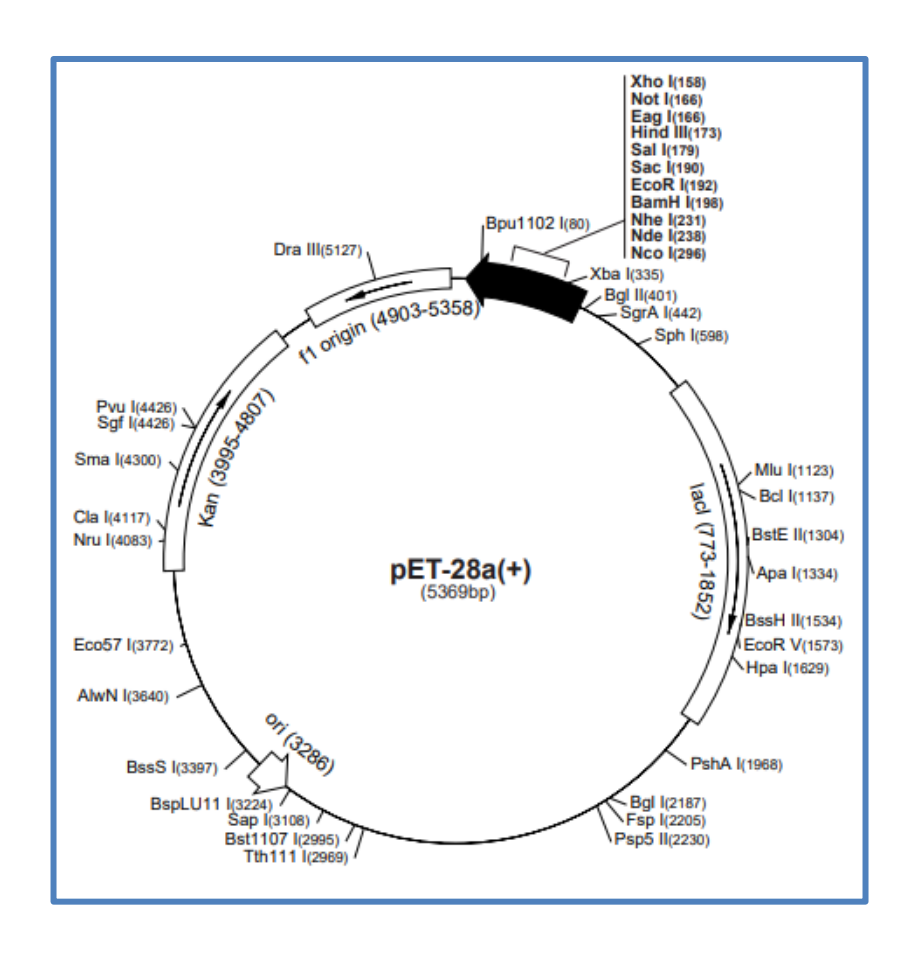


Fig. 3.1. pET28a(+) vector map (adapted from Novagen)

b) Recombinant protein synthesis mechanism in E. coli

The *AtAOXIA* is cloned into the pET28a(+) vector downstream of the T7 promoter and transformed into *E. coli* BL21(DE3). The most popular method for synthesizing the recombinant protein in *E. coli* is the T7 RNA polymerase system. The addition of IPTG causes the expression of T7 RNA polymerase in *E. coli*. The synthesized T7 RNA polymerase binds to the T7 promoter present in the pET vector in the presence of IPTG and initiates the transcription of the gene of interest (*AtAOXIA*). After transcription, endogenous protein translation machinery synthesizes the desired protein (**Fig. 3.2**).

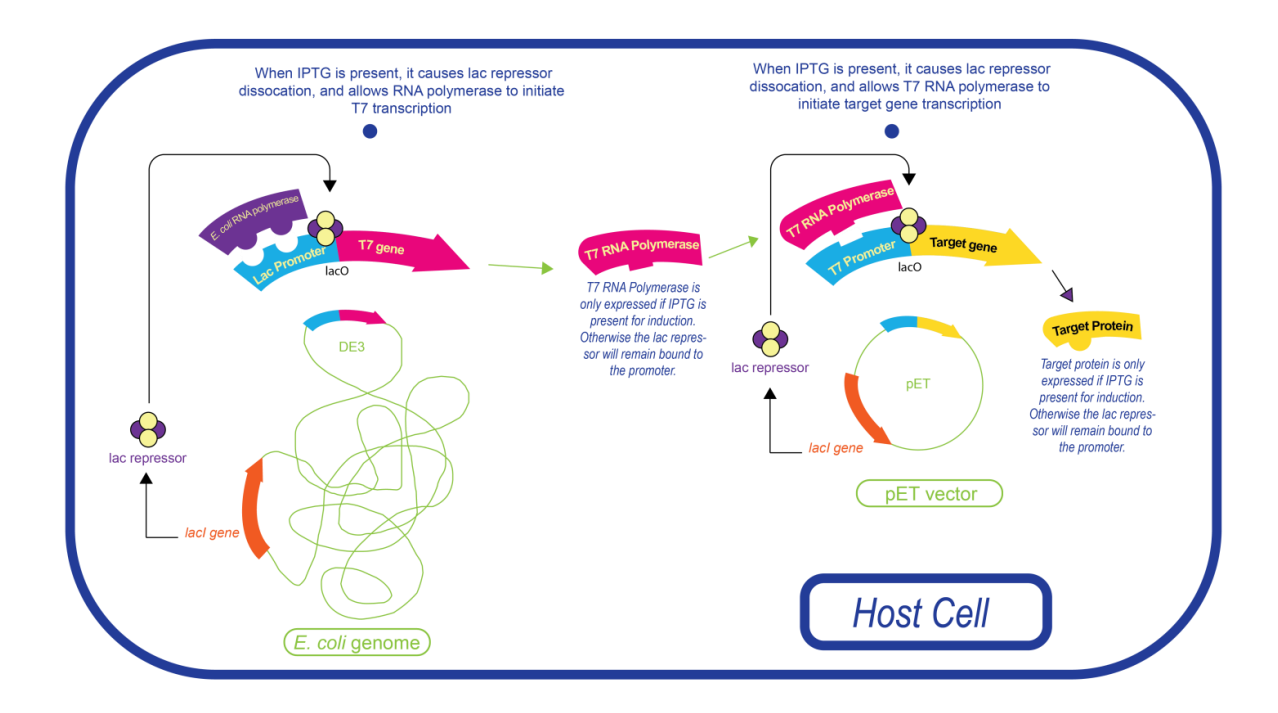


Fig. 3.2. Recombinant protein synthesis in *E. coli*. The mechanism of recombinant protein synthesis in *E. coli* cells is shown in the figure, where IPTG induces the T7 RNA polymerase synthesis and this polymerase starts synthesizing the gene of interest (Adapted from Louis, 2019).

3.3. E. coli cell growth measurement

The *E. coli* strain BL21(DE3) cells transformed with pET28a (*E. coli*/pET28a) and recombinant pET28a with AtAOX1A (*E. coli*/pAtAOX1A) were inoculated into 3 ml of LB medium containing 50 μg/ml of kanamycin and incubated overnight at 37°C (pre-culture). The pre-culture was inoculated into 20 ml of LB medium with 50μg/ml of kanamycin and allowed to grow. As the OD₆₀₀ of the culture reached 0.15, IPTG (0.1 mM) was added to the culture medium to induce rAtAOX1A. To ascertain the functions of rAtAOX1A in promoting the *E. coli* growth cultures were treated with each of the following mitochondrial inhibitors at a wider range of concentrations: 0.05–1 mM KCN (inhibitor of COX pathway), 0.025–0.5 mM n-PG and 0.5–2 mM SHAM (inhibitors of AOX pathway). Subsequently, both control

(*E. coli*/pET28a) and transformed (*E. coli*/pAtAOX1A) cells were incubated for 5 h at 37°C, and OD₆₀₀ was monitored at regular intervals of 30 min (Kumar and Söll, 1992; Berthold, 1998; Fukai et al., 1999).

3.4. Assay of cell respiration

After induction of rAtAOX1A with IPTG as described above, $E.\ coli$ cells were extracted and suspended in a suitable volume of LB medium to achieve a cell density of 20 at OD₆₀₀. The cellular respiration of both $E.\ coli/pET28a$ and $E.\ coli/pAtAOX1A$ were measured in terms of rates of oxygen consumption with or without the addition of KCN, n-PG, and SHAM. Respiration rates were measured with a total of 4.8×10^8 cells/ml for each reaction (As the 1.0 OD₆₀₀ of the $E.\ coli$ cells is equal to 8×10^8 cells/ml, the culture was diluted so as to get the required cell number) using the Clark-type oxygen electrode (Kirimura et al., 1999; Ajayi et al., 2002; Oxygraph plus, Hansatech instruments, UK).

3.5. Purification of rAtAOX1A from E. coli/pAtAOX1A

Since AOX is a membrane-bound protein, it is possible that rAtAOX1A expressed in recombinant *E. coli* cells is targeted to the *E. coli* membranes. The following protocol is applied to purify the rAtAOX1A from *E. coli*/pAtAOX1A. Purification of rAtAOX1A was done according to Kido et al. (2010) and Elliott et al. (2014), with minor modifications (**Fig. 3.3**).

(a) Preparation of *E. coli/pAtAOX1A* membrane sample

The *E. coli* carrying recombinant AtAOX1A was pre-cultured overnight at 37°C in 10 ml of LB medium containing 50 µg/ml of kanamycin. About 5 ml of pre-culture was inoculated into

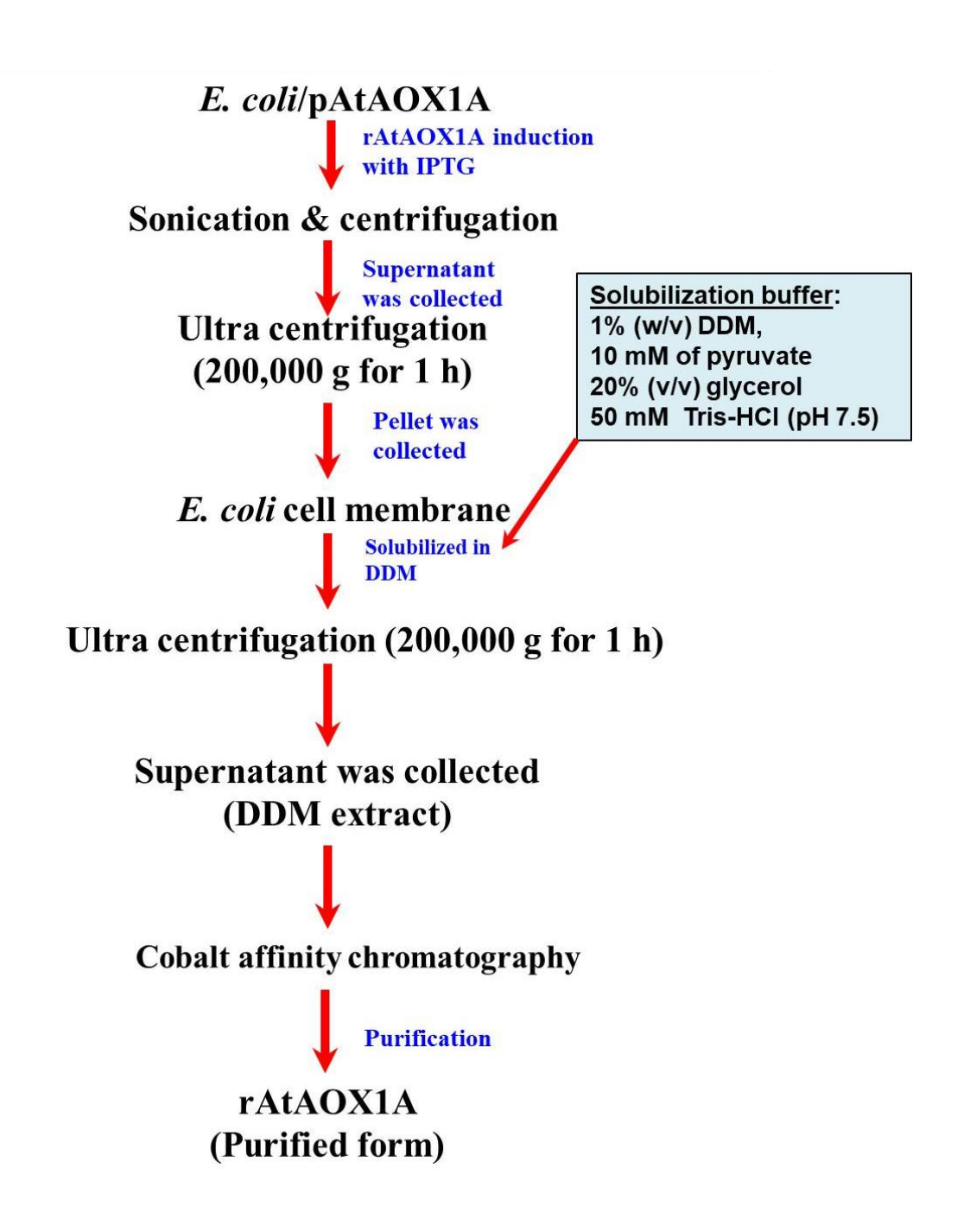


Fig. 3.3. Flow chart. Procedure for the purification of rAtAOX1A from *E. coli*/pAtAOX1A membranes by using affinity chromatography.

500 ml of LB medium containing 50 μg/ml kanamycin and grown at 37°C with 200 rpm. The culture was allowed to grow until OD₆₀₀ reached 0.4 and 0.1 mM IPTG and 0.1 mM ferrous sulfate was added to induce the expression of rAtAOX1A. Subsequently, the culture was allowed to grow at 28°C for 4 h, and cells were harvested by centrifugation at 5,000 rpm for 10 min at 4°C. The pellet obtained was resuspended in 50 mM Tris-HCl containing 10 mM pyruvate at pH 7.5. *E. coli* cells were lysed by sonication with an amplitude of 35 for 20 min by switching on/off of the probe at regular intervals of 30 s each, in the presence of a protease inhibitor cocktail and 1 mM phenylmethylsulfonyl fluoride (PMSF). After lysis, cell debris was removed in a single step by centrifugation at 12,000 g for 30 min. The supernatant was centrifuged at 200,000 g for 1 h at 4°C to separate cytoplasm from membrane fraction. The membrane pellet was resuspended in a minimal volume of 50 mM Tris-HCl (pH 7.5) containing 10 mM of pyruvate.

(b) Solubilization of rAtAOX1A from E. coli membranes

The solubilization (10 ml) buffer, which contains 1% (w/v) n-dodecyl-β-D-maltopyranoside (DDM) in 50 mM of Tris-HCl, along with 10 mM of pyruvate and 20% (v/v) glycerol at pH 7.5, was used to solubilize the membrane fraction obtained from *E. coli*/pAtAOX1A as described above. The buffer was added dropwise with gentle mixing and immediately centrifuged for 2 h at 200,000 g. All the steps were performed at 4°C. The supernatant enriched in rAtAOX1A is labeled as DDM extract.

(c) Affinity chromatography

The cobalt resin (selective for His-tag) was equilibrated with an equilibration buffer at a 1:3 ratio for 1 h. The equilibration buffer contained 0.5% (w/v) DDM and 0.5% (w/v) n-octyl- β -D-

glucopyranoside (OG) in 50 mM of Tris-HCl (pH 7.5), along with 10 mM of pyruvate, 20% (v/v) glycerol and 100 mM of MgSO₄. After equilibration, 10 ml of DDM extract was added to the resin and allowed to mix gently overnight at 4°C. Further, the resin, which is bound with rAtAOX1A, was washed with 10 ml of wash buffer, which contained 0.5% (w/v) DDM and 0.5% (w/v) OG in 50 mM Tris-HCl (pH 7.5), along with 10 mM of pyruvate, 20% (v/v) glycerol, 100 mM MgSO₄ and 50 mM of imidazole. Subsequently, the resin was transferred onto a column and rAtAOX1A was eluted as 1-ml fractions using elution buffer, which contained 0.5% (w/v) DDM and 0.5% (w/v) OG in 50 mM of Tris-HCl (pH 7.5) along with 10 mM of pyruvate, 250 mM of imidazole, 20% (v/v) glycerol and 100 mM of MgSO₄ at pH 7.5. Protein purification was visualized on 12.5% SDS-PAGE under reducing conditions.

3.6. SDS-PAGE

The *E. coli* cells were pelleted after suspending in 50 mM of Tris-HCl (pH 7.5) and protein estimation was done by a BCA protein estimation kit. Similarly, purified rAtAOX1A was estimated and separated by SDS-PAGE according to Laemmli (1970) using standard/mini gels.

a) Buffers and chemicals used for SDS-PAGE

The SDS-PAGE resolving gel was prepared by using the following buffers and chemicals: 12.5% acrylamide, 0.375M Tris-HCl (pH 8.8), 0.1% SDS (w/v), 0.05% ammonium persulfate (APS) and 0.01 % N,N,N',N-tetramethyl ethylenediamine (TEMED). The stacking gel was made of 4% acrylamide, 0.125M Tris-HCl (pH 6.8), 0.1% SDS (w/v), 0.04% APS and TEMED. The protein sample was added with the sample buffer containing 0.250M Tris-HCl (pH 6.8), 8% (w/v) SDS, 50% (v/v) glycerol, 10% (v/v) β-mercaptoethanol and 0.04%

(w/v) bromophenol blue, and boiled at 100°C for 3-5 min. The *E. coli* pellets/protein samples were stored at -80°C until loaded onto the gel. The electrophoresis was performed initially at 80V (until the dye moved into the resolving gel) and then shifted to 120V. Power was supplied through Amersham Biosciences Electrophoresis Power Supply EPS-601 units. The gels were visualized by the coomassie brilliant blue staining method.

b) Gel staining: Coomassie Brilliant Blue (CBB)

For staining the SDS-PAGE gel, the CBB staining solution composed of CBB R250 (0.1%) dissolved in methanol, acetic acid and distilled water in a 40:10:50 ratio at room temperature was prepared and kept under stirring for 5-6 hrs. Further, this solution was filtered using Whatman No.1 filter paper. Then the SDS-PAGE gel was stained by adding the CBB stain and kept overnight under gentle shaking. The excess stain was removed by the destaining solution composed of methanol, acetic acid and water in a 40:10:50 ratio under gentle shaking until the protein bands were visible clearly.

3.7. Western Blot

The purity of rAtAOX1A was examined using the western blot. Approximately 30 µg of total protein was loaded onto each well and performed SDS-PAGE to detect rAtAOX1A. In the present study, we used a polyvinylidene difluoride (PVDF) membrane for blotting. The membrane was cut according to the size of the SDS-PAGE gel and placed in 100% methanol for 5 min under shaking. After that, the methanol was discarded and distilled water was added to the membrane and kept for shaking for 5 min. Then the membrane was transferred to a transfer buffer composed of 25 mM Tris-HCl (pH 8.3), 192 mM glycine and methanol 20% (v/v). The PVDF membrane was laid on the gel carefully without any air

bubbles in between the membrane and the gel. The gel and the membrane were kept in between two layers of Whatman No. 3 chromatography papers, like a sandwich. Further, on either side of the Whatman No. 3 chromatography papers, a single layer of a sponge was placed. This entire sandwich was placed in the western blot unit cassette (Amersham Biosciences, Hoefer mini vertical electrophoresis system) and connected to a power pack (Amersham Biosciences Electrophoresis Power Supply EPS-601). A power supply of 30V was given for 8-10 hrs at 4°C. The proteins were electrophoretically transferred from the gel to PVDF membranes (Towbin et al., 1979). Further, to saturate the non-specific binding sites on the membrane, the PVDF membrane was blocked with blocking buffer [5% (w/v) nonfat milk powder in Tris-Buffered Saline (TBS) containing 25 mM Tris-HCl pH 7.5 and 150 mM NaCl] for 1 hr with constant shaking at room temperature. After blocking, the PVDF membrane was incubated at 4°C with a mouse monoclonal anti-His antibody (1:5,000 dilution) for 5-6 h, which is conjugated with horseradish peroxidase (Cell signaling technology). The blot was washed with tris buffered saline containing 0.2% of tween 20 (TBST) 3 times (3 x 15 min). The blot was developed using Enhanced chemiluminescence (ECL) western blotting reagents and rAtAOX1A protein was detected with the help of the ChemiDoc imaging system (BioRad).

3.8. Oxygen uptake activity

The activity of rAtAOX1A was measured polarographically by monitoring the oxygen uptake rates using an S1 Clark-type oxygen electrode (**Fig. 3.4 and 3.5**). The oxygen electrode chamber was first calibrated with air-saturated distilled water according to the manufacturer's instructions (Oxygraph plus, Hansatech Instruments, UK). The activity assay was performed by adding the 0.7 µg of purified protein in 400 µl of air-saturated reaction medium (50 mM of

Tris-HCl, pH 7.5), and the reaction was started by the addition of 600 μ M duroquinol (DQH₂) as a substrate (**Fig. 3.5**). The reduced form of the substrate can only be used for AOX activity. The reduction of Duroquinone (DQ) to DQH₂ was performed in the laboratory (Rich, 1978).

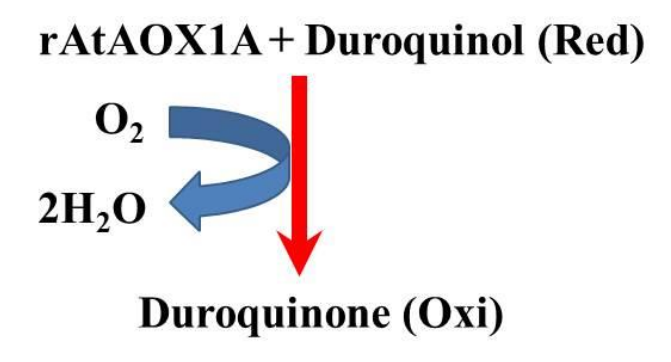


Fig. 3.4. Schematic representation of oxygen uptake activity of AOX purified rAtAOX1A.

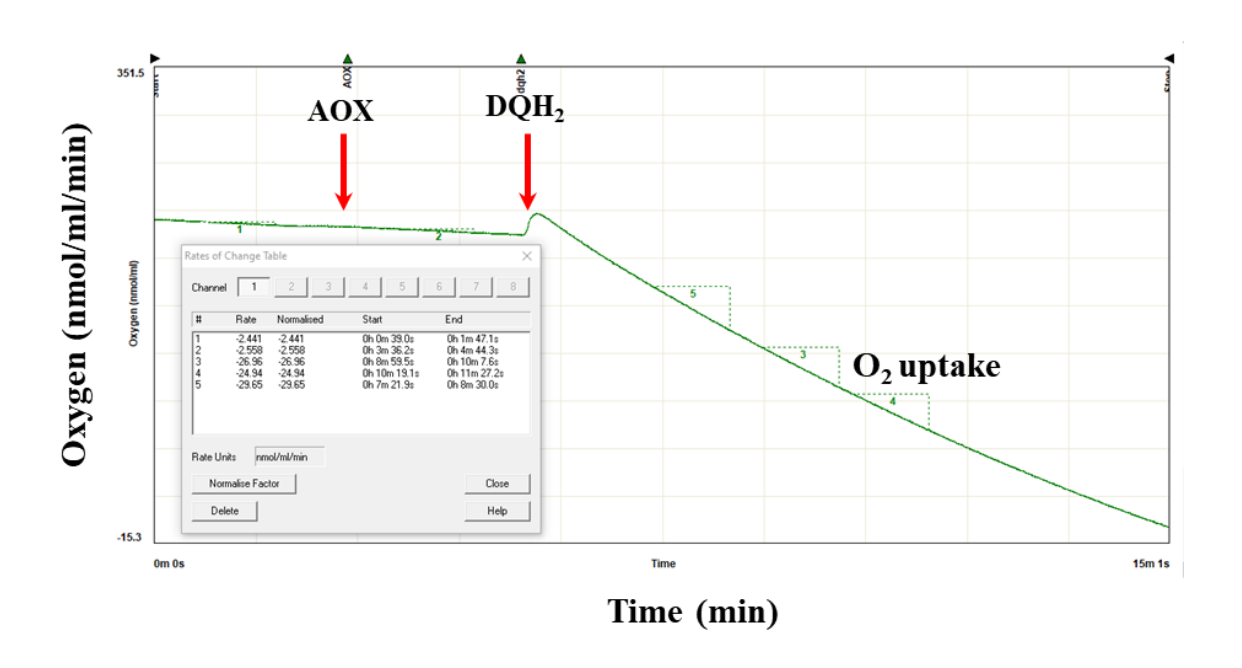


Fig. 3.5. Recording: Oxygen uptake record trace of purified rAtAOX1A upon the addition of duroquinol as substrate using Clark-type O₂ electrode. The addition of enzyme and substrate is indicated in red colored arrows.

3.9. DQH₂ preparation

A 250 mg of duroquinone (DQ) was dissolved in 50 ml diethyl ether which gives a transparent yellow-orange color solution. On the other hand, 1 g of sodium dithionite was dissolved in 50 ml of distilled water. The sodium dithionite solution was added to the DQ solution in a separating funnel and was mixed vigorously for 5 min. Initially, due to the formation of semiduroquinone, the color of the solution increased and then slowly became colorless, which indicates that the DQ is totally reduced to DQH₂. After that, the aqueous phase was discarded slowly so that only the upper ethereal layer was present in the separating funnel. This colorless solution is further shaken with another 50 ml of sodium dithionite solution to reduce any residual DQ. The aqueous solution was removed from the ethereal layer. This ethereal layer was washed with 100 ml of saturated sodium chloride solution to remove any excess water. The ethereal layer, which contains duroquinol, was passed through anhydrous sodium sulfate powder (30g) in a sintered glass funnel. The ethereal solution was dried down in order to remove water by vacuum desiccation at 25°C. White duroquinol powder obtained after vacuum desiccation is stored in eppendorf tubes sealed using parafilm (Alcan) in the dark at room temperature until required (**Fig. 3.6**). The stocks of DQH_2 were prepared on the day of use by suspending the DQH₂ powder in acidified ethanol (96% ethanol, which contained 10 mM HCI). The resuspended DQH₂ stock solution can be stored at -20°C for a few weeks and at -80°C for a few months. The stock concentration of DQH₂ was determined by monitoring the O.D at 283 nm in water using a molar extinction coefficient (2.15 mM⁻¹ cm⁻¹) and cuvette pathlength (1 cm) in a UV-Visible spectrophotometer (Shimadzu UV-1700). The acidified ethanol blank was subtracted from the assay while measuring the oxygen uptake activity (Rich, 1978).

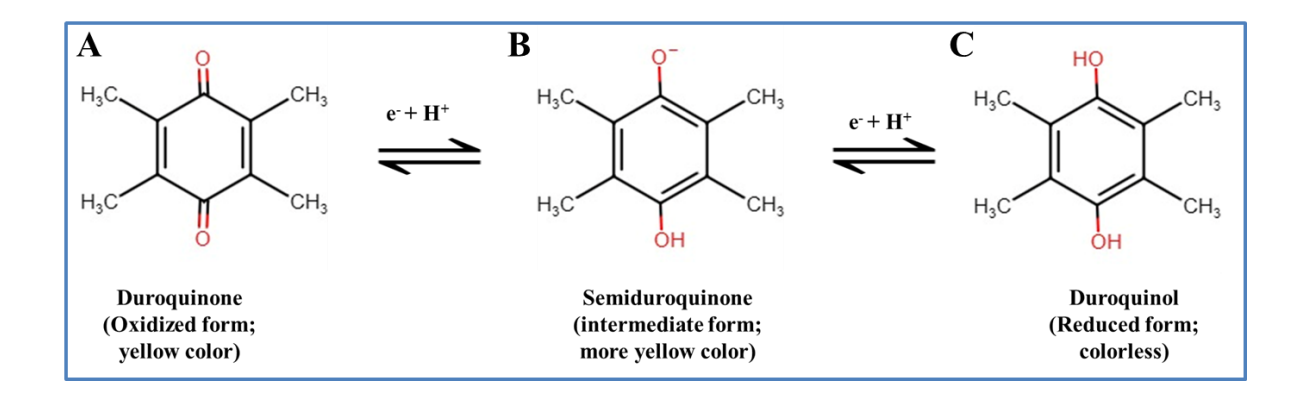


Fig. 3.6. The reduction mechanism and structure of DQ. The reduction is carried out using sodium dithionite, which reduces DQ (**A**) to semiduroquinone (**B**) and DQH₂ (**C**). This DQH₂ is used as a substrate for purified rAtAOX1A. The structures were drawn by using the chemspace online server.

3.10. MALDI TOF/TOF analysis

The purified recombinant protein band was excised with a sharp and sterile scalpel from the gel after performing SDS-PAGE and kept in a 1.5 ml tube. Later, the gel plug was reduced with DTT (10 mM) and alkylated with iodoacetamide (55 mM) before subjecting to digestion with trypsin (12.5 μ g/ μ l). The tryptic-digested protein sample was analyzed by using matrix-assisted laser desorption ionization time-of-flight mass spectrometry (MALDI-TOF MS). The method uses an Autoflex III smart beam instrument (Bruker Daltonics, Bremen, Germany), equipped with a nitrogen laser (355 nm) and operated in a reflection mode for peptide mass and sequencing in the presence of α -cyano4-hydroxycinnamic acid as a matrix, as described by Swathi et al. (2014). The spectra from MALDI-MS and MALDI-MS/MS ionization were searched with the MASCOT search engine. The biotools software (Bruker Daltonics, version 3.1) was used to analyze the lift spectra, while the sequence similarity analysis was performed by the National Center for Biotechnology Information (NCBI) blast tool.

3.11. Dialysis and lyophilization

The purified rAtAOX1A present in the elution buffer described in **section 3.7** was transferred into a 10 mM phosphate buffer (pH 7.5) through the process of step-down dialysis for performing CD, fluorescence and SPR studies. The dialysis buffer composition is described in **Table 3.1**.

Table 3.1 Buffers used for the dialysis of purified rAtAOX1A at a ratio of 10:500 (sample volume to buffer volume). The protein sample was dialyzed in each buffer for a period of 4 h at 4°C under continuous stirring.

S.No	Dialysis buffer	Composition
1	Buffer 1	20 mM Tris-HCl (pH 7.5), 10 mM of pyruvate,
		0.03% of DDM and 10% of Glycerol
2	Buffer 2	10 mM of phosphate buffer (pH 7.5) containing
		0.03% of DDM and 1% of glycerol
3	Buffer 3	10 mM of phosphate buffer (pH 7.5)

Further, the dialyzed protein present in 10 mM phosphate buffer (pH 7.5) was transferred into 50 ml falcon tubes and frozen in liquid nitrogen for 15 min. Then the sample is allowed for lyophilization for 10-12 hrs based on the sample volume until we get around 1 ml. The concentration of the protein in the solution was measured by the BCA protein estimation kit and used for further analysis.

3.12. Circular dichroism (CD) and thermal stability studies

The CD spectrophotometer (Jasco J-1500, Japan) coupled with a thermostat was used to analyze purified rAtAOX1A (0.8 mg/ml). The parameters used for the CD scan were as follows: wavelength, 190 to 260 nm; speed, 50 nm/min; step resolution, 1 nm; bandwidth, 1

nm; response, 3 s; temperature, 25°C, and sensitivity, 50 mdegrees. Similarly, the secondary structural stability of rAtAOX1A at different pH, from 2 to 12, was determined after incubating rAtAOX1A in different buffers [5 mM Glycine-HCl (pH 2), 10 mM sodium phosphate (pH 7.5) control sample and 5 mM Glycine-NaOH (pH 10-12)] at 37°C for 1 h. Conversely, for the temperature melting studies, the parameters used were as follows: wavelength, 190 to 260 nm; response, 1 s; temperature, 4 to 90°C; speed, 50 nm/min; and sensitivity, 50 mdegrees (Kelly et al., 2005; Elliott et al., 2014). Furthermore, different concentrations (0.05, 0.1, and 0.5 mM) of SHAM and n-PG were added separately to 0.4 mg/ml of purified rAtAOX1A to analyze the changes induced in the secondary structure of rAtAOX1A during its interaction with the inhibitors. Similarly, different concentrations of AOX activator (pyruvate), TCA cycle metabolites (citrate, α-KG, succinate, fumaric acid, malic acid and OAA) and redox metabolites (GSH, GSSG, AsA, DHA, NAD, NADH, NADP and NADPH) were added to 0.4 mg/ml of purified rAtAOX1A to study the changes induced in the secondary structure of rAtAOX1A during its interaction with these metabolites. The changes in secondary structural elements of rAtAOX1A upon interaction were analyzed by submitting the raw CD data to the Dichroweb online server (Whitmore and Wallace, 2008) using the CDSSTR algorithm with a reference set 4 (Sreerama and Woody, 2000). The final CD spectrum of each concentration represented is an average of four to five scans.

3.13. Fluorescence spectroscopic studies

The changes in the conformation of protein upon interacting with the ligand can be studied conveniently using fluorescence spectroscopy. The changes in the fluorescence intensity of tryptophan residues present in the protein reflect the changes in the tertiary structural conformation (Lakowicz, 2006). The fluorescence spectroscopy was used to better

understand the effects of microenvironmental changes on fluorophore residues during the interaction of purified rAtAOX1A (10 μM) with different concentrations of AOX inhibitors (SHAM and n-PG), activator (pyruvate), TCA cycle metabolites (citrate, α-KG, succinate, fumaric acid, malic acid and OAA) and redox metabolites (GSH, GSSG, AsA, DHA, NAD, NADH, NADP and NADPH). The AtAOX1A protein contains nine Trp residues at 108, 123, 125, 131, 158, 165, 211, 237, and 305 positions (**Fig. 3.7**). The emission spectra fluorescence was recorded using a fluorescence spectrofluorometer (Jasco FP-8500, Japan) fitted with a thermostatic bath. A Quartz cell with a path length of 1.0 cm was used and the spectra were observed at 25°C. Excitation at 295 nm was used to determine the emission spectra of various metabolites with rAtAOX1A, and the emissions were evaluated in the wavelength range of 300 to 450 nm. Sigma plot version 12.0 was used to plot the experimental data. The final fluorescence emission spectrum of each concentration represented is an average of four to five scans.

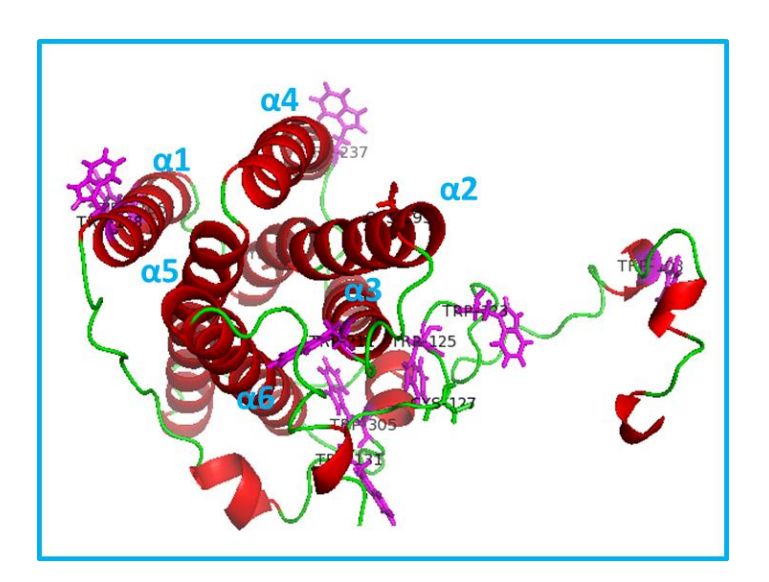


Fig. 3.7. The figure represents the AtAOX1A model of Pennisi et al. (2016), which is visualized by the PyMOL tool. The tryptophan residues present in the protein structure are indicated in pink color.

3.14. Surface plasmon resonance (SPR) studies

SPR (Biacore T200) is used for measuring interactions between immobilized ligand on the special gold-coated chip surface and biomolecules or drugs with high accuracy and is label-free. The purified rAtAOX1A protein sample was dialyzed into a 10 mM phosphate buffer (pH 7.5) by the step-down dialysis procedure and concentrated by lyophilization (See section 3.13). The Biacore T200 SPR, sample flow and light path, and the sensorgram are shown in **Fig. 3.8.**

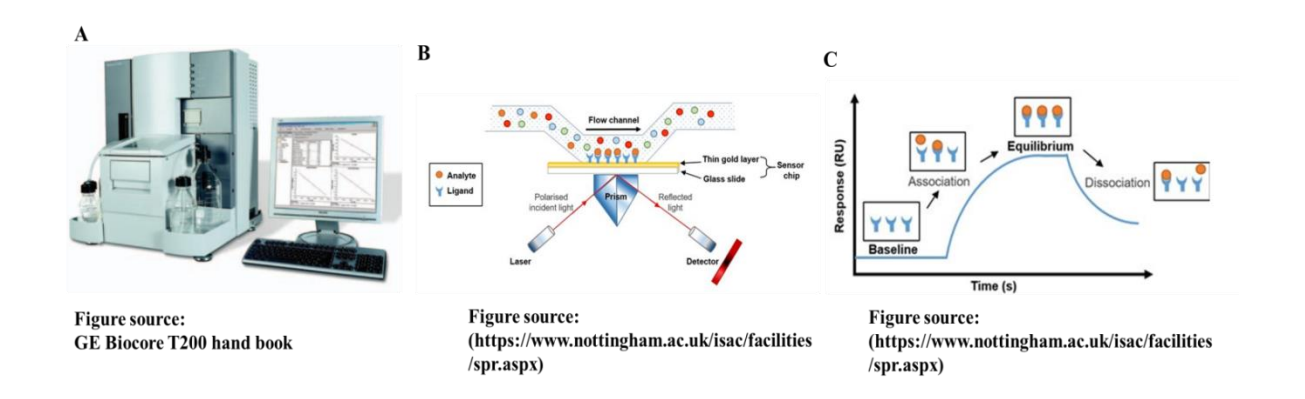


Fig. 3.8. Overview of SPR analysis. A) Biocore T200 system; B) SPR setup, indicating the sample flow and light path; C) Sensorgram showing different phases of interaction like association, equilibrium and dissociation.

a) Immobilization of the rAtAOX1A on the CM5 sensor chip

The following steps are performed to immobilize the rAtAOX1A on the CM5 sensor chip as shown in **Fig. 3.9**: (i) a mixture of 40 mM of 1-ethyl3-(3-dimethylaminopropyl) carbodiimide (EDC) and 10 mM of N-hydroxysuccinimide (NHS) are passed through the reference (blank) flow cell (Fc-3), as well as the sample flow cell (Fc-4) of CM5 sensor chip at a flow rate of 30 µl/min for 300 s, to generate reactive succinimide esters; (ii) the rAtAOX1A (100µg/ml)

prepared in sodium acetate buffer (pH 5) was injected into the activated flow cell (Fc-4), where the NHS esters spontaneously react with uncharged amino groups of rAtAOX1A (ligand) and covalently link it to the dextran matrix; (iii) the residual active NHS esters in Fc-4 are blocked by passing 1 M of ethanolamine-HCl (pH 8.5) for 300 s, at a flow rate of 30 µl/min; (iv) all the active NHS esters of the reference (blank) flow cell (Fc-3), which is devoid of rAtAOX1A are blocked with ethanolamine-HCl (pH 8.5). The immobilization of rAtAOX1A is confirmed by the increase in the RU of FC-4 (**Fig. 3.10**).

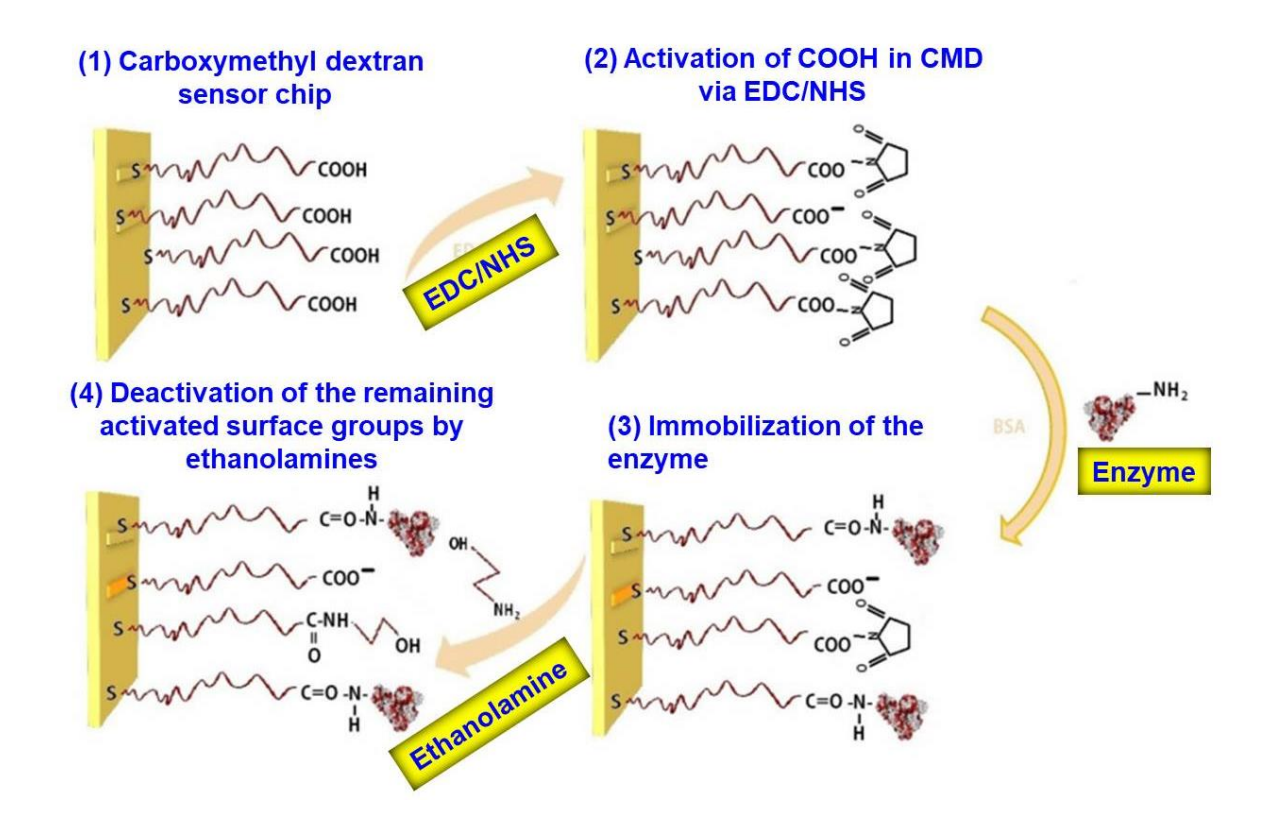


Fig. 3.9. The mechanism of immobilization of purified rAtAOX1A on to CM5 sensor chip (Adapted from Sharifi et al., 2017).

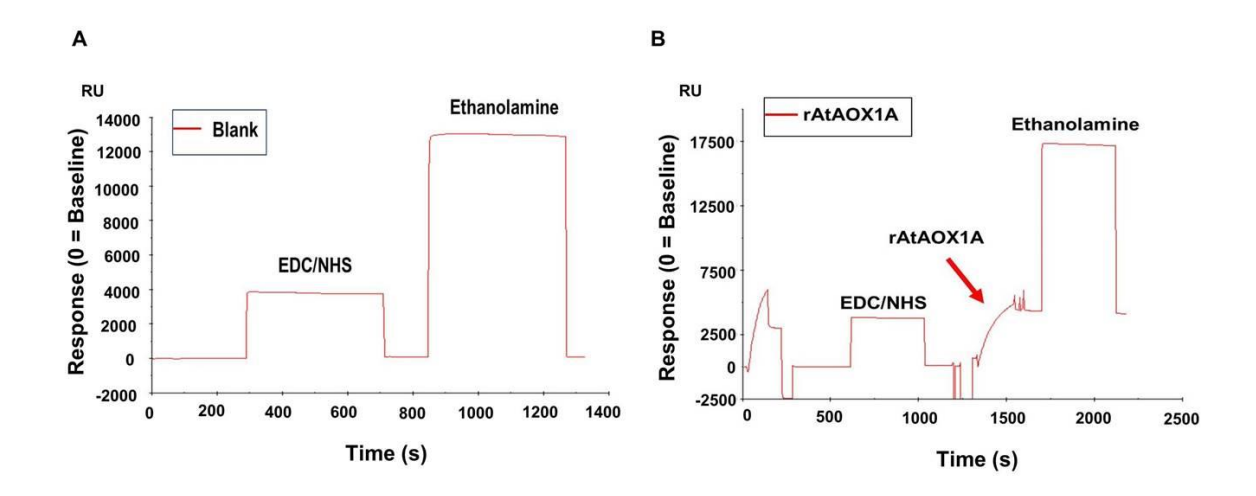


Fig. 3.10. Purified rAtAOX1A is immobilized onto Series S Sensor Chip CM5. (A) Blank immobilization on flow cell Fc-3; (B) $100\mu g/ml$ of purified rAtAOX1A (ligand) immobilization on flow cell Fc-4. Arrow indicates rAtAOX1A injection, which resulted in \sim 4,117 RU.

b) Sample injection

The AOX inhibitors (SHAM and n-PG), activator (pyruvate), TCA cycle metabolites (citrate, α-KG, succinate, fumaric acid, malic acid and OAA) and redox metabolites (GSH, GSSG, AsA, DHA, NAD, NADH, NADP and NADPH) are used as analytes. The analytes (1 to 5 mM concentration) dissolved in double distilled water are injected independently into the flow cells (Fc-3 & Fc-4) in a running buffer composed of PBS (2 mM of KH₂PO₄, 10 mM of Na₂HPO₄, 2.7 mM of KCl, and 137 mM of NaCl at pH 7.4) containing 0.005% P20 surfactant, at a flow rate of 30 μl/min at 25°C. In the association phase (120 s), the analytes were allowed to bind to the rAtAOX1A, while in the dissociation phase (120 s), they were separated from each other. In the regeneration phase (30 s), the analytes are disposed of from the flow cells using 10 mM of Glycine-HCl (pH 2.5) and 0.5 M of NaCl, as described in the Biacore T-200 manual (GE Healthcare Life Sciences). The experiment was performed twice. In each experiment, three

cycles of association, dissociation, and regeneration were carried out against each concentration of inhibitors, activators, TCA cycle and redox metabolites tested in the present study.

c) Kinetic analysis

The acquired data were analyzed using BIA evaluation software (version 2.0, GE Healthcare Life Sciences) with the Langmuir fit model of 1:1 binding. To determine the kinetic constants (k_a , k_d , and K_D), the sensorgrams were fitted to a 1:1 kinetic model using the pooled data analysis option. The k_a represents the association constant, k_d represents the dissociation constant, and K_D represents the equilibrium dissociation constant. The affinity of inhibitors, activators, TCA cycle and redox metabolites with rAtAOX1A was derived by measuring the kinetic parameters at five different concentrations (1, 2, 3, 4, and 5 mM).

3.15 Molecular docking

The homology model of the AtAOX1A monomer (PMDB Accession number: PM0080189) was chosen as the target protein for the docking study (Pennisi et al., 2016). The 3-dimensional models of the ligands [AOX inhibitors (SHAM and n-PG); substrates (DQ, DQH2, ubiquinone-1 (UQ₁) ubiquinol-1 (Q₁H₂); activator (pyruvate), TCA cycle metabolites (citrate, α-KG, succinate, fumaric acid, malic acid and OAA) and redox metabolites (GSH, GSSG, AsA, DHA, NAD, NADH, NADP and NADPH] were generated using PubChem (Kim et al., 2021) and CHARMM-GUI (Jo et al., 2008) programs. The binding affinities of different ligands with AtAOX1A are studied using the SwissDock program (Grosdidier et al., 2011a, b). To identify the potent residues that may have a direct impact on the binding of the ligands, mutational docking studies were performed, i.e., point mutations were introduced in silico in WT-

AtAOX1A by replacing amino acid residues whose side chains are located in the binding pocket (within 3Å region) with alanine/arginine.

3.16 Statistical analysis

In general, the data shown are the Mean \pm SE of three replicates. The statistical differences were evaluated by one-way ANOVA with the Tukey test integrated into Sigma plot, version 12.0, Systat Software Inc., San Jose, CA, USA, at a significance level of P \leq 0.05.

Chapter 4

Cloning, Expression and Purification of Functionally Active rAtAOX1A from *E. coli* BL21(DE3)

Cloning, Expression and Purification of Functionally Active rAtAOX1A from *E. coli* BL21(DE3)

4.1. Introduction

In higher plants, under different stress conditions, a cyanide-resistant AOX pathway operates in mitochondria, along with a conventional COX pathway (Rich and Moore, 1976; Vanlerberghe and McIntosh, 1997; McDonald et al., 2009; Moore et al., 2013). The AOX pathway is involved in a non-phosphorylating electron transport mechanism and dissipates excess energy as heat (Wagner and Moore, 1997; Siedow and Umbach, 2000; Millar et al., 2011; Moore et al., 2013). The physiological significance of AOX in biotic/abiotic stress tolerance is well-documented (Dinakar et al., 2010b; Yoshida et al., 2011; Liao et al., 2012, 2021; Gandin et al., 2014; Zhu et al., 2015; Zhang et al., 2016). A remarkable increase in the expression of AOX1A in A. thaliana at a wide range of stress conditions and during the impairment of respiratory metabolism indicates its primary role in stress response as compared to other AOX genes (Clifton et al., 2005, 2006; Ho et al., 2008; Vishwakarma et al., 2015). In higher plants, SHAM and n-PG are frequently used to inhibit the activity of AOX and, thereby, the AOX pathway under both in vitro and in vivo conditions to reveal its physiological function(s) during normal growth, as well as biotic/abiotic stress conditions (Diethelm et al., 1990; Padmasree and Raghavendra, 1999a,b; Yoshida et al., 2006; Giraud et al., 2008; Dinakar et al., 2010b; Florez-Sarasa et al., 2011; Zhang et al., 2011).

Several attempts have been made by various scientists to purify AOX from mitochondria of different plant sources (Huq and Palmer, 1978; Rich, 1978; Kay and Palmer, 1985; Bonner et al., 1986; Elthon and McIntosh, 1986, 1987; Berthold and Siedow, 1993; Zhang et al., 1996; Affourtit and Moore, 2004). However, the low yield and thermal

instability of AOX impeded the studies related to its structural and biophysical properties and its crystal structure is not yet revealed in plants (Moore et al., 2013). In this context, the rDNA technology helped the expression of plant AOX in *Escherichia coli* (*E. coli*). The AOX from *A. thaliana* and Trypanosoma were expressed in a ΔhemA *E. coli* strain, which is deficient in the cytochrome pathway (Kumar and Söll, 1992; Nihei et al., 2003; Kido et al., 2010; Xu et al., 2021). Besides, the supplementation of iron in the form of Fe²⁺/Fe³⁺ was in ambiguity during the heterologous expression of AOX to acquire it in pure and active form (Minagawa et al., 1990; Ajayi et al., 2002; Affourtit and Moore, 2004).

The present study is aimed to purify the functionally active rAtAOX1A from *E. coli* membranes, which is a general laboratory stain for recombinant protein expression and to confirm it by western blot and MALDI-TOF-TOF studies.

4.2. Results

Cloning and expression of *Arabidopsis thaliana AOX1A* (*AtAOX1A*)

The cDNA of *AtAOX1A* coding for mature protein was amplified (**Fig. 4.1**) using *AOX1A* specific primers and cloned into a pET28a(+) vector (**Fig. 4.2**). The pAtAOX1A construct was transformed into BL21(DE3) cells. Transformed positive colonies (*E. coli/*pAtAOX1A) were selected by colony polymerase chain reaction (PCR) (**Fig. 4.3**). Recombinant plasmids from these colonies were isolated and confirmed by restriction digestion with *Eco*RI and *Xho*I (**Fig. 4.4**), and DNA sequencing using T7 primers (**Fig. 4.5**). After confirming the *AtAOX1A* sequence, these colonies were used for recombinant protein synthesis. The expression of rAtAOX1A protein (~37 kDa) in *E. coli/*pAtAOX1A after induction with IPTG was visualized on 12.5% (w/v) SDS-PAGE under reducing conditions (**Fig. 4.6**).

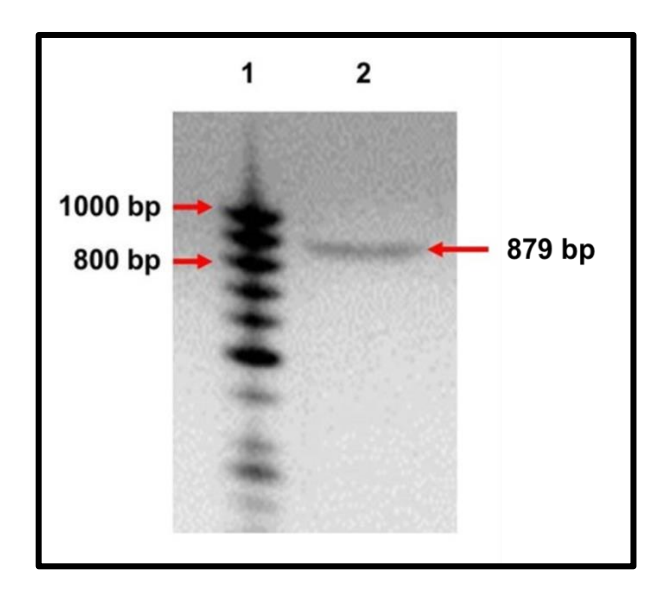


Fig. 4.1. Agarose-gel electrophoresis of PCR-amplified AtAOX1A DNA fragment. PCR was carried out with *AtAOX1A* specific forward and reverse primers as described in materials and methods. Lane 1, 50-1000 bp DNA ladder; lane 2, PCR amplified *AtAOX1A* (879 bp) was indicated with an arrow.

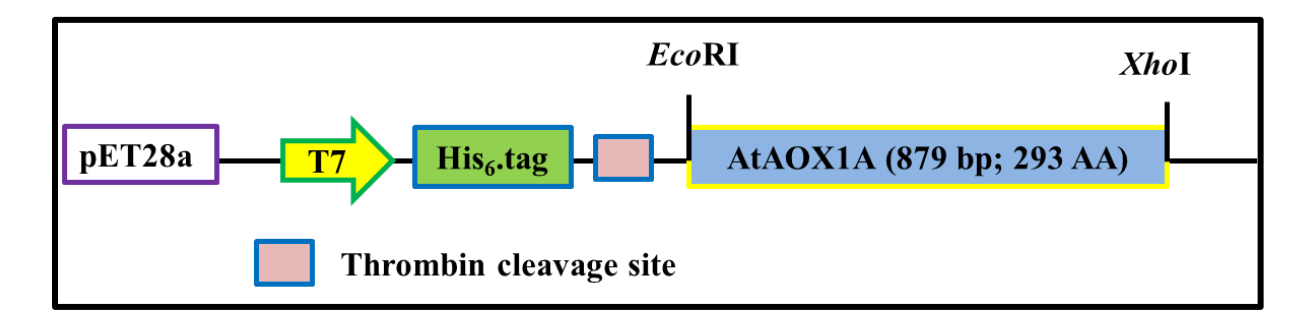


Fig. 4.2. Schematic diagram of the expression vector construction. Cloning of AtAOX1A into pET28a vector. The gene sequences were cloned into restriction endonuclease *Eco*RI and *Xho*I recognition sites of the pET28a vector to produce N-terminal His₆-tag recombinant AtAOX1A protein.

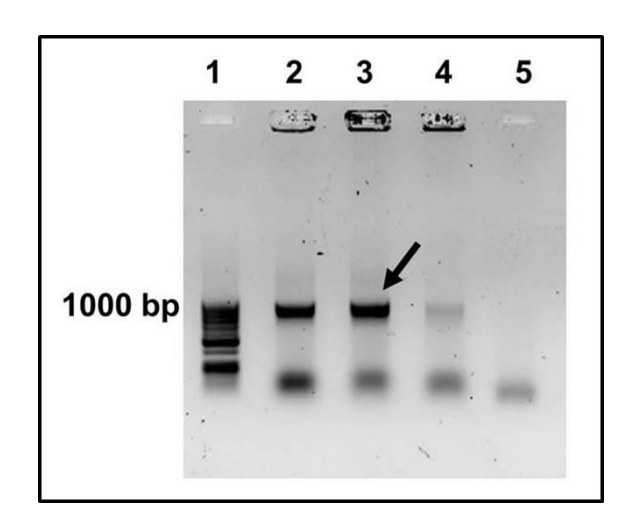


Fig. 4.3. Confirmation of the clone (pAtAOX1A). Colony PCR: A single colony of *E. coli* [BL21(DE3)] cells transformed with pAtAOX1A construct was used as a DNA source to amplify AtAOX1A using gene specific primers. Lane 1, 50-1000 bp DNA ladder; lane 2, colony 1; lane 3, colony 2; lane 4, colony 3 and lane 5, non-template control. Amplified AtAOX1A from colony 2 (indicated with an arrow) was chosen for further studies. An aliquot of 20 μl of the sample was loaded in each well.

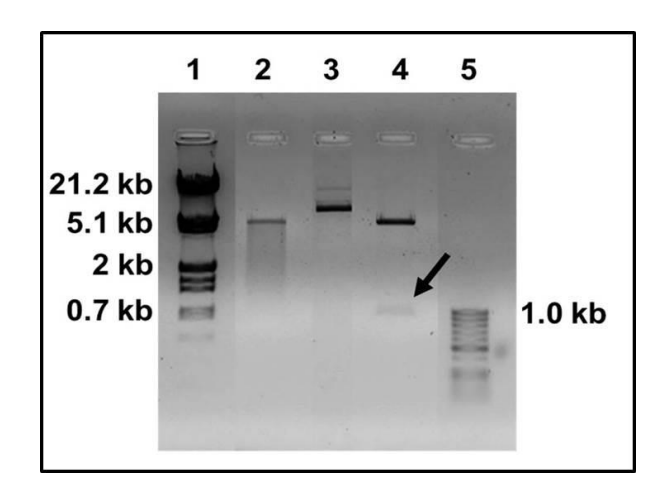


Fig. 4.4. Confirmation of the clone (pAtAOX1A). Restriction Digestion: pET28a and pAtAOX1A plasmids were digested with *Eco*RI and *Xho*I restriction endonucleases. Lane 1, 0.5–10 kb DNA ladder; lane 2, restriction digested pET28a vector; lane 3, pAtAOX1A vector; lane 4, restriction digested pAtAOX1A; lane 5, 50–1000 bp DNA ladder. The inserted gene (*AtAOX1A*) release is indicated with an arrow in lane 4. An aliquot of 20 μl of the sample was loaded in each well.

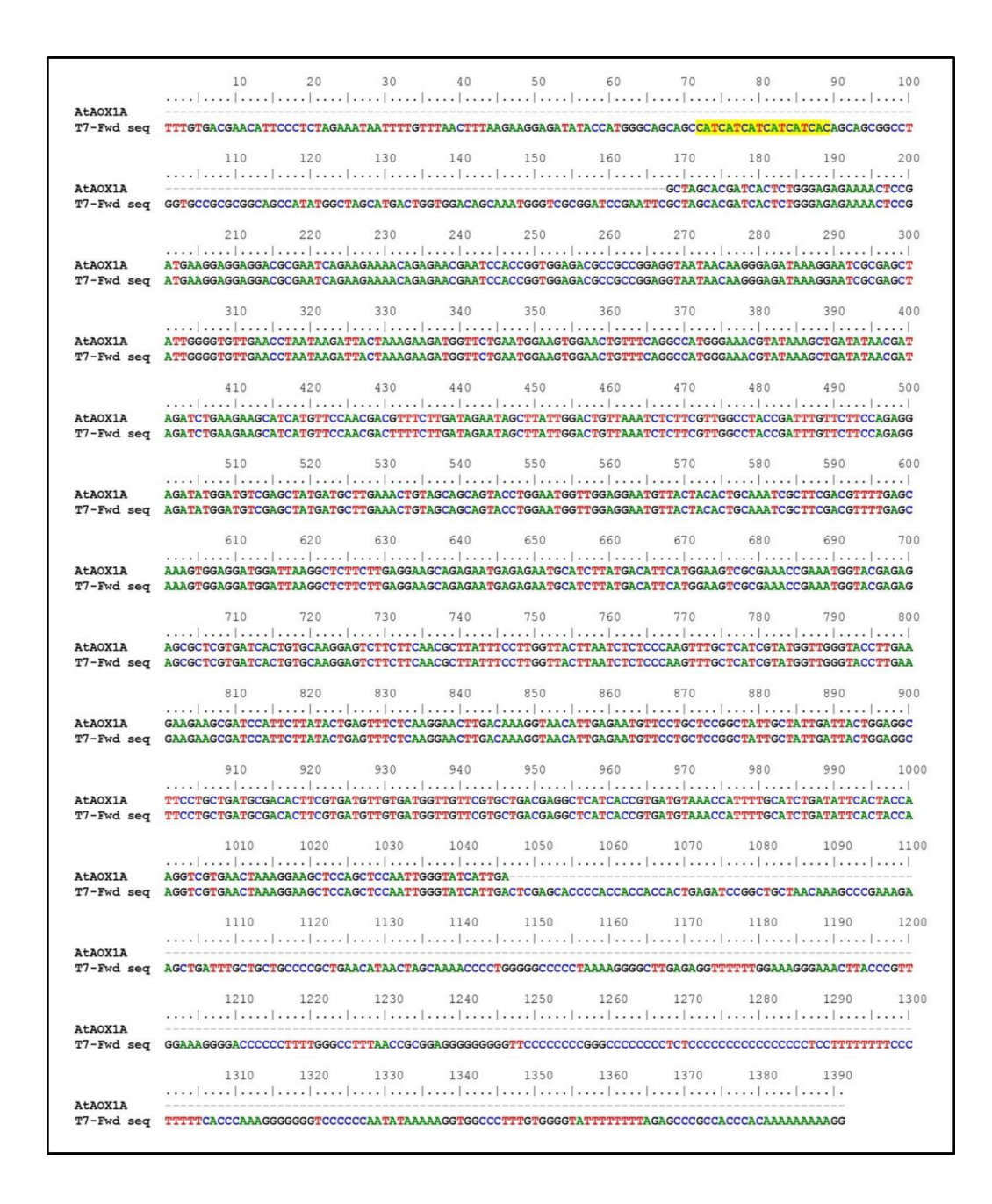


Fig. 4.5. Confirmation of the clone (pAtAOX1A). The colony PCR-positive clones were sequenced (Eurofins Pvt. Ltd.) with T7 forward primer (TAATACGACTCACTATAGGG). DNA sequence obtained from clone (pAtAOX1A) was aligned with original *AtAOX1A* gene sequence from NCBI database using ClustalW Multiple alignments. DNA sequence alignment results showed 100% similarity. The highlighted (yellow) region represents Histag sequences.

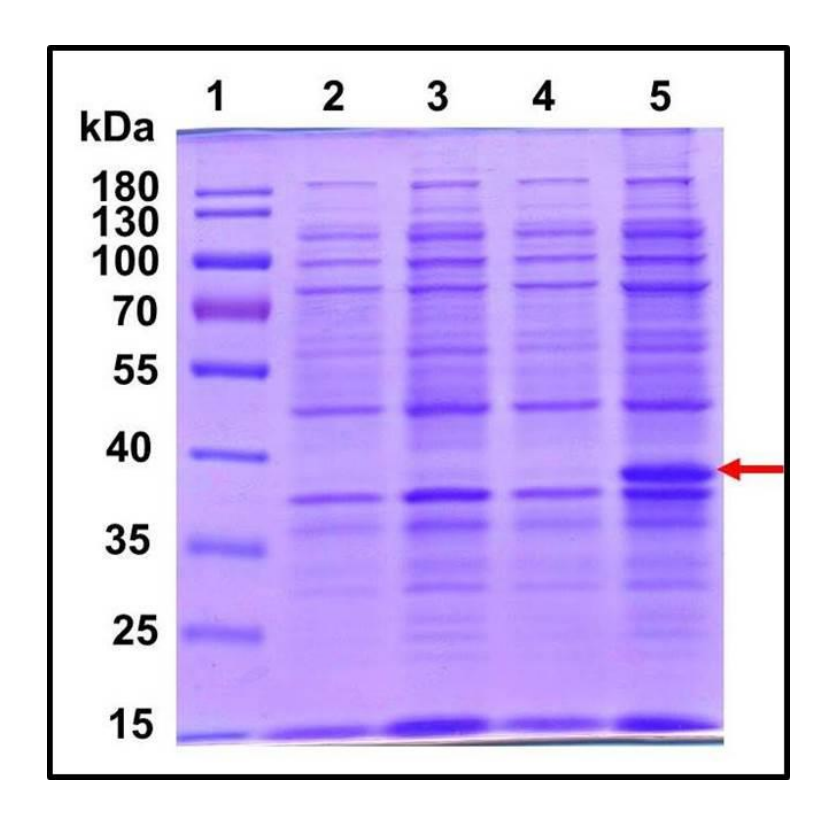


Fig. 4.6. Total protein of both *E. coli*/pET28a and *E. coli*/pAtAOX1A cells were separated on 12.5% (w/v) sodium dodecyl sulfate-polyacrylamide gel electrophoresis (SDS-PAGE) for recombinant protein expression analysis. Each well was loaded with 40 μg of protein. Lane 1, 10–180 kDa protein marker; lane 2, *E. coli*/pET28a; lane 3, *E. coli*/pET28a induced with 0.1 mM IPTG; lane 4, *E. coli*/pAtAOX1A; lane 5, *E. coli*/pAtAOX1A induced with 0.1 mM IPTG. The induced rAtAOX1A is indicated with an arrow.

Functional characterization of rAtAOX1A in E. coli

To identify whether the expressed rAtAOX1A is functionally active or not, both E. coli/pET28a and E. coli/pAtAOX1A were evaluated for their respiratory and growth rates in the presence of KCN, n-PG, and SHAM at a wide range of concentrations (Figs. 4.7 and **4.8**). In the absence of any inhibitor, both *E. coli*/pET28a ($34.52 \pm 0.5 \mu moles O_2 min^{-1}$) and E. coli/pAtAOX1A (32 ± 0.74 µmoles $O_2 min^{-1}$) showed comparable respiratory O_2 uptake rates per 4.8 x 10⁸ cells ml⁻¹. However, supplementation of KCN at an increasing concentration from 0.05 to 1 mM caused a significant reduction in the O₂ uptake (up to 90%) of E. coli/pET28a due to inhibition of COX-catalyzed respiration, whereas it only caused a 37% reduction in respiratory rate of E. coli/pAtAOX1A, suggesting that the remaining O₂ uptake in transformed cells is contributed by AOX-catalyzed respiration (Fig. 4.7A). In contrast to KCN, supplementation of n-PG, a commonly used inhibitor of AOX, has shown only a marginal (<13%) effect on respiratory O₂ uptake rates of E. coli/pET28a even at a concentration as high as 0.5 mM due to the lack of AOX-catalyzed respiration. Conversely, at this concentration, n-PG caused a 50% reduction in respiratory rates of E. coli/pAtAOX1A (**Fig. 4.7B**). In the case of SHAM supplementation, another inhibitor of the AOX respiratory pathway decreased the respiratory rates of E. coli/pAtAOX1A remarkably up to 33%, as its concentration increased from 0.5 to 2 mM. However, treatment of E. coli/pET28a with 2 mM SHAM caused only a 2.5% reduction in its respiratory rate (Fig. 4.7C). To examine the effect of respiratory inhibitors on the growth of the E. coli/pET28a and E. coli/pAtAOX1A, the bacterial growth was compared at the end of 5 h. Interestingly, E. coli/pET28a achieved a stationary phase after 4 h (Fig. 4.8A, C and E), while E. coli/pAtAOX1A cells remained in a

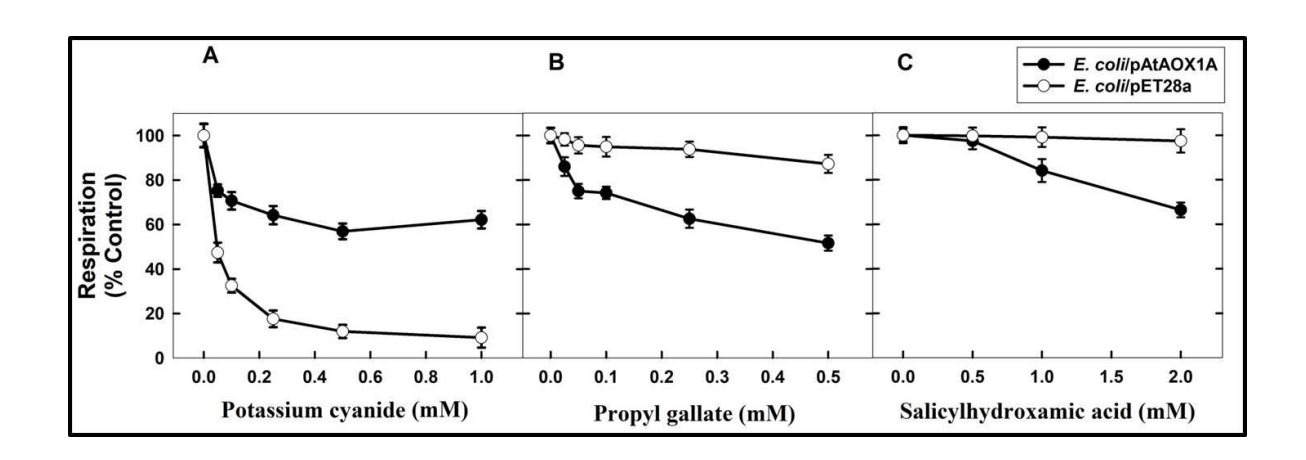


Fig. 4.7. Functional characterization of rAtAOX1A in *E. coli*. Oxygen consumption (respiratory) rates (%) of *E. coli* expressing AtAOX1A (*E. coli*/pAtAOX1A) and *E. coli* containing an empty vector (*E. coli*/pET28a) in presence of (**A**) KCN (0.05, 0.1, 0.25, 0.5 and 1.0 mM), (**B**) n-PG (0.025, 0.05, 0.1, 0.25 and 0.5 mM) and (**C**) SHAM (0.5, 1, and 2 mM).

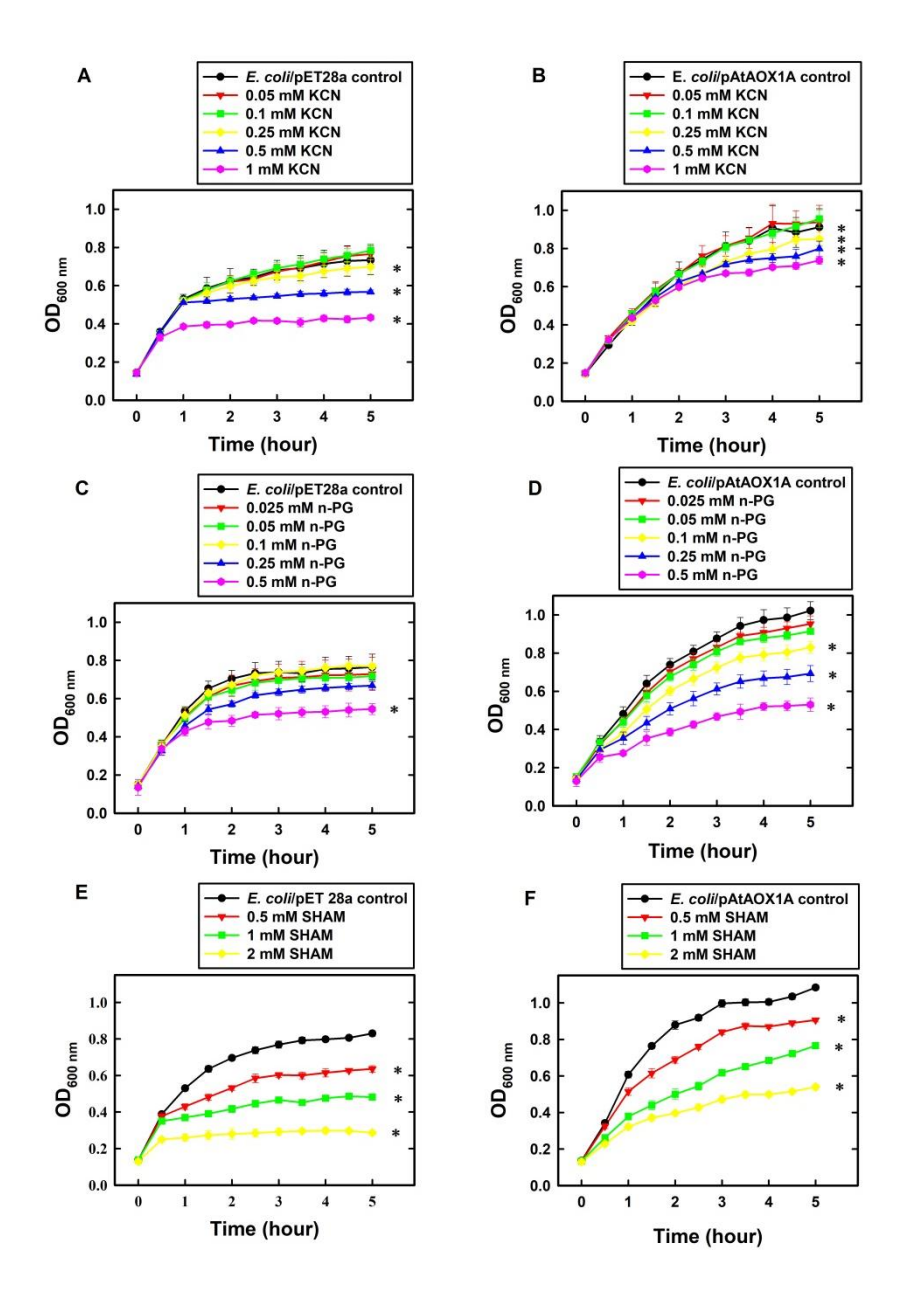


Fig. 4.8. Functional characterization of rAtAOX1A in *E. coli*. The growth pattern of *E. coli* cells was monitored for 5 h in the absence or presence of respiratory inhibitors: **(A)** Growth pattern of *E. coli*/pET28a and **(B)** *E. coli*/pAtAOX1A in the absence or presence of KCN; **(C)** Growth pattern of E. coli/pET28a and **(D)** *E. coli*/pAtAOX1A in the absence or presence of n-PG; **(E)** Growth pattern of *E. coli*/pET28a and **(F)** *E. coli*/pAtAOX1A in the absence or presence of SHAM. Each value represents the mean \pm SD of three experiments. The statistical significance difference (P <0.05) was calculated for the endpoint of the growth curve and indicated with asterisks.

log phase even after 5 h of growth (Fig. 4.8B, D and F), suggesting the role of AOXcatalyzed respiration in enhancing the metabolic activities of E. coli. The supplementation of KCN at an increasing concentration (0.05 to 1 mM) has suppressed the growth of E. coli/pET28a significantly by 51%. However, KCN has suppressed only 23% of growth in E. coli/pAtAOX1A (Fig. 4.8A, B). When E. coli/pET28a was supplemented with n-PG, it caused only a trivial (14%) effect on its growth even at 0.25 mM concentration, whereas it suppressed the growth of E. coli/pAtAOX1A up to 38% at the same concentration. However, n-PG at a higher concentration (0.5 mM) showed a remarkable growth inhibitory effect on both E. coli/pET28a (34%) and E. coli/pAtAOX1A (54%), respectively (Fig. 4.8C, D). On the contrary, SHAM has suppressed the growth of E. coli/pET28a and E. coli/pAtAOX1A by 88 and 57%, respectively, as its concentration was raised from 0.5 to 2 mM (Fig. 4.8E, F). However, the greater effect of SHAM on the growth of E. coli/pET28a, as compared to E. coli/pAtAOX1A, might be due to the non-specific inhibitory effect on other oxidases of E. coli, besides its specific effect on AOX. These results, taken together, suggest that rAtAOX1A expressed in E. coli/pAtAOX1A is functionally active.

Purification of rAtAOX1A and its analysis by MALDI TOF/TOF

As the expression cassette contains an N-terminal His₆-tag, cobalt column affinity chromatography was used to purify rAtAOX1A from the soluble fraction of *E. coli*/pAtAOX1A membrane. To get active protein: (1) rAtAOX1A was induced by IPTG in the presence of FeSO₄ (0.1 mM) and (2) after induction, the harvested cells were suspended in 50 mM Tris-HCl containing 10 mM of pyruvate at pH 7.5. The purified rAtAOX1A with a molecular mass of ~37 kDa was observed in reducing SDS-PAGE, which includes AtAOX1A mature protein (33.44 kDa) and pET28a(+) vector sequence (3.83 kDa)

(Fig. 4.9A). Furthermore, western blot analysis with anti-His antibody showed a single band correlating with the molecular mass observed in SDS-PAGE (Fig. 4.9B). The rAtAOX1A has shown a specific activity of 3.86 µmol O₂ min⁻¹ mg⁻¹ protein and a 15% recovery rate, where 600 µM of duroquinol was used as a substrate (Table 4.1). Moreover, the purified recombinant protein band (~37 kDa) from SDS-PAGE (**Fig. 4.9A**) was digested with trypsin and subjected to MALDI-TOF/TOF analysis (Fig. 4.10A). The Biotools software revealed the following sequence 'LPADATLRDVVMVVR' for lift spectra corresponding to the peak 1656.258 Da (Fig. 4.10B, C). The MS-MS ion search in the Mascot search database resulted in matching with partial AtAOX (ID: gi/1872517) with a significant score of 308 (Fig. **4.10D**). The six major peptide peaks (m/z 1209.854, m/z 1365.972, m/z 1566.099, m/z 1656.258, m/z 2385.628 and m/z 2476.697) in peptide mass fingerprint (PMF) spectrum covered 24% of partial A. thaliana AOX (ID: gi/1872517) protein sequence from NCBI database (Fig. 4.10E). A blast search of the sequence (LPADATLRDVVMVVR) showed 100% identity with the AtAOX1A in the NCBI database (Fig. 4.10F). These results confirm that the purified protein is rAtAOX1A.

4.3. Discussion

Differential respiratory and growth responses of *E. coli*/pET28a and *E. coli*/pAtAOX1A on exposure to mitochondrial inhibitors

In the present study, BL21(DE3) *E. coli* strain was chosen to examine in vivo functional expression of pAtAOX1A and robust expression of rAtAOX1A protein for purification and in vitro characterization. AOX is known to be resistant to cyanide and sensitive to n-PG and

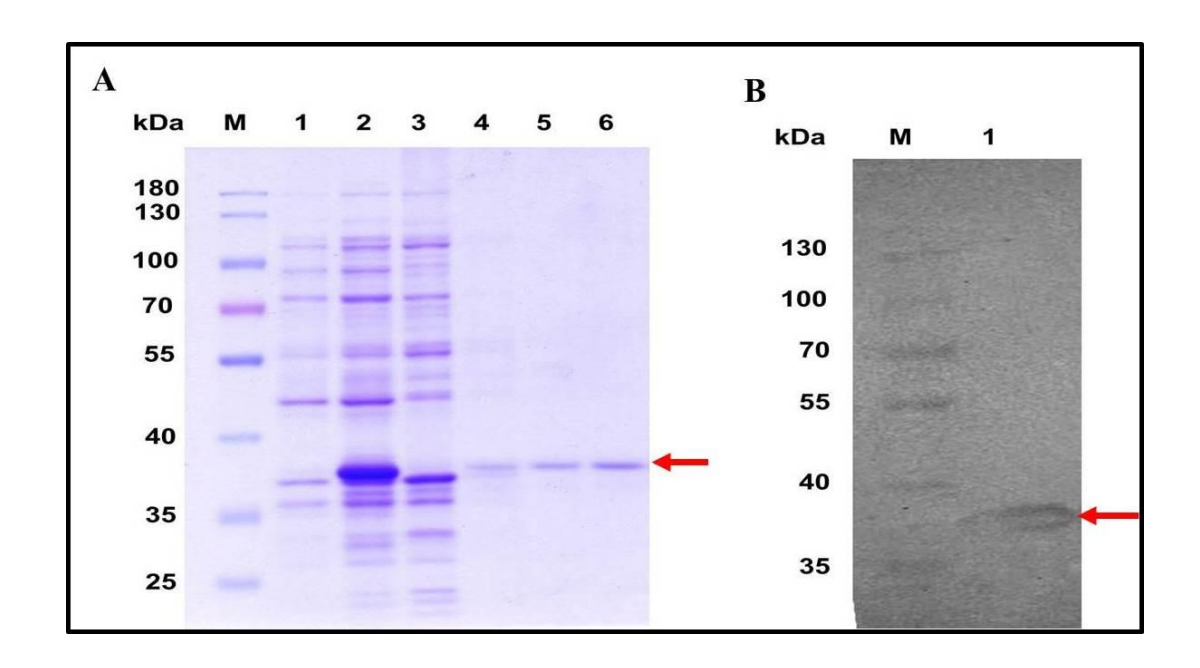
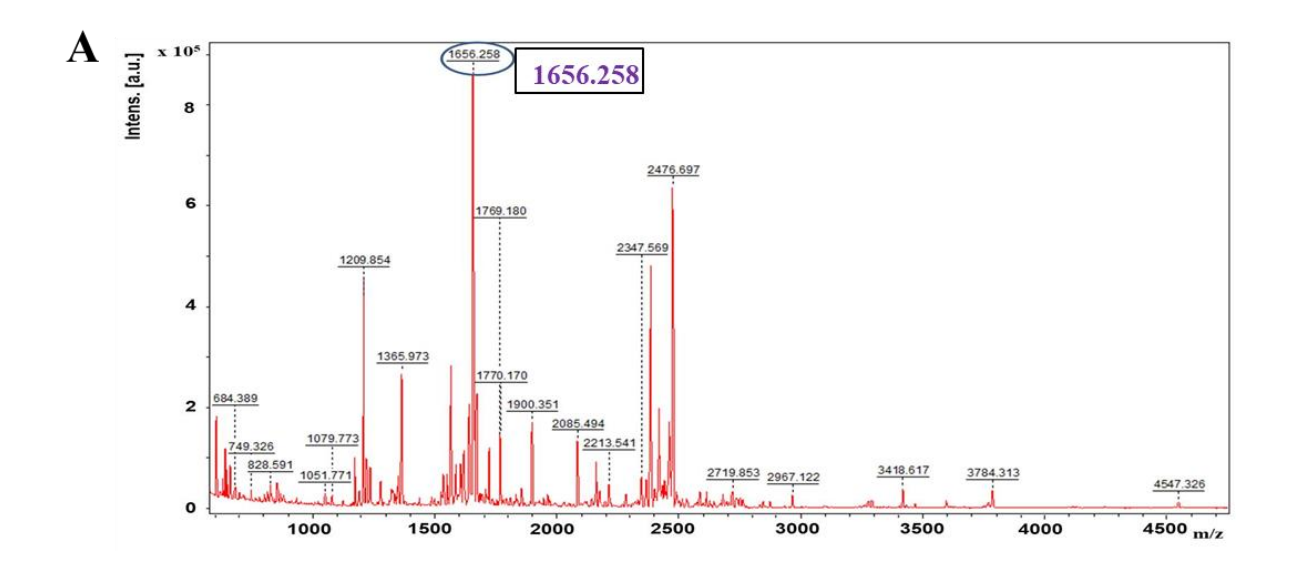


Fig. 4.9. Purification and validation of rAtAOX1A protein using SDS-PAGE and western blotting. **(A)** SDS-PAGE visualizing purification profile of rAtAOX1A from *E. coli* membrane. Lane M, 10-180 kDa protein marker; lane 1, protein from *E. coli*/pAtAOX1A; lane 2, protein from *E. coli*/pAtAOX1A induced with IPTG; lane 3, flow-through; lane 4, washing fraction; lanes 5 and 6, elution fractions, arrow indicates purified rAtAOX1A with ~37 kDa molecular mass. **(B)** Western blot showing purified rAtAOX1A: lane M, 10-180 kDa protein marker; lane 1, purified rAtAOX1A. 40 μg of protein sample is loaded in each well.

Table 4.1. The membrane fractions of *E. coli* were prepared from 500 mL of *E. coli*/pAtAOX1A culture and used for rAtAtAOX1A purification. Oxygen uptake activities were measured using an oxygen electrode in the presence of duroquinol as a substrate. The specific activity shown here is representative of three independent experiments.

Fraction	Total activity (µmol O ₂ min ⁻¹)	Protein yield (mg/500 ml culture)	Recovery (%)	Specific activity (µmol O ₂ min ⁻¹ mg ⁻¹ protein)	Fold increase in specific activity
E. coli lysate	14.57	44.17	100	0.33 ± 0.061	1.0
Inner membrane	29.95	19.2	43.4	0.56 ± 0.137	4.7
DDM extract	20.76	17.16	39.8	1.21 ± 0.196	3.7
Purified rAtAOX1A	25.47	6.6	14.94	3.86 ± 0.182	11.7



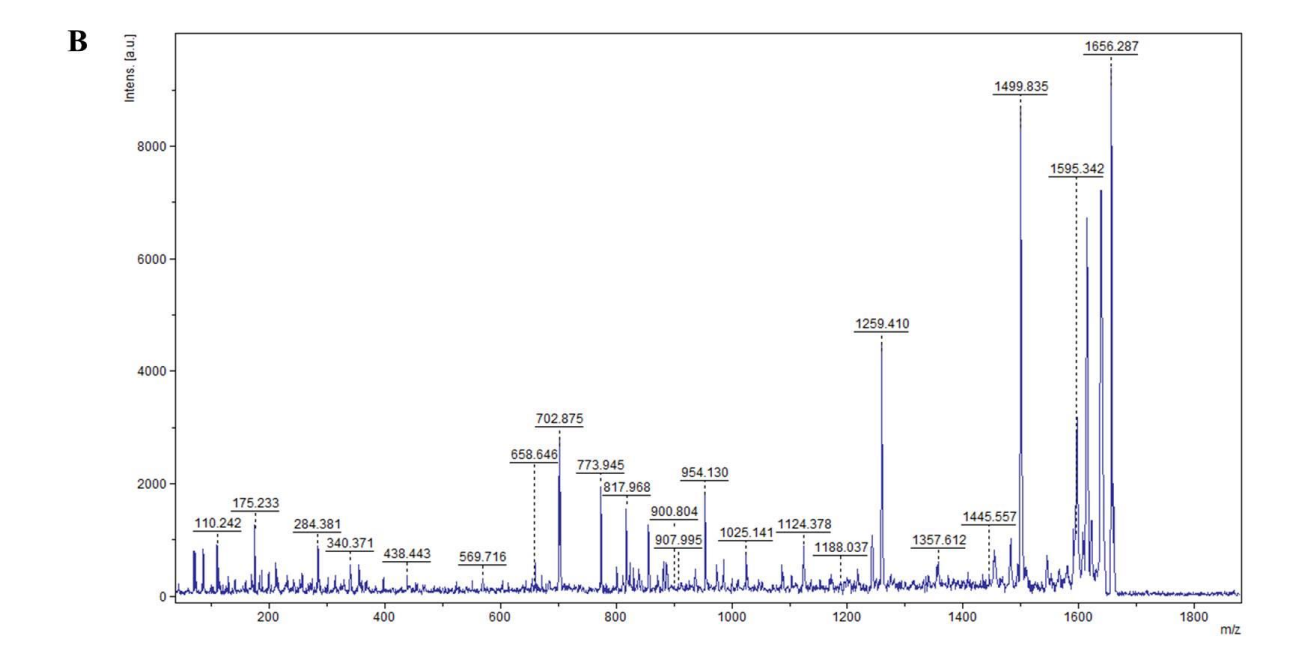
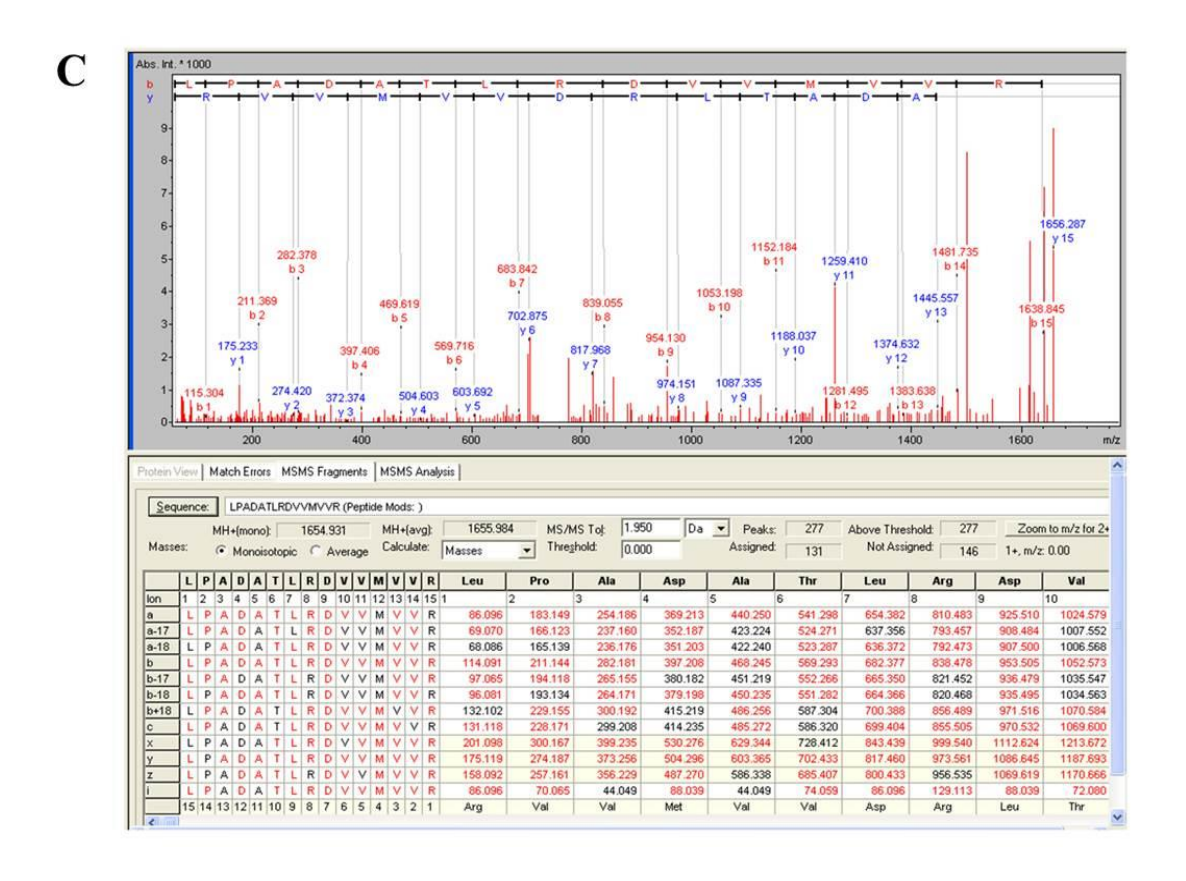
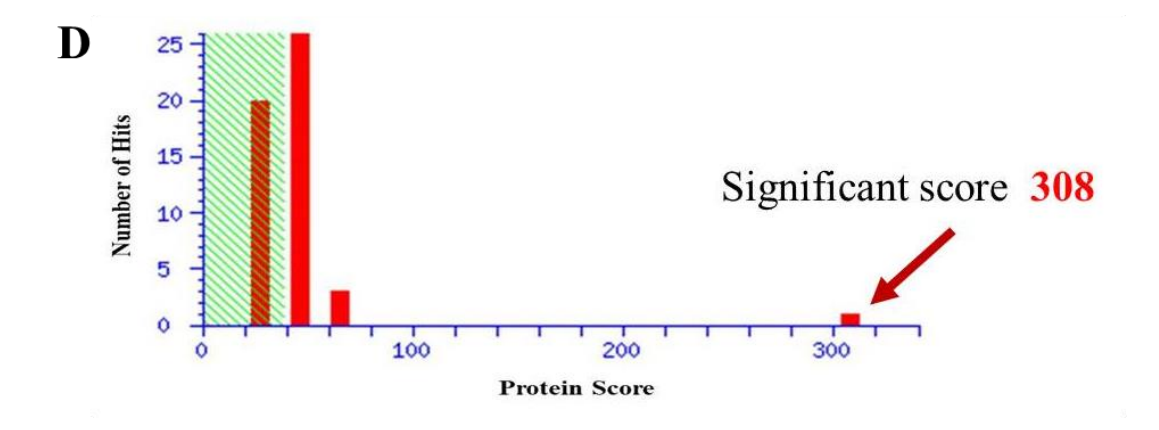


Fig. 4.10. Validation of purified rAtAOX1A protein using MALDI-MS-MS. (**A**) MALDI TOF/TOF mass spectrum of purified rAtAOX1A between 500-5,000 m/z obtained after digestion with trypsin. Peaks corresponding to 1209.854, 1365.972, 1566.099, 1656.258, 2385.628, and 2476.697 Da are subjected to MS-MS analysis. (**B**) The lift spectrum of the peak corresponds to the 1656.258 Da.





_						
${f E}$	1	LGEKTPMKEE	DANQKKTENE	STGGDAAGGN	NKGDKGIASY	WGVEPNKITK
	51	EDGSEWKWNC	FRPWETYKAD	ITIDLKKHHV	PTTFLDRIAY	WTVKSLRWPT
	101	DLFFQRRYGC	RAMMLETVAA	VPGMVGGMLL	HCKSLRRFEQ	SGGWIKALLE
	151	EAENERMHLM	TFMEVAKPKW	YERALVITVQ	GVFFNAYFLG	YLISPKFAHR
	201	MVGYLEEEAI	HSYTEFLKEL	DKGNIENVPA	PAIAIDYWRL	PADATLRDVV
	251	MVVRADEAHH	RDVNHFASDI	HYQGRELKEA	PAPIGYH	

Fig. 4.10. (**C**) Biotools display of the peptide peak 1656.258 Da. (**D**) its Mascot score; (**E**) *A. thaliana* partial AOX (gi/1872517) sequence from NCBI database. The sequence of MS peaks (1209.854, 1365.972, 1566.099, 1656.258, 2385.628, and 2476.697 Da) of rAtAOX1A are indicated in bold red font and sequence coverage from these six major peaks is about 24%. The sequence obtained from the MS peak with 1656.258 is underlined.

S. No	Plant Source	Accession No. (NCBI)	Sequence	Similarity (%)	
1 2 3 4 5 6 7 8	rAtAOXIA Arabidopsis thaliana (alternative oxidase 1A) Arabidopsis thaliana (alternative oxidase) Brassica rapa (ubiquinol oxidase 1A, mitochondrial) Brassica juncea (mitochondrial alternative oxidase 1A) Camelina sativa (PREDICTED: ubiquinol oxidase 1A) Brassica napus (ubiquinol oxidase 1A, mitochondrial) Brassica rapa (ubiquinol oxidase 1A, mitochondrial) Camelina sativa (PREDICTED: ubiquinol oxidase 1A) Tanacetum cinerariifolium (ubiquinol oxidase 1A)	NP_188876.1 CAA10364.1 XP_009135803.1 AEB00555.1 XP_010511278.1 XP_013683733.1 XP_009145388.1 XP_010466517.1 GFD53721.1	LPADATLRDVVMVVR	100 100 100 100 100 100 100 100	

Fig. 4.10. (F) The sequence obtained from peptide peak m/z 1656.258 ('LPADATLRDVVMVVR') has shown 100% identity with AtAOX1A in the BLAST search.

SHAM, while *E. coli* oxidases are found to be sensitive to cyanide but not to AOX inhibitors (Bendall and Bonner, 1971; Siedow and Girvin, 1980; Fukai et al., 1999). Thus, consistent with the properties of different oxidases, the respiratory rates of *E. coli*/pAtAOX1A are resistant to KCN and sensitive to n-PG and SHAM when compared with *E. coli*/pET28a (Fig. 4.7A–C).

In the absence of any inhibitor, after 5 h, E. coli/pAtAOX1A exhibited higher growth $(OD_{600} = \sim 1)$ when compared with E. coli/pET28a $(OD_{600} = \sim 0.8)$ due to the beneficial effects rendered by AtAOX1A expression in E. coli/pAtAOX1A. Consequently, the growth rates of E. coli/pAtAOX1A are found to be resistant to KCN and sensitive to n-PG and SHAM, which is not the case with E. coli/pET28a (Fig. 4.8A-F). Thus, the differential observed in respiration and growth rates of E. responses coli/pET28a and E. coli/pAtAOX1A, upon treatment with mitochondrial inhibitors, clearly demonstrates that the rAtAOX1A expressed in E. coli in the present study is functionally active (Berthold, 1998). The previous report on the expression of AOX from A. thaliana in hemA E. coli strain (deficient in cytochrome-mediated aerobic respiration) allowed it to grow under aerobic conditions (Kumar and Söll, 1992). Also, the expression of TAO in E. coli and rAtAOX1A in yeast cells has shown cyanide-insensitive and ascofuranone/SHAM-sensitive growth (Fukai et al., 1999; Nihei et al., 2003; Vishwakarma et al., 2016). Nevertheless, the results from this study suggest the concentration of n-PG to be restricted to ≤ 0.25 mM, as treatment with higher concentrations leads to non-specific inhibitory effects on E. coli oxidase(s) and/or cellular redox enzymes, as well as hydrolases (Boyd and Beveridge, 1979; Han and Park, 2009; Fig. 4.8C). Similarly, a high concentration of SHAM (2 mM) showed an inhibitory effect on the growth of E. coli/pET28a (88%), possibly due to its non-specific

effect on *E. coli* cytochrome oxidases (**Fig. 4.8E**). However, the non-specific effects are exacerbated more with SHAM than n-PG. Further, the studies of Berthold (1998) reported such ambiguity in the usage of these inhibitors. The results from their studies using cytochrome *bd* oxidase mutants indicated that partial inhibition in the duroquinol oxidase activity of the *E. coli* membrane was observed with SHAM but not n-PG.

Purification of rAtAOX1A in its active form

In the present study, the rAtAOX1A is overexpressed in *E. coli* BL21(DE3) and purified from *E. coli* membranes (**Fig. 4.9A**). To obtain a pure as well as active rAtAOX1A, it is found to be essential to maintain the following conditions during its induction and purification procedure.

Supplementation of Fe²⁺ is essential for the expression of active rAtAOX1A

The studies of Minagawa et al. (1990) and Ajayi et al. (2002) have reported that iron supplementation is essential during the heterologous expression of AOX. In this study, Fe²⁺ was added to the culture medium at the time of induction along with IPTG, which resulted in an active rAtAOX1A (**Table 4.1**). However, when rAtAOX1A was purified without Fe²⁺ supplementation, its activity was not detectable, despite the presence of pyruvate in all purification steps (data not shown). This could be due to a lack of formation of the hydroxobridged binuclear iron center, which is involved in the reduction of molecular oxygen to water, as evident by electron paramagnetic resonance studies (Berthold et al., 2002; Moore et al., 2008). Similarly, in this study, supplementation of Fe⁺³ ion to the culture medium could not retrieve AOX in pure form (data not shown).

Pyruvate supplementation is essential during all the steps of purification

Pyruvate stabilizes the active enzyme conformation, although the specific mechanism of AOX activation by pyruvate is unclear (Carré et al., 2011; Elliott et al., 2014; Xu et al., 2021). In this study, the addition of pyruvate (10 mM) in all purification steps resulted in the retrieval of active rAtAOX1A from *E. coli* membranes (**Table 4.1**). However, the AOX activity was found to be insensitive to pyruvate when examined in mitochondria isolated from thermogenic plants, such as *Arum italicum* (Hoefnagel et al., 1997), *Sauromatum guttatum* (Crichton et al., 2005) and *A. maculatum* (Ito et al., 2011).

Detergent choice to solubilize the rAtAOX1A from E. coli membranes

The choice of detergent usage also plays a major role in retaining AOX activity during the process of purification. For solubilizing the recombinant trypanosomal alternative oxidase (rTAO), OG was proven to be efficient (Kido et al., 2010). However, in the case of recombinant *S. guttatum* alternative oxidase (rSgAOX), OG caused a decrease in enzyme activity, while DDM improved its activity (Elliott et al., 2014). In this study, DDM was used to solubilize rAtAOX1A from *E. coli*/pAtAOX1A membranes. The protocol used in this study resulted in a 15% recovery of rAtAOX1A. Further, the oxygen uptake activity of purified rAtAOX1A in the presence of duroquinol was found to be 3.8 μ mol O₂ min⁻¹ mg⁻¹ protein at pH 7.5 in Tris-HCl (**Table 4.1**). Nevertheless, the activity obtained in the present study was found to be comparable (4 μ mol Q₁H₂ min⁻¹ mg⁻¹ protein) with that of rAtAOX1A, which is purified from the Δ hemA deficient *E. coli* strain (FN102), which lacks the quinol oxidase activity for cytochrome *bo* and *bd* complexes (Xu et al., 2021). In contrast, the activity of rTAO measured as quinol oxidizing activity was found to be 207

μmol min⁻¹ mg⁻¹ protein (Kido et al., 2010), while rSgAOX measured as oxygen uptake activity was found to be 20 μmol min⁻¹ mg⁻¹ protein (Elliott et al., 2014), respectively. The lower activity levels of rAtAOX1A in the present study could be due to its origin from a non-thermogenic plant *A. thaliana* (Moore et al., 2013). The docking studies of May et al. (2017) and Xu et al. (2021) indicated that the differences in the polar residues surrounding the hydrophobic cavity of the quinol binding site might change the size of the cavity, which, in turn, may lead to the differences in the strength of attraction of quinol into the active site, and, thereby, affect the activity of AOX enzyme in *A. thaliana*.

Highlights of the study

- ✓ AtAOX1A was successfully cloned into pET28a(+) vector and expressed in *E. coli* BL21(DE3) cells.
- ✓ E. coli/pAtAOX1A showed cyanide resistance, SHAM and n-PG sensitive respiration as well as growth, which indicates that the expressed rAtAOX1A is functionally active in E. coli.
- ✓ rAtAOX1A was separated from *E. coli* membranes by solubilizing in DDM and purified by passing through the His-tag cobalt affinity column.
- ✓ The rAtAOX1A possessed a molecular mass of ~37 kDa and purified to 11-fold with a specific activity of 3.86 µmol oxygen uptake/min/mg protein.
- ✓ Western blot and MALDI TOF/TOF analysis confirmed that the purified protein is rAtAOX1A.

Chapter 5

Structural and Biophysical Characterization of Purified rAtAOX1A with its Inhibitors

Structural and Biophysical Characterization of Purified rAtAOX1A with its Inhibitors

5.1. Introduction

The secondary structure of AOX from plants source was revealed for the first time by Elliott et al. (2014) in the thermogenic plant S. guttatum. The AOX belongs to the non-heme diiron carboxylate protein superfamily with six long ($\alpha 1 - \alpha 6$) and four short ($\alpha S1 - \alpha S4$) α -helices (Moore et al., 2013; Shiba et al., 2013). The helices α1 and α4 of TAO are bound to the IMM, and the other helices $(\alpha 2, \alpha 3, \alpha 5)$ and $\alpha 6$ form a four-helix bundle with catalytic diiron core, which catalyzes the reduction of O₂ upon binding with its substrate (UQH₂) (Moore et., 2013; Pennisi et al., 2016; May et al., 2017). However, from the non-thermogenic plants, the secondary structure of AOX is yet to be elusive. The protein secondary and tertiary structures are stabilized by the inter and intramolecular forces, which may get affected by the addition of interacting compounds. These inter and intramolecular structural changes can be studied using CD spectroscopic signals (Kelly and Price, 2005). The aim of the present study is (i) Secondary structural analysis and structural stability of purified rAtAOX1A at a wide range of temperature and pH conditions; (ii) Characterize the purified rAtAOX1A protein and its interaction with inhibitors, such as SHAM and n-PG, using biophysical studies like SPR, CD spectroscopy, fluorescence spectroscopy, and in silico molecular docking; (iii) Identifying the binding pockets of AOX substrates (DQ, DQH₂, UQ₁ and Q₁H₂) on AtAOX1A and comparing the inhibitor binding site with the substrate binding site on the AtAOX1A.

5.2. Results

CD spectroscopic analysis of secondary structure of rAtAOX1A and its stability at a wide range of temperatures and pH

CD spectroscopy is frequently used to study the secondary structure and its conformational state in proteins. It detects the difference in the absorption of left and right-handed circularly polarized light in optically active molecules such as proteins and is expressed in terms of ellipticity. In the CD spectroscopy graph, a combination of positive and negative peaks at defined wavelengths describe the nature of secondary structure, such as: (1) A positive peak at 192 nm and negative peaks at 208 and 222 nm represent an α-helical structure; (2) A positive peak at 195 nm, and a negative peak at 216 nm indicates a β-sheet structure; (3) A positive peak at 205 nm represents a β-turn, and (4) A negative peak at 200 nm, and a positive peak at 212 nm represents a random coil (Kelly and Price, 2000; Kelly et al., 2005). The secondary structural analysis of rAtAOX1A in Far-UV (190–260 nm) CD spectra indicated that it possesses an α -helical structure (Fig. 5.1). The presence of two negative peaks at 208 nm and 222 nm is a characteristic feature of the typical α-helical structure. The high tension (HT) voltage trace was shown as an inset in Fig. 5.1. Further, any change in the pH (2-12) caused only a marginal variation in the ellipticity of rAtAOX1A, as compared to the ellipticity observed at optimal pH 7.5 (Fig. 5.2). Similarly, the thermal treatment of rAtAOX1A showed only a marginal decrease in its ellipticity with a gradual increase in the temperature from 4° to 90°C (Fig. 5.3A). However, this effect was reversed by gradually cooling down the temperature from 90° to 4°C (Fig. 5.3B), suggesting that rAtAOX1A is structurally stable to heat treatment. Also, the protein has retained its helical absorbance signal (222 nm) up to \sim 67% despite an increase in temperature from 25° to 90°C (**Fig. 5.4**).

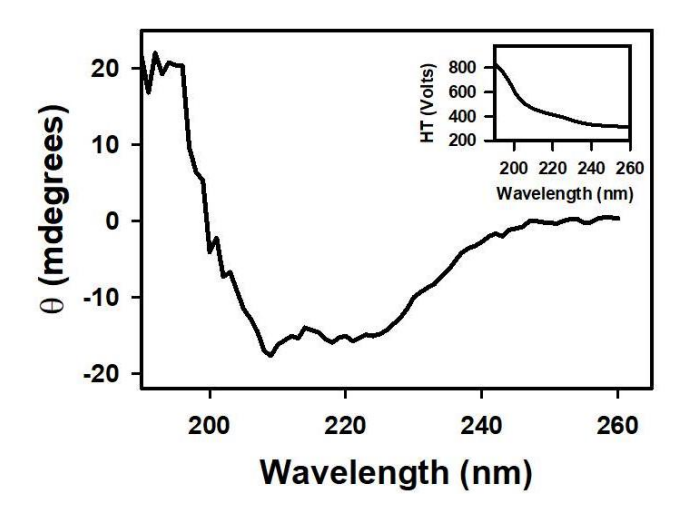


Fig. 5.1. Secondary structure of rAtAOX1A. CD spectra of purified rAtAOX1A at far-UV (190-260 nm) in 10 mM phosphate buffer (pH 7.5). Ellipticity in θ (mdeg) of rAtAOX1A (0.8 mg/ml) was plotted against the wavelength. Inset: High Tension profile of voltage trace. The final spectrum is an average of three scans, as described in the Materials and Methods section.

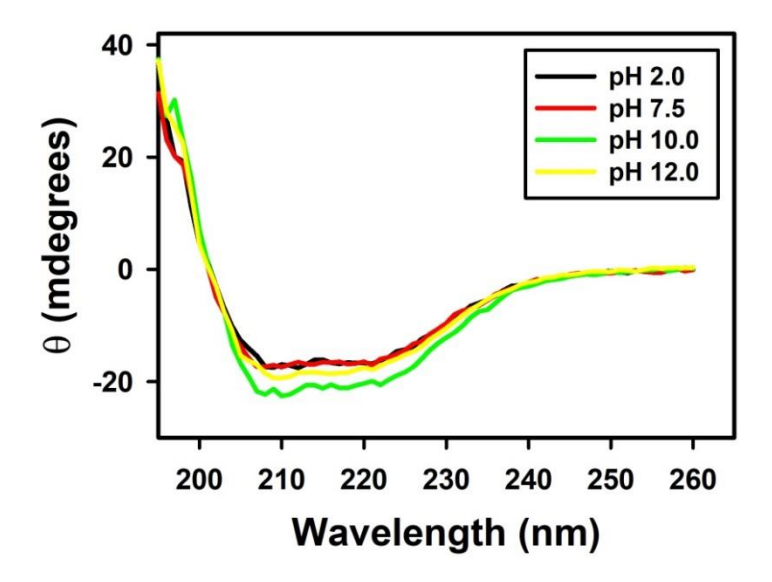


Fig. 5.2. CD spectra of rAtAOX1A (0.8 mg/mL) at far UV (190-260 nm), and the secondary structural stability was determined at different pH (2.0, 7.5, 10.0 and 12.0).

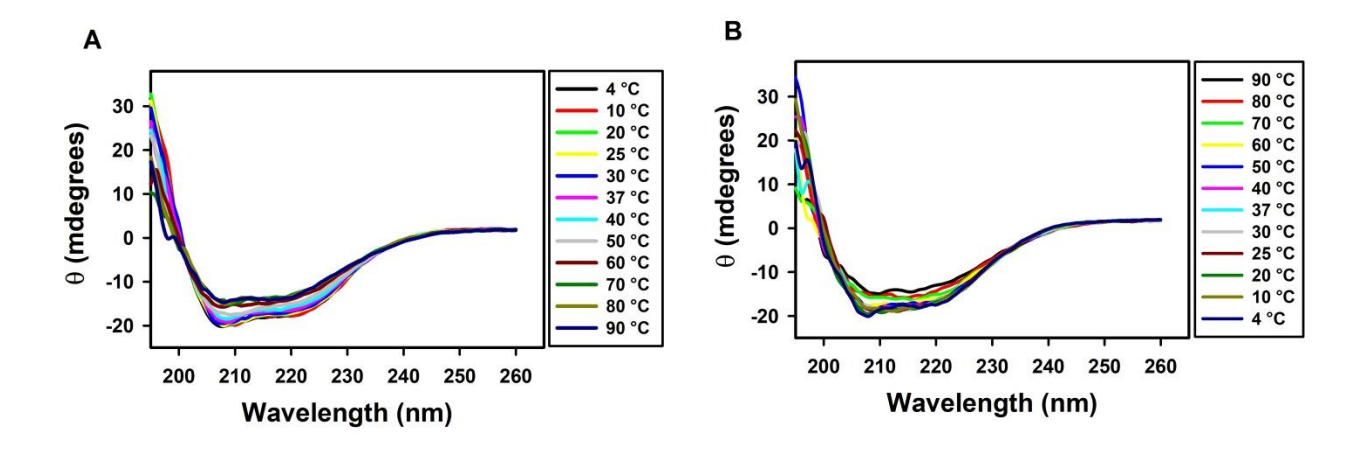


Fig. 5.3. The secondary structural stability of rAtAOX1A at far UV (190-260 nm) was determined at different temperatures. (**A**) Temperature from 4 to 90°C; (**B**) Temperature from 90 to 4°C.

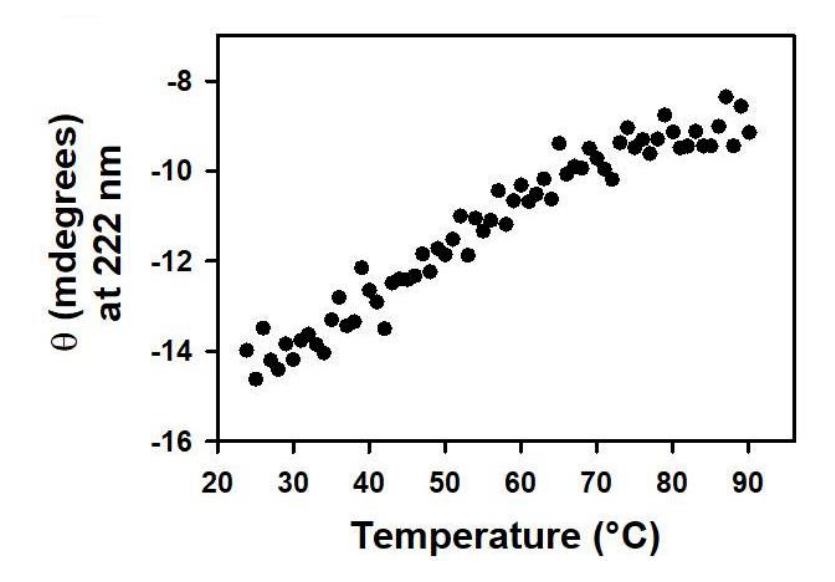


Fig. 5.4. Variation in the ellipticity of rAtAOX1A was measured at 222 nm between the 25°C to 90°C temperature range.

These results suggest that rAtAOX1A is highly stable at a wide range of pH and temperature conditions.

Molecular interaction analysis of rAtAOX1A with SHAM and n-PG

The alterations in secondary structural elements of purified rAtAOX1A upon the addition of SHAM and n-PG were determined separately by CD spectroscopy. The addition of different concentrations of SHAM and n-PG to rAtAOX1A has not shown any deviation in the helical absorbance signal in the CD spectrum observed between 190–260 nm. However, a marginal deviation in the negative peaks was observed (**Fig. 5.5A, B**). Further, the changes in the secondary structure composition of the rAtAOX1A in the presence of SHAM and n-PG were summarized in **Table 5.1**. The addition of both inhibitors (SHAM and n-PG) to the rAtAOX1A caused an increase in β -sheets (\sim 7%) with a concomitant decrease in α -helical (\sim 10%) content, while the changes in β -turns and random coils (together) are negligible (\sim 3%).

As the AtAOX1A protein contains nine Trp residues at 108, 123, 125, 131, 158, 165, 211, 237, and 305 positions (**Fig. 3.5**; **Chapter 3**), the fluorescence emission spectra of rAtAOX1A have shown a peak at 339 nm upon excitation (λ_{ex}) at 295 nm. The fluorescence emission spectra of rAtAOX1A, in the presence of different concentrations (0.05, 0.1 and 0.5 mM) of SHAM and n-PG, have shown significant changes in fluorescence intensity. The fluorescence emission profile of rAtAOX1A has shown a red shift (**Fig. 5.6A, B**), with maximum wavelength emission spectra changing from 339 nm (in the absence of inhibitors) to 358 nm at 0.5 mM SHAM and 378 nm at 0.5 mM n-PG indicating the protein

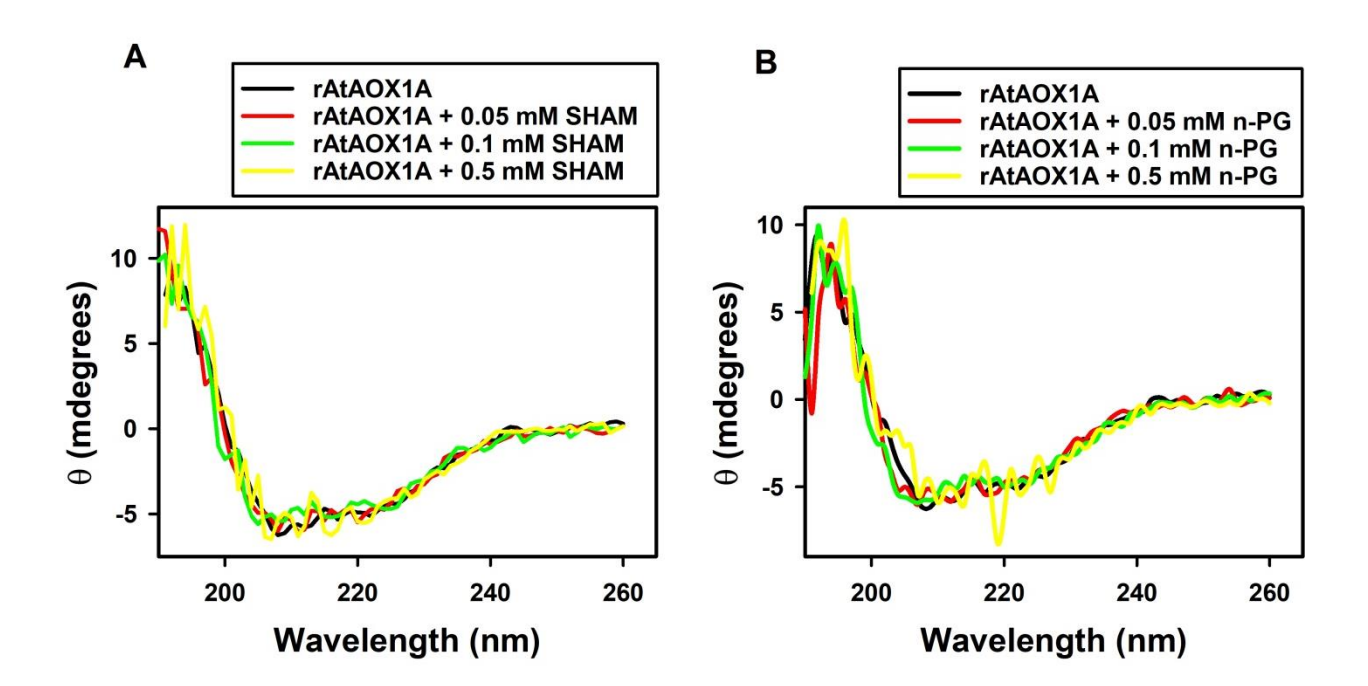


Fig. 5.5. CD spectra of rAtAOX1A at far UV (190–260 nm) with (**A**) 0.05, 0.1, and 0.5 mM SHAM, and without inhibitor; (**B**) 0.05, 0.1, and 0.5 mM n-PG and without inhibitor in 10 mM phosphate buffer (pH 7.5). The concentration of purified rAtAOX1A used to obtain the CD spectrum (SHAM and n-PG) was 0.4 mg/ml. The final spectrum is an average of three scans, as described in the Materials and Methods section.

Table 5.1. Modulation in rAtAOX1A secondary structural elements during interaction with SHAM and n-PG. The data is analyzed using the CDSSTR algorithm and reference set 4. Values represent the average of four to five scans.

Sample	Concentration of inhibitor	Predicted secondary structure elements (%)			
	or immortor	α-helix	β-sheet	β-turn	Random coil
rAtAOX1A	Control	53	22	5	20
rAtAOX1A	0.05 mM	42	29	7	21
+	0.1 mM	42	30	7	21
SHAM	0.5 mM	44	27	7	21
	0.025 mM	42	30	7	21
rAtAOX1A	0.05 mM	44	29	7	21
+	0.1 mM	48	26	6	21
n-PG	0.5 mM	42	30	7	21

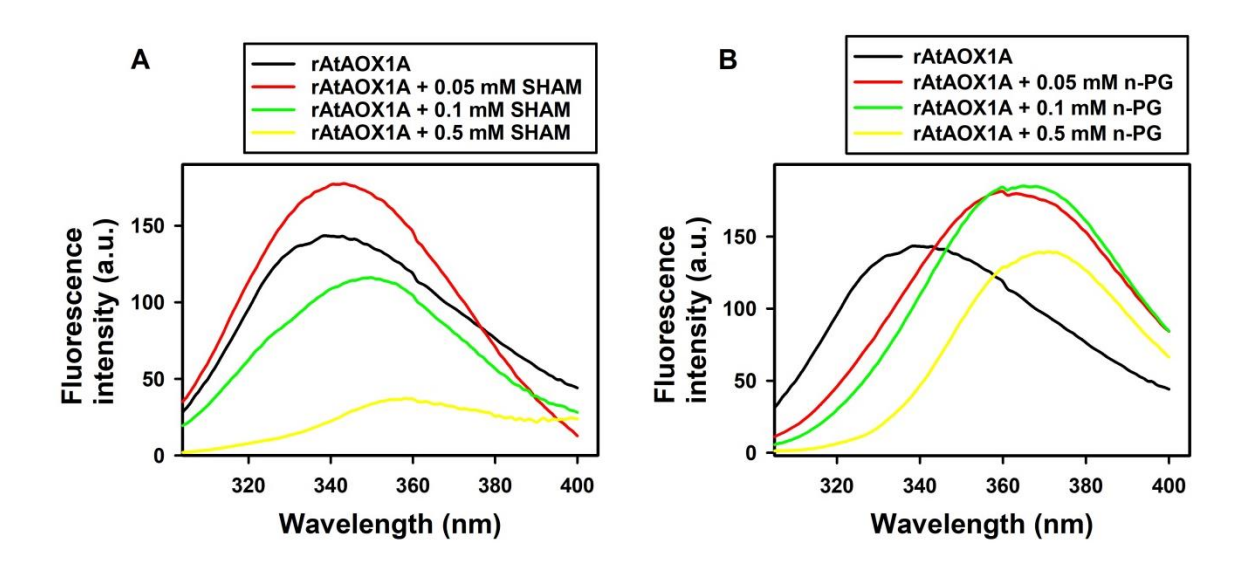


Fig. 5.6. Intrinsic fluorescence emission spectra of purified rAtAOX1A in the absence and presence of different concentrations (0.05, 0.1 and 0.5 mM) of inhibitors (**A**) SHAM and (**B**) n-PG. A 10 μM protein sample (rAtAOX1A) was prepared in 5 mM phosphate buffer at pH 7.5. Fluorescence emission spectra were obtained at 25°C, from 300 to 450 nm, with excitation at 295 nm. The final spectrum is an average of three scans, as described in the Materials and Methods section.

unfolding in the presence of inhibitor and tryptophan residues are in a more polar environment.

The SPR technique has been extensively used to study the molecular interaction of proteins with small-molecule(s) and in drug discovery due to its improved selectivity, stability, and sensitivity (Homola, 2003; Olaru et al., 2015). The binding events of the immobilized ligand and analytes are ascertained by monitoring the changes in the SPR signal (Response unit).

As the analyte is passed on an immobilized ligand through a microfluidic channel, the interaction between ligand and analyte leads to the formation of a complex structure, which causes a change in the mass on the sensor chip surface and, thereby, a change in the SPR signal of the sensorgram. This change/difference in the signal is used to derive kinetic constants for both complex formation (association) and its dissociation in a particular molecular interaction between a ligand and an analyte (Nguyen et al., 2015). The mechanism of rAtAOX1A interaction with SHAM and n-PG is characterized by the SPR technique. The analytes (SHAM and n-PG) are allowed to pass independently through both Fc-3 (reference/blank flow cell) and Fc-4 (rAtAOX1A immobilized flow cell). The binding of SHAM and n-PG with immobilized rAtAOX1A at different concentrations (1 to 5 mM) was visualized in the sensorgrams as the rate of increase in RU of Fc-4 [note: The RU of corresponding analytes in blank/reference flow cell (Fc-3) is subtracted automatically] (Fig. **5.7A, B).** From these sensorgrams, association, dissociation, and steady-state interaction kinetics of SHAM and n-PG with rAtAOX1A were calculated. SHAM has shown an equilibrium dissociation constant $K_D = 3.08 \times 10^{-9} \text{ M}$ with the following association

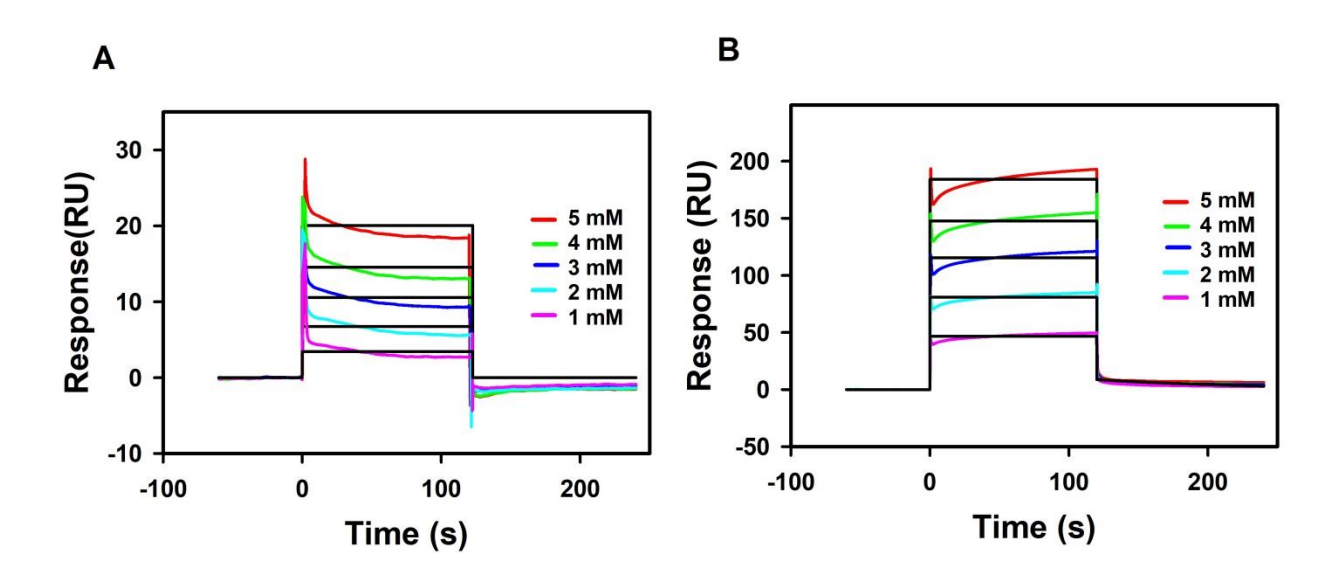


Fig. 5.7. SPR kinetics of SHAM and n-PG with rAtAOX1A. Binding curves for **(A)** SHAM and **(B)** n-PG with rAtAOX1A at 25°C. The colored lines represent the concentrations of SHAM/n-PG (1, 2, 3, 4, and 5 mM), the black lines correspond to the fit lines to the data, and each fit line is a result of a global fit. The final sensorgram is representative of three cycles.

 $(k_a = 1.11 \text{ x } 10^5 \text{ M}^{-1} \text{ s}^{-1})$ and dissociation $(k_d = 3.40 \text{ x } 10^{-4} \text{ s}^{-1})$ rate constants. Similarly, the kinetic parameters measured for n-PG have shown equilibrium dissociation constant $K_D = 4.91 \text{ x } 10^{-10} \text{ M}$ with the following association $(k_a = 1.80 \text{ x } 10^7 \text{ M}^{-1} \text{ s}^{-1})$ and dissociation $(k_d = 8.85 \text{ x } 10^{-3} \text{ s}^{-1})$ rate constants. These results suggest that the n-PG (~0.49 nM) has more affinity to rAtAOX1A than SHAM (~3 nM). However, both the inhibitors bind reversibly to the rAtAOX1A, which is evident by the changes in the RU observed during their association and dissociation in corresponding sensorgrams (**Fig. 5.7A, B**).

The interaction of the ligands (SHAM and n-PG) with AtAOX1A was examined by the in silico molecular docking and mutational docking studies. SHAM and n-PG inhibit the transfer of electrons through the AOX pathway. Panel (a) in **Fig. 5.8Aa**, **Ba** shows the most probable binding sites on AtAOX1A for SHAM & n-PG and panel (b) shows their corresponding binding pocket. According to the SwissDock results, SHAM and n-PG bind to the same binding pocket made up of Met191, Val192, Met195, Leu196, Phe251, and Phe255 (**Fig. 5.8Ab**, **Bb**). The binding energies of SHAM and n-PG are found to be –6.01 and –6.13 kcal/mol, respectively.

Mutational docking studies of AtAOX1A with SHAM and n-PG

To identify the potent residues on AtAOX1A that may have a direct impact on the binding of SHAM and n-PG, point mutations were performed concerning three hydrophobic residues: (i) Met195 to Ala, (ii) Leu196 to Ala, and (iii) Phe255 to Ala in the inhibitor binding pocket (**Fig. 5.9A, B**). The side chains of these residues lie within 3Å from the ligand as the hydrophobic interactions between the ligand and side chains hold the ligand in its binding

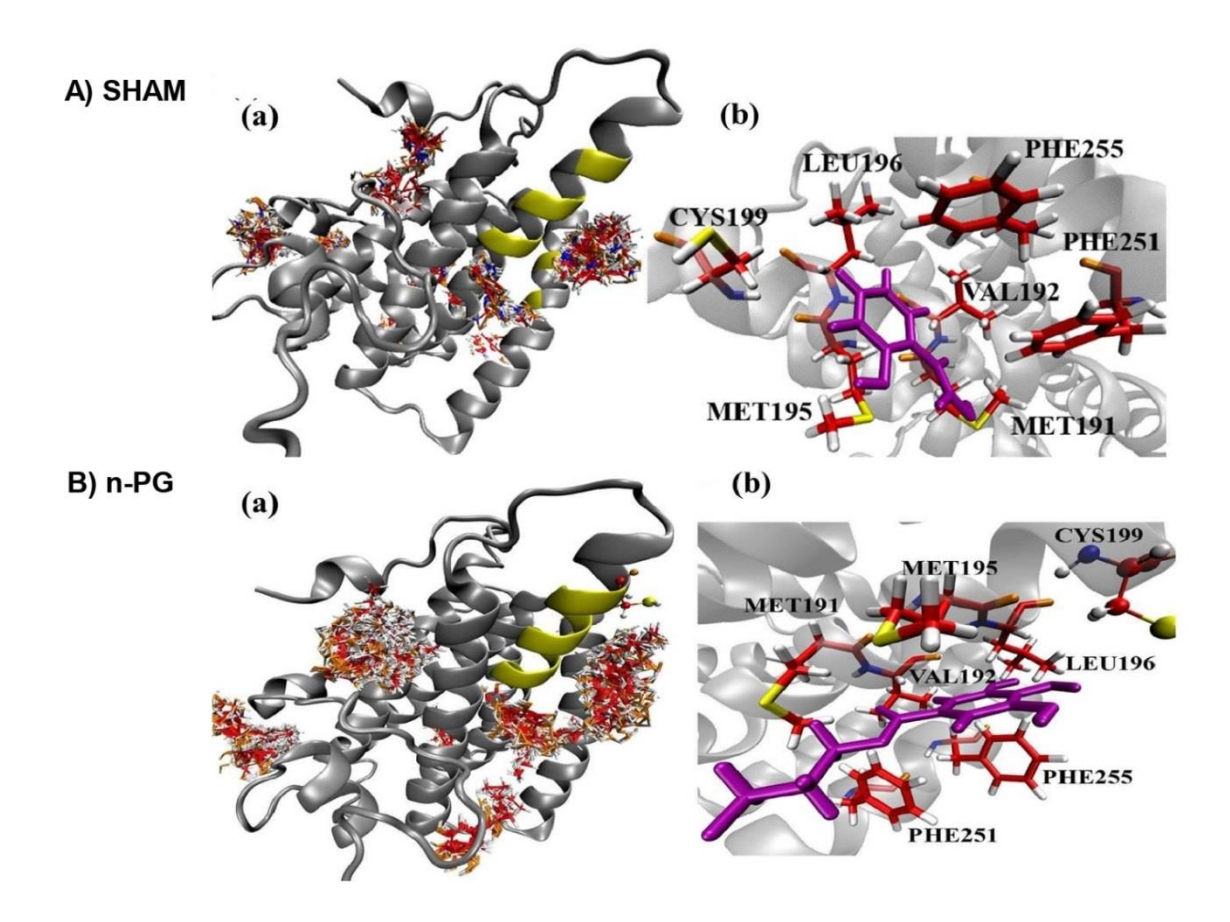


Fig. 5.8. Molecular docking of AtAOX1A with (**A**) SHAM and (**B**) n-PG. (a) All possible binding pockets of a specific ligand on AtAOX1A. The yellow region on AtAOX1A secondary structure indicates the best-fit binding pocket of a particular ligand. (b) residues of AtAOX1A that are involved in forming the binding pocket of the best model (Cluster 0 Element 0), according to SwissDock results. SHAM and n-PG are shown in purple. Color scheme: carbon (red), oxygen (orange), sulfur (yellow), nitrogen (blue), and hydrogen (white).

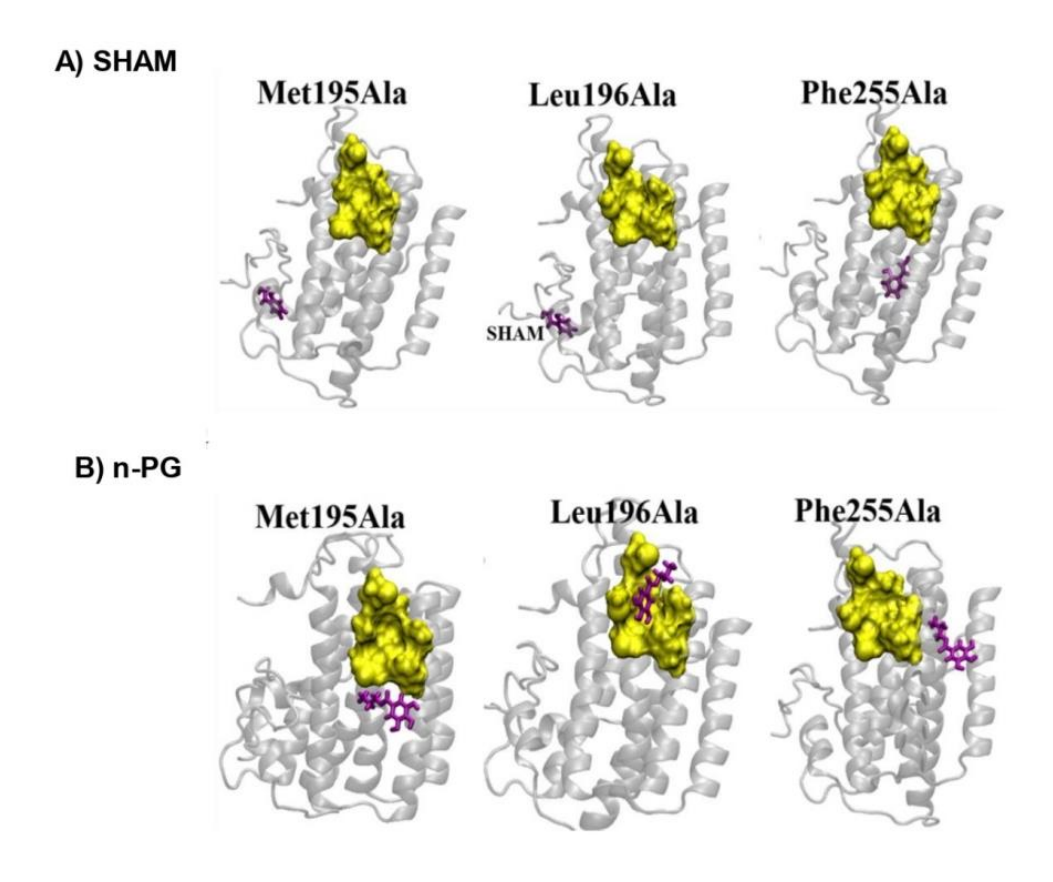


Fig. 5.9. Effect of mutation on the binding affinities of SHAM (**A**) and n-PG (**B**). The yellow surface indicates the location of the binding pocket in wild-type (WT) AtAOX1A. The location of the ligand on the mutant AtAOX1A is shown in purple.

pocket. Interestingly, upon mutations of Met195, Leu196, and Phe255 to alanine, the SHAM and n-PG binding locations are drastically altered in comparison to that of the WT AtAOX1A (**Fig. 5.9A**, **B**). However, the mutation of Leu196 did not alter the binding pocket of n-PG (**Fig. 5.9B**).

Identification of substrate binding location and comparison with inhibitor binding location using molecular docking

The interaction of the following ligands with AtAOX1A was examined by the in silico molecular docking and mutational studies: (i) Q₁H₂ (reduced form of ubiquinone), which plays a significant role in the transfer of electrons from complex I and complex II of miETC to AOX and its oxidized form (UQ₁), which is released from the AOX after the donation of electrons by Q₁H₂ to its catalytic center under in vivo conditions; (ii) DQH₂ (reduced form of duroquinone), an analog of UQH₂ and electron donor to AOX under in vitro conditions, and its oxidized form (DQ) that is released from AOX after electron donation by DQH₂ to its catalytic center.

Panel (a) in **Fig. 5.10** shows the most probable binding sites on AtAOX1A for (I) UQ₁, (II) Q₁H₂, (III) DQ and (IV) DQH₂ and panel (b) shows their corresponding binding pocket. The Q₁H₂ binding site (**Fig. 5.10IIb**) is composed of Trp131, Glu132, Thr133, Tyr134, Lys135, Ile138, Trp305, Arg306, Leu307, Pro308, and Asp315, while Q₁H₂ makes hydrogen bonds with Trp131 and Arg306, and forms a stable complex with $\Delta G = -7.05$ kcal/mol. The ubiquinone or ubiquinone-1 (with one isoprenoid unit) binding pocket (**Fig. 5.10Ib**) is made up of Leu163, Thr167, Phe171, Met181, Leu182, Val185, Leu242, Thr245, Val246, Val249, and Phe250, respectively, and the ligand is mostly hydrophobic due to the

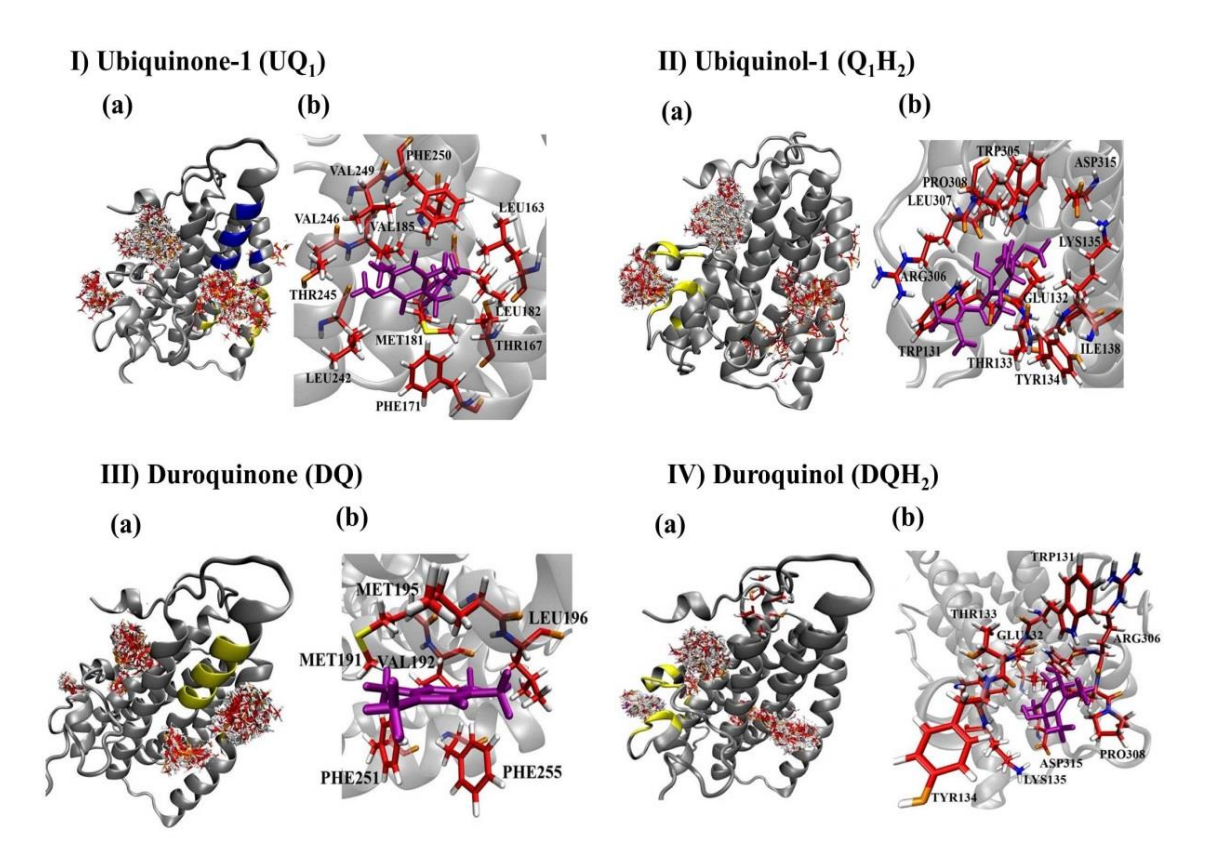


Fig. 5.10. Molecular docking of AtAOX1A with its substrates (**I-IV**). (**a**) All possible binding pockets of a specific ligand on AtAOX1A. The yellow region on AtAOX1A secondary structure indicates the best-fit binding pocket of a particular ligand. The Blue region in panel (**IIa**) represents the inhibitor binding pocket to compare with that of UQ, and (**b**) residues of AtAOX1A that are involved in forming the binding pocket of the best model (Cluster 0 Element 0) according to SwissDock results. The ligands (**I**) UQ₁, (**II**) Q₁H₂, (**III**) DQ and (**IV**) DQH₂ are shown in purple. Color scheme: carbon (red), oxygen (orange), sulfur (yellow), nitrogen (blue), and hydrogen (white).

presence of five methyl groups. The binding energy of UQ₁ in this pocket is $\Delta G = -6.74$ kcal/mol. The binding pocket for DQH₂ consists of Trp131, Glu132, Thr133, Tyr134, Lys135, Arg306, Pro308, and Asp315 (**Fig. 5.10IVb**). The binding energy of DQH₂ to the AtAOX1A is $\Delta G = -6.63$ kcal/mol. Interestingly, DQH₂ and Q₁H₂ bind in the same location that is close to the diiron cavity (**Fig. 5.11A**). According to the SwissDock results, the binding pocket of DQ is made up of Met191, Val192, Met195, Leu196, Phe251, and Phe255 (**Fig. 5.10IIIb**). The binding energy of DQ to the AtAOX1A is $\Delta G = -6.11$ kcal/mol. This surface-exposed, hydrophobic region of DQ is located on the 2nd and 4th α -helices and is \sim 27Å away from the diiron center. According to the SwissDock results, SHAM and n-PG bind to the same binding pocket (**Fig. 5.8Ab, Bb**) as that of DQ. The **Figure 5.11A, B** compares the location of the diiron cavity with the inhibitor and Q₁H₂/ DQH₂ and UQ₁ binding sites, respectively. It was observed that the UQ₁ binding site bridges the diiron cavity and the inhibitor binding site.

5.3. Discussion

Structural characterization of purified rAtAOX1A and its interaction with inhibitors

In this study, the structure of rAtAOX1A and the changes in the corresponding structure during interaction with its inhibitory (SHAM and n-PG) molecules are revealed by CD spectroscopy. Besides, the docking and SPR studies identified the specific binding pockets for these molecules on AtAOX1A and revealed their binding energies/affinities during interaction with rAtAOX1A.

Analysis of far-UV (190–260 nm) CD spectra reveals the secondary structural elements such as α -helices and β -sheets present in a protein. The CD results from the present

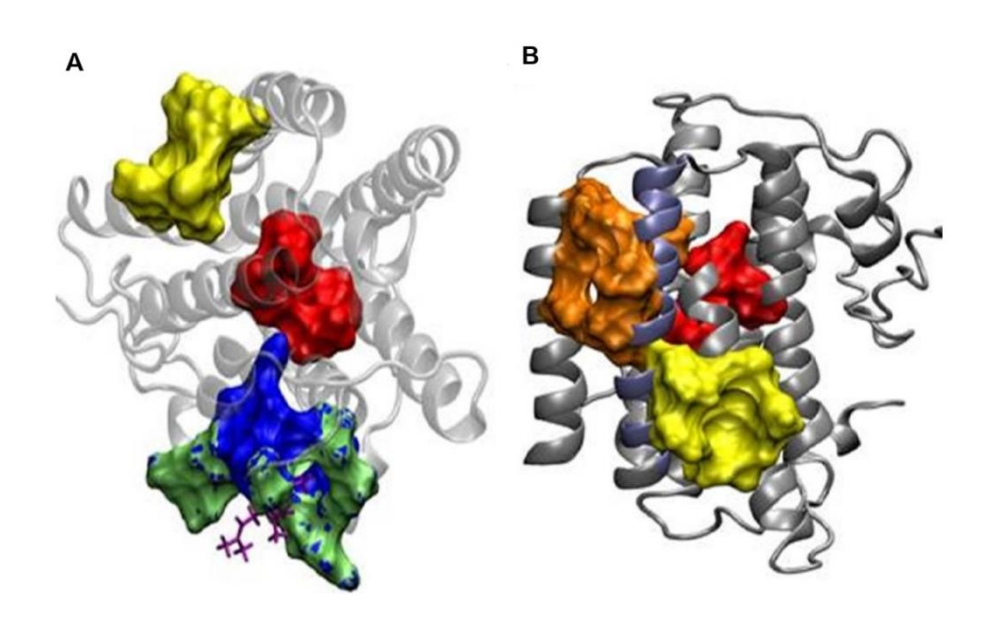


Fig. 5.11. Molecular docking of AtAOX1A with substrates and inhibitors. (**A**) Binding pockets of inhibitor (yellow), DQH_2 (green surface), Q_1H_2 (blue surface), and diiron binding cavity (red surface). DQH_2 is shown with purple sticks. (**B**) Binding pockets of inhibitor (yellow surface), UQ_1 (orange surface), and diiron cavity (red surface).

study have revealed that the purified rAtAOX1A possessed α -helices predominantly over β -sheets in its secondary structure (**Fig. 5.1** and **Table 5.1**), and this result is consistent with the secondary structural elements of rTAO and rSgAOX (Elliott et al., 2014). Besides, the following observations in this study, such as (i) stability in the ellipticity of rAtAOX1A to a wide range of temperatures (**Fig. 5.3A, B**) and (ii) retention of its helical absorbance signal up to 67% even at temperatures as high as 90°C (**Fig. 5.4**), indicated that the thermal stability of rAtAOX1A isoform from a non-thermogenic plant *A. thaliana* is comparable to that of rAOX from thermogenic plant *S. guttatum* and rTAO from a parasitic protozoan (Elliott et al., 2014). Further, the retention of the helical signal even at a wide range of pH conditions indicated the stability of the rAtAOX1A to changes in pH (**Fig. 5.2**). Besides, a decrease in the α -helical content and a rise in the β -sheets in rAtAOX1A upon interaction with SHAM and n-PG demonstrated the conformational changes occurring in the protein, possibly due to a rearrangement in the hydrogen bond network of the secondary structural elements (Hebia et al., 2014; Yu et al., 2021; **Fig. 5.5A, B** and **Table 5.1**).

Further, a red shift in the fluorescence emission spectra of rAtAOX1A with its inhibitors (SHAM and n-PG) was observed (Fig. 5.6A, B), which indicates that the hydrophobic groups of the protein are exposed to the polar environment and this might be due to the unfolding of rAtAOX1A upon interaction with its inhibitors. These results demonstrate that the rAtAOX1A interacts with its inhibitors and this interaction was associated with a remarkable change in the microenvironment of tryptophan residues of the protein.

Furthermore, the SPR technique, which is known to provide real-time label-free binding kinetics, is used to analyze the interaction of rAtAOX1A with its inhibitors. The

kinetic data obtained for n-PG and SHAM during their interaction with rAtAOX1A fitted well with the 1:1 Langmuir model. Also, n-PG ($K_D = 0.49$ nM) showed a higher affinity with rAtAOX1A than SHAM ($K_D = 3$ nM), as the K_D is inversely proportional to the binding affinity (**Fig. 5.7A, B**). Also, a positive correlation was observed between the K_D values (an indicator of binding affinity) obtained in this study with the IC₅₀ values (an indicator of the inhibition potency) obtained for n-PG and SHAM against rAOX from different sources (Elliott et al., 2014; May et al., 2017; Xu et al., 2021). For example, the results from the studies of Xu et al. (2021) indicated that the n-PG inhibits rAtAOX1A at a concentration of ~1.58µM (IC₅₀), while SHAM inhibits at a concentration of ~33 µM (IC₅₀).

In the case of plants, the crystal structure of AOX is not yet available so far. Therefore, in the docking studies, we used the homology model generated for AtAOX1A (PMDB Accession number: PM0080189), using the crystal structure of TAO (PDB ID: 3VV9) as a template (Pennisi et al., 2016). The studies of Pennisi et al. (2016) also predicted the protein structure for N-terminal 31 residues (residues 63–93) of AtAOX1A by ab initio/threading program. Thus, irrespective of the origin, AOX possessed a common structural trend of forming a four-α-helix bundle with a diiron catalytic center.

The AOX1A from *A. thaliana* contained three domains: (i) a mitochondrial recognition signal peptide domain between residues 1 and 62, which detaches from AOX after mitochondrial recognition; (ii) a predicted region in the N-terminus between residues 63 and 93; and (iii) a catalytic domain between residues 94 and 354 that is responsible for the oxidation of ubiquinol, binding of activators and inhibitors, and reduction of an oxygen molecule to water. However, the model generated by Pennisi et al. (2016) includes only the catalytic domain of AtAOX1A, and the tunnel formed by four α -helices (α 2, α 3, α 5, and α 6)

in this model has two prominent hydrophobic regions: (i) a catalytic cavity consisting of conserved glutamate and histidine residues (Glu183, Glu222, Glu273, Glu324, His225, and His327) hosting the diiron center and (ii) a second region with conserved residues Arg164, Asp168, Arg178, Leu182, Ala186, Leu272, Glu275, and Ala276 connects the first hydrophobic region with the lipid bilayer facing the mitochondrial matrix. Further, the monomer-monomer binding region lies between residues 94 and 127 of each monomer. However, this choice can have the least effect on the binding affinities of SHAM and n-PG as the inhibitor binding sites are far away from the monomer-monomer interacting region.

Furthermore, the analysis of binding sites for the molecules like Q₁H₂, UQ₁, DQH₂, DQ, SHAM, and n-PG on AtAOX1A using the molecular docking method indicated that because the structural and functional similarities between Q₁H₂ and DQH₂, the binding cavities of these two ligands are found to be identical to some extent (Fig. 5.10IIb, IVb). As observed in TAO (Shiba et al., 2013), this binding cavity is near the diiron cavity formed by four glutamate residues (Glu183, Glu222, Glu273, and Glu324), but the inhibitor binding site is far from this Q1H2 and DQH2 binding cavity (Fig. 5.11A). Further, the UQ1 binding site (Fig. 5.10Ib) is somewhat similar to that of the inhibitor (SHAM and n-PG) binding site as both are: (i) composed of hydrophobic residues and (ii) share α -2 and α -4 helices. Our results also show that the UQ₁ binding site is slightly away from that of the inhibitor. The inhibitor and UQ₁ binding pockets and diiron cavity have been shown in the surface model (Fig. **5.11B**). Besides, DQ binding site (**Fig. 5.10IIIb**) is similar to that of the inhibitor (SHAM and n-PG) binding site. Thus, the binding of the inhibitors to a hydrophobic groove formed by the residues Met191, Val192, Met195, Leu196, Phe251, and Phe255 in AtAOX1A might block the electron transport through the AOX pathway (Fig. 5.8Ab, Bb). The mutational docking studies suggest that Met195 and Phe255 of AtAOX1A are the potential candidates to bind the inhibitors (**Fig. 5.9A, B**). Hence, this binding pocket could be a potential "gateway" for the oxidation and reduction process in AtAOX1A.

According to the docking studies of Shiba et al. (2013), the inhibitor AF2279OH binds to the Q_1H_2 binding site on TAO, while the results from the present docking studies indicated that the Q_1H_2 / DQH₂ binding sites are different from that of inhibitors (SHAM and n-PG) binding pocket on AtAOX1A (**Fig. 5.11A**). Also, the UQ₁ (oxidized form of Q₁H₂) binding site is slightly away from that of the inhibitor (**Fig. 5.11B**). However, the inhibitors (SHAM and n-PG) bind at the DQ (oxidized form of DQH₂) binding site. This difference in the inhibitor binding site in TAO and AtAOX1A could be due to the difference in the amino acid sequences, where the sequence similarity between them (TAO and AtAOX1A) is only 31.04% (Xu et al., 2021). Taken together, the results obtained from CD, fluorescence, SPR, and docking studies suggest that binding of SHAM or n-PG to a specific hydrophobic groove associated with α 2 and α 4 helices on AtAOX1A might alter its α -helical conformation, which in turn may lead to the inhibition of AOX pathway.

Highlights of the study

- ✓ CD studies revealed that >50% of rAtAOX1A existed in α-helical conformation and retained its helical absorbance signal (ellipticity) at a wide range of temperatures (4 to 90°C) and pH (2 to 12).
- \checkmark CD spectra showed a decrease in the α- helical content of rAtAOX1A upon interaction with SHAM and n-PG, while fluorescence emission studies showed a red shift in the spectrum, which indicates the unfolding of rAtAOX1A during its interaction with inhibitors.

- ✓ SPR studies revealed that both n-PG and SHAM bind reversibly to rAtAOX1A; however, n-PG showed higher binding affinity SHAM.
- ✓ The molecular docking studies revealed that they bind to the same hydrophobic groove to which Duroquinone (oxidized form AOX substrate Duroquinol) binds in the rAtAOX1A.
- ✓ Mutational docking studies revealed that Met195 and Phe255 are the potential candidates to bind the inhibitor. Hence, this binding pocket could be a potential gateway for the oxidation-reduction process in AtAOX1A.
- ✓ Molecular docking studies revealed that the AOX substrates DQH₂ and UQH₂ bind to the same binding pocket, while the UQ₁ (oxidized form) binding site bridges the diiron cavity and inhibitors binding site.

Chapter 6

Interaction of rAtAOX1A with Pyruvate and TCA cycle Metabolites using Docking and Biophysical Studies

Interaction of rAtAOX1A with Pyruvate and TCA cycle Metabolites using Docking and Biophysical Studies

6.1. Introduction

The AOX from non-thermogenic plants plays an essential physiological role in maintaining the function of the miETC and cellular metabolic homeostasis under stress (Dinakar et al., 2010a; Vanlerberghe, 2013; Vishwakarma et al., 2015, 2016). It is well documented that at the protein level, the activity of AOX is regulated post-translationally by α -keto acids/organic acids under stress conditions (Carré et al., 2011; Moore et al., 2013). This activation of AOX is found to be isoform-specific (Selinski et al., 2018a; Xu et al., 2021). But, how these metabolites interact with AOX and does this interaction cause any subsequent structural changes in AOX is not known. This information might help to understand the activation of AOX by different α-keto acids and TCA cycle metabolites to maintain cellular metabolic homeostasis under various physiological/stress conditions. Therefore, the present study aimed (i) To identify any binding pockets on the surface of rAtAOX1A and the potential amino acid residues involved in binding with pyruvate or other TCA cycle metabolites by the molecular mutational docking studies; (ii) To analyze the real-time binding and kinetic constants of these different metabolites with purified rAtAOX1A using SPR; and (iii) To examine if the binding of these metabolites to rAtAOX1A cause any conformational changes in the structure of rAtAOX1A using CD and fluorescence spectroscopic studies. The chemical structures of pyruvate and TCA cycle metabolites used in the present study are shown in **Table 6.1**.

Table 6.1. Chemical structures of pyruvate and TCA cycle metabolites used in the analysis of interaction with rAtAOX1A

Sl. No	Name of the compound	PubChem CID	Chemical formula	Structure	Mol. Weight
1.	Pyruvate	107735	C ₃ H ₃ O ₃	0	87.05
2.	Citrate	31348	C ₆ H ₅ O ₇ ⁻³	0 - 0 - 0 - 0 - 0 - 0 - 0 - 0 - 0 - 0 -	189.10
3.	α-KG	164533	C ₅ H ₄ O ₅	.0.	144.08
4.	Succinate	160419	C ₄ H ₄ O ₄ ⁻²	0: 0.	116.07
5.	Fumaric acid	444972	C ₄ H ₄ O ₄	H. 0 H	116.07
6.	Malic acid	525	C ₄ H ₆ O ₅	H. O O.H	134.09
7.	OAA	970	C ₄ H ₄ O ₅	H. 0 0 ,H	132.07

6.2. Results

Molecular docking of AtAOX1A with pyruvate and TCA cycle metabolites

The docking studies revealed binding pockets for pyruvate and various TCA cycle metabolites in the wild-type (WT) AtAOX1A and the binding affinity corresponding to each of the metabolites is identified (**Table 6.2**). The metabolites pyruvate and fumaric acid are found to have independent binding sites, while no binding site was identified for succinate on WT AtAOX1A. Contrarily, conserved locations are identified on the protein surface for the binding of the following metabolites: (i) citrate and α -KG and (ii) malate and OAA.

The pyruvate binds in the groove formed by Arg174, Tyr175, Gly176, Cys177, Val232, Ala233, Asn294, and Leu313 with $\Delta G = -6.87$ kcal/mol (**Table 6.2**). Among these residues, the mutation of Arg174, Gly176 or Cys177 to Ala did not allow the binding of pyruvate to its binding pocket (**Table 6.3**; **Sl. No. 1**). Thus, the mutational docking studies revealed the importance of all three residues in interacting with WT-AtAOX1A.

Further, both citrate and α -KG bind in the same groove formed by Thr184, Ala187, Arg223, Leu226, Met227, Met230, Val243, and Gly247 with Δ G of -8.11 and -7.12 kcal/mol, respectively (**Table 6.2, Sl. No. 2 & 3**). Among these amino acid residues, Arg223 and Gly247 are closest (within 3Å) to the ligand and form H-bonds. Further, mutational docking studies with AtAOX1A revealed which among them are potent and involved in binding with citrate and/or α -KG (**Table 6.3, Sl. No. 4-7**). Upon Arg223Ala mutation, citrate could not bind to its WT binding pocket, whereas the mutation of Gly247Ala has not altered the location of the ligand binding site. These results suggest that Arg223 of the binding pocket might play a crucial role in binding with citrate (**Table 6.3, Sl. No. 4 & 5**). Contrarily,

Table 6.2. Molecular docking of pyruvate and TCA cycle metabolites on Wild-Type AtAOX1A. Color scheme: Ligand (purple), carbon (red), nitrogen (blue), oxygen (orange), sulfur (yellow), hydrogen (white). The secondary structure of AtAOX1A is shown in grey color. Parentheses indicate the position of amino acid residue in the AtAOX1A along with α-helical chain number.

Sl. No.	Ligand	Residues in the binding pocket (helix No.)		Binding pocket
1.	Pyruvate	Arg174(loop), Tyr175(α2), Gly176(α2), Cys177(α2), Val232(α3), Ala233(loop), Asn294(loop), Leu313(α6)		ASN294 TYR175 ALA233 GLV176 CYS177 ARG174
2.	Citrate	Thr184(α2) Ala187(α2) Arg223(α3) Leu226(α3) Met227(α3) Met230(α3) Val243(α4) Gly247(α4)	-8.11	ARG223 ALA187 GLY247 THR184 LEU226 WAL243

3.	α-KG	Thr184(α2) Ala187(α2) Arg223(α3) Leu226(α3) Met227(α3) Met230(α3) Val243(α4) Gly247(α4)	-7.12	ARG223 ALA187 THR184 GLY247 LEU226 VAL243
4.	Succinate			Not detected
5.	Fumaric acid	Val160(α1) Leu163(α1) Arg164(α1) Thr167(α1) Asp168(α1) Arg178(α2) Leu182(α2) Val185(α2) Phe250(α4) Leu272(α5) Glu275(α5)	-5.96	ASP168 ARG178 THR167 LEU182 ARG164 VAL185 CLEU272 LEU163 VAL160 PHE250
6.	Malic acid	Trp131(loop) Glu132(loop) Thr133(loop) Tyr134(loop) Lys135(S3) Trp305(S4) Arg306(loop) Leu307(loop) Pro308(loop) Ala311(loop) Asp315(α6) Met318(α6) Val319(α6)	-6.24	TRP131 GLU132 ARG306 THR133 VAL319 TYR134 LEU307 PRO308 ASP315 MET318 LYS135

7.	OAA	Trp131(loop) Glu132(loop) Thr133(loop) Tyr134(loop) Lys135(S3) Trp305(S4) Arg306(loop) Leu307(loop) Pro308(loop) Ala311(loop) Asp315(α6) Met318(α6) Val319(α6)	-6.27	ARG306 TRP131 GLU132 THR133 VAL319 TYR134 LEU307 PRO308 MET318 ALA311 ASP315 LYS135
----	-----	--	-------	--

Table 6.3. Molecular docking of pyruvate and TCA cycle metabolites on mutant AtAOX1A. Parentheses indicate residues within 3Å from the ligand in WT. These potent residues are mutated to Alanine in AtAOX1A to understand their importance in binding with ligands.

Sl. No.	Ligand	Mutation (Residues within 3Å from ligand in WT- AOX1A)	Binding pocket (WT binding surface is in yellow)	Remarks
1.	Pyruvate	Arg174Ala		Ligand does not bind into WT binding pocket upon Arg174Ala mutation. Thus, Arg174 is a potent binding residue to bind pyruvate
2.	Pyruvate	Gly176Ala		Ligand does not bind into WT binding pocket upon Gly176Ala mutation. Thus, Gly176 is a potent binding residue to bind pyruvate
3.	Pyruvate	Cys177Ala		Ligand does not bind into WT binding pocket upon Cys177Ala mutation. Thus, Cys177 is a potent binding residue to bind pyruvate

4.	Citrate	Arg223Ala	Ligand does not bind into WT binding pocket upon Arg223Ala mutation. Thus, Arg223 is a potent binding residue to bind citrate
5.	Citrate	Gly247Ala	Ligand binds into WT binding pocket upon Gly247Ala mutation. Thus, it is not a potent binding residue for citrate
6.	α-KG	Arg223Ala	Ligand does not bind into WT binding pocket upon Arg223Ala mutation. Thus, it is a potent binding residue to bind α-KG
7.	α-KG	Gly247Ala	Ligand does not bind into WT binding pocket upon Gly247Ala mutation. Thus, it is a potent binding residue to bind α-KG

8.	Fumaric acid	Thr167Ala	Ligand does not bind into WT binding pocket upon Thr167Ala mutation. Thus, it is a potent binding residue to bind fumaric acid.
9.	Fumaric acid	Glu275Ala	Ligand does not bind into WT binding pocket upon Glu275Ala mutation. Thus, it is a potent binding residue to bind fumaric acid.
10.	Malic acid	Trp305Ala	Ligand binds into WT binding pocket upon Trp305Ala. Thus, it is not a potent binding residue to bind malic acid.
11.	Malic acid	Asp315Ala	Ligand does not bind into WT binding pocket upon Asp315Ala mutation. Thus, it is a potent binding residue to bind with malic acid.

12.	OAA	Trp305Ala	Ligand binds into WT binding pocket upon Trp305Ala mutation. Thus, it is not a potent residue to bind OAA
13.	OAA	Asp315Ala	Ligand does not bind into WT binding pocket upon Asp315Ala mutation. Thus, it is a potent binding residue to bind with OAA

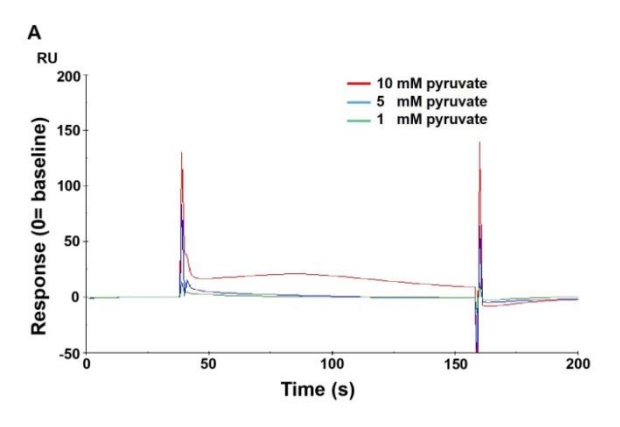
the mutational docking studies revealed that both Arg223 and Gly247 are found to be important for the binding of AtAOX1A with α -KG (**Table 6.3, Sl. No. 6 & 7**).

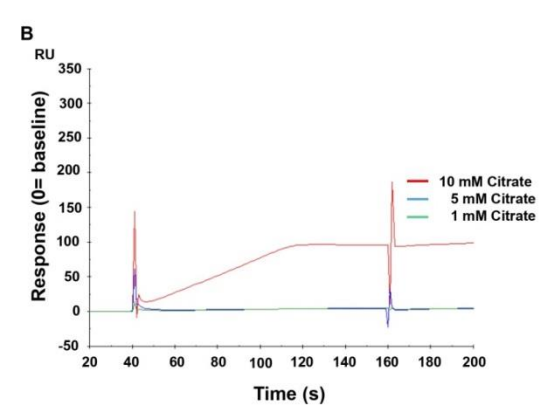
The fumaric acid interacts with a binding pocket of AtAOX1A formed by Val160, Leu163, Arg164, Thr167, Asp168, Arg178, Leu182, Val185, Phe250, Leu272 and Glu275 with ΔG of -5.96 kcal/mol (**Table 6.2, Sl. No. 5**). Among these residues, the side chain of Thr167 and Glu275 are in close proximity with fumaric acid, where the former makes H-bond with the ligand. Also, site-specific mutation of these residues to alanine shifted the binding location away from the site on WT protein, which signifies the importance of both of these residues in binding to fumaric acid (**Table 6.3, Sl. No. 8 & 9**).

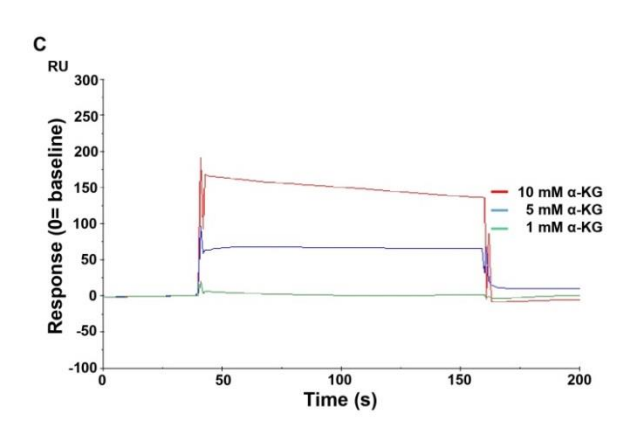
The present study also revealed that both malic acid and OAA bind to the same binding pocket, which is composed of Trp131, Glu132, Thr133, Tyr134, Lys135, Trp305, Arg306, Leu307, Pro308, Ala311, Asp315, Met318 and Val319. Both the ligands bind to AtAOX1A with ΔG of -6.24 and -6.27 kcal/mol, respectively (**Table 6.2, Sl. No. 6 & 7**). The amino acid residues Trp305 and Asp315 are found to be nearest to the ligand(s). However, mutational docking studies showed that Asp315 is a potent residue but not Trp 305 to bind with both malic acid and OAA (**Table 6.3, Sl. No. 10-13**).

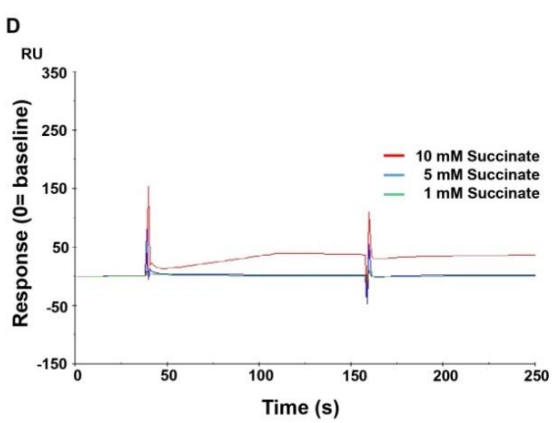
SPR Kinetic analysis to understand the interaction of rAtAOX1A with pyruvate and TCA cycle metabolites

To understand the interaction of pyruvate and TCA cycle metabolites with rAtAOX1A, the binding of these metabolites with immobilized rAtAOX1A was analyzed by passing a wide range of concentrations of each metabolite (1, 5 and 10 mM) onto the CM5 sensor chip (**Fig. 6.1A-G**). However, a prominent increase in RU was identified with α -KG, Fumaric acid,

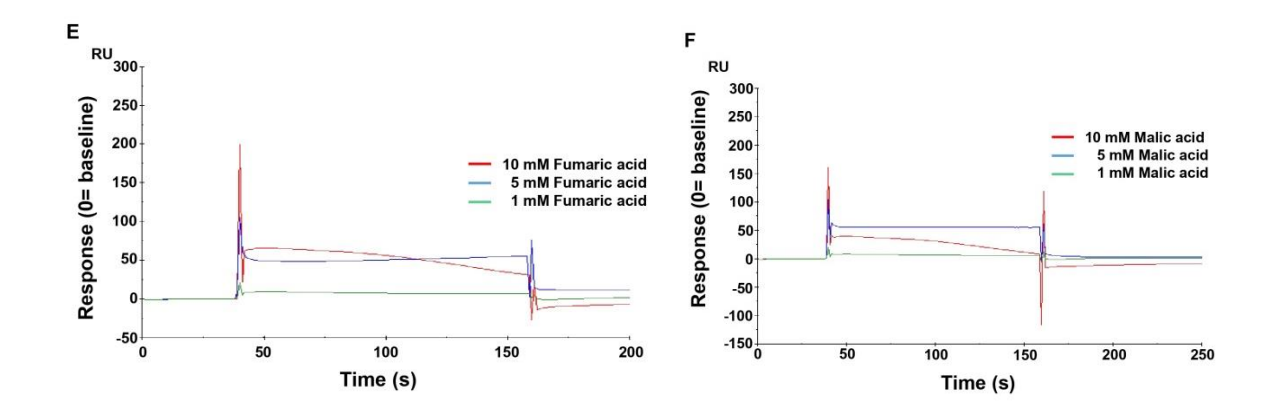








(**P.T.O**)



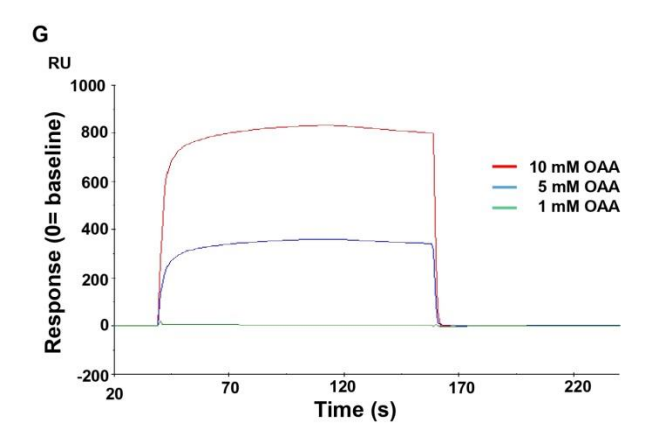


Fig. 6.1. Binding analysis of **(A)** pyruvate, **(B)** citrate, **(C)** α -KG, **(D)** succinate, **(E)** fumaric acid, **(F)** malic acid and **(G)** OAA with rAtAOX1A. Different concentrations of metabolites (1, 5 and 10 mM) are allowed to pass over a CM5 sensor chip with rAtAOX1A immobilized on its surface.

malic acid and OAA but not with pyruvate, citrate and succinate. Therefore, the kinetic parameters were derived for the metabolites which showed a clear increase in RU in sensorgram (Fig. 6.2). The affinity of these metabolites for rAtAOX1A was derived by monitoring kinetic parameters such as association constant (k_a) , dissociation constant (k_d) and equilibrium dissociation constant (K_D) . The experiments were conducted in duplicate and the above kinetic parameters were measured for each analyte from the equilibrium analysis over five (1, 2, 3, 4, and 5 mM) different concentrations (**Fig. 6.2**). The affinity (K_D) of each of the metabolite with rAtAOX1A was almost similar as follows: (A) α -KG = 3.51 nM, (B) fumaric acid = 4.05 nM, (C) malic acid = 4.32 nM and (D) OAA = 4.08 nM (**Table 6.4**). Further, their association and dissociation with rAtAOX1A was reversible. Further, for better visualization and comparison of kinetics between these metabolites (α-KG, fumaric acid, malic acid and OAA) with rAtAOX1A, the SPR kinetic constants were deconvoluted and represented as an iso-affinity graph, which is a plot of association rate constants versus dissociation rate constants (Fig. 6.3). The metabolites α -KG, fumaric acid, malic acid and OAA have shown approximately closer isoaffinity values to AtAOX1A.

CD spectroscopic analysis of the interaction of rAtAOX1A with pyruvate and TCA cycle metabolites

CD spectroscopic study is a highly reliable and relatively easy technique that allows for studying the conformational changes in a protein of interest and is also helpful in ascertaining secondary structural changes in the protein upon binding with its interacting compounds.

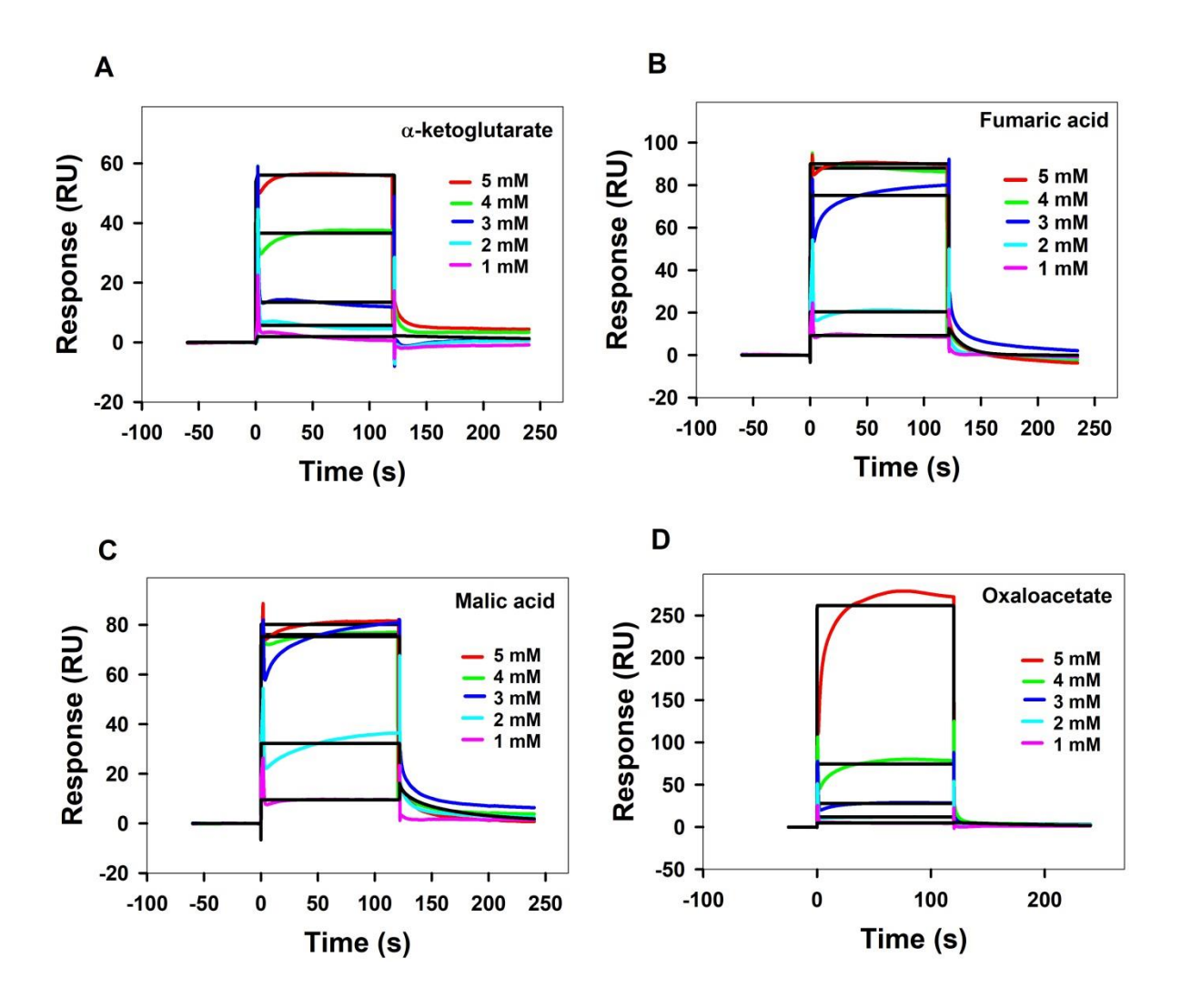


Fig. 6.2. SPR kinetic analysis of rAtAOX1A with TCA cycle metabolites. Sensogram plots generated by SPR kinetic analysis demonstrate the association and dissociation characteristics between immobilized ligand (rAtAOX1A) and TCA cycle metabolites (analytes) such as (A) α -KG, (B) fumaric acid, (C) malic acid, and (D) OAA.

Table 6.4. SPR kinetic constants for the interaction of purified rAtAOX1A with TCA cycle metabolites

Sl. No	Analyte	$k_{\mathbf{a}} (\mathbf{M}^{-1} \mathbf{s}^{-1})$	$k_{\mathbf{d}} \ (\mathbf{s}^{-1})$	$K_{\mathbf{D}}(\mathbf{M})$
1.	Pyruvate			Not detected
2.	Citrate			Not detected
3.	α-KG	1.44×10^{6}	5.07×10^{-3}	3.51×10^{-9}
4.	Succinate			Not detected
5.	Fumaric acid	1.87×10^7	7.59×10^{-2}	4.05×10^{-9}
6.	Malic acid	3.78×10^{7}	1.63×10^{-1}	4.32×10^{-9}
7.	OAA	2.61×10^6	1.06×10^{-2}	4.08×10^{-9}

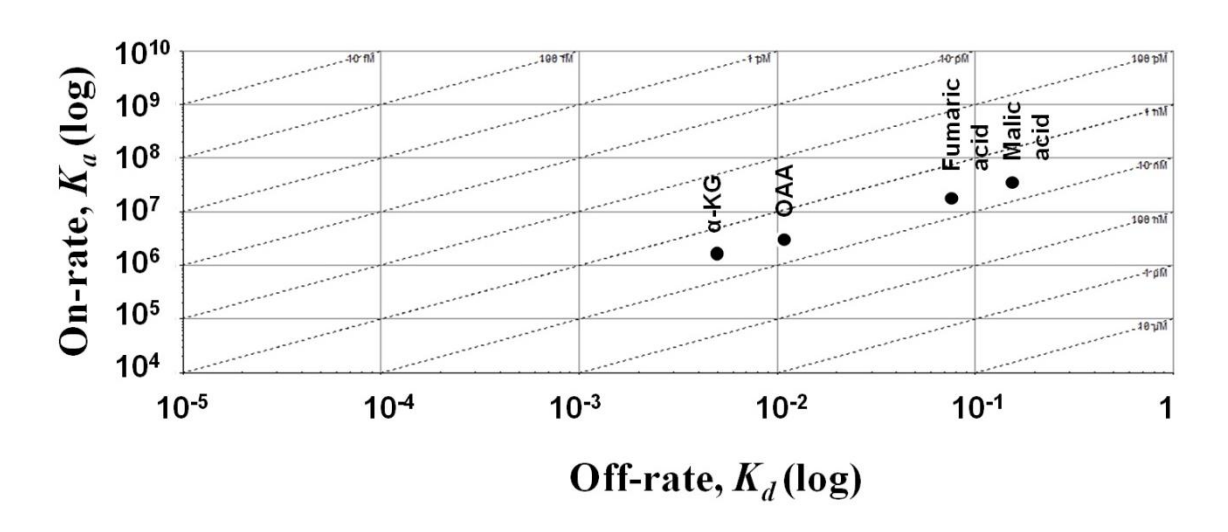
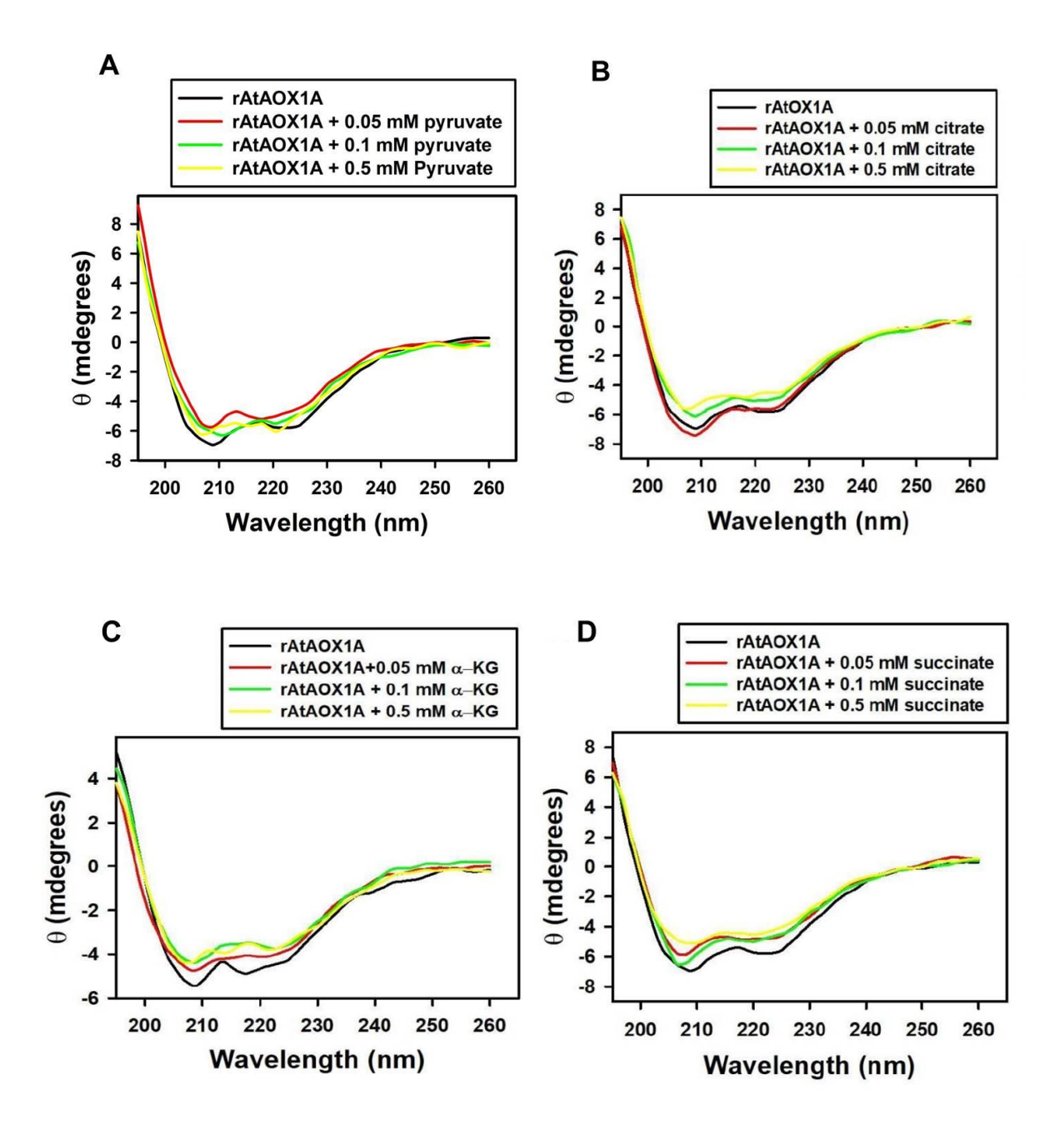


Fig. 6.3. Isoaffinity graph. A plot of the SPR kinetic constants (k_a versus k_d) of α -KG, fumaric acid, malic acid and OAA interaction with purified rAtAOX1A using the 1:1 Langmuir model. Dashed diagonals indicate the isoaffinity lines.

The rAtAOX1A shows a typical α -helical structure consisting of a positive peak at 195 nm and two distinguished negative signals at 208 nm and 222 nm when examined at the far-UV range (190-260 nm) using CD spectroscopy. The addition of pyruvate and TCA cycle metabolites (citrate, α -KG, succinate, fumaric acid, malic acid and OAA) to rAtAOX1A has shown marginal changes in the ellipticity of its CD spectrum (**Fig. 6.4A-G**). However, the changes in the secondary structural elements (α -helices, β -sheets, β -turns and random coils) of rAtAOX1A upon interaction with each of these metabolites were analyzed using the Dichroweb online server with the CDSSTR algorithm. The rAtAOX1A α -helical content is decreased (<10%) while β -sheets (<7%), β -turns and random coils (<3%) increased upon interaction with pyruvate and TCA cycle metabolites at 0.5 mM concentration (**Fig. 6.4A-G** and **Table 6.5**). Further, upon the addition of OAA (0.05 and 0.1 mM), the α -helical content of rAtAOX1A was slightly (55% to 57%) increased (**Fig. 6.4G** and **Table 6.5**).

Fluorescence spectroscopic analysis of the interaction of rAtAOX1A with pyruvate and TCA cycle metabolites

The tertiary structural changes in a protein upon interaction with its ligand can be conveniently studied by monitoring the changes in the fluorescence intensity of tryptophan residues using fluorescence spectroscopy. Hence, the conformational changes in rAtAOX1A upon the addition of different concentrations (0.05, 0.1 and 0.5 mM) of pyruvate and TCA cycle metabolites (citrate, α -KG, succinate, fumaric acid, malic acid and OAA) were monitored by following the changes in the fluorescence emission spectra. In the present study, a decrease in the fluorescence intensity without a shift in the peak (339 nm) upon the addition of these metabolites was observed (**Fig. 6.5A-G**). These results suggest that the



(**P.T.O**)

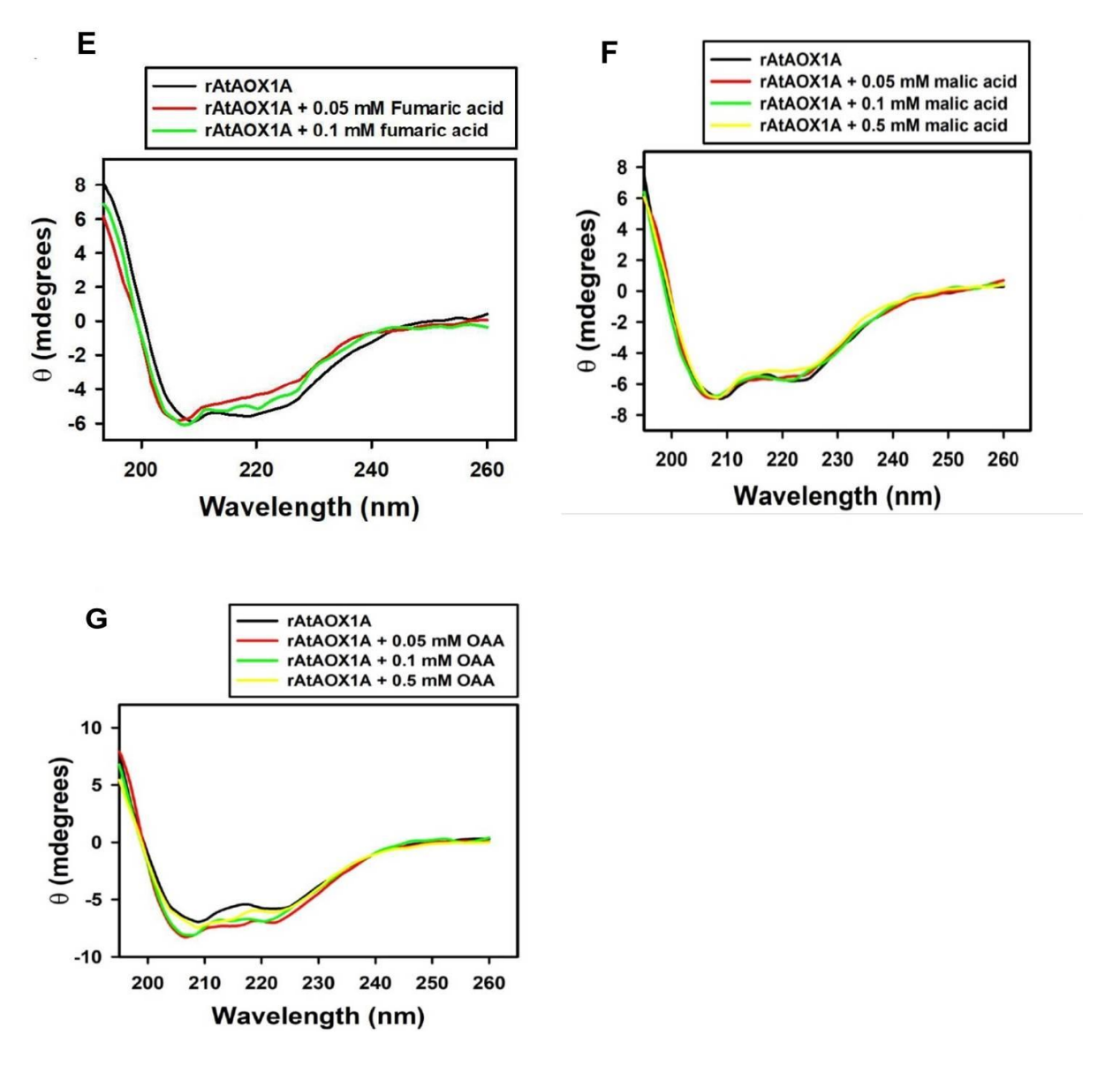
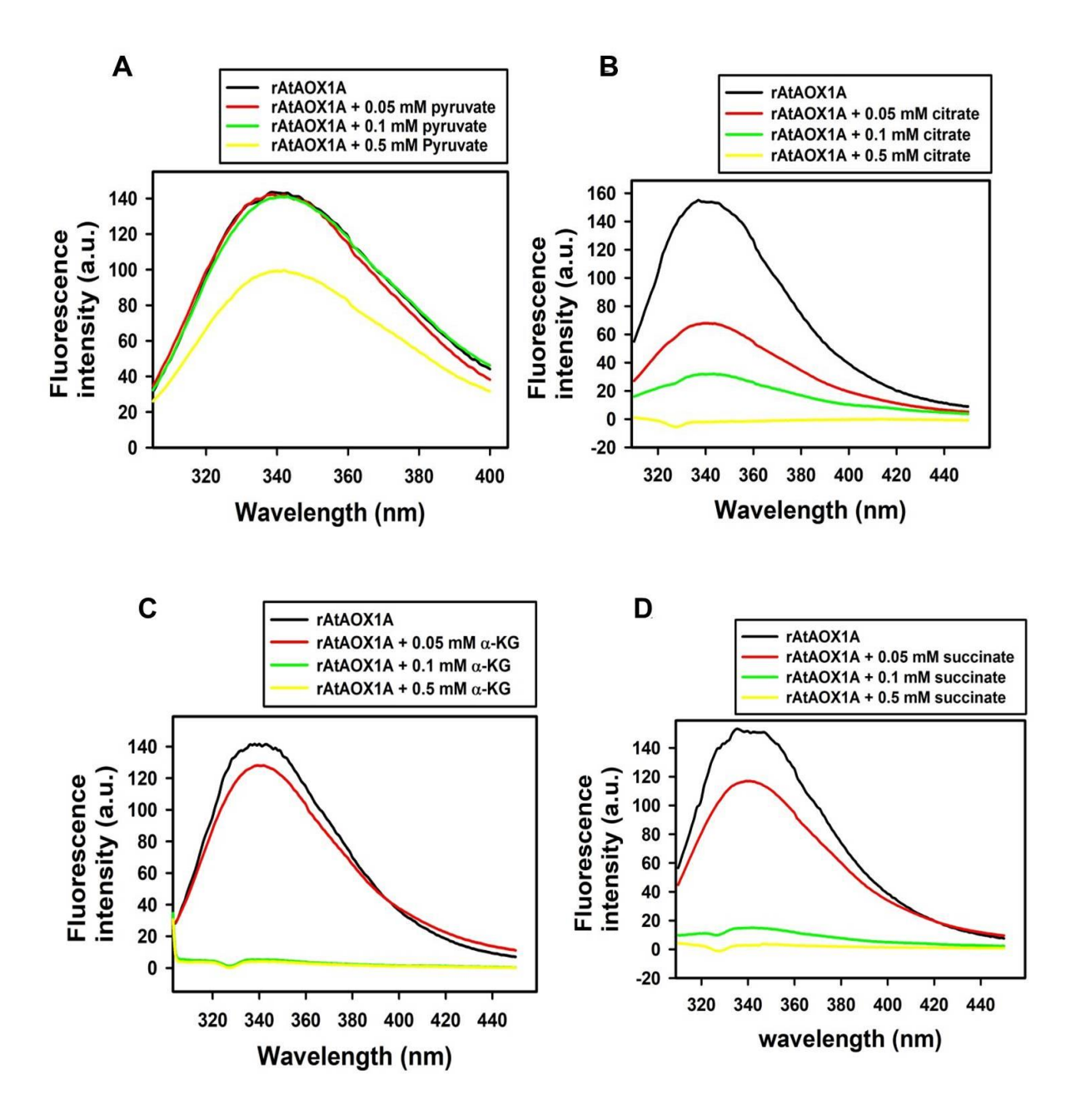


Fig. 6.4. CD spectra of rAtAOX1A at far-UV (190-260 nm). The change in ellipticity upon treatment with different concentrations (0.05, 0.1 and 0.5 mM) of (**A**) pyruvate, (**B**) citrate, (**C**) α-KG, (**D**) succinate, (**E**) fumaric acid, (**F**) malic acid and (**G**) OAA is shown in comparison with control (without metabolite) CD spectra (black line). The concentration of purified rAtAOX1A used to obtain the CD spectra was 0.4 mg/ml in 10 mM phosphate buffer at pH 7.5.

Table 6.5. Modulation in rAtAOX1A secondary structural elements during interaction with pyruvate and TCA cycle metabolites. The data is analyzed using the CDSSTR algorithm and reference set 4. Values represent the average of four to five scans.

Sample	Concentration of	on of Predicted secondary structure elements			lements %
	metabolite	α-helix	β-sheet	β-Turn	Random
					Coil
rAtAOX1A	Control	55	19	9	17
rAtAOX1A	0.05 mM	47	24	10	19
+ Pyruvate	0.1 mM	50	23	9	18
1 yravate	0.5 mM	49	24	9	18
rAtAOX1A	0.05 mM	56	19	10	15
+ Citrate	0.1 mM	48	25	9	18
Chilate	0.5 mM	47	25	9	19
rAtAOX1A	0.05 mM	45	26	11	18
+ α-KG	0.1 mM	49	23	11	17
	0.5 mM	47	24	9	20
rAtAOX1A	0.05 mM	51	23	8	18
Succinate	0.1 mM	52	21	9	18
	0.5 mM	47	24	10	19
rAtAOX1A	0.05 mM	49	25	9	17
Fumaric acid	0.1 mM	49	25	8	18
rAtAOX1A	0.05 mM	53	20	9	18
+ Malic acid	0.1 mM	53	20	10	17
	0.5 mM	54	19	10	17
rAtAOX1A	0.05 mM	57	17	9	17
+ OAA	0.1 mM	57	19	8	16
	0.5 mM	54	20	9	17



(**P.T.O**)

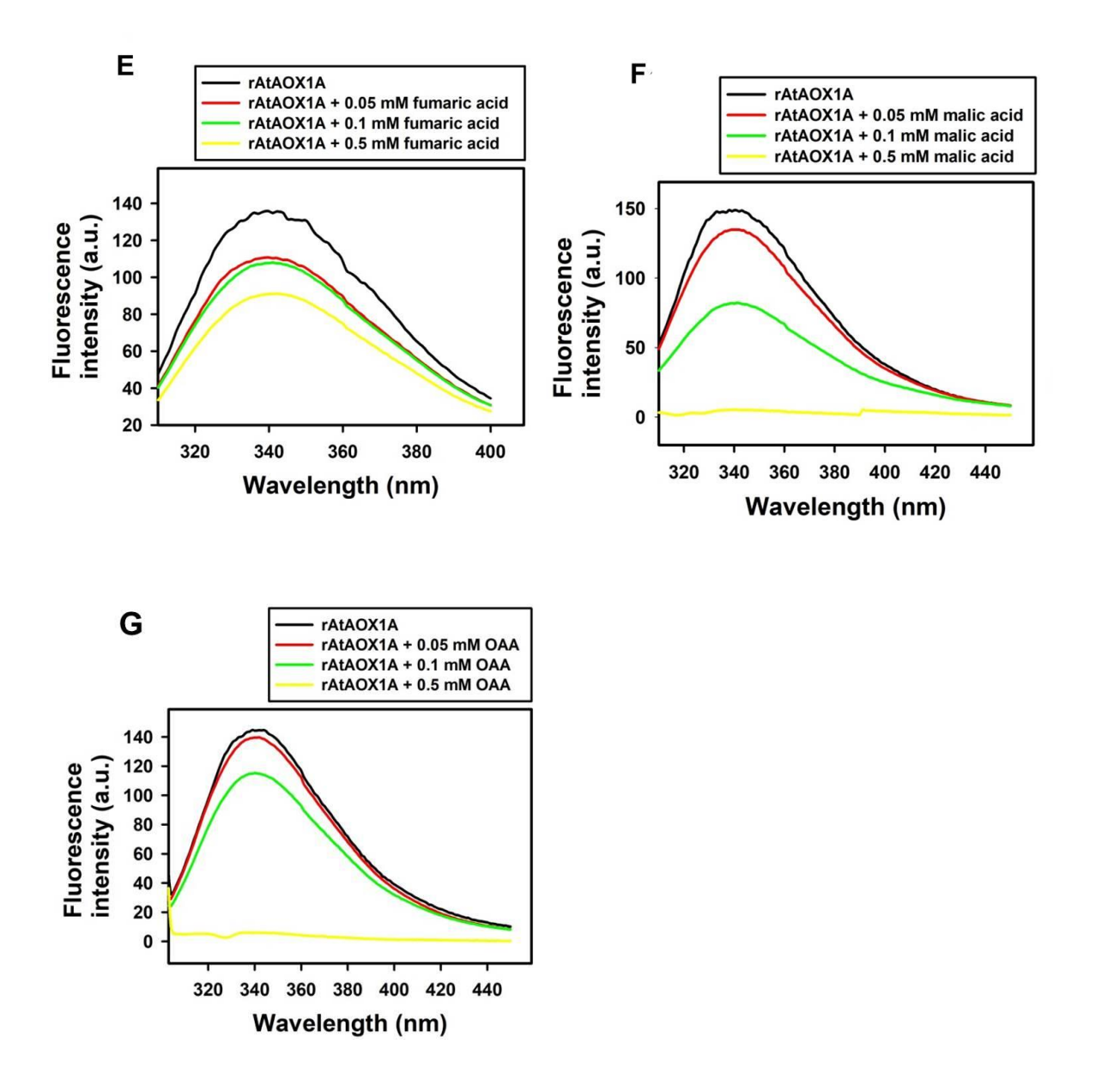


Fig. 6.5. Fluorescence spectroscopic analysis of rAtAOX1A with different TCA metabolites. Intrinsic fluorescence emission spectra of rAtAOX1A in the absence and presence of different concentrations (0.05, 0.1 and 0.5 mM) of metabolites (**A**) pyruvate, (**B**) citrate, (**C**) α-KG, (**D**) succinate, (**E**) fumaric acid, (**F**) malic acid and (**G**) OAA. A 10 μM protein sample (rAtAOX1A) was prepared in 5 mM phosphate buffer at pH 7.5. Fluorescence emission spectra were obtained at 25°C, from 300 to 450 nm, with excitation at 295 nm.

interaction of rAtAOX1A with pyruvate and TCA cycle metabolites caused conformational changes, which may not allow the exposure of hydrophobic groups of the protein to the solvent. Besides, no remarkable shift in the fluorescence emission peak was observed, which indicates that the microenvironment of Trp is not affected by the interaction of rAtAOX1A with pyruvate and TCA cycle metabolites (**Fig. 6.5A-G**).

6.3. Discussion

Generally, in plants, under normal physiological conditions, the mitochondrial AOX activity remained low, possibly due to its low expression levels and existence in inactive dimeric form. However, the exogenous addition of organic acids/TCA cycle metabolites to isolated plant mitochondria has been shown to activate AOX and/or increase the AOX pathway activity (Vanlerberghe et al., 1995; Vanlerberghe and McIntosh, 1996; Vianello et al., 1997). Further, the studies of Wagner et al. (1995) have demonstrated that the addition of succinate, malate, or pyruvate stimulated the AOX-dependent NADH oxidation in mitochondria from potato tuber callus. Contrarily, the studies of Millar et al. (1993; 1996) claimed that malate and succinate do not directly stimulate the AOX activity but may be converted to pyruvate by the malic enzyme present in the mitochondria and aid in the activation of AOX.

The TCA cycle metabolite profile frequently varies in the mitochondrial matrix due to their involvement as substrates in various biosynthetic pathways (Sankar et al., 2002; Sweetlove et al., 2010; Zhang et al., 2018). Moreover, most of the TCA cycle enzymes are sensitive to oxidative stress, which in turn may lead to a significant change in the metabolic profile of TCA cycle metabolites (Verniquet et al., 1991; Lehmann et al., 2009; Savchenko and Tikhonov, 2021). For e.g., the TCA cycle metabolite levels increased in plants under

water stress (Dastogeer et al., 2017) and drought (Vasquez-Robinet et al., 2008) stress while decreased under oxidative stress induced by menadione treatment in *A. thaliana* and *Oryza sativa* (Ishikawa et al., 2010; Obata et al., 2011; Lehmann et al., 2012). The results from these studies indicate that plants modulate their TCA metabolite profile to alleviate stress, perhaps by activating AOX and antioxidative enzymes, respectively (Gray et al., 2004; Vanlerberghe, 2013; Savchenko and Tikhonov, 2021). Further, as plants are immobile, any disturbance in cellular metabolic equilibrium due to various stress conditions has been shown to greatly enhance the AOX activity (Clifton et al., 2005; Vanlerberghe, 2013; Rodziewicz et al., 2014; Vishwakarma et al., 2015; Selinski et al., 2018b; Savchenko and Tikhonov, 2021). Thus, the present study was an attempt to reveal the possible interaction of purified rAtAOX1A with various TCA cycle metabolites and monitored the associated structural changes using in silico and biophysical studies.

rAtAOX1A interacts with pyruvate and TCA cycle metabolites

The AOX is known to exist in several isoforms and each isoform was shown to be activated by different TCA cycle metabolites. For example, the studies of Selinski et al. (2018a) have shown that the TCA cycle metabolites α-KG and OAA increased the activity of membrane-bound rAtAOX1A by 3- and 7-fold, respectively, while its activity has not been affected by other TCA cycle metabolites such as citrate, isocitrate, succinate, fumarate, and malate. Besides, the studies of Xu et al. (2021) have shown that succinate and oxaloacetate play a role in stimulating the membrane-bound rAtAOX1A activity and this stimulation was further enhanced in the presence of well-known activators of AOX such as pyruvate and glyoxylate. Their studies also suggested that not all the TCA cycle metabolites are involved in the strong activation of rAtAOX1A. However, the docking results in the present study have revealed

the presence of binding pockets in AtAOX1A for pyruvate and TCA cycle metabolites, such as citrate, α -KG, fumaric acid, malic acid and OAA, except for succinate (**Table 6.2**). Subsequently, the mutational docking studies have revealed the potent residues involved in the binding of these pyruvate and TCA cycle metabolites to AtAOX1A (**Table 6.3**).

The docking results from the present study revealed that the key activator of the AOX (pyruvate) binding pocket contained Cys177, along with Arg174, Tyr175, Gly176, Val232, Ala233, Asn294, and Leu313 (**Table 6.2**), substantiating the involvement of second cysteine (Cys177) residue in regulating the post-translational activation of AOX during its interaction with pyruvate (Polidoros et al., 2009; Moore et al., 2013). The studies of Crichton et al. (2005) identified four potential regions in AtAOX1A that played an important role in the interaction of organic acids. The Arg174, Gly176 and Cys177 present in the pyruvate binding pocket of the present study corroborated well with the residues identified in region 2, while Asn294 matched with the "N" in the ENV motif of region 3. Further, mutational docking studies performed with Arg174Ala, Gly176Ala, and Cys177Ala in AtAOX1A identified them as potential candidates for binding to pyruvate (Table 6.3, Sl. No. 1-3). Further, the changes observed in the secondary structural elements of AtAOX1A upon interaction with pyruvate may not allow the protein to form an inactive dimeric form and might give more access to the substrate to bind, which, in turn, could lead to the full enzyme activity (Xu et al., 2021) (**Tables 6.2 & 6.3**).

Further, the present study revealed the binding of two other known AOX α -keto activators, i.e., α -KG and OAA, at distinct locations on AtAOX1A (**Table 6.2, Sl. No. 3 &** 7). The binding pocket where the metabolite α -KG interacts are formed by the helices α 2, α 3, and α 4 in AtAOX1A. Mutational docking studies have demonstrated that the amino acid

residues Arg223 (helix- α 3) and Gly247 (helix- α 4) are important for this binding. The binding pocket for OAA contained loops, short helices (S3 and S4), and helix- α 6 in AtAOX1A. According to mutational docking experiments, Asp315 is found to be the key residue involved in the interaction between OAA and AtAOX1A. However, between the two activators, α -KG showed a higher binding affinity (Δ G = -7.12 kcal/mol) to AtAOX1A than OAA (Δ G = -6.27 kcal/mol) (**Table 6.2, Sl. No. 3 & 7**). The docking results are further supported by SPR kinetic data, where the binding affinities (KD) of α -KG and OAA are 3.51 nM and 4.08 nM, respectively (**Figs. 6.2 and 3; Tables 6.2 and 6.4**). Besides, both docking and SPR studies revealed that malic acid had shown little less binding affinity (Δ G = -6.24 kcal/mol; KD = 4.32 nM) to rAtAOX1A than α -KG and OAA (**Tables 6.2, Sl. No. 6 and 6.4**). Thus, a positive correlation was observed between Δ G and KD of α -KG, OAA and malic acid towards rAtAOX1A.

Interestingly, the binding pocket of fumaric acid on AtAOX1A is overlapped with the binding pocket of ubiquinone-1 (UQ₁; an oxidized form of AOX substrate) in containing Leu163, Thr167, Leu182, Val185 and Phe250, although the chemical composition of these ligands is different (**Table 6.2, Sl. No. 5**; Sankar et al., 2022). This partial overlap in binding pockets of fumaric acid and UQ₁ indicates the possibility of fumaric acid acting as a natural inhibitor of AtAOX1A. It is reported in the literature that this fumaric acid acts as a natural inhibitor of tyrosinase, an enzyme involved in the melanogenesis of skin and eyes (Gou et al., 2017). The closest residues to the fumaric acid on AtAOX1A are Glu275 and Thr167. Sitespecific mutational docking studies revealed that both of these amino acid residues are important for the binding of fumaric acid to AtAOX1A (**Table 6.3, Sl. No. 8 & 9**). Further, Glu275 is close to Glu273, a highly conserved residue that coordinates with the di-iron

catalytic core in AtAOX1A (Pennisi et al., 2016). In trypanosomal alternative oxidase (TAO), Thr219 is found to be crucial for binding with ubiquinol/ubiquinone (Moore et al., 2013; Shiba et al., 2013; Shiba et al., 2019). In this line, Thr167 of AtAOX1A might play a similar role as Thr219 in TAO in binding with UQ₁, as described above. Nevertheless, these observations need further investigation using different approaches to validate the role of fumaric acid as a natural inhibitor of AOX since the crystal structure of plant AOX/AtAOX1A is not yet resolved.

In the present study, the results obtained from docking studies complemented the real-time binding kinetics of immobilized rAtAOX1A (purified from *E. coli* membranes) with TCA cycle metabolites using the SPR technique. The studies with SPR revealed that purified rAtAOX1A interacted with some of the TCA cycle metabolites, such as α -KG, fumaric acid, malic acid and OAA, but not with pyruvate, citrate and succinate (**Fig. 6.1, 6.2** and **Table 6.4**). Further, the results obtained with SPR studies showed the following affinity order of TCA cycle metabolites with rAtAOX1A: α -KG > fumaric acid \geq OAA \geq malic acid (**Fig. 6.2, 3 and Table 6.4**). However, the rAtAOX1A could not show any binding response with citrate and succinate in SPR analysis (**Fig. 6.1**), possibly due to some technical limitations such as the sensitivity of SPR instrumentation (**Fig. 6.2, 3 and Table 6.4**). However, further investigations using CD and fluorescence spectroscopy further confirmed the interaction of these metabolites with rAtAOX1A.

Structural changes are induced in rAtAOX1A upon interaction with pyruvate and TCA cycle metabolites

Protein secondary and tertiary structures are stabilized by inter and intra-molecular forces, and they might get distorted in the presence of interacting compounds. In the present study, the structural changes that occurred in rAtAOX1A upon interaction with pyruvate and TCA cycle metabolites were examined using techniques such as CD and fluorescence spectroscopy (Kelly et al., 2005; Lakowicz, 2006). The rAtAOX1A showed a typical α-helical signal, as evidenced by the CD spectra taken from the far-UV region (**Fig 5.1**; **chapter 5**). Besides, a concentration range (0.05, 0.1 and 0.5 mM) of different metabolites was used to obtain CD spectra from the far-UV region. Due to the high HT voltage, the study could not be continued beyond the concentrations mentioned above. The secondary structural content of rAtAOX1A bound to pyruvate and TCA cycle metabolites was compared with that of rAtAOX1A (control).

The addition of different concentrations (0.05, 0.1 and 0.5 mM) of pyruvate to the rAtAOX1A caused an increase in β -sheets with a concomitant decrease in α -helical content, while the changes in β -turns and random coils (together) are negligible (**Fig. 6.4A and Table 6.5**). Upon the addition of different concentrations (0.05, 0.1 and 0.5 mM) of α -KG, and 0.5 mM citrate, succinate, and 0.05 and 0.1 mM fumaric acid, the α -helical content of rAtAOX1A decreased with a concomitant increase in the β -sheets. Only a marginal increase in β -turns and random coils was observed (**Fig. 6.4B-G and Table 6.5**). Upon the addition of different concentrations (0.05, 0.1 and 0.5 mM) of malic acid, the secondary structural content did not vary much (**Fig. 6.4F and Table 6.5**). Contrary to the other TCA cycle metabolites, the addition of OAA to the rAtAOX1A caused a slight increase in its α - helical content compared to the control (**Fig. 6.4G and Table 6.5**). Taken together, the results suggest that, although a transition in the secondary structural conformation occurred from α -

helix to β -sheet, the typical α -helical signal was retained even upon binding with pyruvate and TCA cycle metabolites. Nevertheless, all the decreased α -helical content might have been converted to mostly β -sheets and, to some extent, turns and random coils. Also, the binding of the pyruvate and TCA cycle metabolites at their cognate binding sites probably might caused a rearrangement in the hydrogen bond network among the amino acid residues in the binding pocket, resulting in local conformation changes in the rAtAOX1A (Varlan and Hillebrand, 2010; Suryawanshi et al., 2016; Sankar et al., 2022).

Further, the tryptophan fluorescence is used as a probe to understand the conformational changes in a protein upon interaction with the analyte molecule. In the present study, a decrease in the fluorescence intensity, without any shift (red or blue) in the spectral peak of rAtAOX1A, was observed upon the addition of pyruvate and TCA cycle (citrate, α-KG, succinate, fumaric acid, malic acid or OAA) metabolites (**Fig. 6.5A-G**). These results indicated that the TCA cycle metabolites interact with rAtAOX1A. However, this interaction was not associated with a remarkable change in the microenvironment of tryptophan residues of the protein (Wang et al., 2014; Gheibi et al., 2016; Gou et al., 2017; Maji et al., 2017). But, the observed decrease in the fluorescence intensity upon binding with these metabolites could be due to structural changes associated with fluorescence quenching, possibly due to the further folding of rAtAOX1A into the hydrophobic region. As the AtAOX1A contained nine tryptophan residues, the fluorescence quenching observed in the present study might be due to the tryptophan residues located near the metabolite binding pocket (Lelis et al., 2020; Duysak et al., 2021; Pennisi et al., 2016).

Highlights of the study

- ✓ Molecular docking studies revealed that the pyruvate (key activator of AOX) binding pocket on AtAOX1A contained Cys177 (a second cysteine residue) along with other residues.
- ✓ Molecular docking studies have shown some important conserved binding pockets in rAtAOX1A for different TCA metabolites, as shown below:
 - Citrate & α -Ketoglutarate (α 2, α 3, and α 4)
 - Malic acid & Oxaloacetate (S3, S4 and α6)
- ✓ Fumaric acid and UQ₁ (Oxidized form of AOX substrate) share few residues in their binding pocket to binding to AtAOX1A.
- ✓ Mutational docking studies revealed potential residues for the binding of pyruvate and different TCA cycle metabolites to AtAOX1A.
- ✓ SPR studies of rAtAOX1A with TCA cycle metabolites revealed reversible binding with binding affinities as shown in the following order: α-KG > fumaric acid ≥ OAA ≥ malic acid.
- ✓ Upon interaction of rAtAOX1A with pyruvate and TCA cycle metabolites, the α-helical content decreased while β-sheet, β-turn and random coils were increased. These results confirm the changes in the secondary structural conformation of rAtAOX1A in the presence of pyruvate and TCA cycle metabolites.
- ✓ A decrease in the fluorescence intensity with no shift (red or blue) in the spectral peak of rAtAOX1A upon interaction with pyruvate and TCA metabolites demonstrated that the interaction caused an overall conformational change in rAtAOX1A, however without disturbing the hydrophobic environment surrounding tryptophan residues.

Chapter 7

Interaction of rAtAOX1A with Redox Metabolites using Docking and Biophysical Studies

Interaction of rAtAOX1A with Redox Metabolites using Docking and Biophysical Studies

7.1. Introduction

The redox metabolites work together to maintain the redox environment in a cell. The major cellular redox metabolites are NAD, NADH, NADP, NADPH, AsA, DHA, GSH and GSSG (Noctor and Foyer, 1998; Schafer and Buettner, 2001, 2003; Noctor, 2006; Møller et al., 2020). The AOX expression is induced more under various stress and unfavorable environmental conditions (Vanlerberghe and McIntosh, 1992a, b; Simons et al., 1999; Bartoli et al., 2005; Fiorani et al., 2005; Ribas-Carbo et al., 2005). Further, AtAOX1A is known to play an important role in optimizing photosynthesis by maintaining cellular redox homeostasis under oxidative stress. The studies of Dinakar et al. (2016) and Vishwakarma et al. (2015) monitored the changes in the redox ratios of the redox metabolites like Asc, glutathione, NAD(H), and NADP(H) under stress using the mesophyll cell protoplast of pea and A. thaliana knock-out mutants of AOX1A and wild type plants. Chapter 4 of this study revealed the purification of rAtAOX1A from E. coli in its active state. The present study is aimed to (i) identify the binding pockets for the redox metabolites (GSSG, GSH, AsA, DHA, NAD, NADH, NADP and NADPH) from four redox couples on the surface of rAtAOX1A; (ii) analyze the real-time binding and kinetics of these redox metabolites with the purified rAtAOX1A; (iii) study the structural changes in the rAtAOX1A upon interaction with the redox metabolites using CD and fluorescence spectroscopy. The chemical structures of redox metabolites used in the present study are shown in **Table 7.1**.

Table 7.1. Chemical structures of redox metabolites used in the analysis of the interaction with rAtAOX1A.

Sl. No	Name of the compound	PubChem CID	Chemical formula	Structures from PubChem	Mol. Weight
1.	GSH	124886	$C_{10}H_{17}N_3O_6S$	HOW HOW H	307.33
2.	GSSG	65359	$C_{20}H_{32}N_6O_{12}S_2$		612.6
3.	AsA	54670067	$\mathrm{C_6H_8O_6}$	H	176.12
4.	DHA	4613280	C ₁₂ H ₁₂ O ₁₂	H H H H H H H H H H H H H H H H H H H	348.22
5.	NAD	925	C ₂₁ H ₂₇ N ₇ O ₁₄ P ₂	HON	663.4
6.	NADH	11250888	C ₂₁ H ₂₉ N ₇ O ₁₄ P ₂	HON HOUSE HO	665.4
7.	NADP	91972139	C ₂₁ H ₂₈ N ₇ O ₁₇ P ₃	H O O O O O O O O O O O O O O O O O O O	743.4
8.	NADPH	5884	C ₂₁ H ₃₀ N ₇ O ₁₇ P ₃	HOPO OF HOPO O	745.4

7.2. Results

Molecular docking of AtAOX1A with different redox metabolites

The binding pockets for different redox metabolites on AtAOX1A and the binding affinities are shown in **Table 7.2**. Several conserved binding locations are detected on the surface of AtAOX1A for the redox metabolites chosen in the present study.

The metabolites GSH, NADH and NADP are bound to the same binding pocket formed by Phe128, Arg129, Pro130, Trp131, Glu132, Ala214, Glu217, Glu218, Asn221, Arg306, Ala322, Asp323, His326, His327, Ala349, Pro350, Tyr353 and His354, but with a different ΔG of -8.34, -10.61 and -10.52 kcal/mol, respectively, on WT-AtAOX1A (Table 7.2, Sl. No. 1, 6 & 7) Besides, the most probable binding site for GSSG (an oxidized form of GSH) is similar to that of GSH possessing ten residues in common (Phe128, Ala214, Glu217, Glu218, Asn221, His326, His327, Ala349, Pro350 and Tyr353) along with a few additional residues (Lys213, Leu215, Val330 and Asn331) and a ΔG of -8.76 kcal/mol on WT-AtAOX1A (Table 7.2, Sl. No. 2).

The mutational docking studies with AtAOX1A revealed Glu217 and His326 as potent residues to bind GSH and NADP, respectively, as the point mutations of these residues to Ala altered the binding sites relative to the WT-AtAOX1A (**Table 7.3, Sl. No. 1 & 7**). In the case of GSSG and NADH, though the potent residues are not identified on the rAtAOX1A, the collective interaction of all the binding site residues with these ligands might hold them in their binding pockets (**Table 7.3, Sl. No. 2 & 6**).

The ligands NAD and AsA possessed several residues in common in their binding pocket on AtAOX1A. The binding pocket of NAD possessed the following residues: Trp131,

Table 7.2. Molecular docking of redox metabolites (GSH, GSSG, AsA, DHA, NAD, NADH, NADP and NADPH) on WT AtAOX1A. Color scheme: Ligand (purple), carbon (red), nitrogen (blue), oxygen (orange), sulfur (yellow), hydrogen (white). The secondary structure of AtAOX1A is shown in grey color. Parentheses indicate the position of amino acid residue in the AtAOX1A and the chain number of α -helices.

Sl. No.	Ligand	Residues in the binding pocket	Binding free energy (ΔG in kcal/mol)	Binding pocket
1.	GSH	Phe128 (loop) Arg129 (loop) Pro130 (loop) Trp131 (loop) Glu132 (loop) Ala214 (α3) Glu217 (α3) Glu218 (α3) Asn221 (α3) Arg306 (loop) Ala322 (α6) Asp323 (α6) His326 (α6) His327 (α6) Ala349 (loop) Pro350 (loop) Tyr353 (loop) His354(loop)	-8.34	GLU218 HSD327 ASN331 LEU215 VAL330 GLU217 LYS213 PRO350 PHE128
2.	GSSG	Phe128 (loop) Lys213 (α3) Ala214 (α3) Leu215 (α3) Glu217 (α3) Glu218 (α3) Asn221 (α3) His326 (α6) His327 (α6) Val330 (α6) Asn331 (α6) Ala349 (loop) Pro350 (loop) Tyr353 (loop)	-8.76	ASN221 HSD327 ASP323 GLU132 ARG306 HSD326 ARG129 GLU217 PHE128 TRP131 TYR353 PRO350 HSE354

3.	AsA	Trp131 (loop) Glu132 (loop) Thr133 (loop) Tyr134 (loop) Lys135 (s3) Ile138 (s3) Leu307 (loop) Pro308 (loop) Ala311 (loop) Asp315 (α6) Met318 (α6) Val319 (α6)	-6.39	LYS135 MET318 LYS135 MET318 LLE138 THR133 ALA311 PRO308 VAL319 LEU307 TRP131
4.	DHA (monomer)	Met191 (α2) Val192 (α2) Gly193 (α2) Gly194 (α2) Met195 (α2) Leu196 (α2) His198 (α2) Cys199 (α2) Phe251 (α4) Phe255 (α4)	-5.73	CYS199 LEU196 GLY194 MET195 MET191 LEU196 VAL192 PHE255
5.	NAD	Trp131 (loop) Glu132 (loop) Thr133 (loop) Tyr134 (loop) Lys135 (s3) Ile138 (s3) Arg306 (loop) Leu307 (loop) Pro308 (loop) Ala309 (loop) Ala311 (loop) Arg314 (α6) Asp315 (α6) Val316 (α6) Met318 (α6) Val319 (α6)	-8.19	ARG306 TRP131 LEU307 PR03(8) ALA311 VAL316 GLU132 VAL319 ASP315 THR133 TYR134 LYS135 VAL319 ARG314 MFT318

6.	NADH	Phe128 (loop) Arg129 (loop) Pro130 (loop) Trp131 (loop) Glu132 (loop) Ala214 (α3) Glu217 (α3) Glu218 (α3) Asn221 (α3) Arg306 (loop) Ala322 (α6) Asp323 (α6) His326 (α6) His327 (α6) Ala349 (loop) Pro350 (loop) Tyr353 (loop) His354(loop)	-10.61	ASP323 HSD327 (CASP322) ALA322 ASN221 ARG306 ARG129 HSD326 ALA214 TRP131 ALA349 PHE128 PRO350 TYR353
7.	NADP	Phe128 (loop) Arg129 (loop) Pro130 (loop) Trp131 (loop) Glu132 (loop) Ala214 (α3) Glu217 (α3) Glu218 (α3) Asn221 (α3) Arg306 (loop) Ala322 (α6) Asp323 (α6) His326 (α6) His327 (α6) Ala349 (loop) Pro350 (loop) Tyr353 (loop) His354(loop)	-10.52	ASP323 ALA322 GLU132 ARG306 ARG129 AHSD326 PHE128 GLU217 ALA349 TYR353 PRO350 HSE354

8.	NADPH	Trp123 (loop) Lys124 (loop) Asn126 (loop) Ala187 (α2) Val188 (α2) Met191 (α2) Leu215 (α3) Leu216 (α3) Glu217 (α3) Ala219 (α3) Glu220 (α3) Arg223 (α3)	-9.79	ASN1264 GLU217 TRP123 LEU216 LEU215 GLU220 MET191 ARG223 VAL188 PHE251 GLN247 6
		` ,		
		` ′		ARG223
		Glu217 (a3)		VAL188
		` /		PHE251
		` ′		GLN247 6 4 5
		` ` /		
		Ile244 (α 4)		ILE244
		Thr245 (α 4)		VAL246
		Val246 (α4)		THR245
		$Gln247 (\alpha 4)$		11111/243
		Gly248 (α4)		•
		Phe251 (α4)		
		Phe252 (α4)		

Table 7.3. Molecular docking of different cellular redox metabolites on mutant AtAOX1A. Parentheses indicate residues within 3Å from the ligand in WT. These potent residues are mutated to alanine/arginine in AtAOX1A to understand their importance in binding with ligands.

Sl. No.	Ligand	Mutation (Residues within 3Å from ligand in WT- AtAOX1A)	Binding pocket (WT binding surface is in yellow)	Remarks
1.	GSH	Glu217Ala		Ligand does not bind into WT binding pocket upon Glu217Ala mutation. Thus, it is a potent binding residue to bind GSH
2.	GSSG			Due to the collective interactions of GSSG with all the binding site residues, no potent residue was identified
3.	AsA	Asp315Ala		Ligand does not bind into WT binding pocket upon Asp315Ala mutation. Thus, it is a potent binding residue to bind AsA

4.	DHA (monomer)	Val192Arg	Ligand does not bind into WT binding pocket upon Val192Arg mutation. Thus, it is a potent binding residue to bind DHA.
5.	NAD	Thr133Ala	Ligand does not bind into WT binding pocket upon Thr133Ala mutation. Thus, it is a potent binding residue to bind NAD.
6.	NADH		 Due to the collective interactions of GSSG with all the binding site residues, no potent residue was identified
7.	NADP	His326Ala	Ligand does not bind into WT binding pocket upon His326Ala mutation. Thus, it is a potent binding residue to bind NADP.

8.	NADPH	Met191Arg	Ligand does not bind into WT binding pocket upon Met191Arg mutation. Thus, it is a potent binding residue to bind NADPH.
9.		Glu220Ala	Ligand does not bind into WT binding pocket upon Glu220Ala mutation. Thus, it is a potent binding residue to bind NADPH.

Glu132, Thr133, Tyr134, Lys135, Ile138, Arg306, Leu307, Pro308, Ala309, Ala311, Arg314, Asp315, Val316, Met318 and Val319 and a ΔG of -6.39 kcal/mol. However, the binding pocket for AsA is devoid of Arg306, Ala309, Arg314, and Val316 as compared to the binding pocket of NAD and possessed ΔG of -8.19 kcal/mol on WT AtAOX1A (**Table 7.2, Sl. No. 5 & 3**). Also, the potent residues which hold the ligand in the binding pocket varied. It is found that Thr133 is the potent residue for the binding of NAD, while Asp315 is the potent residue for the binding of AsA (**Table 7.3, Sl. No. 5 & 3**).

Contrarily, the binding site residues for DHA and NADPH varied significantly on WT AtAOX1A. However, two residues, Met191 and Phe251, were found to be present in common in their binding sites (**Table 7.2 Sl. No. 4 & 8**), with a ΔG of -5.73 and -9.79 kcal/mol, respectively. The amino acid Val192 is found to be the potent residue for binding of DHA as the point mutation of Val192 to Arg altered the binding site on WT-AtAOX1A (**Table 7.3, Sl. No. 4**). In the case of NADPH, Met191 and Glu220 are found to be potent residues to interact with AtAOX1A since the point mutation of these residues to Arg and Ala altered the binding site on WT-AtAOX1A (**Table 7.3 Sl. No. 8 & 9**).

SPR Kinetic analysis of different redox metabolites with rAtAOX1A

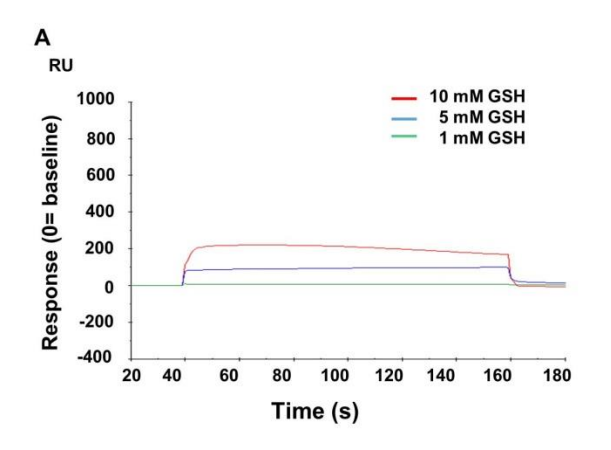
The label-free technique 'SPR' allows monitoring of real-time interaction and kinetics between immobilized molecules and the analyte, for e.g., protein-metabolite, etc. It detects the changes occurring in the refractive index of metal film immobilized with a protein whenever it interacts with a metabolite. The change in the refractive index is measured as a response unit (RU). To study the interaction of rAtAOX1A with redox metabolites, the real-time binding was performed by passing these metabolites onto the CM5 sensor chip

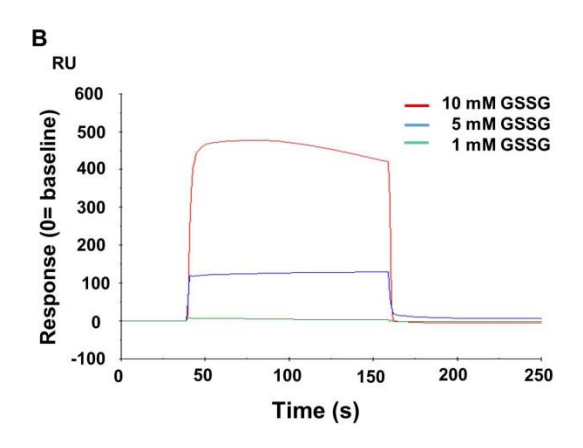
immobilized with rAtAOX1A at different concentrations (1, 5 and 10 mM). The binding of metabolites to rAtAOX1A is revealed by the increase in the RU (Fig. 7.1A-H).

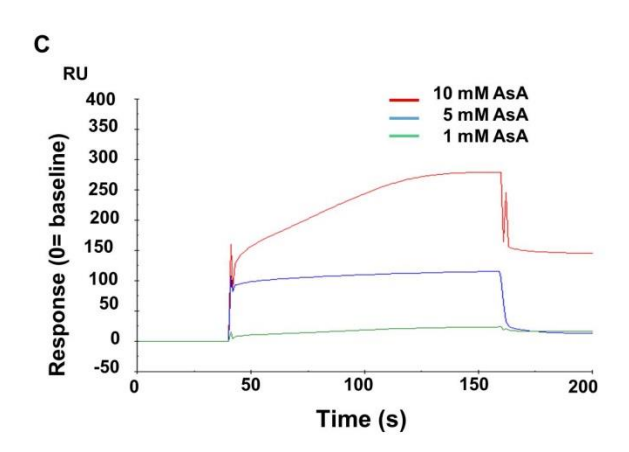
The affinity of each of the redox metabolite with rAtAOX1A was derived from kinetic parameters: k_a (association constant), k_d (dissociation constant) and K_D (equilibrium dissociation constant) (Fig. 7.2A-F and Table 7.4). The SPR kinetics data revealed that both metabolites in the redox couple GSH-GSSG possessed closer binding affinity to rAtAOX1A with $K_D = 0.551$ nM (GSH) and 0.531 nM (GSSG), respectively. But, in the case of AsA-DHA redox couple, the metabolite AsA showed less affinity ($K_D = 6.60$ nM) to rAtAOX1A than DHA ($K_D = 2.74$ nM). Further, in the redox couple NAD-NADH, the metabolite NAD showed affinity ($K_D = 0.054$ nM), while NADH did not show any binding to rAtAOX1A. Similarly, the metabolite NADP from redox couple NADP-NADPH showed affinity to rAtAOX1A with $K_D = 0.729$ nM, while NADPH did not show any binding to rAtAOX1A (Fig. 7.2A-F and Table 7.4).

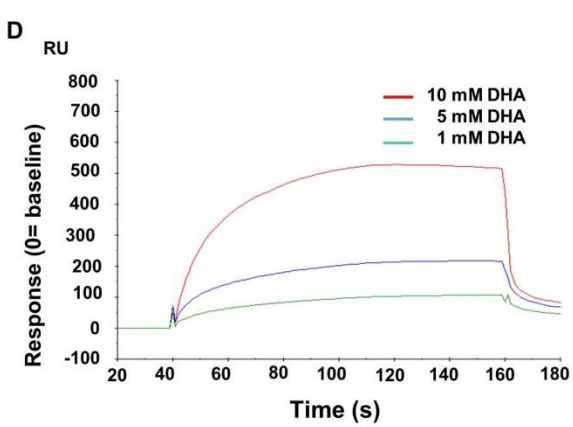
Thus, the data obtained from SPR studies revealed a faster association and dissociation kinetics, which indicate that the binding of these redox metabolites to rAtAOX1A is reversible. Based on the K_D values, the metabolite NAD showed a considerably higher affinity with the rAtAOX1A compared to other redox metabolites in the following order: NAD > GSSG \geq GSH \geq NADP > DHA > AsA (**Fig. 7.2A-F and Table 7.4**). The association and dissociation of NADH and NADPH with rAtAOX1A were not traceable using SPR (**Fig. 7.1F, H and Table 7.4**).

CD spectroscopic analysis of rAtAOX1A with different redox metabolites









(**P.T.O**)

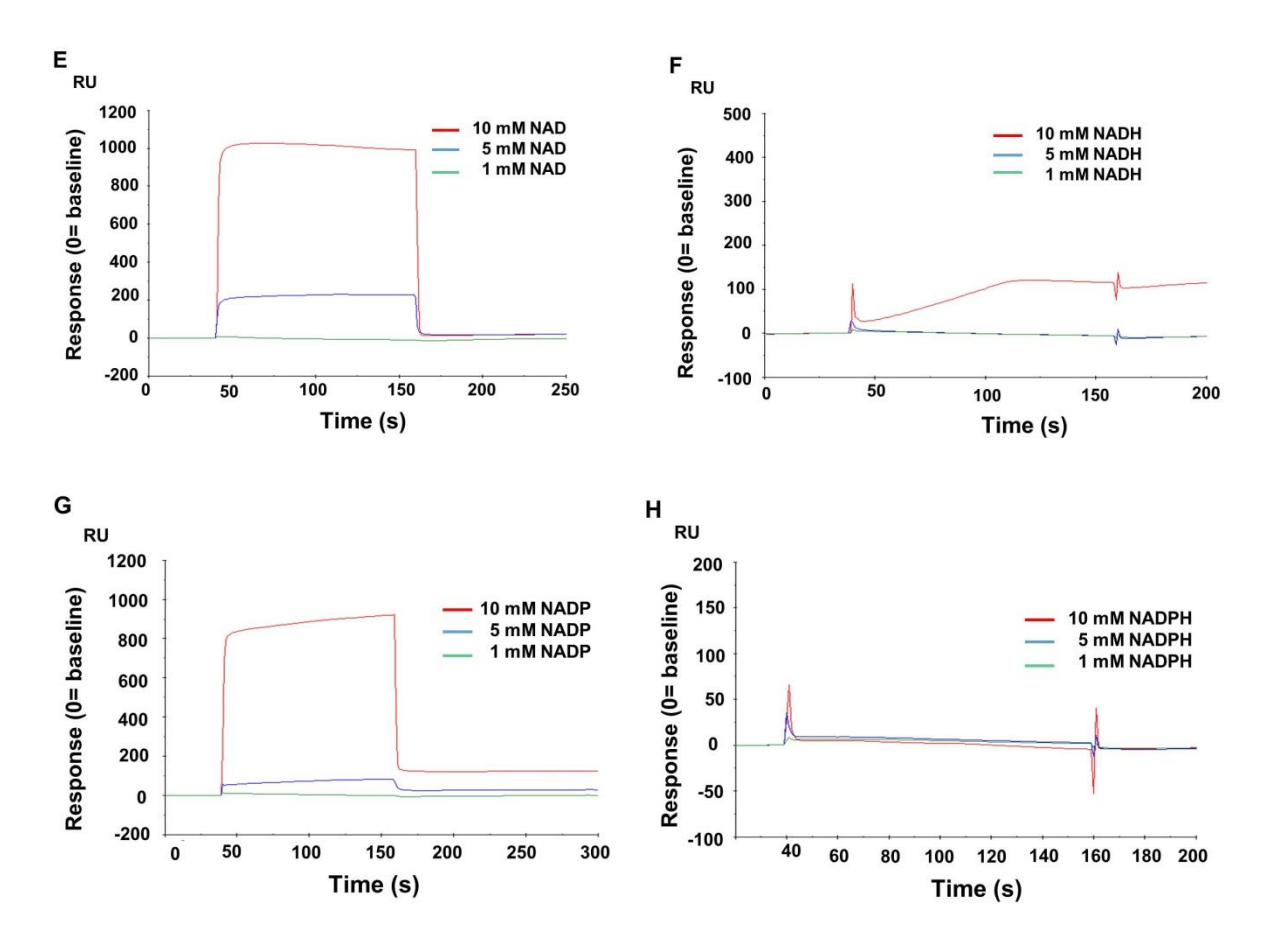


Fig. 7.1. Binding analysis of redox metabolites (**A**) GSH, (**B**) GSSG, (**C**) AsA, (**D**) DHA, (**E**) NAD, (**F**) NADH, (**G**) NADP and (**H**) NADPH with rAtAOX1A. Different concentrations (1, 5 and 10 mM) of redox metabolites have flowed over a CM5 sensor chip with rAtAOX1A immobilized on the surface.

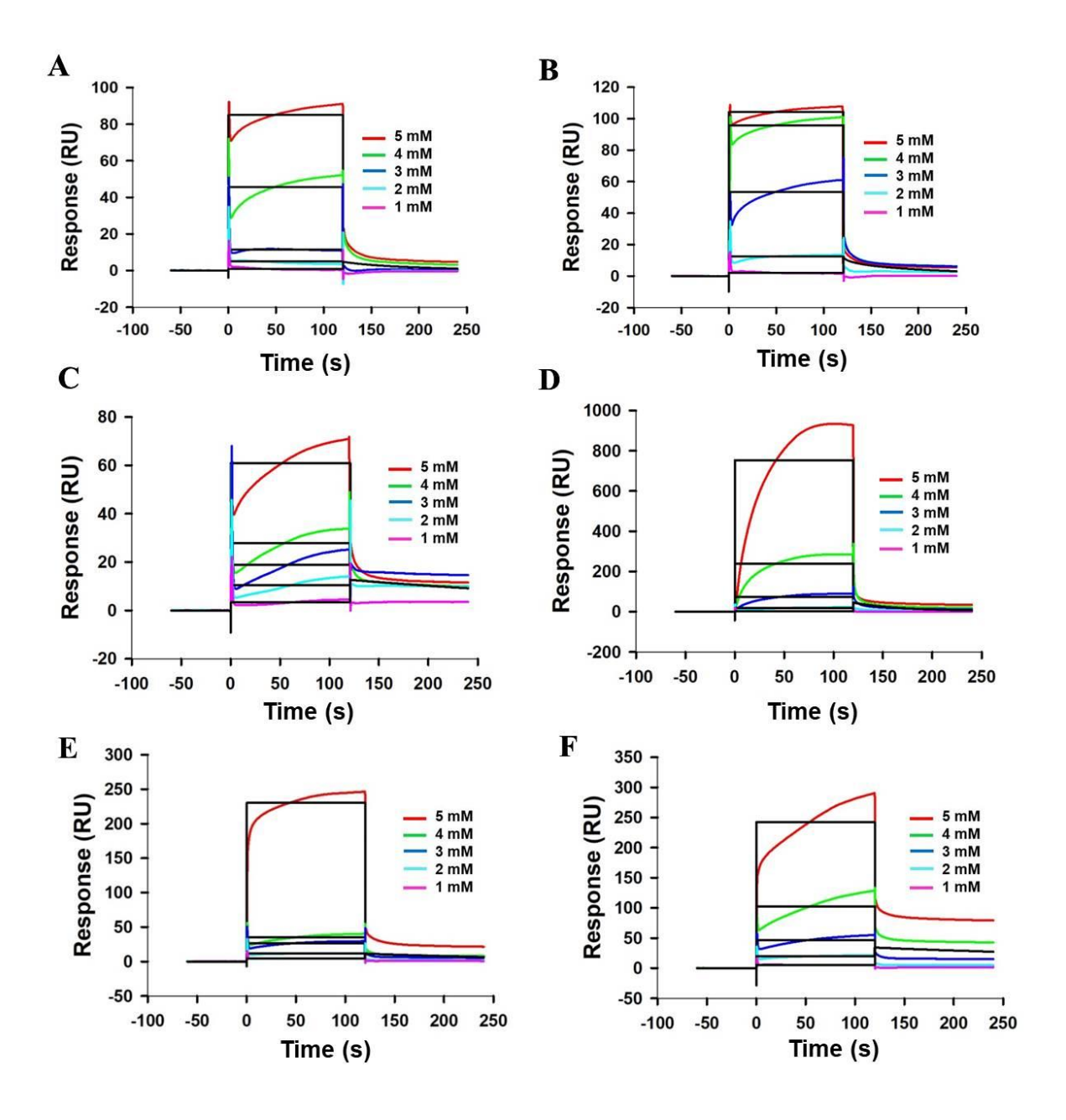


Fig. 7.2. Biacore surface plasmon resonance (SPR) analysis of rAtAOX1A. Sensorgram plots generated by SPR kinetic analysis demonstrate the association and dissociation characteristics between immobilized ligand (rAtAOX1A) and analytes, (**A**) GSH, (**B**) GSSG, (**C**) AsA, (**D**) DHA, (**E**) NAD and (**F**) NADP.

Table 7.4. Binding constants for the interaction between purified rAtAOX1A and redox metabolites

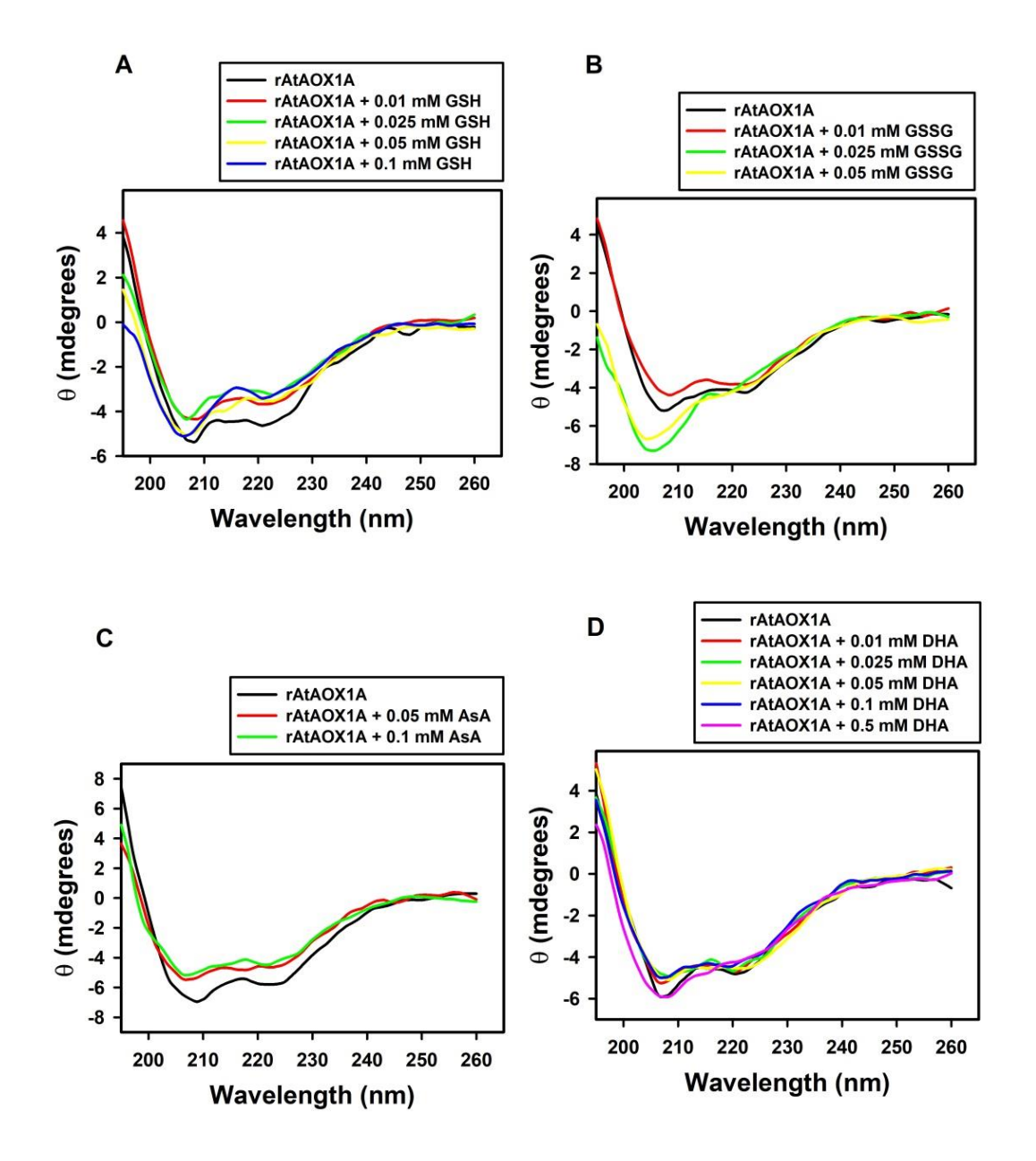
Sl. No	Compound	$k_{\mathbf{a}} (\mathbf{M}^{-1} \mathbf{s}^{-1})$	$k_{\rm d} (\rm s^{-1})$	$K_{\mathbf{D}}(\mathbf{M})$
1.	GSH	3.08×10^7	1.70×10^{-2}	0.551×10^{-9}
2.	GSSG	3.75×10^8	1.99×10^{-1}	0.531×10^{-9}
3.	AsA	5.25×10^5	3.46×10^{-3}	6.60×10^{-9}
4.	DHA	8.11×10^{6}	2.22×10^{-2}	2.74×10^{-9}
5.	NAD	4.86×10^7	2.64×10^{-3}	0.054×10^{-9}
6.	NADH			Not detected
7.	NADP	3.22×10^6	2.35×10^{-3}	0.729×10^{-9}
8.	NADPH			Not detected

CD spectroscopy is a powerful technique that is widely used to study the secondary structure of proteins and it provides valuable information about structural changes that occur in proteins upon interaction with other molecules.

The CD studies from **Chapter 5** revealed that the secondary structure of purified rAtAOX1A possessed a typical α -helical structure. In this chapter, the changes in the secondary structure of rAtAOX1A were examined to monitor its interaction with various redox metabolites. The ellipticity at 208 and 222 nm did not vary significantly upon interaction with different metabolites at the chosen concentrations in the CD spectrum (**Fig. 7.3A-H**). However, a significant change in the secondary structural elements (α -helices, β -sheets, β -turns and random coils) of rAtAOX1A was observed upon interaction with these redox metabolites (**Table 7.5**). The α -helical content is decreased (<21%) while β -sheets (<7%), β -turns (<14%) and random coils (<7%) are increased in rAtAOX1A upon interaction with various redox metabolites at a range of concentrations against each metabolite used in the present study except for GSSG (**Fig. 7.3A-H and Table 7.5**). The addition of GSSG (0.025 and 0.05 mM) increased the α -helical content of rAtAOX1A by <3% and it is reflected in the increase of ellipticity between 205-208 nm (**Fig. 7.3B and Table 7.5**).

Fluorescence spectroscopic analysis of rAtAOX1A with different redox metabolites

Fluorescence spectroscopy uses the intrinsic fluorescence of tryptophan residues as a probe to monitor the protein conformational changes during interaction with any other molecule. In the present study, the conformational changes in the tertiary structure of rAtAOX1A, which contains nine tryptophan residues, were monitored upon the addition of different redox



(**P.T.O**)

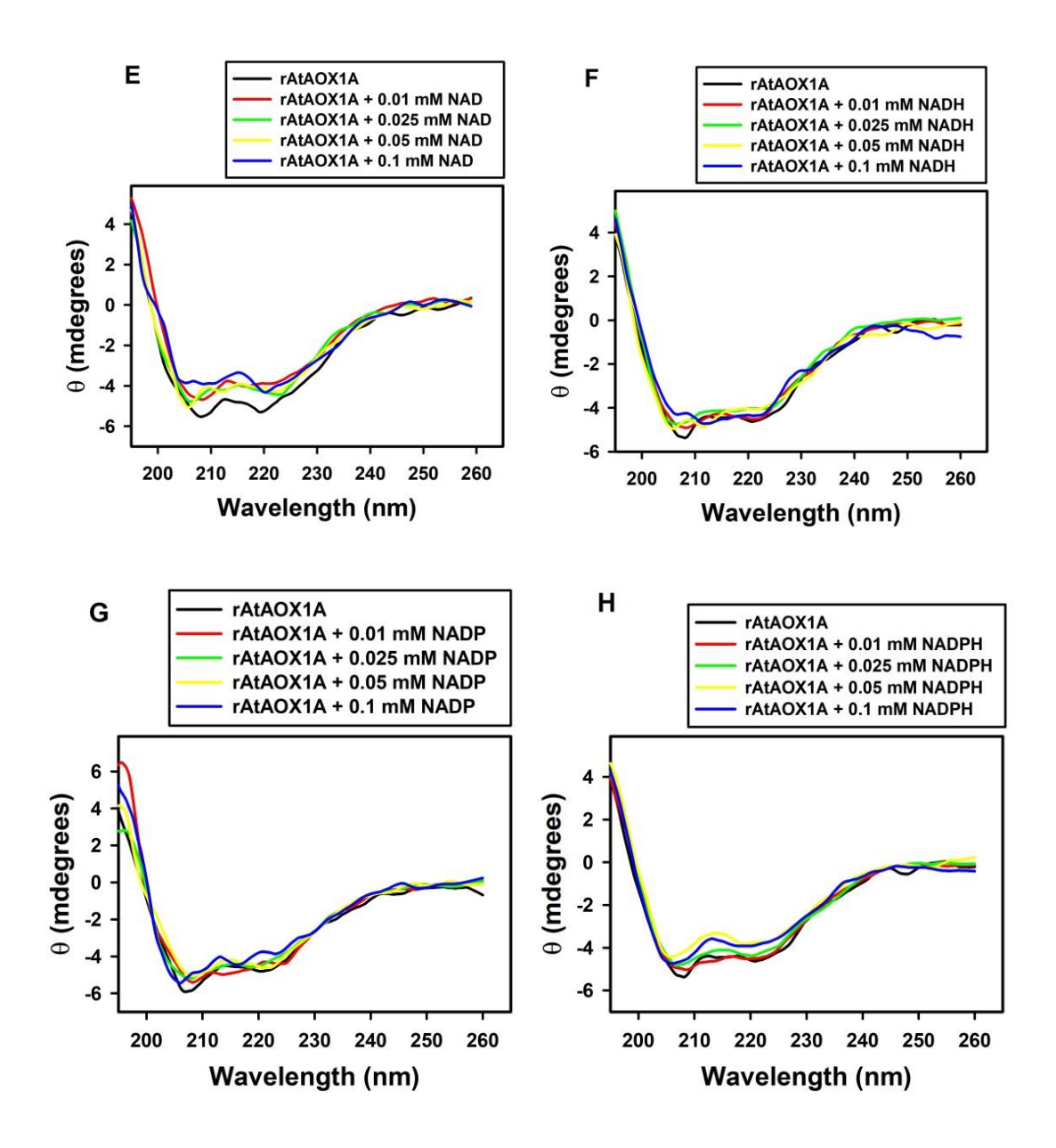


Fig. 7.3. CD spectra of rAtAOX1A at far UV (190-260 nm). The change in ellipticity upon treatment with different concentrations of **(A)** GSH, **(B)** GSSG, **(C)** AsA, **(D)** DHA, **(E)** NAD, **(F)** NADH, **(G)** NADP and **(H)** NADPH is shown in comparison with control (rAtAOX1A) CD spectra (black line). The concentration of purified rAtAOX1A used to obtain the CD spectra was 0.4 mg/ml in 10 mM phosphate buffer at pH 7.5.

Table 7.5. Modulation in rAtAOX1A secondary structural elements during interaction with GSSG, GSH, AsA, DHA, NAD, NADH, NADP and NADPH. The data is analyzed using the CDSSTR algorithm and reference set 4. Values represent the average of four to five scans.

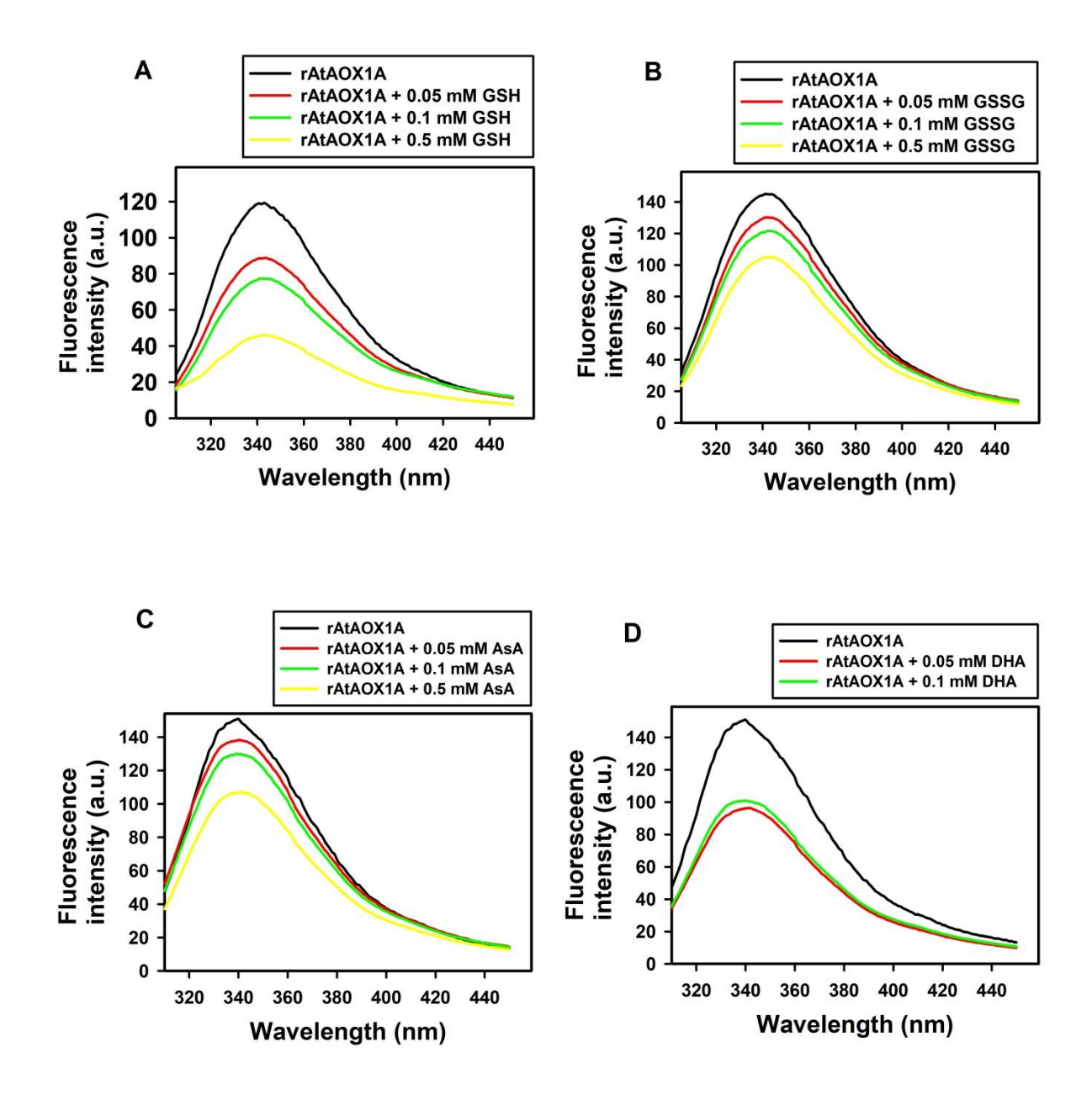
Sample	Concentration of metabolite	Predicted secondary structure elements %			
		α-helix	β-Sheet	β-Turn	Random coil
rAtAOX1A	Control	51	21	9	19
	0.01 mM	46	26	10	18
rAtAOX1A+	0.025 mM	37	28	18	17
GSH	0.05mM	47	25	10	18
	0.1mM	49	25	9	17
rAtAOX1A	0.01 mM	39	18	17	26
+ GSSG	0.025 mM	54	22	9	15
	0.05mM	52	24	9	15
rAtAOX1A	0.05 mM	48	25	9	18
AsA	0.1 mM	48	26	9	17
	0.01 mM	45	25	10	20
rAtAOX1A+	0.025 mM	45	26	10	19
DHA	0.05mM	45	25	11	19
	0.1mM	46	25	10	19
	0.5 mM	49	26	8	17
	0.01 mM	46	24	11	19
rAtAOX1A+	0.025 mM	47	26	9	18
NAD	0.05mM	47	25	9	19
	0.1mM	32	28	19	21
	0.01 mM	44	25	12	19
rAtAOX1A+	0.025 mM	47	26	9	18
NADH	0.05mM	46	26	10	18
	0.1mM	30	23	23	24

rAtAOX1A+ NADP	0.01 mM	46	24	11	19
	0.025 mM	46	25	10	19
	0.05mM	45	24	12	19
	0.1mM	46	26	9	19
rAtAOX1A+ NADPH	0.01 mM	45	25	11	19
	0.025 mM	44	25	11	20
	0.05mM	45	26	10	19
	0.1mM	46	26	10	18

metabolites. The fluorescence intensity of emission spectra of rAtAOX1A was measured before and after the addition of different concentrations of redox metabolites such as GSH, GSSG, AsA, DHA, NAD, NADH, NADP and NADPH. The fluorescence emission spectra of rAtAOX1A have shown a peak at 339 nm upon excitation (λex) at 295 nm. The addition of redox metabolites caused a decrease in the fluorescence intensity of emission spectra of rAtAOX1A without any shift in the peak observed at 339 mn compared to the control (**Fig. 7.4A-H**). These results suggest that the interaction of rAtAOX1A with the redox metabolites caused conformational changes in its tertiary structure that may not allow the exposure of hydrophobic groups of the protein to the solvent. Hence, there is no shift in the fluorescence emission peak.

7.3. Discussion

As the plants are sessile, they are often exposed to different biotic and abiotic stress conditions, which in turn might affect redox metabolism. Therefore, restoration of redox homeostasis is essential for the survival of plants under such conditions. The AOX from the mitochondrial electron transport chain is known to play a significant role in maintaining cellular redox homeostasis under different stress conditions. Also, the knock-out plants for *AOX1a* emphasized the crucial role of AOX in the maintenance of cellular redox homeostasis during oxidative stress caused by highlight or restricting the flow of electrons through the COX pathway (Vishwakarma et al., 2014, 2015). Besides, inhibition of AOX pathway using SHAM in mesophyll protoplasts of pea disturbed the cellular redox homeostasis under hyperosmotic and sub-optimal temperature stress (Dinakar et al., 2010a; Dinakar et al., 2016). These studies showed an increase in the cellular ROS followed by an increase in redox ratios of malate/OAA, NAD(P)H/NAD(P), Asc/DHA and GSH/GSSG under stress conditions.



(**P.T.O**)

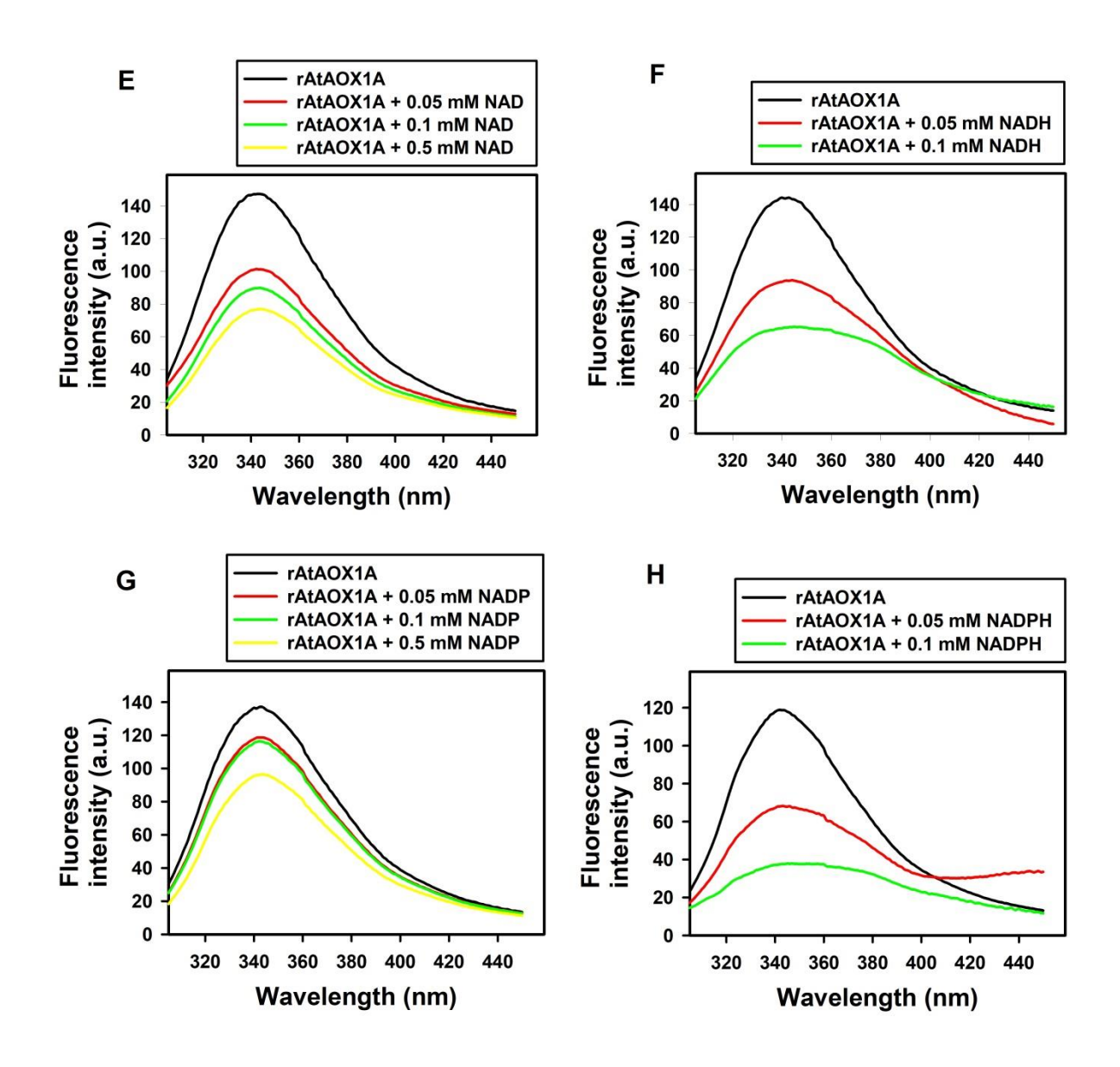


Fig. 7.4. Fluorescence spectroscopic analysis of rAtAOX1A with different redox metabolites. Intrinsic fluorescence emission spectra of rAtAOX1A in the absence and presence of different concentrations of redox metabolites (**A**) GSH, (**B**) GSSG, (**C**) AsA, (**D**) DHA, (**E**) NAD, (**F**) NADH, (**G**) NADP and (**H**) NADPH. A 10 μM protein sample (rAtAOX1A) was prepared in 5 mM phosphate buffer at pH 7.5. Fluorescence emission spectra were obtained at 25°C, from 300 to 450 nm, with excitation at 295 nm.

The present study is aimed to understand the interaction of plant cellular redox metabolites with the rAtAOX1A by employing in silico and biophysical techniques like SPR, CD and fluorescence spectroscopy.

rAtAOX1A possessed binding pockets which interact with redox metabolites

Among the different redox metabolites that are investigated in the present study, the redox metabolites GSH, GSSG, NADH and NADP are found to bind to a conserved binding pocket on the AtAOX1A (Table 7.2, Sl. No. 1, 2, 6 & 7). The mutational docking studies revealed that the potent residues Glu217 & His326 involved in the binding of the ligands GSH & NADP on AtAOX1A varied with one another in finding their location on α -3 and α -6 helices, respectively (**Table 7.3, Sl. No. 1 & 7**). However, all the residues were found to be equally important for the binding of GSSG & NADH (data not shown). Further, the Glu217 (Table **7.3, Sl. No. 1**) is closer to Glu222 (α-helix-3); hence, GSH may coordinate with the diiron center of AtAOX1A through Glu217 and Glu222 for the transfer of reducing equivalents (Pennisi et al., 2016). Further, a close relation between AOX1A expression and GSH content observed in the roots of A. thaliana under cadmium stress support this hypothesis (Keunen et al., 2016). Besides, AOX pathway-mitigated oxidative stress also increased the GSH/GSSG ratio in waterlogging stress-tolerant variety of watermelon (Zheng et al., 2021). Thus, the interaction of GSH with Glu217 may possibly activate AtAOX1A by sharing reducing equivalents to the diiron center, which plays a role in the reduction of O₂ to H₂O. Similar to Glu217, His326, which plays a role in the binding of NADP, is closer to His327 (α -helix-6), which forms a hydrogen bond with highly conserved Glu residues in catalytic diiron center (Table 7.3, Sl. No. 7; Pennisi et al., 2016). This hypothesis is further supported by SPR

studies, which showed that both GSH and NADP bind to rAtAOX1A with closer binding affinities (Table 7.4, Sl. No. 1 & 7).

In the literature, a positive correlation between AOX and AsA levels was observed under highlight stress in *A. thaliana* leaves (Bartoli et al., 2006). The redox metabolites AsA and NAD are found to bind to a binding pocket on AtAOX1A, where short helix-3 (S3) and α -helix-6 are involved. The potent residue for the binding of AsA with AtAOX1A is Asp315 (α -helix-6). The interaction of AsA with rAtAOX1A was also observed in the present study (Table 7.3, Sl. No. 3). In the case of NAD, Thr133 is the potent residue which is present on loop region (Table 7.3, Sl. No. 5). The redox metabolites DHA and NADPH shares Met191 (α -helix-2) and Phe251 (α -helix-4). The potent residue for the binding of DHA is Val192 (α -helix-2), whereas, Val188 (α -helix-2) and Arg223 (α -helix-3) are the potent residues for binding of NADPH (Table 7.3, Sl. No. 4, 8 & 9). Overall, the interaction between redox metabolites and AtAOX1A appears to be charge based (hydrophobic/hydrophilic).

In the present study, different redox metabolites were passed on to the immobilized rAtAOX1A to measure the real-time kinetic constants. According to the SPR kinetic analysis data (**Fig. 7.2A-F and Table 7.4**), the metabolite NAD has shown higher affinity ($K_D = 0.054 \text{ nM}$) with rAtAOX1A as compared to all other redox metabolites. Further, both components in redox couple GSH-GSSG has an almost similar binding affinity with $K_D = 0.551$ and 0.531 nM, respectively, but the affinities of these redox metabolites are tenfold less than that of NAD. The redox metabolite AsA has shown lower affinity ($K_D = 6.60 \text{ nM}$) as compared to DHA ($K_D = 2.74 \text{ nM}$) in the redox couple Asc-DHA. The redox metabolite DHA has shown higher affinity than that of AsA ($K_D = 6.60 \text{ nM}$) (**Table 7.4**). The previous reports suggest that DHA keeps thiol groups of protein in the oxidized state. Whereas, under

stress conditions, there is a decrease in the DHA levels and an increase in AsA levels which in turn may lead to the activation of AOX (Arrigoni and Tullio, 2002; Bartoli et al., 2006). The redox metabolite NADP has a $K_D = 0.729$ nM for rAtAOX1A, while the affinity for its counterpart (NADPH) in NADP- NADPH is not detected in the SPR studies. Similarly, the affinity for NADH, the counterpart of NAD - NADH redox couple, is also not detected in the SPR studies. These results showed the following order of affinity of redox metabolites with rAtAOX1A: NAD > GSSG \geq GSH \geq NADP > DHA > AsA (**Figs 7.1, 7.2 and Table 7.4**).

Structural changes are induced in rAtAOX1A upon interaction with redox metabolites

The CD spectra from the far-UV region of rAtAOX1A on binding with different redox metabolites have not shown significant changes in its ellipticity as compared with the control spectrum, which displayed the characteristic shape of an α -helical protein. In the present work, different concentration of the redox metabolites was used to obtain CD spectra from the far-UV region. Due to the high HT voltage, we could not go beyond the concentration mentioned in the materials and methods. However, a significant decrease in the α -helical content (<21%) with a concomitant increase in β -sheets (<7%), β -turns (<14%) and random coils (<7%) was observed in the secondary structural content of rAtAOX1A when the redox metabolites interact with rAtAOX1A except for GSSG where the α -helical content increased at 0.025 and 0.05 mM concentration (**Fig. 7.3A-H and Table 7.5**).

These results indicate that there is a transition in the secondary structural conformation from α -helices to β -sheets, β -turns and random coils. The interaction of the redox metabolites with the rAtAOX1A might cause the rearrangement in the hydrogen bond network of the amino acid residues resulting in conformational changes in the AOX protein.

The addition of GSSG caused a marginal blue shift with an increase in the ellipticity of the spectral peaks (**Fig. 7.3B**). Together, these results indicate that local conformational changes occur in the AOX protein when it interacts with redox metabolites.

The tryptophan fluorescence is usually used as a probe to understand the conformational changes of the protein upon interaction with the analyte molecule. A decrease in the fluorescence intensity with no shift (red or blue) in the spectral peak was observed upon the addition of different redox metabolites (**Fig. 7.4A-H**). These results indicate that the metabolites are interacting with rAtAOX1A. The decrease in the fluorescence intensity of rAtAOX1A upon binding with redox metabolites could be due to structural changes associated with fluorescence quenching (**Fig. 7.4A-H**; Lelis et al., 2020; Duysak et al., 2021).

Nevertheless, these observations need further investigation to validate potent residues involved in the binding with different redox metabolites and their role in AOX function since the crystal structure of plant AOX/AtAOX1A is not yet resolved.

Highlights of the study

- ✓ Molecular docking studies have shown some important conserved binding pockets or residues in rAtAOX1A for different redox metabolites, as shown below:
- NADH, NADP, GSH and GSSG (α3 and α6)
- NAD and Ascorbic acid (S3 and α6)
- NADPH & DHA shares Met191(α 2) and Phe251(α 4)
- ✓ Point mutational studies revealed that the potential candidates involved in binding to different types of redox metabolites are either polar or/and hydrophobic in nature.

- ✓ SPR kinetic studies have shown that rAtAOX1A is able to interact with redox couples in a reversible binding fashion, however, in the following order of affinity: NAD > GSSG ≥ GSH ≥ NADP > DHA > AsA.
- \checkmark When rAtAOX1A interact with redox metabolites, the α-helical content decreases with a concomitant rise in β-sheets, indicating possible conformational changes in its secondary structure.
- ✓ Also, a decrease in the fluorescence intensity with no shift (red or blue) in the spectral peak indicates that the interaction of rAtAOX1A with redox metabolites caused an overall change in its conformation without disturbing the hydrophobic environment of tryptophan residues.

Chapter 8

Summary and Conclusions

Summary and Conclusions

The present study aimed to characterize the purified rAtAOX1A protein and its interaction with known AOX inhibitors (SHAM and n-PG), pyruvate, TCA cycle metabolites, and redox metabolites using biophysical and in silico studies. For this, we need a large amount of purified AtAOX1A. Hence, in this study, the cDNA, which encodes mature AtAOX1A protein, was amplified and cloned into a pET28a(+) vector (Figs. 4.1–4.2). The pAtAOX1A plasmid construct was transformed into BL21(DE3) *E. coli* cells and the positive colonies were selected by colony PCR and restriction digestion (Figs. 4.3–4.4). Recombinant plasmids from these positive colonies were isolated and confirmed by DNA sequencing (Fig. 4.5). After confirming the *AtAOX1A* sequence; these colonies were used for recombinant protein synthesis. The rAtAOX1A protein (~37 kDa) expression was visualized on 12.5% (w/v) SDS-PAGE (Fig. 4.6). *To identify whether the heterologously expressed protein is functionally active or not, E. coli*/pET28a (control *E. coli*) and *E. coli*/pAtAOX1A (recombinant *E. coli*) were tested for concentration-dependent cyanide resistance, as well as n-PG & SHAM sensitive respiration and growth (Figs. 4.7A-C and 4.8A-F).

In order to get active protein, rAtAOX1A was induced by IPTG in the presence of 0.1 mM FeSO₄ and 10 mM pyruvate. The expressed rAtAOX1A was extracted from the *E. coli* membranes by solubilizing with DDM and purified using cobalt column affinity chromatography, as the expression cassette contains an N-terminal His₆-tag. The purified rAtAOX1A possessed a molecular mass of ~37 kDa, which includes AtAOX1A mature protein (33.44 kDa) and pET28a(+) vector sequence (3.83 kDa) (**Fig. 4.9A**). The purified rAtAOX1A was confirmed by western blot (**Fig. 4.9B**) and MALDI-TOF/TOF analysis (**Figs. 4.10A-F**). The rAtAOX1A in its soluble form has shown a specific activity of 3.86

 μ mol O₂ min⁻¹ mg⁻¹ in the presence of duroquinol (**Table 4.1**). All further experiments (SPR, CD and fluorescence spectroscopy) are carried out with the soluble form of AtAOX1A (monomeric form).

The Far-UV (190-260 nm) CD spectra of purified rAtAOX1A have shown that it possessed a typical α -helical structure and it is structurally stable at different temperatures and pH (Figs. 5.1-5.4). The changes in the secondary structure of rAtAOX1A in the presence of its inhibitors were studied by using CD spectroscopy in the far-UV region from 190–260 nm. Both the inhibitors have not shown significant changes in the CD spectra except for little deviations (Figs. 5.5A, B). However, changes in secondary structural elements were observed upon analysis of the CD data using the Dichroweb online server. The rAtAOX1A α -helical content is decreased (<10%) while β -sheets (<7%), β -turns and random coils (<3%) increased upon interaction with the inhibitors SHAM and n-PG, which resulted in a change in the protein conformation (Table 5.1).

The AtAOX1A protein contains nine Trp residues and the fluorescence emission profile of rAtAOX1A has shown a red shift, with maximum wavelength emission spectra changing from 339 nm (in the absence of inhibitors) to 358 nm in the presence of SHAM and 378 nm in the presence of n-PG, respectively (**Figs. 5.6A, B**). These results indicate that protein gets unfolded in the presence of inhibitor(s) and tryptophan residues are exposed to the more polar environment.

The real-time binding affinity (SPR) studies of rAtAOX1A with its known inhibitors, such as SHAM and n-PG, indicated that n-PG has more affinity than SHAM for rAtAOX1A, suggesting that n-PG is a better inhibitor than SHAM (**Figs. 5.7A, B**). Also, SPR results

revealed that the immobilized rAtAOX1A is able to interact with its inhibitors in a reversible binding fashion.

Further, molecular docking studies have revealed that the SHAM and n-PG bind at the same hydrophobic cavity to which DQ binds in the AtAOX1A (**Figs. 5.8A**, **B and Fig 5.10IIIb**). The residues, Met195 and Phe255 were identified as potent residues using mutational docking studies (**Figs. 5.9A**, **B**). Further, the binding pockets for AOX substrates such as duroquinol and ubiquinol and oxidized products, ubiquinone and duroquinone were identified (**Figs. 5.10I-IV**) and compared the location of the diiron cavity with the inhibitors and substrates/products binding sites. The AOX substrates (Q₁H₂ and DQH₂) binding sites are far from the inhibitor binding site, while the UQ₁ (oxidized form) binding site bridges the diiron cavity and inhibitors binding site (**Figs. 5.10I-VI and 5.11A**, **B**).

The literature reveals that pyruvate, the end product of glycolysis, and a few TCA cycle metabolites such as α -KG, OAA and malate are known to enhance mitochondrial respiration through the AOX pathway. However, their interaction with AOX is not revealed so far. In this study, the molecular interaction of purified rAtAOX1A with pyruvate and TCA cycle metabolites (citrate, α -KG, succinate, fumaric acid, malic acid and OAA) (**Table 6.1**) was studied.

Molecular docking studies have shown binding pockets on the AtAOX1A surface for these metabolites. However, few metabolites, such as (i) citrate & α -KG and (ii) malic acid & OAA, bind to the same groove (**Table 6.2**). Further, mutational docking studies revealed the potent residues in the binding pocket on AtAOX1A for each of the TCA cycle metabolites or pyruvate. In the case of citrate and α -KG, Arg223 of AtAOX1A plays a crucial role in the interaction; for the interaction of fumaric acid, two residues of AtAOX1A (Glu275 and

Thr167) play an important role; for malic acid and OAA interaction, Asp315 is found important, while for pyruvate interaction three residues Arg174, Gly176, and Cys177 were found to be important (**Table 6.3**).

The SPR kinetic results showed the following order of binding affinity of TCA cycle metabolites with rAtAOX1A: α -KG > fumaric acid \geq OAA \geq malic acid (**Figs. 6.2A-D & 6.3** and **Table 6.4**). Contrarily, though pyruvate, citrate, and succinate are used for binding analysis, we could not get proper binding signals with these metabolites (**Figs. 6.1A, B and D**).

The addition of pyruvate and TCA cycle metabolites to rAtAOX1A has shown marginal deviations in the ellipticity of its CD spectrum taken in the far-UV region from 190–260 nm (**Figs. 6.4A-G**). But, the rAtAOX1A α -helical content is decreased (<10%) while β -sheets (<7%), β -turns and random coils (<3%) increased upon interaction with pyruvate and TCA cycle metabolites (**Table 6.5**). Further, the results suggest that, although a transition in the secondary structural conformation occurred from α -helix to β -sheet, the typical α -helical signal was retained in the CD spectrum even upon binding with pyruvate or TCA cycle metabolite(s).

The conformational changes in rAtAOX1A upon the addition of different concentrations of pyruvate and TCA cycle metabolites were monitored by following the changes in the fluorescence emission spectra. Also, in the present study, a decrease in the fluorescence intensity was observed without a shift in the peak (339 nm) upon the addition of these metabolites (**Figs. 6.5A-G**). These results indicate that the interaction with pyruvate and TCA cycle metabolites caused an overall conformational change in the rAtAOX1A without disturbing the hydrophobic environment of Trp residues.

From the literature, it is known that in plants, under different biotic and abiotic stress conditions, the mitochondrial alternative oxidase (AOX) activity is increased dramatically to maintain cellular redox homeostasis. But, the physical interaction of the cellular redox metabolites (GSH, GSSG, Asc, DHA, NAD, NADH, NADP and NADPH) with AtAOX1A and the concurrent structural changes that occur in AOX is not yet revealed. In this study, the molecular interaction of purified rAtAOX1A with different redox metabolites (**Table 7.1**) was analyzed using molecular docking, SPR, CD and fluorescence spectroscopy.

The molecular docking studies have shown several conserved locations on the rAtAOX1A surface for different redox metabolites. For e.g., the metabolites GSH, NADH and NADP are bound to the same binding pocket on WT-AtAOX1A. Besides, the most probable binding site for GSSG and GSH on AtAOX1A possessed ten residues in common on WT-AtAOX1A. Further, the ligands NAD and AsA possessed several residues in common in their binding pocket on AtAOX1A, while the binding sites for ligands DHA and NADPH have not shown any commonality with other binding pockets but shared two residues in common (**Table 7.2**). It is found that Thr133 is the potent residue for the binding of NAD and Asp315 is the potent residue for the binding of AsA. Besides, the amino acid Val192 is found to be the potent residue for the binding of DHA and in the case of NADPH, Met191 and Glu220 are found to be important residues for binding with AtAOX1A (**Table 7.3**).

The redox metabolites have shown reversible binding with rAtAOX1A in the following order in the SPR analysis: $NAD > GSSG \ge GSH \ge NADP > DHA > Ascorbic acid$ (Figs. 7.2A-F and Table 7.4). However, the metabolites NADH and NADPH did not show binding signals to rAtAOX1A (Figs. 7.1F and H).

The addition of redox metabolites to purified rAtAOX1A has shown a marginal change in the ellipticity of the CD spectrum (**Figs. 7.3A-H**). However, the rAtAOX1A α -helical content is decreased (<21%) while β -sheets (<7%), β -turns (<14%) and random coils (<7%) are increased in rAtAOX1A upon interaction with various redox metabolites at the chosen concentrations used in the present study (**Table 7.5**).

Also, the addition of redox metabolites caused a decrease in the fluorescence intensity of emission spectra of rAtAOX1A without any shift in the peak observed at 339 nm in the control (**Figs. 7.4A-H**). These results suggest that the interaction of rAtAOX1A with the redox metabolites caused minute changes in its tertiary structure that may not allow the hydrophobic groups of the protein to get exposed to the solvent.

The following conclusions are drawn from the present study

- 1. The rAtAOX1A expressed in *E. coli* BL21(DE3) cells is found to be functionally active, as evident by its sensitivity to respiratory and growth rates in the presence of metabolic inhibitors SHAM and n-PG.
- 2. The rAtAOX1A purified by affinity chromatography was confirmed by Western blot and MALDI TOF/TOF analysis and possessed a molecular mass of ~37 kDa. Also, the purified rAtAOX1A has shown moderate specific activity with duroquinol as substrate in Tris-HCl (pH 7.5).
- 3. Secondary structural analysis of rAtAOX1A has shown strong negative bands at 222 nm and 208 nm and a positive band at 193 nm, which indicates that purified rAtAOX1A is in α helical conformation.
- 4. The rAtAOX1A, which is purified from the non-thermogenic plant *Arabidopsis thaliana*, is stable at a wide range of temperatures, as shown in the case of thermogenic plants.

- 5. The binding of SHAM or n-PG binds to the hydrophobic groove of rAtAOX1A, unfolds it and causes a decrease in its helical structure, which in turn may not allow the binding of its substrate.
- 6. Mutational docking studies revealed that Met195 and Phe255 are the potential candidates to bind the inhibitor. Hence, this binding pocket could be a potential gateway for the oxidation-reduction process in AtAOX1A.
- 7. Molecular docking, together with mutational docking studies, confirmed the presence of binding pockets on rAtAOX1A for pyruvate, TCA cycle, and redox metabolites examined in the present study, while few metabolites shared common binding pockets.
- 8. The SPR kinetic analysis has shown the following order of affinity of (i) TCA cycle: α -KG > fumaric acid \geq OAA \geq malic acid and (ii) redox metabolites: NAD > GSSG \geq GSH \geq NADP > DHA > AsA with rAtAOX1A in a reversible binding fashion.
- 9. The interaction of rAtAOX1A with redox metabolites caused significant changes in the secondary structural elements (α -helix, β -sheet, β -turn, and random coils) as compared to pyruvate or TCA cycle metabolites.
- 10. A decrease in the fluorescence intensity with no shift (red or blue) in the spectral peak of rAtAOX1A indicates that the interaction of pyruvate, TCA cycle or redox metabolites caused an overall conformational change in the tertiary structure of rAtAOX1A without disturbing the hydrophobic environment of tryptophan residues.

Future Directions

- Crystallization: Although the present study gave some knowledge on the molecular interaction mechanism of AOX with its inhibitors and different cellular metabolites (Chapters 4, 5, 6 and 7), proper crystal structure with high resolution is yet to be solved from non-thermogenic plants, which is essential for the better understanding of the structure-function biology of AOX from plants.
- ❖ Agricultural use: Several abiotic and biotic stress conditions cause less crop yield in the crop plant. The results from the present study (Chapters 6 and 7) have shown the metabolites interacting with AOX. Exogenous application of AOX-activating metabolites on the crop plant may increase crop yield under stress conditions (Godoy et al., 2021), which will be time-saving and legally risk-free compared to the transgenic approach.
- ❖ Therapeutic use: Proteoliposome formulation with purified rAOX, which can target specific tissues as a remedy for miETC over-reduction or dysfunction in animals, including humans.

Literature Cited

- **Affourtit, C., & Moore, A. L. (2004).** Purification of the plant alternative oxidase from *Arum maculatum*: Measurement, stability and metal requirement. *Biochimica et Biophysica Acta Bioenergetics*, **1608(2–3)**, 181–189.
- Affourtit, C., Albury, M. S., Crichton, P. G., & Moore, A. L. (2002). Exploring the molecular nature of alternative oxidase regulation and catalysis. *FEBS Letters*, *510*(3), 121–126.
- **Ajayi, W. U., Chaudhuri, M., & Hill, G. C.** (2002). Site-directed mutagenesis reveals the essentiality of the conserved residues in the putative diiron active site of the trypanosome alternative oxidase. *Journal of Biological Chemistry*, **277(10)**, 8187–8193.
- Alber, N. A., & Vanlerberghe, G. C. (2021). The flexibility of metabolic interactions between chloroplasts and mitochondria in *Nicotiana tabacum* leaf. *Plant Journal*, 106(6), 1625–1646.
- **Albury, M. S., Elliott, C., & Moore, A. L. (2009).** Towards a structural elucidation of the alternative oxidase in plants. *Physiologia Plantarum*, **137(4)**, 316–327.
- Anraku, Y., & Gennis, R. B. (1987). The aerobic respiratory chain of *Escherichia coli*.

 Trends in Biochemical Sciences, 12(C), 262–266.
- Arrigoni, O., & De Tullio, M. C. (2002). Ascorbic acid: Much more than just an antioxidant. *Biochimica et Biophysica Acta General Subjects*, **1569**(1–3), 1–9.
- Aziz, S., Germano, T. A., Thiers, K. L. L., Batista, M. C., de Souza Miranda, R., Arnholdt-Schmitt, B., & Costa, J. H. (2022). Transcriptome analyses in a selected gene set indicate alternative oxidase (AOX) and early enhanced fermentation as critical for salinity tolerance in rice. *Plants*, *11*(16), 2145.
- Balmer, Y., Vensel, W. H., Tanaka, C. K., Hurkman, W. J., Gelhaye, E., Rouhier, N., ... & Buchanan, B. B. (2004). Thioredoxin links redox to the regulation of fundamental processes of plant mitochondria. *Proceedings of the national academy of*

- sciences, 101(8), 2642-2647.
- Barreto, P., Counago, R. M., & Arruda, P. (2020). Mitochondrial uncoupling protein-dependent signaling in plant bioenergetics and stress response. *Mitochondrion*, 53, 109-120.
- Barsottini, M. R. O., Copsey, A., Young, L., Baroni, R. M., Cordeiro, A. T., Pereira, G. A. G., & Moore, A. L. (2020). Biochemical characterization and inhibition of the alternative oxidase enzyme from the fungal phytopathogen Moniliophthora perniciosa. *Communications Biology*, 3(1).
- Bartoli, Carlos G., Gomez, F., Gergoff, G., Guiamét, J. J., & Puntarulo, S. (2005). Upregulation of the mitochondrial alternative oxidase pathway enhances photosynthetic electron transport under drought conditions. *Journal of Experimental Botany*, 56(415), 1269–1276.
- Bartoli, Carlos G., Yu, J., Gómez, F., Fernández, L., McIntosh, L., & Foyer, C. H. (2006). Inter-relationships between light and respiration in the control of ascorbic acid synthesis and accumulation in *Arabidopsis thaliana* leaves. *Journal of Experimental Botany*, 57(8), 1621–1631.
- Bartoli, Carlos Guillermo, Gómez, F., Martínez, D. E., & Guiamet, J. J. (2004). Mitochondria are the main target for oxidative damage in leaves of wheat (*Triticum aestivum* L.). *Journal of Experimental Botany*, 55(403), 1663–1669.
- Baxter, C. J., Redestig, H., Schauer, N., Repsilber, D., Patil, K. R., Nielsen, J., ... Sweetlove, L. J. (2007). The metabolic response of heterotrophic Arabidopsis cells to oxidative stress. *Plant Physiology*, *143*(1), 312–325.
- **Bendall, D. S., & Bonner Jr, W. D.** (1971). Cyanide-insensitive respiration in plant mitochondria. *Plant physiology*, 47(2), 236-245.
- **Berthold, D. A. (1998).** Isolation of mutants of the *Arabidopsis thaliana* alternative oxidase (ubiquinol:oxygen oxidoreductase) resistant to salicylhydroxamic acid. *Biochimica et Biophysica Acta Bioenergetics*, **1364(1)**, 73–83.

- **Berthold, D. A., & Siedow, J. N.** (1993). Partial purification of the cyanide-resistant alternative oxidase of skunk cabbage (*Symplocarpus foetidus*) mitochondria. *Plant Physiology*, **101**(1), 113–119.
- **Berthold, D. A., & Stenmark, P.** (2003). MEMBRANE-BOUND DIIRON CARBOXYLATE PROTEINS . *Annual Review of Plant Biology*, **54(1)**, 497–517.
- Berthold, D. A., Andersson, M. E., & Nordlund, P. (2000). New insight into the structure and function of the alternative oxidase. *Biochimica et Biophysica Acta (BBA)-Bioenergetics*, **1460**(2-3), 241-254.
- Berthold, D. A., Voevodskaya, N., Stenmark, P., Gräslund, A., & Nordlund, P. (2002). EPR studies of the mitochondrial alternative oxidase: Evidence for a diiron carboxylate center. *Journal of Biological Chemistry*, 277(46), 43608–43614.
- Bonner, W. D., Clarke, S. D., & Rich, P. R. (1986). Partial Purification and Characterization of the Quinol Oxidase Activity of *Arum maculatum* Mitochondria. *Plant Physiology*, 80(4), 838–842.
- Borecký, J., Nogueira, F. T., De Oliveira, K. A., Maia, I. G., Vercesi, A. E., & Arruda, P. (2006). The plant energy-dissipating mitochondrial systems: depicting the genomic structure and the expression profiles of the gene families of uncoupling protein and alternative oxidase in monocots and dicots. *Journal of Experimental Botany*, 57(4), 849-864.
- Borisov, V. B., Gennis, R. B., Hemp, J., & Verkhovsky, M. I. (2011). The cytochrome *bd* respiratory oxygen reductases. *Biochimica et Biophysica Acta Bioenergetics*, *1807*(11), 1398–1413.
- **Boyd, I., & Beveridge, E. G. (1979).** Relationship between the antibacterial activity towards *Escherichia coli* NCTC 5933 and the physico-chemical properties of some esters of 3,4,5-trihydroxybenzoic acid (Gallic acid). *Microbios*, **24(97–98)**, 173–184.
- **Braun, H. P.** (2020). The oxidative phosphorylation system of the mitochondria in plants. *Mitochondrion*, 53, 66-75.

- Bykova, N. V., Egsgaard, H., & Møller, I. M. (2003). Identification of 14 new phosphoproteins involved in important plant mitochondrial processes. *FEBS letters*, 540(1-3), 141-146.
- Bykova, N. V., Stensballe, A., Egsgaard, H., Jensen, O. N., & Møller, I. M. (2003). Phosphorylation of formate dehydrogenase in potato tuber mitochondria. *Journal of Biological Chemistry*, 278(28), 26021-26030.
- Carré, J. E., Affourtit, C., & Moore, A. L. (2011). Interaction of purified alternative oxidase from thermogenic *Arum maculatum* with pyruvate. *FEBS Letters*, 585(2), 397–401.
- Chadee, A., Mohammad, M., & Vanlerberghe, G. C. (2022). Evidence that mitochondrial alternative oxidase respiration supports carbon balance in source leaves of Nicotiana tabacum. *Journal of Plant Physiology*, 279, 153840.
- Challabathula, D., Analin, B., Mohanan, A., & Bakka, K. (2022). Differential modulation of photosynthesis, ROS and antioxidant enzyme activities in stress-sensitive and tolerant rice cultivars during salinity and drought upon restriction of COX and AOX pathways of mitochondrial oxidative electron transport. *Journal of Plant Physiology*, 268, 153-583.
- Chen, Y., & Hoehenwarter, W. (2015). Changes in the phosphoproteome and metabolome link early signaling events to rearrangement of photosynthesis and central metabolism in salinity and oxidative stress response in arabidopsis. *Plant Physiology*, *169*(4), 3021–3033.
- Chew, O., Whelan, J., & Millar, A. H. (2003). Molecular Definition of the Ascorbate-Glutathione Cycle in Arabidopsis Mitochondria Reveals Dual Targeting of Antioxidant Defenses in Plants. *Journal of Biological Chemistry*, 278(47), 46869–46877.
- Clifton, R., Lister, R., Parker, K. L., Sappl, P. G., Elhafez, D., Millar, A. H., ... Whelan, J. (2005). Stress-induced co-expression of alternative respiratory chain components in *Arabidopsis thaliana*. *Plant Molecular Biology*, 58, 193–212.

- Clifton, R., Millar, A. H., & Whelan, J. (2006). Alternative oxidases in Arabidopsis: A comparative analysis of differential expression in the gene family provides new insights into function of non-phosphorylating bypasses. *Biochimica et Biophysica Acta Bioenergetics*, 1757(7), 730–741.
- Considine, M. J., Holtzapffel, R. C., Day, D. A., Whelan, J., & Millar, A. H. (2002). Molecular distinction between alternative oxidase from monocots and dicots. *Plant Physiology*, 129(3), 949–953.
- Costa, J. H., Dos Santos, C. P., da Cruz Saraiva, K. D., & Arnholdt-Schmitt, B. (2017).

 A step-by-step protocol for classifying AOX proteins in flowering plants. *Plant Respiration and Internal Oxygen: Methods and Protocols*, 225-234.
- Costa, J. H., Dos Santos, C. P., e Lima, B. D. S., Netto, A. N. M., da Cruz Saraiva, K. D., & Arnholdt-Schmitt, B. (2017). In silico identification of alternative oxidase 2 (AOX2) in monocots: A new evolutionary scenario. *Journal of plant physiology*, 210, 58-63.
- Crichton, P. G., Affourtit, C., Albury, M. S., Carré, J. E., & Moore, A. L. (2005). Constitutive activity of *Sauromatum guttatum* alternative oxidase in *Schizosaccharomyces pombe* implicates residues in addition to conserved cysteines in α-keto acid activation. *FEBS Letters*, *579*, 331–336.
- Cvetkovska, M., & Vanlerberghe, G. C. (2012). Alternative oxidase modulates leaf mitochondrial concentrations of superoxide and nitric oxide. *New Phytologist*, 195(1), 32–39.
- Cvetkovska, M., & Vanlerberghe, G. C. (2013). Alternative oxidase impacts the plant response to biotic stress by influencing the mitochondrial generation of reactive oxygen species. *Plant, Cell and Environment*, *36*(3), 721–732.
- **Dahal, K., & Vanlerberghe, G. C.** (2017). Alternative oxidase respiration maintains both mitochondrial and chloroplast function during drought. *New Phytologist*, 213(2), 560–571.

- Dastogeer, K. M. G., Li, H., Sivasithamparam, K., Jones, M. G. K., Du, X., Ren, Y., & Wylie, S. J. (2017). Metabolic responses of endophytic *Nicotiana benthamiana* plants experiencing water stress. *Environmental and Experimental Botany*, 143, 59–71.
- Day, D. A., Whelan, J., Millar, A. H., Siedow, J. N., & Wiskich, J. T. (1995). Regulation of the alternative oxidase in plants and fungi. *Australian Journal of Plant Physiology*, 22(3), 497–509.
- Del-Saz, N. F., Ribas-Carbo, M., McDonald, A. E., Lambers, H., Fernie, A. R., & Florez-Sarasa, I. (2018). An In Vivo Perspective of the Role(s) of the Alternative Oxidase Pathway. *Trends in Plant Science*, 23(3), 206–219.
- **Diethelm, R., Miller, M. G., Shibles, R., & Stewart, C. R. (1990).** Effect of Salicylhydroxamic Acid on Respiration, Photosynthesis, and Peroxidase Activity in Various Plant Tissues. *Plant and Cell Physiology*, **31(2)**, 179–185.
- Dinakar, C., Vishwakarma, A., Raghavendra, A. S., & Padmasree, K. (2016). Alternative oxidase pathway optimizes photosynthesis during osmotic and temperature stress by regulating cellular ROS, malate valve and antioxidative systems. *Frontiers in Plant Science*, 7, 68.
- **Dinakar, C., Vishwakarma, A., Yearla, S. R., Raghavendra, A. S., & Padmasree, K.** (2010a). Importance of ROS and antioxidant system during the beneficial interactions of mitochondrial metabolism with photosynthetic carbon assimilation. *Planta*, 231(2), 461–474.
- **Dinakar, Challabathula, Raghavendra, A. S., & Padmasree, K.** (2010b). Importance of AOX pathway in optimizing photosynthesis under high light stress: Role of pyruvate and malate in activating AOX. *Physiologia Plantarum*, 139(1), 13–26.
- Du, C., Zhang, B., He, Y., Hu, C., Ng, Q. X., Zhang, H., ... ZhifenLin. (2017). Biological effect of aqueous C60 aggregates on *Scenedesmus obliquus* revealed by transcriptomics and non-targeted metabolomics. *Journal of Hazardous Materials*, 324, 221–229.
- Dunn, A. K. (2023). Alternative oxidase in bacteria. Biochimica et Biophysica Acta (BBA)-

- Bioenergetics, 148929.
- **Duysak, T., Afzal, A. R., & Jung, C. H.** (2021). Determination of glutathione-binding to proteins by fluorescence spectroscopy. *Biochemical and Biophysical Research Communications*, 557, 329–333.
- Elliott, C., Young, L., May, B., Shearman, J., Albury, M. S., Kido, Y., ... Moore, A. L. (2014). Purification and characterisation of recombinant DNA encoding the alternative oxidase from *Sauromatum guttatum*. *Mitochondrion*, 19, 261–268.
- Elthon, T. E., & McIntosh, L. (1987). Identification of the alternative terminal oxidase of higher plant mitochondria. *Proceedings of the National Academy of Sciences USA*, 84(23), 8399–8403.
- Elthon, Thomas E., & McIntosh, L. (1986). Characterization and Solubilization of the Alternative Oxidase of *Sauromatum guttatum* Mitochondria . *Plant Physiology*, 82(1), 1–6.
- Escobar, M. A., Geisler, D. A., & Rasmusson, A. G. (2006). Reorganization of the alternative pathways of the Arabidopsis respiratory chain by nitrogen supply: Opposing effects of ammonium and nitrate. *Plant Journal*, 45(5), 775–788.
- **Eulgem, T., & Somssich, I. E. (2007).** Networks of WRKY transcription factors in defense signaling. *Current Opinion in Plant Biology*, **10(4)**, 366–371.
- **Fedotova, O. A., Polyakova, E. A., & Grabelnych, O. I.** (2023). Ca 2+-dependent oxidation of exogenous NADH and NADPH by the mitochondria of spring wheat and its relation with AOX capacity and ROS content at high temperatures. *Journal of Plant Physiology*, 283, 153943-153943.
- **Finnegan, P. M., Umbach, A. L., & Wilce, J. A.** (2003). Prokaryotic origins for the mitochondrial alternative oxidase and plastid terminal oxidase nuclear genes. *FEBS Letters*, 555(3), 425–430.
- Fiorani, F., Umbach, A. L., & Siedow, J. N. (2005). The alternative oxidase of plant mitochondria is involved in the acclimation of shoot growth at low temperature. A study

- of Arabidopsis AOX1a transgenic plants. *Plant Physiology*, 139(4), 1795–1805.
- **Florez-Sarasa, I., Fernie, A. R., & Gupta, K. J.** (2020). Does the alternative respiratory pathway offer protection against the adverse effects resulting from climate change? *Journal of Experimental Botany*, 71(2), 465–469.
- Florez-Sarasa, I., Flexas, J., Rasmusson, A. G., Umbach, A. L., Siedow, J. N., & Ribas-Carbo, M. (2011). In vivo cytochrome and alternative pathway respiration in leaves of Arabidopsis thaliana plants with altered alternative oxidase under different light conditions. *Plant, Cell & Environment*, 34(8), 1373-1383.
- **Friedle, S., Reisner, E., & Lippard, S. J.** (2010). Current challenges of modeling diiron enzyme active sites for dioxygen activation by biomimetic synthetic complexes. *Chemical Society Reviews*, 39(8), 2768–2779.
- **Friedrich, T., Steinmüller, K., & Weiss, H.** (1995). The proton-pumping respiratory complex I of bacteria and mitochondria and its homologue in chloroplasts. *FEBS Letters*, 367(2), 107–111.
- Fujita, M., Fujita, Y., Noutoshi, Y., Takahashi, F., Narusaka, Y., Yamaguchi-Shinozaki, K., & Shinozaki, K. (2006). Crosstalk between abiotic and biotic stress responses: a current view from the points of convergence in the stress signaling networks. Current Opinion in Plant Biology, 9(4), 436–442.
- Fukai, Y., Amino, H., Hirawake, H., Yabu, Y., Ohta, N., Minagawa, N., ... Kita, K. (1999). Functional expression of the ascofuranone-sensitive *Trypanosoma brucei brucei* alternative oxidase in the cytoplasmic membrane of *Escherichia coli*. *Comparative Biochemistry and Physiology C Pharmacology Toxicology and Endocrinology*, 124(2), 141–148.
- Gandin, A., Koteyeva, N. K., Voznesenskaya, E. V., Edwards, G. E., & Cousins, A. B. (2014). The acclimation of photosynthesis and respiration to temperature in the C₃-C₄ intermediate *Salsola divaricata*: Induction of high respiratory CO₂ release under low temperature. *Plant Cell and Environment*, 37(11), 2601–2612.

- **Garmash, E. V.** (2023). Suppression of mitochondrial alternative oxidase can result in upregulation of the ROS scavenging network: Some possible mechanisms underlying the compensation effect. *Plant Biology*, 25(1), 43-53.
- Garmash, E. V., Velegzhaninov, I. O., Ermolina, K. V., Rybak, A. V., & Malyshev, R. V. (2020). Altered levels of AOX1a expression result in changes in metabolic pathways in *Arabidopsis thaliana* plants acclimated to low dose rates of ultraviolet B radiation. *Plant Science*, 291, 110332.
- Gheibi, N., Asghari, H., Chegini, K. G., Sahmani, M., & Moghadasi, M. (2016). The role of calcium in the conformational changes of the recombinant S100A8/S100A91. *Molecular Biology*, 50(1), 118–123.
- Giraud, E., Ho, L. H. M. M., Clifton, R., Carroll, A., Estavillo, G., Tan, Y. F., ... Whelan, J. (2008). The absence of Alternative Oxidase1a in Arabidopsis results in acute sensitivity to combined light and drought stress. *Plant Physiology*, 147(2), 595–610.
- Giraud, E., van Aken, O., Ho, L. H. M., & Whelan, J. (2009). The transcription factor ABI4 is a regulator of mitochondrial retrograde expression of ALTERNATIVE OXIDASE1a. *Plant Physiology*, *150*(3), 1286–1296.
- Godoy, F., Olivos-Hernández, K., Stange, C., & Handford, M. (2021). Abiotic Stress in Crop Species: Improving Tolerance by Applying Plant Metabolites. *Plants*, *10*(2), 186.
- Gou, L., Lee, J., Yang, J. M., Park, Y. D., Zhou, H. M., Zhan, Y., & Lü, Z. R. (2017). Inhibition of tyrosinase by fumaric acid: Integration of inhibition kinetics with computational docking simulations. *International Journal of Biological Macromolecules*, 105, 1663–1669.
- Gray, G. R., Maxwell, D. P., Villarimo, A. R., & McIntosh, L. (2004). Mitochondria/nuclear signaling of alternative oxidase gene expression occurs through distinct pathways involving organic acids and reactive oxygen species. *Plant Cell Reports*, 23(7), 497–503.

- Grosdidier, A., Zoete, V., & Michielin, O. (2011a). Fast docking using the CHARMM force field with EADock DSS. *Journal of computational chemistry*, 32(10), 2149-2159.
- Grosdidier, A., Zoete, V., & Michielin, O. (2011b). SwissDock, a protein-small molecule docking web service based on EADock DSS. *Nucleic Acids Research*, 39(2), 270–277.
- Gupta, K. J., Fernie, A. R., Kaiser, W. M., & van Dongen, J. T. (2011). On the origins of nitric oxide. *Trends in Plant Science*, 16(3), 160–168.
- Gupta, K. J., Shah, J. K., Brotman, Y., Jahnke, K., Willmitzer, L., Kaiser, W. M., ... Igamberdiev, A. U. (2012). Inhibition of aconitase by nitric oxide leads to induction of the alternative oxidase and to a shift of metabolism towards biosynthesis of amino acids. *Journal of Experimental Botany*, 63(4), 1773–1784.
- Han, Y. H., & Park, W. H. (2009). Propyl gallate inhibits the growth of HeLa cells via regulating intracellular GSH level. *Food and Chemical Toxicology*, 47(10), 2531–2538.
- He, C., Berkowitz, O., Hu, S., Zhao, Y., Qian, K., Shou, H., ... & Wang, Y. (2023). Coregulation of mitochondrial and chloroplast function–molecular components and mechanisms. *Plant Communications*.
- Hebia, C., Bekale, L., Chanphai, P., Agbebavi, J., & Tajmir-Riahi, H. A. (2014). Trypsin inhibitor complexes with human and bovine serum albumins: TEM and spectroscopic analysis. *Journal of Photochemistry and Photobiology B: Biology*, 130, 254–259.
- Herrero, E., Ros, J., Bellí, G., & Cabiscol, E. (2008). Redox control and oxidative stress in yeast cells. *Biochimica et Biophysica Acta General Subjects*, 1780(11), 1217–1235.
- Ho, L. H., Giraud, E., Uggalla, V., Lister, R., Clifton, R., Glen, A., ... & Whelan, J. (2008). Identification of regulatory pathways controlling gene expression of stress-responsive mitochondrial proteins in Arabidopsis. *Plant physiology*, 147(4), 1858-1873.
- Hoefnagel, M. H. N., Wiskich, J. T., Madgwick, S. A., Patterson, Z., Oettmeier, W., & Rich, P. R. (1995). New Inhibitors of the Ubiquinol Oxidase of Higher Plant Mitochondria. *European Journal of Biochemistry*, 233(2), 531–537.

- Hoefnagel, M. H., Rich, P. R., Zhang, Q., & Wiskich, J. T. (1997). Substrate kinetics of the plant mitochondrial alternative oxidase and the effects of pyruvate. *Plant Physiology*, 115(3), 1145-1153.
- **Homola, J. (2003).** Present and future of surface plasmon resonance biosensors. *Analytical and Bioanalytical Chemistry*, **377(3)**, 528–539.
- **Huq, S., & Palmer, J. M.** (1978). Isolation of a cyanide-resistant duroquinol oxidase from arum maculatum mitochondria. *FEBS Letters*, *95*(2), 217–220.
- **Igamberdiev, A. U., & Bykova, N. V.** (2018). Role of organic acids in the integration of cellular redox metabolism and mediation of redox signalling in photosynthetic tissues of higher plants. *Free Radical Biology and Medicine*, 122, 74-85.
- **Igamberdiev, A. U., & Gardeström, P. (2003).** Regulation of NAD- and NADP-dependent isocitrate dehydrogenases by reduction levels of pyridine nucleotides in mitochondria and cytosol of pea leaves. *Biochimica et Biophysica Acta Bioenergetics*, **1606(1–3)**, 117–125.
- Ishikawa, T., Takahara, K., Hirabayashi, T., Matsumura, H., Fujisawa, S., Terauchi, R., ... Kawai-Yamada, M. (2010). Metabolome Analysis of Response to Oxidative Stress in Rice Suspension Cells Overexpressing Cell Death Suppressor Bax Inhibitor-1. *Plant and Cell Physiology*, 51(1), 9–20.
- Ito, K., Ogata, T., Kakizaki, Y., Elliott, C., Albury, M. S., & Moore, A. L. (2011). Identification of a gene for pyruvate-insensitive mitochondrial alternative oxidase expressed in the thermogenic appendices in *Arum maculatum*. *Plant Physiology*, *157*(4), 1721–1732.
- Jarmuszkiewicz, W., Czarna, M., & Sluse, F. E. (2005). Substrate kinetics of the *Acanthamoeba castellanii* alternative oxidase and the effects of GMP. *Biochimica et Biophysica Acta Bioenergetics*, 1708(1), 71–78.
- **Jiménez, A., Hernández, J. A.,** del Río, L. A., & Sevilla, F. (1997). Evidence for the presence of the ascorbate-glutathione cycle in mitochondria and peroxisomes of pea

- leaves. *Plant physiology*, **114**(1), 275-284.
- Jo, S., Kim, T., Iyer, V. G., Im, W. (2008). CHARMM-GUI a web-based graphical user interface for CHARMM. *Journal of Computational Chemistry*, 29, 1859–1865
- **Joseph-Horne, T., Hollomon, D. W., & Wood, P. M.** (2001). Fungal respiration: a fusion of standard and alternative components. *Biochimica et Biophysica Acta* (*BBA*) *Bioenergetics*, **1504**(2–3), 179–195.
- **Kay, C. J., & Palmer, J. M. (1985).** Solubilization of the alternative oxidase of cuckoo-pint (*Arum maculatum*) mitochondria. Stimulation by high concentrations of ions and effects of specific inhibitors. *The Biochemical Journal*, **228(2)**, 309–318.
- Kelly, S. M., Jess, T. J., & Price, N. C. (2005). How to study proteins by circular dichroism. *Biochimica et Biophysica Acta (BBA)-Proteins and Proteomics*, 1751(2), 119-139.
- **Kelly, S., and Price, N.** (2000). The use of circular dichroism in the investigation of protein structure and function. *Current protein and peptide science*, **1(4)**, 349–384.
- **Kerscher, S. J.** (2000). Diversity and origin of alternative NADH:ubiquinone oxidoreductases. *Biochimica et Biophysica Acta (BBA) Bioenergetics*, **1459(2–3)**, 274–283.
- Keunen, E., Florez-Sarasa, I., Obata, T., Jozefczak, M., Remans, T., Vangronsveld, J., ... & Cuypers, A. (2016). Metabolic responses of Arabidopsis thaliana roots and leaves to sublethal cadmium exposure are differentially influenced by ALTERNATIVE OXIDASE1a. Environmental and Experimental Botany, 124, 64-78.
- Kido, Y., Shiba, T., Inaoka, D. K., Sakamoto, K., Nara, T., Aoki, T., ... Kita, K. (2010). Crystallization and preliminary crystallographic analysis of cyanide-insensitive alternative oxidase from *Trypanosoma brucei brucei*. Acta Crystallographica Section F: Structural Biology and Crystallization Communications, 66(3), 275–278.
- Kim, S., Chen, J., Cheng, T., Gindulyte, A., He, J., He, S., ... Bolton, E. E. (2021). New data content and improved web interfaces. *Nucleic Acids Research*, 49(1), 1388–1395.

- **Kirimura, K., Yoda, M., & Usami, S.** (1999). Cloning and expression of the cDNA encoding an alternative oxidase gene from *Aspergillus niger* WU-2223L. *Current Genetics*, 34(6), 472–477.
- **Kita, K., Konishi, K., & Anraku, Y. (1984a).** Terminal oxidases of *Escherichia coli* aerobic respiratory chain. I. Purification and properties of cytochrome b₅₆₂-o complex from cells in the early exponential phase of aerobic growth. *Journal of Biological Chemistry*, **259(5)**, 3368–3374.
- Kita, K., Konishi, K., & Anraku, Y. (1984b). Terminal Oxidases of *Escherichia coli* Aerobic Respiratory Chain. *Journal of Biological Chemistry*, 259(5), 3368–3374.
- König, A. C., Hartl, M., Boersema, P. J., Mann, M., & Finkemeier, I. (2014). The mitochondrial lysine acetylome of Arabidopsis. *Mitochondrion*, 19, 252-260.
- Kumar, A. M., & Söll, D. (1992). Arabidopsis alternative oxidase sustains *Escherichia coli* respiration. *Proceedings of the National Academy of Sciences of the USA*, 89(22), 10842–10846.
- **Laemmli, U. K.** (1970). Cleavage of structural proteins during the assembly of the head of bacteriophage T4. *Nature*. 227, 680–685.
- **Lakowicz, J. R.** (2006). Principles of fluorescence spectroscopy (Third ed.). Boston, MA: springer US.
- **Lehmann, M., Laxa, M., Sweetlove, L. J., Fernie, A. R., & Obata, T. (2012).** Metabolic recovery of *Arabidopsis thaliana* roots following cessation of oxidative stress. *Metabolomics*, **8(1)**, 143-153.
- Lehmann, M., Schwarzländer, M., Obata, T., Sirikantaramas, S., Burow, M., Olsen, C. E., ... Laxa, M. (2009). The Metabolic Response of Arabidopsis Roots to Oxidative Stress is Distinct from that of Heterotrophic Cells in Culture and Highlights a Complex Relationship between the Levels of Transcripts, Metabolites, and Flux. *Molecular Plant*, 2(3), 390–406.
- Lelis, C. A., Nunes, N. M., de Paula, H. M. C., Coelho, Y. L., da Silva, L. H. M., & Pires,

- **A. C. dos S. (2020).** Insights into protein-curcumin interactions: Kinetics and thermodynamics of curcumin and lactoferrin binding. *Food Hydrocolloids*, *105*, 105-825
- Liao, Y. W. K., Shi, K., Fu, L. J., Zhang, S., Li, X., Dong, D. K., ... Yu, J. Q. (2012). The reduction of reactive oxygen species formation by mitochondrial alternative respiration in tomato basal defense against TMV infection. *Planta*, 235(2), 225–238.
- Liao, Y., Cui, R., Xu, X., Cheng, Q., & Li, X. (2021). Jasmonic Acid- and Ethylene-Induced Mitochondrial Alternative Oxidase Stimulates *Marssonina brunnea* Defense in Poplar. *Plant & Cell Physiology*, 61(12), 2031–2042.
- **Liu, J., Li, Z., Wang, Y., & Xing, D.** (2014). Overexpression of ALTERNATIVE OXIDASE1a alleviates mitochondria-dependent programmed cell death induced by aluminium phytotoxicity in Arabidopsis. *Journal of Experimental Botany*, **65**(15), 4465–4478.
- Liu, Q., Liu, M., Wu, S., Xiao, B., Wang, X., Sun, B., & Zhu, L. (2020). Metabolomics Reveals Antioxidant Stress Responses of Wheat (*Triticum aestivum L.*) Exposed to Chlorinated Organophosphate Esters. *Journal of Agricultural and Food Chemistry*, 68(24), 6520–6529.
- Liu, Z., & Butow, R. A. (2006). Mitochondrial Retrograde Signaling. *Annual Review of Genetics*, 40(1), 159–185.
- Louis, S. (2019). A Deep Dive Into Induction with IPTG. Gold Biotechnology, FM-000008.
- **Lyubarev, A. E., & Kurganov, B. I.** (1989). Supramolecular organization of tricarboxylic acid cycle enzymes. *BioSystems*, 22(2), 91–102.
- Maji, A., Beg, M., Mandal, A. K., Das, S., Jha, P. K., Kumar, A., ... Chakrabarti, P. (2017). Spectroscopic interaction study of human serum albumin and human hemoglobin with *Mersilea quadrifolia* leaves extract mediated silver nanoparticles having antibacterial and anticancer activity. *Journal of Molecular Structure*, 1141, 584–592.

- Maréchal, A., Kido, Y., Kita, K., Moore, A. L., & Rich, P. R. (2009). Three redox states of *Trypanosoma brucei* alternative oxidase identified by infrared spectroscopy and electrochemistry. *Journal of Biological Chemistry*, 284(46), 31827–31833.
- Martí, M. C., Jiménez, A., & Sevilla, F. (2020). Thioredoxin network in plant mitochondria: cysteine S-posttranslational modifications and stress conditions. *Frontiers in Plant Science*, 11, 571288.
- Maxwell, D. P., Wang, Y., & McIntosh, L. (1999). The alternative oxidase lowers mitochondrial reactive oxygen production in plant cells. *Proceedings of the National Academy of Sciences*, 96(14), 8271-8276.
- May, B., Young, L., & Moore, A. L. (2017). Structural insights into the alternative oxidases: Are all oxidases made equal? *Biochemical Society Transactions*, 45(3), 731–740.
- **McDonald, A. E. (2008).** Alternative oxidase: An inter-kingdom perspective on the function and regulation of this broadly distributed "cyanide-resistant" terminal oxidase. *Functional Plant Biology*, **35(7)**, 535–552.
- McDonald, A. E., Vanlerberghe, G. C., & Staples, J. F. (2009). Alternative oxidase in animals: Unique characteristics and taxonomic distribution. *Journal of Experimental Biology*, 212(16), 2627–2634.
- Meeuse, B J D. (1975). Thermogenic Respiration in Aroids. *Annual Review of Plant Physiology*, 26(1), 117–126.
- Meeuse, Bastiaan J. D., & Buggeln, R. G. (1969). Time, Space, Light and Darkness in the Metabolic Flare-Up of the Sauromatum Appendix*. *Acta Botanica Neerlandica*, 18(1), 159–172.
- Melo, A. M. P., Bandeiras, T. M., & Teixeira, M. (2004). New Insights into Type II NAD(P)H:Quinone Oxidoreductases. *Microbiology and Molecular Biology Reviews*, 68(4), 603–616.
- Meyer, E. H., Letts, J. A., & Maldonado, M. (2022). Structural insights into the assembly

- and the function of the plant oxidative phosphorylation system. *New Phytologist*, **235(4)**, 1315-1329.
- Meyer, E. H., Welchen, E., & Carrie, C. (2019). Assembly of the Complexes of the Oxidative Phosphorylation System in Land Plant Mitochondria. *Annual Review of Plant Biology*, 70, 23–50.
- Millar, A. H., Eubel, H., Jänsch, L., Kruft, V., Heazlewood, J. L., & Braun, H. P. (2004). Mitochondrial cytochrome c oxidase and succinate dehydrogenase complexes contain plant specific subunits. *Plant molecular biology*, *56*(1), 77-90.
- Millar, A. H., Hoefnagel, M. H., Day, D. A., & Wiskich, J. T. (1996). Specificity of the organic acid activation of alternative oxidase in plant mitochondria. *Plant Physiology*, 111(2), 613-618.
- Millar, A. H., Whelan, J., Soole, K. L., & Day, D. A. (2011). Organization and regulation of mitochondrial respiration in plants. *Annual Review of Plant Biology*, 62, 79–104.
- Millar, A. H., Wiskich, J. T., Whelan, J., & Day, D. A. (1993). Organic acid activation of the alternative oxidase of plant mitochondria. *FEBS Letters*, *329*(3), 259–262.
- **Millenaar, F. F., & Lambers, H.** (2003). The alternative oxidase: In vivo regulation and function. *Plant Biology*, 5(1), 2–15.
- Minagawa, N., Sakajo, S., Komiyama, T., & Yoshimoto, A. (1990). Essential role of ferrous iron in cyanide-resistant respiration in *Hansenula anomala*. *FEBS Letters*, 267(1), 114–116.
- **Mittler, R., & Zilinskas, B.** (1994). Drought Stress and Following Recovery From Drought. *The Plant Journal*, **5(3)**, 397–405.
- Mogi, T., Nakamura, H., & Anraku, Y. (1994). Molecular structure of a heme-copper redox center of the *Escherichia coli* ubiquinol oxidase: Evidence and model. *Journal of Biochemistry*, 116(3), 471–477.
- Møller, I Max., Igamberdiev, A. U., Bykova, N. V, Finkemeier, I., Rasmusson, A. G., &

- **Schwarzländer, M.** (2020). Matrix redox physiology governs the regulation of plant mitochondrial metabolism through posttranslational protein modifications. *Plant Cell*, 32(3), 573–594.
- **Møller, I. M.** (2001). Plant mitochondria and oxidative stress: Electron transport, NADPH turnover, and metabolism of reactive oxygen species. *Annual Review of Plant Biology*, 52, 561–591.
- Møller, I. M., & Rasmusson, A. G. (1998). The role of NADP in the mitochondrial matrix.

 Trends in Plant Science, 3(1), 21–27.
- Møller, I. M., Jensen, P. E., & Hansson, A. (2007). Oxidative modifications to cellular components in plants. *Annual Review of Plant Biology*, 58, 459-481.
- **Moore, A. L., & Albury, M. S. (2008).** Further insights into the structure of the alternative oxidase: From plants to parasites. *Biochemical Society Transactions*, **36(5)**, 1022–1026.
- Moore, A. L., Albury, M. S., Crichton, P. G., & Affourtit, C. (2002). Function of the alternative oxidase: Is it still a scavenger? *Trends in Plant Science*, **7(11)**, 478–481.
- Moore, A. L., Carré, J. E., Affourtit, C., Albury, M. S., Crichton, P. G., Kita, K., & Heathcote, P. (2008). Compelling EPR evidence that the alternative oxidase is a diiron carboxylate protein. *Biochimica et Biophysica Acta Bioenergetics*, 1777(4), 327–330.
- Moore, A. L., Shiba, T., Young, L., Harada, S., Kita, K., & Ito, K. (2013). Unraveling the heater: New insights into the structure of the alternative oxidase. *Annual Review of Plant Biology*, 64, 637–663.
- **Murphy, M. P.** (2009). How mitochondria produce reactive oxygen species. *Biochemical Journal*, 417, 1–13.
- Navrot, N., Rouhier, N., Gelhaye, E., & Jacquot, J. P. (2007). Reactive oxygen species generation and antioxidant systems in plant mitochondria. *Physiologia Plantarum*, 129(1), 185–195.
- Netto, L. E., Kowaltowski, A. J., Castilho, R. F., & Vercesi, A. E. (2002). [25] Thiol

- enzymes protecting mitochondria against oxidative damage. *Methods in enzymology*, *348*, 260-270.
- Ng, S., De Clercq, I., Van Aken, O., Law, S. R., Ivanova, A., Willems, P., ... Whelan, J. (2014). Anterograde and retrograde regulation of nuclear genes encoding mitochondrial proteins during growth, development, and stress. *Molecular Plant*, 7, 1075–1093.
- Ng, S., Giraud, E., Duncan, O., Law, S. R., Wang, Y., Xu, L., ... Ivanova, A. (2013). Cyclin-dependent kinase E1 (CDKE1) provides a cellular switch in plants between growth and stress responses. *Journal of Biological Chemistry*, 288(5), 3449–3459.
- Nguyen, H. H., Park, J., Kang, S., & Kim, M. (2015). Surface plasmon resonance: A versatile technique for biosensor applications. *Sensors*, *15*(5), 10481–10510.
- Nietzel, T., Mostertz, J., Ruberti, C., Née, G., Fuchs, P., Wagner, S., ... & Schwarzländer, M. (2020). Redox-mediated kick-start of mitochondrial energy metabolism drives resource-efficient seed germination. *Proceedings of the National Academy of Sciences*, 117(1), 741-751.
- Nihei, C., Fukai, Y., Kawai, K., Osanai, A., Yabu, Y., Suzuki, T., ... Kita, K. (2003). Purification of active recombinant trypanosome alternative oxidase. *FEBS Letters*, 538(1–3), 35–40.
- **Noctor, G.** (2006). Metabolic signalling in defence and stress: The central roles of soluble redox couples. *Plant, Cell and Environment*, 29(3), 409–425.
- **Noctor, G., & Foyer, C. H. (1998).** Ascorbate and Glutathione: Keeping Active Oxygen under Control. *Annual Review of Plant Biology*, **49**, 249–279.
- Noctor, G., Queval, G., Mhamdi, A., Chaouch, S., & Foyer, C. H. (2011). Glutathione. *The Arabidopsis Book/American Society of Plant Biologists*, 9.
- Noguchi, K., Taylor, N. L., Millar, A. H., Lambers, H., & Day, D. A. (2005). Response of mitochondria to light intensity in the leaves of sun and shade species. *Plant, Cell and Environment*, 28(6), 760–771.

- Obata, T., Matthes, A., Koszior, S., Lehmann, M., Araújo, W. L., Bock, R., ... Fernie, A. R. (2011). Alteration of mitochondrial protein complexes in relation to metabolic regulation under short-term oxidative stress in Arabidopsis seedlings. *Phytochemistry*, 72(10), 1081–1091.
- Olaru, A., Bala, C., Jaffrezic-Renault, N., & Aboul-Enein, H. Y. (2015). Surface Plasmon Resonance (SPR) Biosensors in Pharmaceutical Analysis. *Critical Reviews in Analytical Chemistry*, 45(2), 97–105.
- **Padmasree, K., & Raghavendra, A. S. (1999a).** Importance of oxidative electron transport over oxidative phosphorylation in optimizing photosynthesis in mesophyll protoplasts of pea (*Pisum sativum L.*). *Physiologia Plantarum*, **105(3)**, 546–553.
- **Padmasree, K., & Raghavendra, A. S.** (1999b). Response of photosynthetic carbon assimilation in mesophyll protoplasts to restriction on mitochondrial oxidative metabolism: Metabolites related to the redox status and sucrose biosynthesis. *Photosynthesis Research*, 62(2), 231–239.
- **Padmasree, K., Padmavathi, L., & Raghavendra, A. S.** (2002). Essentiality of mitochondrial oxidative metabolism for photosynthesis: optimization of carbon assimilation and protection against photoinhibition. *Critical Reviews in Biochemistry and Molecular Biology*, 37(2), 71-119.
- **Pascal, N., Dumas, R., & Douce, R.** (1990). Comparison of the kinetic behavior toward pyridine nucleotides of NAD⁺-linked dehydrogenases from plant mitochondria. *Plant Physiology*, 94(1), 189–193.
- Pennisi, R., Salvi, D., Brandi, V., Angelini, R., Ascenzi, P., & Polticelli, F. (2016). Molecular Evolution of Alternative Oxidase Proteins: A Phylogenetic and Structure Modeling Approach. *Journal of Molecular Evolution*, 82(4–5), 207–218.
- Planchet, E., Gupta, K. J., Sonoda, M., & Kaiser, W. M. (2005). Nitric oxide emission from tobacco leaves and cell suspensions: Rate limiting factors and evidence for the involvement of mitochondrial electron transport. *Plant Journal*, 41(5), 732–743.

- Polidoros, A. N., Mylona, P. V., & Arnholdt-Schmitt, B. (2009). Aox gene structure, transcript variation and expression in plants. *Physiologia Plantarum*, 137(4), 342-353.
- **Poole, R. K., & Cook, G. M. (2000).** Redundancy of aerobic respiratory chains in bacteria? Routes, reasons and regulation. *Advances in Microbial Physiology*, **43**, 165–224.
- **Purvis, A. C.** (1997). Role of the alternative oxidase in limiting superoxide production by plant mitochondria. *Physiologia Plantarum*, 100(1), 165–170.
- Qiao, K., Yao, X., Zhou, Z., Xiong, J., Fang, K., Lan, J., ... & Lin, H. (2023). Mitochondrial alternative oxidase enhanced ABA-mediated drought tolerance in Solanum lycopersicum. *Journal of Plant Physiology*, 280, 153892.
- **Raghavendra, A S, Padmasree, K., & Saradadevi, K.** (1994). Interdependence of photosynthesis and respiration in plant cells: interactions between chloroplasts and mitochondria. *Plant Science*, 97(1), 1–14.
- **Raghavendra, Agepati S., & Padmasree, K.** (2003). Beneficial interactions of mitochondrial metabolism with photosynthetic carbon assimilation. *Trends in Plant Science*, 8(11), 546–553.
- Rasmusson, A. G., & Møller, I. M. (1990). NADP-Utilizing Enzymes in the Matrix of Plant Mitochondria. *Plant Physiology*, 94(3), 1012–1018.
- Rasmusson, A. G., Soole, K. L., & Elthon, T. E. (2004). Alternative NAD(P)H dehydrogenases of plant mitochondria. *Annual Review of Plant Biology*, 55, 23–39.
- **Reid, G. A., & Ingledew, W. J. (1979).** Characterization and phenotypic control of the cytochrome content of *Escherichia coli*. *Biochemical Journal*, **182(2)**, 465–472.
- **Rhoads, D. M., & Subbaiah, C. C. (2007).** Mitochondrial retrograde regulation in plants. *Mitochondrion*, **7**, 177–194.
- Rhoads, D. M., Umbach, A. L., Sweet, C. R., Lennon, A. M., Rauch, G. S., & Siedow, J.
 N. (1998). Regulation of the Cyanide-resistant Alternative Oxidase of Plant Mitochondria. *Journal of Biological Chemistry*, 273(46), 30750–30756.

- Ribas-Carbo, M., Taylor, N. L., Giles, L., Busquets, S., Finnegan, P. M., Day, D. A., ... Flexas, J. (2005). Effects of water stress on respiration in soybean leaves. *Plant Physiology*, 139(1), 466–473.
- **Rich, P. R.** (1978). Quinol oxidation in *Arum maculatum* mitochondria and its application to the assay, solubilisation and partial purification of the alternative oxidase. *FEBS Letters*, 96(2), 252–256.
- **Rich, P. R., & Moore, A. L. (1976).** The involvement of the protonmotive ubiquinone cycle in the respiratory chain of higher plants and its relation to the branchpoint of the alternate pathway. *FEBS Letters*, **65(3)**, 339–344.
- **Rietsch, A., & Beckwith, J.** (1998). The genetics of disulfide bond metabolism. *Annual review of genetics*, 32, 163.
- **Robson, C. A., & Vanlerberghe, G. C. (2002).** Transgenic plant cells lacking mitochondrial alternative oxidase have increased susceptibility to mitochondria-dependent and independent pathways of programmed cell death. *Plant Physiology*, *129*(4), 1908–1920.
- Rodziewicz, P., Swarcewicz, B., Chmielewska, K., Wojakowska, A., & Stobiecki, M. (2014). Influence of abiotic stresses on plant proteome and metabolome changes. *Acta Physiologiae Plantarum*, 36, 1-19.
- Rushton, P. J., Macdonald, H., Huttly, A. K., Lazarus, C. M., & Hooley, R. (1995). Members of a new family of DNA-binding proteins bind to a conserved cis-element in the promoters of α -Amy2 genes. Plant Molecular Biology, 29(4), 691–702.
- Rushton, P. J., Somssich, I. E., Ringler, P., & Shen, Q. J. (2010). WRKY transcription factors. *Trends in Plant Science*, 15(5), 247–258.
- Rushton, P. J., Torres, J. T., Parniske, M., Wernert, P., Hahlbrock, K., & Somssich, I.
 E. (1996). Interaction of elicitor-induced DNA-binding proteins with elicitor response elements in the promoters of parsley PR1 genes. *EMBO Journal*, 15(20), 5690–5700.
- Saisho, D., Nambara, E., Naito, S., Tsutsumi, N., Hirai, A., & Nakazono, M. (1997). Characterization of the gene family for alternative oxidase from *Arabidopsis thaliana*.

- *Plant Molecular Biology*, **35(5)**, 585–596.
- Salvato, F., Havelund, J. F., Chen, M., Rao, R. S. P., Rogowska-Wrzesinska, A., Jensen,
 O. N., ... & Møller, I. M. (2014). The potato tuber mitochondrial proteome. *Plant physiology*, 164(2), 637-653.
- Sankar, T. V., Saharay, M., Santhosh, D., Vishwakarma, A., & Padmasree, K. (2022). Structural and Biophysical Characterization of Purified Recombinant *Arabidopsis thaliana's* Alternative Oxidase 1A (rAtAOX1A): Interaction With Inhibitor(s) and Activator. *Frontiers in Plant Science*, 13, 1–21.
- Savchenko, T., & Tikhonov, K. (2021). Oxidative Stress-Induced Alteration of Plant Central Metabolism. *Life*, 11, 304.
- Schafer, F. Q., & Buettner, G. R. (2001). Redox environment of the cell as viewed through the redox state of the glutathione disulfide/glutathione couple. *Free radical biology and medicine*, 30(11), 1191-1212.
- Schafer, F. Q., & Buettner, G. R. (2003). Redox state and redox environment in biology. Signal transduction by reactive oxygen and nitrogen species: pathways and chemical principles, 1-14.
- **Scheibe, R.** (2019). Maintaining homeostasis by controlled alternatives for energy distribution in plant cells under changing conditions of supply and demand. *Photosynthesis research*, 139(1-3), 81-91.
- Selinski, J., & Scheibe, R. (2019). Malate valves: old shuttles with new perspectives. *Plant Biology*, 21, 21–30.
- Selinski, J., Hartmann, A., Höfler, S., Deckers-Hebestreit, G., & Scheibe, R. (2016). Refined method to study the posttranslational regulation of alternative oxidases from Arabidopsis thaliana in vitro. *Physiologia Plantarum*, 157(3), 264-279.
- Selinski, Jennifer, Hartmann, A., Deckers-Hebestreit, G., Day, D. A., Whelan, J., & Scheibe, R. (2018a). Alternative oxidase isoforms are differentially activated by tricarboxylic acid cycle intermediates. *Plant Physiology*, 176(2), 1423–1432.

- Selinski, Jennifer, Hartmann, A., Kordes, A., Deckers-Hebestreit, G., Whelan, J., & Scheibe, R. (2017). Analysis of posttranslational activation of alternative oxidase isoforms. *Plant Physiology*, 174(4), 2113–2127.
- Selinski, Jennifer, Scheibe, R., Day, D. A., & Whelan, J. (2018b). Alternative Oxidase Is Positive for Plant Performance. *Trends in Plant Science*, 23(7), 588–597.
- Shan, X., & Que, L. (2005). Intermediates in the oxygenation of a nonheme diiron(II) complex, including the first evidence for a bound superoxo species. *Proceedings of the National Academy of Sciences of the USA*, 102(15), 5340–5345.
- Sharifi, M., Dolatabadi, J. E. N., Fathi, F., Rashidi, M., Jafari, B., Tajalli, H., & Rashidi, M. R. (2017). Kinetic and thermodynamic study of bovine serum albumin interaction with rifampicin using surface plasmon resonance and molecular docking methods. *Journal of biomedical optics*, 22(3), 037002-037002.
- Shiba, T., Inaoka, D. K., Takahashi, G., Tsuge, C., Kido, Y., Young, L., ... & Kita, K. (2019). Insights into the ubiquinol/dioxygen binding and proton relay pathways of the alternative oxidase. *Biochimica et Biophysica Acta (BBA)-Bioenergetics*, 1860(5), 375-382.
- Shiba, T., Kido, Y., Sakamoto, K., Inaoka, D. K., Tsuge, C., Tatsumi, R., ... Kita, K. (2013). Structure of the trypanosome cyanide-insensitive alternative oxidase. *Proceedings of the National Academy of Sciences of the USA*, 110(12), 4580–4585.
- **Siedow, J. N., & Girvin, M. E. (1980).** Alternative respiratory pathway: its role in seed respiration and its inhibition by propyl gallate. *Plant Physiology*, **65(4)**, 669-674.
- **Siedow, J. N., & Umbach, A. L. (2000).** The mitochondrial cyanide-resistant oxidase: Structural conservation amid regulatory diversity. *Biochimica et Biophysica Acta Bioenergetics*, **1459**, 432–439.
- Simons, B. H., Millenaar, F. F., Mulder, L., Van Loon, L. C., & Lambers, H. (1999). Enhanced expression and activation of the alternative oxidase during infection of Arabidopsis with *Pseudomonas syringae pv tomato*. *Plant Physiology*, **120**(2), 529-538.

- **Singh Gill, S., & Tuteja, N.** (2010). Polyamines and abiotic stress tolerance in plants. *Plant Signaling & Behavior*, **5(1)**, 26–33.
- Sipari, N., Lihavainen, J., Shapiguzov, A., Kangasjärvi, J., & Keinänen, M. (2020). Primary metabolite responses to oxidative stress in early-senescing and Paraquat resistant Arabidopsis thaliana rcd1 (radical-induced cell Death1). Frontiers in plant science, 11, 194.
- Smirnoff, N., & Pallanca, J. E. (1996). Ascorbate metabolism in relation to oxidative stress. *Biochemical Society Transactions*, 24(2), 472-478.
- Smirnoff, N., & Wheeler, G. L. (2000). Ascorbic acid in plants: Biosynthesis and function. *Critical Reviews in Plant Sciences*, **19(4)**, 267–290.
- Smith, C. A., Melino, V. J., Sweetman, C., & Soole, K. L. (2009). Manipulation of alternative oxidase can influence salt tolerance in *Arabidopsis thaliana*. *Physiologia Plantarum*, 137(4), 459–472.
- **Sreerama, N., & Woody, R. W. (2000).** Estimation of protein secondary structure from circular dichroism spectra: Comparison of CONTIN, SELCON, and CDSSTR methods with an expanded reference set. *Analytical Biochemistry*, **287(2)**, 252–260.
- Strodtkötter, I., Padmasree, K., Dinakar, C., Speth, B., Niazi, P. S., Wojtera, J., ... Scheibe, R. (2009). Induction of the AOX1D isoform of alternative oxidase in *A. thaliana* T-DNA insertion lines lacking isoform AOX1A is insufficient to optimize photosynthesis when treated with antimycin a. *Molecular Plant*, 2(2), 284–297.
- Suryawanshi, V. D., Walekar, L. S., Gore, A. H., Anbhule, P. V., & Kolekar, G. B. (2016). Spectroscopic analysis on the binding interaction of biologically active pyrimidine derivative with bovine serum albumin. *Journal of Pharmaceutical Analysis*, 6(1), 56-63.
- Suzuki, N., Koussevitzky, S., Mittler, R., & Miller, G. (2012). ROS and redox signalling in the response of plants to abiotic stress. *Plant, Cell and Environment*, *35*(2), 259–270.
- Sweetlove, L. J., Beard, K. F., Nunes-Nesi, A., Fernie, A. R., & Ratcliffe, R. G. (2010).

- Not just a circle: flux modes in the plant TCA cycle. *Trends in plant science*, **15(8)**, 462-470.
- Szarka, A., Horemans, N., Bánhegyi, G., & Asard, H. (2004). Facilitated glucose and dehydroascorbate transport in plant mitochondria. *Archives of Biochemistry and Biophysics*, 428(1), 73–80.
- **Taniguchi, M., & Miyake, H.** (2012). Redox-shuttling between chloroplast and cytosol: Integration of intra-chloroplast and extra-chloroplast metabolism. *Current Opinion in Plant Biology*, **15(3)**, 252–260.
- **Tovar-Méndez, A., Miernyk, J. A., & Randall, D. D.** (2003). Regulation of pyruvate dehydrogenase complex activity in plant cells. *European Journal of Biochemistry*, **270**(6), 1043–1049.
- **Towbin, H., Staehelin, T., and Gordon, J. (1979).** Electrophoretic transfer of proteins from polyacrylamide gels to nitrocellulose sheets: procedure and some applications. *Biotechnology*, **24**, 145–149.
- Umbach, A. L., & Siedow, J. N. (1993). Covalent and noncovalent dimers of the cyanideresistant alternative oxidase protein in higher plant mitochondria and their relationship to enzyme activity. *Plant Physiology*, 103(3), 845–854.
- Umbach, A. L., & Siedow, J. N. (1996). The reaction of the soybean cotyledon mitochondrial cyanide-resistant oxidase with sulfhydryl reagents suggests that α-Keto acid activation involves the formation of a thiohemiacetal. *Journal of Biological Chemistry*, 271(40), 25019–25026.
- Umbach, A. L., Gonzàlez-Meler, M. A., Sweet, C. R., & Siedow, J. N. (2002). Activation of the plant mitochondrial alternative oxidase: Insights from site-directed mutagenesis. *Biochimica et Biophysica Acta - Bioenergetics*, 1554(1-2), 118–128.
- Umbach, A. L., Ng, V. S., & Siedow, J. N. (2006). Regulation of plant alternative oxidase activity: A tale of two cysteines. *Biochimica et Biophysica Acta Bioenergetics*, 1757(2), 135–142.

- Van Aken, O., Giraud, E., Clifton, R., & Whelan, J. (2009). Alternative oxidase: A target and regulator of stress responses. *Physiologia Plantarum*, 137(4), 354–361.
- Van Aken, O., Zhang, B., Law, S., Narsai, R., & Whelan, J. (2013). AtWRKY40 and AtWRKY63 Modulate the Expression of Stress-Responsive Nuclear Genes Encoding Mitochondrial and Chloroplast Proteins. *Plant Physiology*, *162*(1), 254–271.
- **Vanlerberghe, G C. (2013).** Alternative oxidase: A mitochondrial respiratory pathway to maintain metabolic and signaling homeostasis during abiotic and biotic stress in plants. *International Journal of Molecular Sciences*, **14(4)**, 6805–6847.
- Vanlerberghe, G. C., & Mcintosh, L. (1992a). Alternative Pathway Capacity. *Plant Physiology*, 100(1), 115–119.
- Vanlerberghe, G. C., & McIntosh, L. (1992b). Coordinate regulation of cytochrome and alternative pathway respiration in tobacco. *Plant Physiology*, *100*(4), 1846–1851.
- Vanlerberghe, G. C., & Ordog, S. H. (2002). Alternative oxidase: integrating carbon metabolism and electron transport in plant respiration. *Photosynthetic nitrogen assimilation and associated carbon and respiratory metabolism*, 173-191.
- Vanlerberghe, Greg C, Dahal, K., Alber, N. A., & Chadee, A. (2020). Photosynthesis, respiration and growth: A carbon and energy balancing act for alternative oxidase. *Mitochondrion*, 52, 197–211.
- Vanlerberghe, Greg C., & McIntosh, L. (1996). Signals regulating the expression of the nuclear gene encoding alternative oxidase of plant mitochondria. *Plant Physiology*, 111(2), 589–595.
- Vanlerberghe, Greg C., & McIntosh, L. (1997). ALTERNATIVE OXIDASE: From Gene to Function. *Annual Review of Plant Physiology and Plant Molecular Biology*, **48**(1), 703–734.
- Vanlerberghe, Greg C., Cvetkovska, M., & Wang, J. (2009). Is the maintenance of homeostatic mitochondrial signaling during stress a physiological role for alternative oxidase? *Physiologia Plantarum*, 137(4), 392–406.

- Vanlerberghe, Greg C., Day, D. A., Wiskich, J. T., Vanlerberghe, A. E., & McIntosh, L. (1995). Alternative oxidase activity in tobacco leaf mitochondria: Dependence on tricarboxylic acid cycle-mediated redox regulation and pyruvate activation. *Plant Physiology*, 109(2), 353–361.
- Vanlerberghe, Greg C., Martyn, G. D., & Dahal, K. (2016). Alternative oxidase: a respiratory electron transport chain pathway essential for maintaining photosynthetic performance during drought stress. *Physiologia Plantarum*, 157, 322–337.
- Varlan, A., & Hillebrand, M. (2010). Bovine and human serum albumin interactions with 3-carboxyphenoxathiin studied by fluorescence and circular dichroism spectroscopy. *Molecules*, 15(6), 3905-3919.
- Vasquez-Robinet, C., Mane, S. P., Ulanov, A. V, Watkinson, J. I., Stromberg, V. K., De Koeyer, D., ... Grene, R. (2008). Physiological and molecular adaptations to drought in Andean potato genotypes. *Journal of Experimental Botany*, 59(8), 2109–2123.
- Vassileva, V., Simova-Stoilova, L., Demirevska, K., & Feller, U. (2009). Variety-specific response of wheat (*Triticum aestivum* L.) leaf mitochondria to drought stress. *Journal of Plant Research*, 122(4), 445–454.
- Vercesi, A. E., Borecký, J., Maia, I. D. G., Arruda, P., Cuccovia, I. M., & Chaimovich,
 H. (2006). Plant uncoupling mitochondrial proteins. *Annual Review of Plant Biology*, 57, 383-404.
- **Verniquet, F., Gaillard, J., Neuberger, M., & Douce, R.** (1991). Rapid inactivation of plant aconitase by hydrogen peroxide. *Biochemical Journal*, 276(3), 643–648.
- Vianello, A., Braidot, E., Petrussa, E., & Macri, F. (1997). ATP synthesis driven by α-keto acid-stimulated alternative oxidase in pea leaf mitochondria. *Plant and cell physiology*, 38(12), 1368-1374.
- Vishwakarma, A., Bashyam, L., Senthilkumaran, B., Scheibe, R., & Padmasree, K. (2014). Physiological role of AOX1a in photosynthesis and maintenance of cellular redox homeostasis under high light in *Arabidopsis thaliana*. *Plant Physiology and*

- *Biochemistry*, **81**, 44–53.
- Vishwakarma, A., Dalal, A., Tetali, S. D., Kirti, P. B., & Padmasree, K. (2016). Genetic engineering of AtAOX1a in Saccharomyces cerevisiae prevents oxidative damage and maintains redox homeostasis. FEBS Open Bio, 6(2), 135–146.
- Vishwakarma, A., Kumari, A., Mur, L. A. J., & Gupta, K. J. (2018). A discrete role for alternative oxidase under hypoxia to increase nitric oxide and drive energy production. *Free Radical Biology and Medicine*, 122, 40–51.
- Vishwakarma, A., Tetali, S. D., Selinski, J., Scheibe, R., & Padmasree, K. (2015). Importance of the alternative oxidase (AOX) pathway in regulating cellular redox and ROS homeostasis to optimize photosynthesis during restriction of the cytochrome oxidase pathway in *Arabidopsis thaliana*. *Annals of Botany*, 116(4), 555–569.
- Voss, I., Sunil, B., Scheibe, R., & Raghavendra, A. S. (2013). Emerging concept for the role of photorespiration as an important part of abiotic stress response. *Plant Biology*, 15(4), 713–722.
- Wagner, A. M., & Moore, A. L. (1997). Structure and function of the plant alternative oxidase: Its putative role in the oxygen defence mechanism. *Bioscience Reports*, 17(3), 319–333.
- Wagner, A. M., van den Bergen, C. W., & Wincencjusz, H. (1995). Stimulation of the alternative pathway by succinate and malate. *Plant physiology*, 108(3), 1035-1042.
- Wang, Y., Berkowitz, O., Selinski, J., Xu, Y., Hartmann, A., & Whelan, J. (2018). Stress responsive mitochondrial proteins in Arabidopsis thaliana. *Free Radical Biology and Medicine*, 122, 28-39.
- Wang, Y., Zhang, G., Yan, J., & Gong, D. (2014). Inhibitory effect of morin on tyrosinase: Insights from spectroscopic and molecular docking studies. *Food Chemistry*, *163*, 226–233.
- Wheeler, G. L., & Grant, C. M. (2004). Regulation of redox homeostasis in the yeast Saccharomyces cerevisiae. *Physiologia Plantarum*, 120(1), 12–20.

- Whelan, J., Millar, A. H., & Day, D. A. (1996). The alternative oxidase is encoded in a multigene family in soybean. *Planta*, 198(2), 197-201.
- Whitmore, L., & Wallace, B. A. (2008). Protein secondary structure analyses from circular dichroism spectroscopy: Methods and reference databases. *Biopolymers*, 89(5), 392–400.
- Xiao, W., Wang, R. S., Handy, D. E., & Loscalzo, J. (2018). NAD(H) and NADP(H) Redox Couples and Cellular Energy Metabolism. *Antioxidants and Redox Signaling*, 28(3), 251–272.
- Xu, F., Copsey, A. C., Young, L., Barsottini, M. R., Albury, M. S., & Moore, A. L. (2021). Comparison of the Kinetic Parameters of Alternative Oxidases From *Trypanosoma brucei* and *Arabidopsis thaliana*—A Tale of Two Cavities. *Frontiers in Plant Science*, 12.
- Xu, F., Peng, Y., He, Z. Q., & Yu, L. L. (2023). The role of cyanoalanine synthase and alternative oxidase in promoting salt stress tolerance in Arabidopsis thaliana. *BMC Plant Biology*, 23(1), 1-13.
- Yao, X., Li, J., Liu, J., & Liu, K. (2015). An Arabidopsis mitochondria-localized RRL protein mediates abscisic acid signal transduction through mitochondrial retrograde regulation involving ABI4. *Journal of Experimental Botany*, 66(20), 6431–6445.
- Yap, L. L., Lin, M. T., Ouyang, H., Samoilova, R. I., Dikanov, S. A., & Gennis, R. B. (2010). The quinone-binding sites of the cytochrome *bo3* ubiquinol oxidase from *Escherichia coli*. *Biochimica et Biophysica Acta Bioenergetics*, 1797(12), 1924–1932.
- **Ying, W.** (2008). NAD⁺/NADH and NADP⁺/NADPH in cellular functions and cell death: Regulation and biological consequences. *Antioxidants and Redox Signaling*, 10(2), 179–206.
- Yoshida K, Watanabe CK, Hachiya T, Tholen D, Shibata M, Terashima I, Noguchi K. (2011). Distinct responses of the mitochondrial respiratory chain to long- and short-term high-light environments in *Arabidopsis thaliana*. *Plant Cell Environ*, *34*, 618-28.

- **Yoshida, K., & Hisaboria, T.** (2016). Two distinct redox cascades cooperatively regulate chloroplast functions and sustain plant viability. *Proceedings of the National Academy of Sciences of the USA*, 113(27), 3967–3976.
- Yoshida, K., Terashima, I., & Noguchi, K. (2006). Distinct roles of the cytochrome pathway and alternative oxidase in leaf photosynthesis. *Plant and Cell Physiology*, 47(1), 22–31.
- Yu, Y., Guan, Y., Liu, J., Hedi, W., Yu, Y., & Zhang, T. (2021). Molecular structural modification of egg white protein by pH-shifting for improving emulsifying capacity and stability. *Food Hydrocolloids*, *121*, 107-071.
- **Zechmann, B., Mauch, F., Sticher, L., & Müller, M.** (2008). Subcellular immunocytochemical analysis detects the highest concentrations of glutathione in mitochondria and not in plastids. *Journal of Experimental Botany*, **59(14)**, 4017–4027.
- Zhang, L. T., Zhang, Z. S., Gao, H. Y., Xue, Z. C., Yang, C., Meng, X. L., & Meng, Q. W. (2011). Mitochondrial alternative oxidase pathway protects plants against photoinhibition by alleviating inhibition of the repair of photodamaged PSII through preventing formation of reactive oxygen species in Rumex K-1 leaves. *Physiologia Plantarum*, 143(4), 396–407.
- **Zhang, L., Oh, Y., Li, H., Baldwin, I. T., & Galis, I.** (2012). Alternative oxidase in resistance to biotic stresses: *Nicotiana attenuata* AOX contributes to resistance to a pathogen and a piercing-sucking insect but not *Manduca sexta* Larvae. *Plant Physiology*, **160**(3), 1453–1467.
- **Zhang, Q., Hoefnagel, M. H. N., & Wiskich, J. T. (1996).** Alternative oxidase from Arum and soybean: Its stabilization during purification. *Physiologia Plantarum*, **96(4)**, 551–558.
- Zhang, Y., Swart, C., Alseekh, S., Scossa, F., Jiang, L., Obata, T., ... & Fernie, A. R. (2018). The extra-pathway interactome of the TCA cycle: expected and unexpected metabolic interactions. *Plant Physiology*, 177(3), 966-979.

- Zheng, J., Fang, C., Ru, L., Sun, N., Liu, Y., Huang, Y., ... & He, Y. (2021). Role of glutathione-ascorbate cycle and photosynthetic electronic transfer in alternative oxidase-manipulated waterlogging tolerance in watermelon seedlings. *Horticulturae*, **7(6)**, 130.
- Zhu, F., Deng, X. G., Xu, F., Jian, W., Peng, X. J., Zhu, T., & Lin, H. H. (2015). Mitochondrial alternative oxidase is involved in both compatible and incompatible host-virus combinations in *Nicotiana benthamiana*. *Plant Science*, **239**, 26–35.

Publications

- **1. Sankar, T. V.**, Saharay, M., Santhosh, D., Vishwakarma, A., & Padmasree, K. (2022). Structural and biophysical characterization of purified recombinant *Arabidopsis thaliana's* alternative oxidase 1A (rAtAOX1A): Interaction with inhibitor (s) and activator. *Frontiers in plant science*, 13 (**IF** = **6.627**).
- **2. Sankar TV**, Saharay M, Santhosh D and Padmasree K. Understanding the Interaction of Purified Recombinant *Arabidopsis thaliana's* Alternative Oxidase 1A (rAtAOX1A) with TCA Cycle Metabolites using Molecular Docking and Biophysical Studies (**Under communication**)
- **3. Sankar TV**, Saharay M, Santhosh D and Padmasree K. Understanding the molecular interaction of *Arabidopsis thaliana* Alternative oxidase with cellular redox couples (**Under preparation**).

Conferences attended

Poster presentations

- Sankar T.V, Vishwakarma A and Padmasree K (2016): Physiological role of AOX1A in alleviating oxidative stress and maintenance of cellular redox homeostasis. "National conference of plant physiology-2016" (NCCP-2016) was held on 8th -10th December 2016 at the University of Agriculture Sciences, GKVK, Bengaluru, Karnataka, India-560065.
- 2. **Sankar T.V** and Padmasree K (2019): Molecular Cloning of *Arabidopsis thaliana AOX1A*: Heterologous Expression of Functionally Active Recombinant AtAOX1A in *E. coli*. International Conference on "Biomedical engineering, Bioscience, Bioinformatics, Biochemistry, Cancer Biology, Molecular Biology and Applied Biotechnology" (BCM-2019) held on 1st January at JNU, Delhi, India-110067 (Received best poster award).
- 3. **Sankar T.V** and Padmasree K (2020): Molecular Cloning and Heterologous Expression of *A. thaliana* AOX1A in *E. coli*: Purification and Characterization of rAtAOX1A. "National Conference on Frontiers in Plant Biology," held on 31st January 1st February -2020, at School of Life Sciences, University of Hyderabad, India-500046.
- 4. **Sankar T.V,** Saharay M, and Padmasree K (2022): Molecular Cloning and Heterologous Expression of *A. thaliana AOX1a* in *E. coli*: Purification and Biophysical Characterization of rAtAOX1A. "2nd international conference on INTEGRATIVE BIOLOGY & APPLIED GENETICS (ICIBAG-2022)", held on 20th 22nd July -2022 at Osmania University, Hyderabad 500 007.

Oral presentations

- 1. **Sankar T.V** and Padmasree K (2021): A Proteomic Approach to Confirm the Purity of Recombinant *Arabidopsis thaliana* Alternative Oxidase (rAtAOX1A) Expressed in *E. coli*. "Virtual Conference on Proteomics in Agriculture and Healthcare" held on March 13-14th, 2021, at the School of Life Sciences, University of Hyderabad, India-500046.
- 2. **Sankar T.V**, **Saharay M**, **Santhosh D** and Padmasree K (2022). Molecular Cloning and Heterologous Expression of *A. thaliana AOX1a* in *E. coli*: Purification and Biophysical Characterization of rAtAOX1A. "Bioanveshana, an in-house symposium of Dept. of

Biotechnology & Bioinformatics", held on Nov 7-8th, **2022**, at School of Life Sciences, University of Hyderabad, India-500046.



Structural and Biophysical Characterization of Purified Recombinant *Arabidopsis thaliana's* Alternative Oxidase 1A (rAtAOX1A): Interaction With Inhibitor(s) and Activator

Tadiboina Veera Sankar¹, Moumita Saharay², Dharawath Santhosh¹, Abhaypratap Vishwakarma^{3,4} and Kollipara Padmasree^{1*}

- ¹ Department of Biotechnology and Bioinformatics, School of Life Sciences, University of Hyderabad, Hyderabad, India,
- ² Department of Systems and Computational Biology, School of Life Sciences, University of Hyderabad, Hyderabad, India,
- ³ Department of Plant Sciences, School of Life Sciences, University of Hyderabad, Hyderabad, India, ⁴ Department of Botany, Deshbandhu College, University of Delhi, New Delhi, India

OPEN ACCESS

Edited by:

Anthony L. Moore, University of Sussex, United Kingdom

Reviewed by:

Fei Xu, Wuhan Institute of Bioengineering, China Allison McDonald, Wilfrid Laurier University, Canada

*Correspondence:

Kollipara Padmasree kpssl@uohyd.ac.in

Specialty section:

This article was submitted to Plant Physiology, a section of the journal Frontiers in Plant Science

Received: 07 February 2022 Accepted: 27 April 2022 Published: 16 June 2022

Citation:

Sankar TV, Saharay M, Santhosh D, Vishwakarma A and Padmasree K (2022) Structural and Biophysical Characterization of Purified Recombinant Arabidopsis thaliana's Alternative Oxidase 1A (rAtAOX1A): Interaction With Inhibitor(s) and Activator. Front. Plant Sci. 13:871208. doi: 10.3389/fpls.2022.871208

In higher plants, alternative oxidase (AOX) participates in a cyanide resistant and non-proton motive electron transport pathway of mitochondria, diverging from the ubiquinone pool. The physiological significance of AOX in biotic/abiotic stress tolerance is well-documented. However, its structural and biophysical properties are poorly understood as its crystal structure is not yet revealed in plants. Also, most of the AOX purification processes resulted in a low yield/inactive/unstable form of native AOX protein. The present study aims to characterize the purified rAtAOX1A protein and its interaction with inhibitors, such as salicylhydroxamic acid (SHAM) and n-propyl gallate (n-PG), as well as pyruvate (activator), using biophysical/in silico studies. The rAtAOX1A expressed in E. coli BL21(DE3) cells was functionally characterized by monitoring the respiratory and growth sensitivity of E. coli/pAtAOX1A and E. coli/pET28a to classical mitochondrial electron transport chain (mETC) inhibitors. The rAtAOX1A, which is purified through affinity chromatography and confirmed by western blotting and MALDI-TOF-TOF studies, showed an oxygen uptake activity of 3.86 µmol min⁻¹ mg⁻¹ protein, which is acceptable in non-thermogenic plants. Circular dichroism (CD) studies of purified rAtAOX1A revealed that >50% of the protein content was α -helical and retained its helical absorbance signal (ellipticity) at a wide range of temperature and pH conditions. Further, interaction with SHAM, n-PG, or pyruvate caused significant changes in its secondary structural elements while retaining its ellipticity. Surface plasmon resonance (SPR) studies revealed that both SHAM and n-PG bind reversibly to rAtAOX1A, while docking studies revealed that they bind to the same hydrophobic groove (Met191, Val192, Met195, Leu196, Phe251, and Phe255), to which Duroquinone (DQ) bind in the AtAOX1A. In contrast, pyruvate binds to a pocket consisting of Cys II (Arg174, Tyr175, Gly176, Cys177, Val232, Ala233, Asn294, and Leu313). Further, the mutational docking studies suggest that (i) the Met195 and

1

Characterization of Recombinant Alternative Oxidase 1A from Arabidopsis thaliana and Interaction with Inhibitors, TCA Cycle and Redox Metabolites

by Veera Sankar Tadiboina

Submission date: 07-Aug-2023 03:58PM (UTC+0530)

Submission ID: 2142609957

File name: Veera Sankar Tadiboina.docx (18.41M)

Word count: 30052

Character count: 159188

lihrarian

Indira Gandhi Memorial Library UNIVERSITY OF HYDERABAD Central University P.O.

HYDERABAD-500 046.

Characterization of Recombinant Alternative Oxidase 1A from Arabidopsis thaliana and Interaction with Inhibitors, TCA Cycle and Redox Metabolites

ORIGINA	ALITY REPORT	·			
4 SIMILA	0% ARITY INDEX	38% INTERNET SOURCES	39% PUBLICATIONS	3% STUDENT PAR	PERS
PRIMAR	Y SOURCES				
1	www.ncb	oi.nlm.nih.gov	Fre	m wook	26%
2	www.froi	ntiersin.org	Dr. K.P.M.S. Professor &	V. Padmasree, Ph.D.,	7%
3	WWW.res	earchgate.net	School Univer Hyd	chnology & Bioinformatics of Life Sciences rsity of Hyderabad erabad-500 046 angana, INDIA	1 %
4	Submitte Hyderab Student Paper	ed to University ad	of Hyderabac	d,	<1%
5	academic Internet Source	c.oup.com			<1%
6	Ascorbate-Glutathione Pathway and Stress Tolerance in Plants, 2010. Publication				<1%
7	core.ac.u				<1%